ISSN 2518-1726 (Online),
ISSN 1991-346X (Print)

ҚАЗАҚСТАН РЕСПУБЛИКАСЫ
ҰЛТТЫҚ ҒЫЛЫМ АКАДЕМИЯСЫНЫҢ
Әль-фараби атындағы Қазақ ұлттық университетінің

Х А Б А Р Л А Р Ы

ИЗВЕСТИЯ

НАЦИОНАЛЬНОЙ АКАДЕМИИ НАУК
РЕСПУБЛИКИ КАЗАХСТАН
Казахский национальный университет
имени Аль-фараби

N E W S

OF THE NATIONAL ACADEMY OFSCIENCES
OF THE REPUBLIC OF KAZAKHSTAN
Al-farabi kazakh
national university

SERIES
PHYSICO-MATHEMATICAL

3 (325)

MAY - JUNE 2019

PUBLISHED SINCE JANUARY 1963

PUBLISHED 6 TIMES A YEAR

ALMATY, NAS RK

«ҚР ҰҒА Хабарлары. Физика-математикалық сериясы».

ISSN 2518-1726 (Online), ISSN 1991-346X (Print)

Меншіктенуші: «Қазақстан Республикасының Ұлттық ғылым академиясы» РҚБ (Алматы қ.)
Қазақстан республикасының Мәдениет пен ақпарат министрлігінің Ақпарат және мұрағат комитетінде 01.06.2006 ж. берілген **№5543-Ж** мерзімдік басылым тіркеуіне қойылу туралы куәлік

Мерзімділігі: жылына 6 рет.
Тиражы: 300 дана.

Редакцияның мекенжайы: 050010, Алматы қ., Шевченко көш., 28, 219 бөл., 220, тел.: 272-13-19, 272-13-18,
http://physics-mathematics.kz/index.php/en/archive

Типографияның мекенжайы: «Аруна» ЖК, Алматы қ., Муратбаева көш., 75.

«Известия НАН РК. Серия физико-математическая».

ISSN 2518-1726 (Online), ISSN 1991-346X (Print)

Собственник: РОО «Национальная академия наук Республики Казахстан» (г. Алматы)
Свидетельство о постановке на учет периодического печатного издания в Комитете информации и архивов Министерства культуры и информации Республики Казахстан **№5543-Ж**, выданное 01.06.2006 г.

Периодичность: 6 раз в год.
Тираж: 300 экземпляров.

Адрес редакции: 050010, г. Алматы, ул. Шевченко, 28, ком. 219, 220, тел.: 272-13-19, 272-13-18,
http://physics-mathematics.kz/index.php/en/archive

Адрес типографии: ИП «Аруна», г. Алматы, ул. Муратбаева, 75.

News of the National Academy of Sciences of the Republic of Kazakhstan. Physical-mathematical series.

ISSN 2518-1726 (Online), ISSN 1991-346X (Print)

Owner: RPA "National Academy of Sciences of the Republic of Kazakhstan" (Almaty)
The certificate of registration of a periodic printed publication in the Committee of information and archives of the Ministry of culture and information of the Republic of Kazakhstan N 5543-Ж, issued 01.06.2006

Periodicity: 6 times a year
Circulation: 300 copies

Editorial address: 28, Shevchenko str., of. 219, 220, Almaty, 050010, tel. 272-13-19, 272-13-18,
http://physics-mathematics.kz/index.php/en/archive

Address of printing house: ST "Aruna", 75, Muratbayev str, Almaty

N E W S
OF THE NATIONAL ACADEMY OF SCIENCES OF THE REPUBLIC OF KAZAKHSTAN
PHYSICO-MATHEMATICAL SERIES
ISSN 1991-346X **https://doi.org/10.32014/2019.2518-1726.18**
Volume 3, Number 325 (2019), 5 – 12

UDC 521.1

M.Zh. Minglibayev, A.T. Ibraimova*

Al-Farabi Kazakh National University, Almaty, Kazakhstan
Fesenkov Astrophysical Institute, Almaty, Kazakhstan
minglibayev@gmail.com, ibraimova@aphi.kz

EQUATIONS OF MOTION OF THE RESTRICTED THREE-BODY PROBLEM WITH NON-ISOTROPICALLY VARIABLE MASSES WITH REACTIVE FORCES

Abstract. During the formation of planetary systems, especially at the non-stationary stage, the gravitational field of the central protostar (e.g., protosun) and the most massive protoplanets (e.g., protojupiter) often dominate. In this regard, we consider the restricted three-body problem with variable masses changing non-isotropically at different rates, as a celestial-mechanical model of small-body motion in a non-stationary protoplanet system. Based on the generalized Meshchersky equation, the differential equations of the restricted three-body problem are derived in the absolute coordinate system and in the presence of a reactive forces. At the same time it is assumed that the masses of the bodies are increasing due to accreting particles from the outer space, and decreasing due to the particle loss. Based on the equation of motion obtained in the absolute coordinate system, the equations of motion in a relative coordinate system whose origin is at the center of the protostar are derived in the presence of a reactive forces. Special cases of the obtained differential equations of motion of a non-stationary dynamic system in a relative coordinate system are discussed.

Key words: restricted three-body problem, non-isotropically variable mass, reactive forces.

1. Introduction. One of the actual problems in modern astronomy is the origin and evolution of small bodies (asteroids, comets) in planetary systems. Studying the movement and evolution of small bodies, we will try to understand what the planetary system was in the past and how the planetary system will be in the future. Small bodies collide with planets every day, in particular with the Earth in the Solar system.

In the case of the Earth, in most cases they are small and burn in the atmosphere of the Earth, before falling to the surface [1]. Nevertheless, even if we talk about less than 10 meters in size asteroids, there were many of them in the Earth history. Only in the last century were two such events (at least) - the Tungussky and the Chelyabinsk meteorites. This is one of the important aspects of the small bodies' dynamics in planetary systems.

Now and in most cases, the dynamics of small bodies studies based on the Keplerian motion of the two-body problem with constant masses [2]. However, such an important parameter of small bodies as a mass is variable. Consequences of the small bodies' mass variability, especially during the stage of non-stationarity of the gravitating system, have been little studied [3-7]. We have studied the motion of an infinitesimal body in protoplanetary systems based on a restricted three-body problem with variable mass in the presence of reactive forces. Here we got the differential equations of motion for the restricted three-body problem with non-isotropically with variable mass in the absolute coordinate system and in the relative coordinate system with the origin at the protostar center. The obtained equations of motion describe the dynamic evolution of the considered non-stationary system of gravitating bodies with non-isotropically changing masses in the presence of reactive forces.

2. Problem statement and the equation of motion in the absolute coordinate system

2.1 Problem statement. Let's consider gravitating system consisting of three spherical celestial bodies with variable masses. We assume that the bodies are bodies with spherical mass distributions or points. Suppose, T_0 - the central protostar (more massive body), T_1 - protoplanet (less massive body), T_2 - a body with a small mass. Accordingly, we denote the masses, which are functions of time.

$$m_0 = m_0(t),\ m_1 = m_1(t),\ m_2 = m_2(t). \tag{2.1}$$

Suppose that the masses of the bodies are increasing due to accreting particles, and decreasing due to the particle loss. In this case, the relative speed of the particles separating from the body is different than the relative speed of the accreting particles to the body. Consider the general case when the masses of bodies change not isotropically at different rates [8, 9, 10]

$$\frac{\dot{m}_0}{m_0} \neq \frac{\dot{m}_1}{m_1}, \qquad \frac{\dot{m}_0}{m_0} \neq \frac{\dot{m}_2}{m_2}, \qquad \frac{\dot{m}_1}{m_1} \neq \frac{\dot{m}_2}{m_2}. \tag{2.2}$$

We assume that an infinitesimal body with mass m_2, does not affect the motion of the two massive bodies with the masses m_0 and m_1, this is a restricted formulation of the three bodies problem with variable mass in the presence of reactive forces [11-13]

$$m_0 \gg m_2, \quad m_1 \gg m_2. \tag{2.3}$$

Required description of the dynamical evolution of three gravitating bodies with variable mass in the presence of reactive forces in this formulation.

2.2 Differential equations of motion in the absolute coordinate system. Based on the generalized equations of Meshchersky [12-14], in the presence of reactive forces we get

$$m_0\ddot{\vec{R}}_0 = grad_{\vec{R}_0} U_{01} + \dot{m}_{01}\vec{V}_{01} + \dot{m}_{02}\vec{V}_{02}, \tag{2.4}$$

$$U_{01} = f\left(\frac{m_0 m_1}{R_{01}}\right), \tag{2.5}$$

$$\vec{V}_{01} = \vec{u}_{01} - \dot{\vec{R}}_0, \quad \vec{V}_{02} = \vec{u}_{02} - \dot{\vec{R}}_0, \tag{2.6}$$

$$m_0 = m_0(t_0) - |m_{01}| + m_{02} = m_0(t_0) - \int_{t_0}^{t}\left(|\dot{m}_{01}|\right)dt + \int_{t_0}^{t}\left(\dot{m}_{02}\right)dt. \tag{2.7}$$

$m_0(t_0) = const$ mass of the body T_0 at the initial time t_0, m_{01} - the mass of particles separated from the body T_0 in time t, m_{02} - the mass of particles accreting to the body T_0 in time t.

$$m_1\ddot{\vec{R}}_1 = grad_{\vec{R}_1} U_{10} + \dot{m}_{11}\vec{V}_{11} + \dot{m}_{12}\vec{V}_{12}, \tag{2.8}$$

$$U_{10} = f\left(\frac{m_1 m_0}{R_{10}}\right), \tag{2.9}$$

$$\vec{V}_{11} = \vec{u}_{11} - \dot{\vec{R}}_1, \qquad \vec{V}_{12} = \vec{u}_{12} - \dot{\vec{R}}_1, \tag{2.10}$$

$$m_1 = m_1(t_0) - |m_{11}| + m_{12} = m_1(t_0) - \int_{t_0}^{t}\left(|\dot{m}_{11}|\right)dt + \int_{t_0}^{t}\left(\dot{m}_{12}\right)dt. \tag{2.11}$$

$m_1(t_0) = const$ mass of the body T_1 at the initial time t_0, m_{11} - mass of particles separated from the body T_1 in time t, m_{12} - the mass of particles accreting to the body T_1 in time t.

$$m_2\ddot{\vec{R}}_2 = grad_{\vec{R}_2}\tilde{U} + \dot{m}_{21}\vec{V}_{21} + \dot{m}_{22}\vec{V}_{22}, \tag{2.12}$$

$$\tilde{U} = fm_2\left(\frac{m_0}{R_{20}} + \frac{m_1}{R_{21}}\right), \tag{2.13}$$

$$\vec{V}_{21} = \vec{u}_{21} - \dot{\vec{R}}_2, \qquad \vec{V}_{22} = \vec{u}_{22} - \dot{\vec{R}}_2, \tag{2.14}$$

$$m_2 = m_2(t_0) - |m_{21}| + m_{22} = m_2(t_0) - \int_{t_0}^{t}\left(|\dot{m}_{21}|\right)dt + \int_{t_0}^{t}(\dot{m}_{22})dt. \tag{2.15}$$

$m_2(t_0) = const$ mass of the body T_2 at the initial time t_0, m_{21} - mass of particles separated from the body T_2 in time t, m_{22} - the mass of particles accreting to the body T_2 in time t.

In equations (2.4) - (2.15) $\vec{u}_{01}$, $\vec{u}_{11}$, $\vec{u}_{21}$ - are the absolute velocities of the separating particles,

$$\vec{V}_{01} = \vec{u}_{01} - \dot{\vec{R}}_0, \ \vec{V}_{11} = \vec{u}_{11} - \dot{\vec{R}}_1, \ \ \vec{V}_{21} = \vec{u}_{21} - \dot{\vec{R}}_2. \tag{2.16}$$

relative velocities of separating particles.

Accordingly, $\vec{u}_{02}$, $\vec{u}_{12}$, $\vec{u}_{22}$ - absolute velocities of the accreting particles,

$$\vec{V}_{02} = \vec{u}_{02} - \dot{\vec{R}}_0, \ \vec{V}_{12} = \vec{u}_{12} - \dot{\vec{R}}_1, \ \vec{V}_{22} = \vec{u}_{22} - \dot{\vec{R}}_1. \tag{2.17}$$

relative velocities of accreting particles. Also marked, that $\vec{R}_j$ - the radius vector of the center of mass bodies in the absolute coordinate system $(j = 0,1,2)$, $\vec{R}_{ij}$ – the mutual distances of the mass bodies center $(j,i = 0,1,2,\ j \neq i)$, f - gravitational constant.

From equations (2.4) - (2.5), (2.8) - (2.9), (2.12) - (2.13) follows

$$\ddot{\vec{R}}_0 = grad_{\vec{R}_0}U_{01} + \frac{1}{m_0}\left(\dot{m}_{01}\vec{V}_{01} + \dot{m}_{02}\vec{V}_{02}\right) \tag{2.18}$$

$$U_{01} = f\left(\frac{m_1}{R_{01}}\right), \tag{2.19}$$

$$\ddot{\vec{R}}_1 = grad_{\vec{R}_1}U_{10} + \frac{1}{m_1}\left(\dot{m}_{11}\vec{V}_{11} + \dot{m}_{12}\vec{V}_{12}\right) \tag{2.20}$$

$$U_{10} = f\left(\frac{m_0}{R_{10}}\right), \tag{2.21}$$

$$\ddot{\vec{R}}_2 = grad_{\vec{R}_2}\tilde{U}^* + \frac{1}{m_2}\left(\dot{m}_{21}\vec{V}_{21} + \dot{m}_{22}\vec{V}_{22}\right) \tag{2.22}$$

$$\tilde{U}^* = f\left(\frac{m_0}{R_{20}} + \frac{m_1}{R_{21}}\right). \tag{2.23}$$

Equations (2.18) - (2.19), (2.20) - (2.21) define the problem of two bodies with variable masses in the presence of reactive forces for the absolute coordinate system.

Equations (2.22) - (2.23) define a restricted three body problem with variable masses in the presence of reactive forces for the absolute coordinate system.

Following L.G. Lukyanov [15] we assume that the reactive forces is applied to the inertia center of the corresponding spherical celestial bodies.

3. Equations of motion of bodies in a relative coordinate system

We introduce the relative coordinate system with the origin at the center of the central protostar T_0, whose axes are parallel to the corresponding axes of the absolute coordinate system. Denote

$$\vec{R}_{01} = \vec{R}_1 - \vec{R}_0 \,,\ \vec{R}_{02} = \vec{R}_2 - \vec{R}_0 \,. \tag{3.1}$$

Then in relative coordinates equations of motion for the two primary bodies problem has the form

$$\ddot{\vec{R}}_{01} = grad_{\vec{R}_{01}} \tilde{U}_{01} + \frac{1}{m_1}\left(\dot{m}_{11}\vec{V}_{11} + \dot{m}_{12}\vec{V}_{12}\right) - \frac{1}{m_0}\left(\dot{m}_{01}\vec{V}_{01} + \dot{m}_{02}\vec{V}_{02}\right), \tag{3.2}$$

$$\tilde{U}_{01} = f\frac{m_0 + m_1}{R_{01}} \,. \tag{3.3}$$

In relative coordinates, the equations of motion of a body with a small mass, in the attraction field of two primary bodies, can be written as

$$\ddot{\vec{R}}_{02} = grad_{\vec{R}_{02}} \tilde{U}^* + \frac{1}{m_2}\left(\dot{m}_{21}\vec{V}_{21} + \dot{m}_{22}\vec{V}_{22}\right) - \frac{1}{m_0}\left(\dot{m}_{01}\vec{V}_{01} + \dot{m}_{02}\vec{V}_{02}\right). \tag{3.4}$$

Denote the reactive forces (per unit mass)

$$\vec{\Phi}_{11} = \frac{1}{m_1}\left(\dot{m}_{11}\vec{V}_{11}\right) - \frac{1}{m_0}\left(\dot{m}_{01}\vec{V}_{01}\right),\ \vec{\Phi}_{12} = \frac{1}{m_1}\left(\dot{m}_{12}\vec{V}_{12}\right) - \frac{1}{m_0}\left(\dot{m}_{02}\vec{V}_{02}\right), \tag{3.5}$$

$$\vec{F}_1 = \vec{F}_1(t) = \vec{\Phi}_{11} + \vec{\Phi}_{12} \,. \tag{3.6}$$

$$\vec{\Phi}_{21} = \frac{1}{m_2}\left(\dot{m}_{21}\vec{V}_{21}\right) - \frac{1}{m_0}\left(\dot{m}_{01}\vec{V}_{01}\right),\ \vec{\Phi}_{22} = \frac{1}{m_2}\left(\dot{m}_{22}\vec{V}_{22}\right) - \frac{1}{m_0}\left(\dot{m}_{02}\vec{V}_{02}\right), \tag{3.7}$$

$$\vec{F}_2 = \vec{F}_2(t) = \vec{\Phi}_{21} + \vec{\Phi}_{22} \,. \tag{3.8}$$

Note that the reactive forces (per unit mass) are due to separating particles denoted by

$$\vec{\Phi}_{11} = \frac{1}{m_1}\left(\dot{m}_{11}\vec{V}_{11}\right) - \frac{1}{m_0}\left(\dot{m}_{01}\vec{V}_{01}\right),\ \vec{\Phi}_{21} = \frac{1}{m_2}\left(\dot{m}_{21}\vec{V}_{21}\right) - \frac{1}{m_0}\left(\dot{m}_{01}\vec{V}_{01}\right). \tag{3.9}$$

Similarly, reactive forces (per unit mass) are due to accreting particles indicated by the formulas

$$\vec{\Phi}_{12} = \frac{1}{m_1}\left(\dot{m}_{12}\vec{V}_{12}\right) - \frac{1}{m_0}\left(\dot{m}_{02}\vec{V}_{02}\right),\ \vec{\Phi}_{22} = \frac{1}{m_2}\left(\dot{m}_{22}\vec{V}_{22}\right) - \frac{1}{m_0}\left(\dot{m}_{02}\vec{V}_{02}\right). \tag{3.10}$$

In the notation (3.5) - (3.8) formulas (3.2) (3.4) has the form

$$\ddot{\vec{R}}_{01} = grad_{\vec{R}_{01}} \tilde{U}_{01} + \vec{F}_1, \tag{3.11}$$

$$\ddot{\vec{R}}_{02} = grad_{\vec{R}_{02}} \tilde{U}^* + \vec{F}_2 \,. \tag{3.12}$$

We introduce the following notation.

$$\vec{R}_{01} = \vec{R}_1 - \vec{R}_0 = \vec{r}_1\left(x_1, y_1, z_1\right),\ \ \vec{R}_{02} = \vec{R}_2 - \vec{R}_0 = \vec{r}_2\left(x_2, y_2, z_2\right),\ \ \vec{r}_1 - \vec{r}_2 = \vec{r}_{21}. \quad (3.13)$$

The equations of motion (3.11) - two primary bodies problems with variable masses in the presence of reactive forces (3.6) we can write in the form

$$\ddot{\vec{r}}_1 + f\left(m_0 + m_1\right)\frac{\vec{r}_1}{r_1^3} = \vec{F}_1, \quad (3.14)$$

$$r_1 = \sqrt{x_1^2 + y_1^2 + z_1^2}\,, \quad (3.15)$$

$$\vec{F}_1 = \vec{F}_1\left(t\right) = \vec{\Phi}_{11} + \vec{\Phi}_{12}. \quad (3.16)$$

Accordingly, the equations of motion of a body with a small mass (3.12), in the attraction field of two primary bodies, can be written as

$$\ddot{\vec{r}}_2 = grad_{\vec{r}_2}\tilde{U}^* + \vec{F}_2.$$

The last equation can be written as

$$\ddot{\vec{r}}_2 + f\left(m_0 + m_2\right)\frac{\vec{r}_2}{r_2^3} = grad_{\vec{r}_2}U + \vec{F}_2, \quad (3.17)$$

$$U = fm_1\left(\frac{1}{r_{21}} - \frac{x_1x_2 + y_1y_2 + z_1z_2}{r_1^3}\right), \quad (3.18)$$

$$r_{21} = \sqrt{\left(x_1 - x_2\right)^2 + \left(y_1 - y_2\right)^2 + \left(z_1 - z_2\right)^2}\,, \quad (3.19)$$

$$r_1 = \sqrt{x_1^2 + y_1^2 + z_1^2}\,,\ \ r_2 = \sqrt{x_2^2 + y_2^2 + z_2^2}\,, \quad (3.20)$$

$$\vec{F}_2 = \vec{F}_2\left(t\right) = \vec{\Phi}_{21} + \vec{\Phi}_{22}. \quad (3.21)$$

The obtained equations of relative motion (3.17)-(3.21), a restricted three-body problem with variable masses in the presence of reactive forces, more adequately describe the dynamic evolution of infinitesimal body motion with variable mass in non-stationary gravitating multiple systems than the isotropic change in the masses of bodies [4, 11, 15, 16]. In this case, the relative motion of the two primary bodies is described by equations (3.14)-(3.16). Note that in some exoplanetary systems [17-19], where nonstationary processes, apparently, in still dominates in the formation of planetary systems then the equations obtained can be effectively used.

In orbital coordinate systems, reactive forces (3.16), (3.21) can be written as

$$\vec{F}_2 = \vec{F}_2\left(t\right) = \vec{F}_{2r} + \vec{F}_{2\tau} + \vec{F}_{2n} = \vec{F}_2\left(F_{2r}\left(t\right), F_{2\tau}\left(t\right), F_{2n}\left(t\right)\right), \quad (3.22)$$

$$\vec{F}_1 = \vec{F}_1\left(t\right) = \vec{F}_{1r} + \vec{F}_{1\tau} + \vec{F}_{1n} = \vec{F}_1\left(F_{1r}\left(t\right), F_{1\tau}\left(t\right), F_{1n}\left(t\right)\right), \quad (3.23)$$

where denoted by radial $\vec{F}_{ir}$, transversal $\vec{F}_{i\tau}$ and normal components $\vec{F}_{in}$ of reactive forces.

4. Particular cases of the equation of motion (3.14), (3.17). The obtained equations of motion in the relative coordinate system, with the origin at the body center, describe the bodies dynamics in the considered formulation of the problem in the general case. There is interest to study the problem under consideration in various particular assumptions regarding in the bodies mass change. The possible combination of three bodies mass change for different cases is quite a lot. A full analysis of various particular cases will be performed in another work. In this paper we consider, as an example, one interesting special case.

The case when the masses of three bodies are constant, but with variable composition. Let the changes in the mass of each body be characterized by the fact that the second mass of the accreting

particles of a particular body is equal to the second mass of the same body discarded particles. Then we have

$$-\dot{m}_{01}=\dot{m}_{02}=\dot{m}_0^*,\quad -\dot{m}_{11}=\dot{m}_{12}=\dot{m}_1^*,\quad -\dot{m}_{21}=\dot{m}_{22}=\dot{m}_2^*. \tag{4.1}$$

From formulas (2.7), (2.11), (2.15) it follows that the masses of the bodies are constant, but with variable composition

$$\begin{aligned} m_0&=m_0\left(t_0\right)=m_0^*=const,\\ m_1&=m_1\left(t_0\right)=m_1^*=const,\\ m_2&=m_2\left(t_0\right)=m_2^*=const. \end{aligned} \tag{4.2}$$

From formulas (3.6), (3.5) and (4.1), taking into account (2.6), (2.10), (2.14), we get

$$\begin{aligned} \vec{F}_1&=\vec{F}_1^*=\vec{\Phi}_{11}^*+\vec{\Phi}_{12}^*=\frac{\dot{m}_{11}}{m_1}\vec{V}_{11}-\frac{\dot{m}_{01}}{m_0}\vec{V}_{01}+\frac{\dot{m}_{12}}{m_1}\vec{V}_{12}-\frac{\dot{m}_{02}}{m_0}\vec{V}_{02}=\\ &=\frac{1}{m_1}\left(\dot{m}_{11}\vec{V}_{11}+\dot{m}_{12}\vec{V}_{12}\right)-\frac{1}{m_0}\left(\dot{m}_{01}\vec{V}_{01}+\dot{m}_{02}\vec{V}_{02}\right)=\\ &=\frac{\dot{m}_1^*}{m_1}\left(-\vec{V}_{11}^*+\vec{V}_{12}^*\right)-\frac{\dot{m}_0^*}{m_0}\left(-\vec{V}_{01}^*+\vec{V}_{02}^*\right)=\\ &=\frac{\dot{m}_1^*}{m_1}\left(-\vec{u}_{11}^*+\vec{u}_{12}^*\right)-\frac{\dot{m}_0^*}{m_0}\left(-\vec{u}_{01}^*+\vec{u}_{02}^*\right). \end{aligned} \tag{4.3}$$

Similarly, taking into account formulas (3.8), (3.7), (4.1) and considering these formulas (2.6), (2.10), (2.14), we get

$$\begin{aligned} \vec{F}_2&=\vec{F}_2^*=\vec{\Phi}_{21}^*+\vec{\Phi}_{22}^*=\frac{\dot{m}_{21}}{m_2}\vec{V}_{21}-\frac{\dot{m}_{01}}{m_0}\vec{V}_{01}+\frac{\dot{m}_{22}}{m_2}\vec{V}_{22}-\frac{\dot{m}_{02}}{m_0}\vec{V}_{02}=\\ &=\frac{1}{m_2}\left(\dot{m}_{21}\vec{V}_{21}+\dot{m}_{22}\vec{V}_{22}\right)-\frac{1}{m_0}\left(\dot{m}_{01}\vec{V}_{01}+\dot{m}_{02}\vec{V}_{02}\right)=\\ &=\frac{\dot{m}_2^*}{m_2}\left(-\vec{V}_{21}^*+\vec{V}_{22}^*\right)-\frac{\dot{m}_0^*}{m_0}\left(-\vec{V}_{01}^*+\vec{V}_{02}^*\right)=\frac{\dot{m}_2^*}{m_2}\left(-\vec{u}_{21}^*+\vec{u}_{22}^*\right)-\frac{\dot{m}_0^*}{m_0}\left(-\vec{u}_{01}^*+\vec{u}_{02}^*\right). \end{aligned} \tag{4.4}$$

As a result, we can write

$$\vec{F}_1=\vec{F}_1^*=\frac{\dot{m}_1^*}{m_1}\left(-\vec{V}_{11}^*+\vec{V}_{12}^*\right)-\frac{\dot{m}_0^*}{m_0}\left(-\vec{V}_{01}^*+\vec{V}_{02}^*\right)=\frac{\dot{m}_1^*}{m_1}\left(-\vec{u}_{11}^*+\vec{u}_{12}^*\right)-\frac{\dot{m}_0^*}{m_0}\left(-\vec{u}_{01}^*+\vec{u}_{02}^*\right). \tag{4.5}$$

$$\vec{F}_2=\vec{F}_2^*=\frac{\dot{m}_2^*}{m_2}\left(-\vec{V}_{21}^*+\vec{V}_{22}^*\right)-\frac{\dot{m}_0^*}{m_0}\left(-\vec{V}_{01}^*+\vec{V}_{02}^*\right)=\frac{\dot{m}_2^*}{m_2}\left(-\vec{u}_{21}^*+\vec{u}_{22}^*\right)-\frac{\dot{m}_0^*}{m_0}\left(-\vec{u}_{01}^*+\vec{u}_{02}^*\right). \tag{4.6}$$

Thus, in the particular case of (4.1), in the three-body gravitating system under consideration, each body has a constant mass. But at the same time, the composition of each body changes, which may affect the chemical structure of these bodies [20]. The relative coordinate system in the equation of motion (3.14), (3.17) contains reactive forces according to (4.5) - (4.6).

The obtained equations of motion of the problem under consideration are rather complicated, therefore, in the future they will be investigate by perturbation theory methods [8].

5. Conclusion

The work investigated the movement of an infinitesimal body in the gravitational field of two massive bodies in the framework of a restricted three-body problem with masses that changing at different rates non-isotropically in the presence of reactive forces.

Based on the generalized Meshchersky equation, the differential equations of the restricted three-body problem with masses varying at different rates non-isotropically are derived, in the absolute coordinate system with the presence of reactive forces. At the same time, it is assumed that the masses of the bodies are increasing due to accreting particles from the outer space, and decreasing due to the particle loss. Also obtained equations of the relative motion for a restricted three-body problem with variable masses, varying at non-isotropically different rates, in a relative coordinate system, in the presence of reactive forces, with the origin at the central protostar center.

Discussed particular cases of the obtained differential equations of motion, considered for a nonstationary dynamic system in a relative coordinate system. Considered one case, when the mass of each body is constant, but with variable composition.

The resulting equations of motion of the restricted three-body problem with non-isotropically varying masses in the presence of reactive forces more adequately describe the dynamic evolution of a small-body motion with a variable mass in non-stationary gravitating multiple systems than isotropic changing masses of the bodies.

Acnowledgments

The work is partially supported by the program BR05236322 and PhD training program of the Ministry of Education and Science of the Republic of Kazakhstan.

М.Дж. Минглибаев, А.Т. Ибраимова

Әл-Фараби атындағы КазҰУ, Алматы қ., Қазақстан
В.Г. Фесенков атындағы астрофизика институты, Алматы қ., Қазақстан

РЕАКТИВТІ КҮШ ЕСКЕРІЛГЕН МАССАЛАРЫ ИЗОТРОПТЫ ЕМЕС ӨЗГЕРЕТІН ШЕКТЕЛГЕН ҮШ ДЕНЕ ЕСЕБІНІҢ ҚОЗҒАЛЫС ТЕҢДЕУІ

Аннотация. Планеталық жүйелердің қалыптасуы кезінде, әсіресе стационар емес кезеңде орталық протожұлдыздың (мысалы, протокүн) және ең массивті протопланетаның (мысалы, протоюпитер) гравитациялық өрісі басым. Осыған орай стационар емес протопланеталық жүйелердегі кіші дене қозғалысының негізгі аспан-механикалық моделі ретінде әртүрлі қарқында изотропты емес өзгеретін массасы айнымалы шектелген екі дене есебі қарастырылады. Мещерскийдің жалпылама теңдеуін негізге ала отырып реактивті күштері бар абсолютті координат жүйесіндегі шектелген үш дене есебінің дифференциалдық теңдеулері алынды. Сонымен, ғарыштық ортадан қосылатын бөлшектердің әсерінен массаның өсуі, сондай-ақ лақтырылатын бөлшектердің есебінен массаның азаюы байқалуы мүмкін деген болжам жасалуда. Абсолютті координат жүйесінде алынған қозғалыс теңдеуін ескере отырып салыстырмалы координат жүйесінде орталық протожұлдыздың центрі координаттар басы болып табылатын реактивті күш ескерілген қозғалыс теңдеуі алынды. Салыстырмалы координат жүйесіндегі стационар емес динамикалық жүйеде қарастырылған дифференциалдық теңдеулердің дербес жағдайы талқыланды.

Түйін сөздер: шектелген үш дене есебі, массаның изотропты емес өзгеруі, реактивті күштер.

М.Дж. Минглибаев, А.Т. Ибраимова

КазНУ им. аль-Фараби, Алматы қ., Казахстан
Астрофизический институт им. В.Г. Фесенкова, г.Алматы, Казахстан

УРАВНЕНИЯ ДВИЖЕНИЯ ОГРАНИЧЕННОЙ ЗАДАЧИ ТРЕХ ТЕЛ С НЕИЗОТРОПНО ИЗМЕНЯЮЩИМИСЯ МАССАМИ ПРИ НАЛИЧИИ РЕАКТИВНЫХ СИЛ

Аннотация. В ходе образования планетных систем, особенно в этапе нестационарности, часто доминирует гравитационное поле центральной протозвезды (например, протосолнце) и самой массивной протопланеты (например, протоюпитер). В связи с этим, рассматривается ограниченная задача трех тел с переменными массами, изменяющимися не изотропно в различных темпах, как исходная небесно-механическая модель движений малого тела в нестационарных протопланетных системах. Исходя из обобщенного уравнения Мещерского выведены дифференциальные уравнения ограниченной задачи трех тел в абсолютной системе координат, при наличии реактивных сил. При этом предполагается

одновременно рост массы тел из-за присоединяющихся (налипания) частиц из космической среды, а также уменьшение массы тел за счет отбрасываемых частиц. Исходя из уравнения движения, полученные в абсолютной системе координат, выведены уравнения движения в относительной системе координат с началом в центре центральной протозвезды, при наличии реактивных сил. Обсуждается частные случаи полученных дифференциальных уравнения движения, рассмотренной нестационарной динамической системы, в относительной системе координат.

Ключевые слова: ограниченная задача трех тел, неизотропное изменения масс, реактивные силы.

Information about authors

Minglibayev Mukhtar Zhumabekovich - Post address: Almaty, Zharokov st, 288, 35, Affiliation: al-Farabi Kazakh National University, Fesenkov Astrophysical Institute, Chief Researcher. Tel: 2476086, e-mail: minglibayev@gmail.com

Ibraimova Aigerim - Post address: Almaty, Tattibekova st. 87. Affiliation: al-Farabi Kazakh National University, doctoral student, Fesenkov Astrophysical Institute, Junior Researcher. Tel: +7 777 211 72 62, e-mail: ibraimova@aphi.kz

REFERENCES

[1] Shustova B.M. Ryhlova L.V. Asteroidno-kometnaja opasnost': vchera, segodnja, zavtra M.: Fizmatlit, 2010 (in Russian)

[2] Engelhardt T. et. al. An Observational Upper Limit on the Interstellar Number Density of Asteroids and Comets. The Astronomical Journal. 2017. V.153. Iss.3, 11 pp. (in Eng.)

[3] Omarov T.B. (Editor) Non-Stationary Dynamical Problems in Astronomy. New-York: Nova Science Publ. Inc., 2002. - 260 p. (in Eng.)

[4] Eggleton P. Evolutionary processes in binary and multiple stars, Cambridge University Press, New York, 2006, 322 p. (in Eng.)

[5] Cherepawuk A.M. Tesnye dvojnye zvezdy. Chast' II.-M.: Fizmatlit, 2013. 572 p. (in Russian)

[6] Veras D., Hadjidemetriou J.D., Tout C.A. An Exoplanet's Response to Anisotropic Stellar Mass-Loss During Birth and Death. - MNRAS. 2013. DOI: 10.1093/mnras/stt1451 (in Eng.)

[7] Surdin V.G. Solnechnaja sistema. M.: Fizmatlit, 2017. 460 p. (in Russian)

[8] Minglibaev M.Zh. Dinamika gravitirujuwih tel s peremennymi massami i razmerami. Postupatel'noe i postupatel'no-vrawatel'noe dvizhenie. LAP LAMBERT Academic Publishing, Germanija, 2012, 229 p. (in Russian)

[9] Minglibayev M.Zh. A.N. Prokopenya, M. Mayemerova, Zh.U. Imanova Three-body problem with variable masses that change anisotropically at different rates. Mathematics in Computer Science, 2017, Vol.11, (3-4). P. 383-391 SJR 2016-0.288 (in Eng.)

[10] Jewitt D. The Active Asteroids, The Astronomical Journal. 2012. V.143. Iss.3. 14 pp. (in Eng.)

[11] Poljahova E.N. Nebesno-mehanicheskie aspekty zadach dvuh i treh tel s peremennymi massami // Uchenye zapiski LGU, Ser. matem. nauk. 1989. T.42, №424, vyp. 64. P. 104-143. (in Russian)

[12] Luk'janov L.G., Shirmin G.I. Lekcii po nebesnoj mehanike. Almaty, 2009. 227 p. (in Russian)

[13] Mewerskij I.V. Raboty po mehanike tel peremennoj massy. M.: Gosudarstvennnoe izdatel'stvo tehniko-teoreticheskoj literatury, 1952. 281 p. (in Russian)

[14] Kosmodem'janskij A.A. Kurs teoreticheskoj mehaniki. 2-oj tom. M.:Prosvewenie, 1966. 402 p. (in Russian)

[15] Luk'janov L.G. Dinamicheskaja jevoljucija orbit zvezd v tesnyh dvojnyh sistemah s konservativnym obmenom mass // Astron.zhurn. 2008. T.85, №8. P.755-768. (in Russian)

[16] Bekov A.A., Omarov T.B. The Theory of Orbits in Non-Stationary Stellar Systems. // Astronomical and Astrophysical Transactions. 2003. V.22. P. 145-153. (in Eng.)

[17] http://spacetimes.ru/exoplanets

[18] http://exoplanetarchive.ipac.caltech.edu

[19] http://exoplanet.eu

[20] Busarev V.V. New Notions of Asteroids of Primitive Types. // Modern Star Astronomy. Vol. 1, Astronomy-2018 (XIII Congress of the International Public Organization "Astronomical Society"). Conference Abstracts, Moscow: IZMIRAN, 2018. P. 9-18. (in Eng.).

N E W S
OF THE NATIONAL ACADEMY OF SCIENCES OF THE REPUBLIC OF KAZAKHSTAN
PHYSICO-MATHEMATICAL SERIES
ISSN 1991-346X **https://doi.org/10.32014/2019.2518-1726.19**
Volume 3, Number 325 (2019), 13 – 21

UDC 52-48, 524, 539.14, 539.17

A.V. Dzhazairov-Kakhramanov[1], L.T. Karipbayeva[1]

[1]V.G. Fesenkov Astrophysical Institute "NCSRT" NSA RK, 050020, Observatory 23,
Kamenskoe plato, Almaty, Kazakhstan
albert-j@yandex.ru; larisa_karipbaeva@mail.ru

RADIATIVE PROTON CAPTURE ON ^{3}H AT ASTROPHYSICAL ENERGIES AND ITS ROLE IN THE INITIAL STAGE OF STAR FORMATION

Abstract. Calculations of the astrophysical *S*-factor of the proton radiative capture on ^{3}H at energies from 1 keV to 10 MeV in the frame of the Modified Potential Cluster Model (MPCM) with classification of orbital states of nuclear particles according to Young tableaux and isospin were carried out. The explanation of the used phenomenological model MPCM was done. The classification of the p^3H states according to Young tableaux was given. The p^3H interaction potentials and phase shifts of the p^3H elastic scattering were found.

Key words: Nuclear astrophysics; primordial nucleosynthesis; light atomic nuclei; astrophysical energies; radiative capture; thermonuclear processes; potential cluster model; forbidden states, p^3H system.

1. Introduction

The proton capture on ^{3}H reaction is of certain interest from the theoretical and experimental points of view for understanding the dynamics of photonuclear processes with the lightest atomic nuclei at low and ultralow, i.e., astrophysical energies [1]. In addition, it is able, evidently, to attend in the primordial elements nucleosynthesis in the Universe [1-4], leading to the prestellar formation of ^{4}He nuclei. Therefore, experimental studies of this reaction continue, and new data for the total cross section of the proton radiative capture on ^{3}H and the astrophysical *S*-factor in the energy range from 50 keV to 5 MeV [5] and at 12 and 39 keV [6] (center of mass system) has been obtained. These data will use by us further for comparison with the calculation results.

The considering reaction could play a certain role at the prestellar stage of evolution of the Universe [1-3], when at its cooling down to the temperature about ~0.8 MeV, the processes of the primordial nucleosynthesis [7,8] with the formation of stable ^{2}H, ^{3}He, ^{4}He nuclei, and also stable in the first minutes of the Universe formation ^{3}H nucleus became possible.

1. $p + n \rightarrow {}^2H + \gamma$ (Q = 2.225 MeV),
2. ${}^2H + p \rightarrow {}^3He + \gamma$ (Q = 5.494 MeV),
3. ${}^2H + n \rightarrow {}^3H + \gamma$ (Q = 6.257 MeV),
4. ${}^3H + p \rightarrow {}^3He + n$ (Q = -0.764 MeV),
5. ${}^3He + n \rightarrow {}^3H + p$ (Q = 0.764 MeV),
6. ${}^3H + p \rightarrow {}^4He + \gamma$ (Q = 19.814 MeV),
7. ${}^3He + n \rightarrow {}^4He + \gamma$ (Q = 20.578 MeV),
8. ${}^2H + {}^2H \rightarrow {}^3He + n$ (Q = 3.269 MeV),
9. ${}^2H + {}^2H \rightarrow {}^3H + p$ (Q = 4.033 MeV),
10. ${}^2H + {}^3He \rightarrow {}^4He + p$ (Q = 18.353 MeV),
11. ${}^2H + {}^3H \rightarrow {}^4He + n$ (Q = 17.589 MeV),
12. ${}^2H + {}^2H \rightarrow {}^4He + \gamma$ (Q = 23.847 MeV).

This situation could realize at the live time of the Universe about 100 sec, when the number of protons and neutrons was comparable – approximately 0.2 neutrons from the proton number. The epoch of primordial nucleosynthesis is finished approximately at 200 sec [7]; practically all neutrons are already bound into ^{4}He nuclei, the number of which is about 25% relative to ^{1}H nuclei. At that moment the content of ^{2}H and ^{3}He relative to ^{1}H is about at the level of $10^{-4}\div10^{-6}$ [1-8].

Thus, ^{4}He is the last nucleus at the initial stage of nucleosynthesis because heavier nuclei (such as C, O et al.) could be synthesized only in the process of nuclear reactions in stars. The reason is existence of some instability gap for light nuclei (A = 5,6), that, apparently, can't be bridged in the process of primordial nucleosynthesis. In principle, ^{4}He could generate heavier nuclei (A = 7) in $^4\text{He} + {}^3\text{H} \rightarrow {}^7\text{Li} + \gamma$, $^4\text{He} + {}^3\text{He} \rightarrow {}^7\text{Be} + \gamma$ reactions, but the Coulomb barrier for these reactions is about 1 MeV while the kinetic energy of the nuclei at temperature $\sim9\cdot10^8$ K (≈56 кеV) is of the order of 0.1 MeV [4]. The mechanism of prestellar synthesis of ^{4}He lets to explain its abundance in the Universe, confirms a prestellar stage of ^{4}He generation, and corroborates the Big Bang theory.

However, the abundance of ^{3}H at the first 100–200 sec. after the Big Bang can be not much smaller ^{2}H, since the reaction of the neutron capture, in spite of the reduction their number down to 0.2 from the proton number, can go on deuteron at any energies. In addition, the half-life of ^{3}He equals 4500(8) days [9] and do not take a real contribution in the decrease of the number of ^{3}H at the first minutes after the Big Bang.

The quantity of tritium, except process No.3, increases due to reactions No.5 and No.9, but can decrease due to processes No.6 and 11 (at the energy lower than 0.8 MeV reaction No.4 practically does not contribute in decreasing of tritium). Meanwhile, the known *S*-factor of $^2\text{H} + {}^3\text{H} \rightarrow {}^4\text{He} + \text{n}$ reaction (No.11), for example, at energy 10 keV has the value of order 15 MeV b [10], and of the reaction No.6 about $2\cdot10^{-3}$ keV b that can demonstrate its small relative contribution into the formation of ^{4}He. However, the number of deuterons for reaction No.11 approximately by 4-5 orders less than protons taking part into reaction No.6, therefore the real contribution of such reactions in prestellar formation of ^{4}He will be quite comparable. Consequently, the proton capture reaction on ^{3}H can be of certain interest at consideration of astrophysical problems in regard to formations of stable ^{4}He in the process of primordial nucleosynthesis of the Universe.

It should be noted that formation of the modern understanding of the different forming stages of the Universe, about the processes of nucleosynthesis occurring in it, as well as the properties of new stars is still in progress. Therefore, the acquisition of new information on the primordial nucleosynthesis and mechanisms of the Universe formation on the basis of modern concepts of nuclear astrophysics is very urgent and one of the main tasks of a unified cosmological model construction. All this directly applies to the detailed study of p^3H capture reaction in the astrophysical energy region on the basis of modern nuclear model which, as shown below, has already demonstrated its efficiency in the description of the characteristics of almost 30 such reactions.

2. Used model

Earlier in our works [11-16] the possibility of description of astrophysical *S*-factors or total cross-sections of the radioactive capture for three dozens of processes on the basis of two-body potential cluster model (PCM) was shown and also the preliminary results [17] for p^3H-capture at astrophysical energies have been obtained. The calculations of these reactions are carried out on the basis of the modified variant of PCM with forbidden states (FSs) [18] and classification of states according to Young tableaux (MPCM).

The well-defined success of the MPCM in the description of the total cross sections of this type can be explained by the fact that the potentials of the intercluster interaction in the continuous spectrum are constructed on the basis of the known elastic scattering phase shifts or structure of the resonance spectrum levels of the final nucleus, and for the discrete spectrum - on the basis of the main characteristics of the bound states (BSs) of such nuclei: the excited (ES) or the ground (GS) states. These intercluster potentials are based also on the classification of the cluster states according to Young tableaux [19], which enables one to determine the presence and quantity of the FSs in each partial wave. This means finding the number of wave function (WF) nodes in such cluster systems [16].

Furthermore, such potentials permit us to carry out the calculations of some basic characteristics of the considered particles interaction in the elastic scattering processes and reactions. For instance, these can be the astrophysical *S*-factors of the radiative capture reactions [20] or the total cross sections of these reactions [21]. Including radiative capture cross sections at the astrophysical and thermal energy range which has been considered in our previous papers [11-16]. On the basis of such conception we succeeded in the correct description of the total cross sections of the radiative capture processes of almost thirty reactions for light nuclei at thermal and astrophysical energies [11-16].

Therefore, continuing studying the thermonuclear reactions [11-16] on the basis of the MPCM [16] with separation of orbital states according to Young tableaux let us consider description of the astrophysical *S*-factor of the radiative proton capture on ^{3}H at energies of 1 keV–10 MeV and rate of this reaction from $T_9 = 0.05$ to $T_9 = 2$. Preliminary results on *S*-factor of this reaction at astrophysical energies in the frame of the MPCM were given in our previous work [17]. New results for the rate of the proton capture on ^{3}H were obtained here and comparison of our results from [17], published in 1995, and the newest experimental data also published in 1995 year too, given further and do not take into account in our work [17]. For carrying out of the present calculations the potentials of the scattering processes and bound p^3H states were improved and detailed classification orbital states of p^3H system according to Young tableaux and isospin is given. Basic methods and principles of the MPCM used here recently were partially given in [15], and more detailed in book [16].

3. Classification of p^3H states according to Young tableaux

It is known [19] that states with minimal spin in scattering processes in the certain lightest atomic nuclei are mixed with respect to orbital Young tableaux, for example, the singlet state of p^3H system is mixed according to tableaux {4} and {31} [18]. At the same time, this state in the bound form, for example, singlet p^3H channel of ^{4}He is the pure state with Young tableau {4} [18]. In this case we can suppose [19] that BSs and scattering potentials for N^3H (N^3He) states will be different because of the difference of their Young tableaux. Thus, the explicit dependence of the potential parameters at the given moments *L*, *S* and *J* from Young tableaux $\{f\}$ is permitted in this case.

Now, let's give the classification of states, for example, of N^3H (N^3He) systems according to orbital and spin-isospin Young tableaux and demonstrate how to obtain these results. In the general case, the possible orbital Young tableau $\{f\}$ of some nucleus $A(\{f\})$ consisting of two parts $A_1(\{f_1\}) + A_2(\{f_2\})$ is the direct outer product of orbital Young tableaux of these parts $\{f\}_L = \{f_1\}_L \times \{f_2\}_L$ and is determined by the Littlewood theorem [18,19]. Therefore, the possible orbital Young tableaux of the N^3H (N^3He) systems, in which tableau {3} is used for ^{3}H (^{3}He), are the symmetries $\{4\}_L$ and $\{31\}_L$.

Spin-isospin tableaux are the direct inner product of spin and isospin Young tableaux of the nucleus of *A* nucleons $\{f\}_{ST} = \{f\}_S \otimes \{f\}_T$ and for the system with the number of particles not larger than eight are given in [22]. For any of these moments (spin and isospin), the corresponding tableau of the nucleus consisting of *A* nucleons each of which has an angular moment equals 1/2 is constructed as follows: in the cells of the first row the number of nucleons with the moments pointing in one direction, for example, upward, is indicated. In cells of the second row, if it is required, the number of nucleons with the moments directed in the opposite direction, for example, downward, is indicated. The total number of cells in both rows is equal to the number of nucleons in the nucleus. Moments of nucleons in the first row which have a pair in the second row with the oppositely directed moment are compensated and have, therefore, a zero total moment. The sum of moments of nucleons of the first row, which are not compensated by moments of nucleons of the second one, gives the total moment of the whole system [23].

In this case for N^3H (N^3He) cluster systems at the isospin $T = 0$ and the spin $S = 0$, we have tableau $\{22\}_S$ or $\{22\}_T$; and for *S* or $T = 1$, the Young tableau has the form $\{31\}_S$ or $\{31\}_T$. Upon construction of the spin-isospin Young tableau for the triplet spin state of N^3H (N^3He) systems with $T = 1$, we have $\{31\}_S \otimes \{31\}_T = \{4\}_{ST} + \{31\}_{ST} + \{22\}_{ST} + \{211\}_{ST}$, and for the singlet spin state with $T = 0$, we have $\{22\}_S \otimes \{22\}_T = \{4\}_{ST} + \{22\}_{ST} + \{1111\}_{ST}$ [22].

The total Young tableau of the nucleus is determined in a similar way as the direct inner product of the orbital and spin-isospin tableau $\{f\} = \{f\}_L \otimes \{f\}_{ST}$ [19]. The total wave function of the system in the case of antisymmetrization does not identically vanish only if it does not contain the antisymmetric

component $\{1^N\}$, that is realized upon multiplication of conjugated $\{f\}_L$ and $\{f\}_{ST}$. Therefore, the tableaux $\{f\}_L$ conjugated to $\{f\}_{ST}$ are allowed in this channel and all other symmetries are forbidden, since they result to zero total wave function of the system of particles after its antisymmetrization.

Thus, for p^3H system in the triplet channel, independently from the T values, only the orbital wave function with the symmetry $\{31\}_L$ is allowed and the function with $\{4\}_L$ turns out to be forbidden, since the products $\{211\}_{ST} \otimes \{4\}_L$ or $\{31\}_{ST} \otimes \{4\}_L$ do not result in an antisymmetric component of the total wave function. At the same time, in the singlet channel for $T = 0$, we have $\{1111\}_{ST} \otimes \{4\}_L = \{1111\}$ [22], and we obtain the antisymmetric tableau. At this channel with $T = 1$ we have the product $\{211\}_{ST} \otimes \{31\}_L$ that also gives the antysimmetric component $\{1111\}$ for total wave function. Just that very case when one can conclude that the singlet spin state for p^3H and n^3He systems turns out mixed according to Young orbital tableaux each of which relates to different isospin values.

In other words, p^3H system is mixed with respect to isospin, since it has the projection $T_z = 0$, and the following values of the total isospin are possible: $T = 0$ and 1. Hence, in this system both triplet and singlet phase shifts and, therefore, potentials effectively depend on two isospin values. Mixing with respect to isospin leads to mixing according to Young tableaux. As it was shown above, in the singlet spin state two orbital Young tableaux - {31} and {4} - are allowed [17]. Then it was shown in [17,18] that singlet phase shifts of the p^3H scattering mixed with respect to isospin can be represented in the form of the half-sum of pure with respect to isospin singlet phase shifts

$$\delta^{\{T=1\}+\{T=0\}} = 1/2[\delta^{\{T=1\}} + \delta^{\{T=0\}}], \quad (1)$$

this is equivalent to the following expression for the scattering phase shifts in terms of Young tableaux

$$\delta^{\{4\}+\{31\}} = 1/2[\delta^{\{31\}} + \delta^{\{4\}}].$$

Pure phase shifts with Young tableau {31} correspond to $T = 1$, and phase shifts with {4} to isospin $T = 0$. In this approach we assume that pure phase shifts with isospin $T = 1$ in p^3H system can be matched to phase shifts with $T = 1$ for p^3He channel [17,18]. Therefore p^3He system at $T_z = 1$ is pure by isospin with $T = 1$, so the pure by isospin phase shifts of p^3H scattering with $T = 0$ are extracted from expression (1) on the basis of the known pure scattering phase shifts with $T = 1$ for p^3He system [24-29] and for mixed p^3H with isospin with $T = 0$ and 1 [30-32]. Furthermore, the corresponded pure potentials of p^3H interaction are constructed on their basis, for example, for the GS of ^4He in p^3H channel [17,18].

4. Potentials and p^3H scattering phase shifts

For calculations of the photonuclear processes in the considered system the nuclear part of the intercluster potential of p^3He interactions for each partial wave can be expressed in the form

$$V_{JLS\{f\}}(R) = V_0(JLS\{f\})exp[-\alpha(JLS\{f\})R^2] + V_1(JLS\{f\})exp[-\alpha(JLS\{f\})R] \quad (2)$$

with the point-like coulomb term. This potential, as for p^2H system [11], is constructed so that to correctly describe correspondent partial phase shift of p^3He elastic scattering [24-29].

Consequently, the pure with respect to isospin $T = 1$ potentials of p^3He interactions for the elastic scattering processes were obtained, and their parameters are listed in Table 2 [17,18]. The singlet and pure with respect to isospin S phase shift of p^3He elastic scattering, used later for calculation of the singlet p^3H phase shifts with the isospin $T = 0$, is shown by the solid line in Fig. 1a together with the experimental data from works [24-26].

Therefore, there are several different variants of the phase shift analysis of p^3He elastic scattering, for example [24-29], so the parameters of the potential for the singlet $^1P_1$ and the triplet $^3P_1$ waves given in the Table 2 are chosen in order to receive a certain compromise between different results. The singlet $^1P_1$ phase shift of the elastic p^3He scattering with $T = 1$ used in our calculations of the $E1$ transition to the ground state of ^4He in p^3H channel with $T = 0$ is shown in Fig. 1b by the solid line and the experimental data of works [24-29] are given in this figure too.

Table 2 - The singlet potentials of the form (2) for p^3He scattering, pure with respect to isospin T = 1 [17,18]

System	^{2S+1}L	V_0 (MeV)	α (fm^{-2})	V_1 (MeV)	γ (fm^{-1})
p^3He	^1S	-110.0	0.37	+45.0	0.67
	^1P	-15.0	0.1	–	–

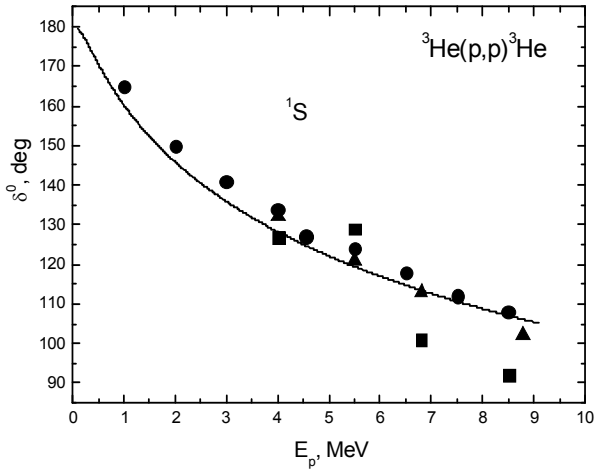

Fig. 1a- Singlet ^1S phase shift of the elastic p^3He scattering. Experimental data: points [24], squares [25], and triangles [26]

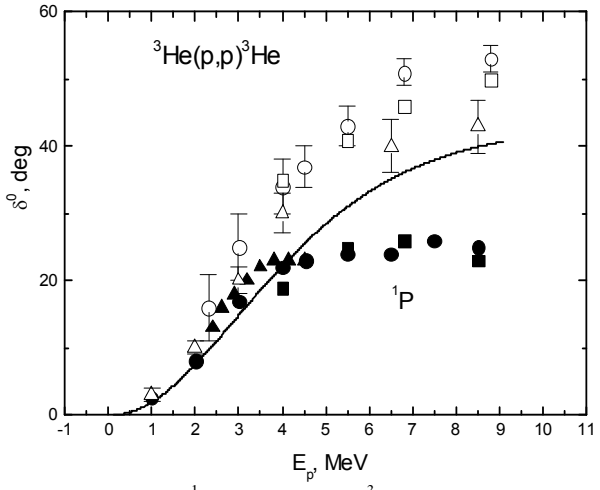

Fig. 1b - Singlet ^1P phase shift of p^3He elastic scattering. Experimental data: points [24], squares [25], triangles [27], circles [28], open squares [26], and open triangles [29]

The singlet and isospin and Young tableaux mixed S phase shift of the elastic p^3H scattering, determining from the experimental differential cross sections and used later for obtaining the pure p^3H phase shifts for potential (2) at $V_1 = 0$ with parameters

$$V_0 = -50 \text{ MeV}, \quad \alpha = 0.2 \text{ fm}^{-2}$$

is shown in Fig. 2 by the solid line together with the experimental data of works [30-32].

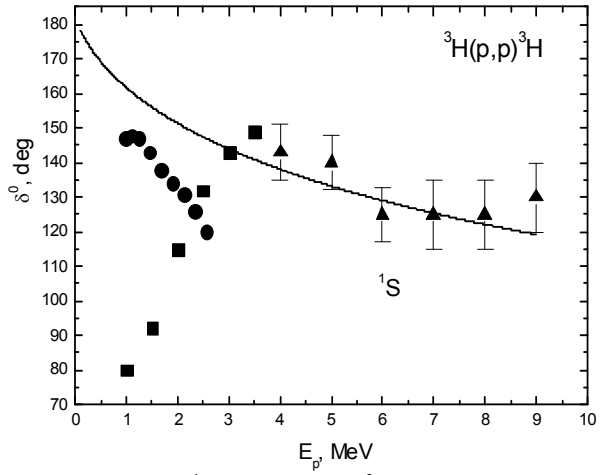

Fig. 2 - Singlet ^1S phase shift of p^3H elastic scattering. Experimental data: points [30], squares [31], and triangles [32]

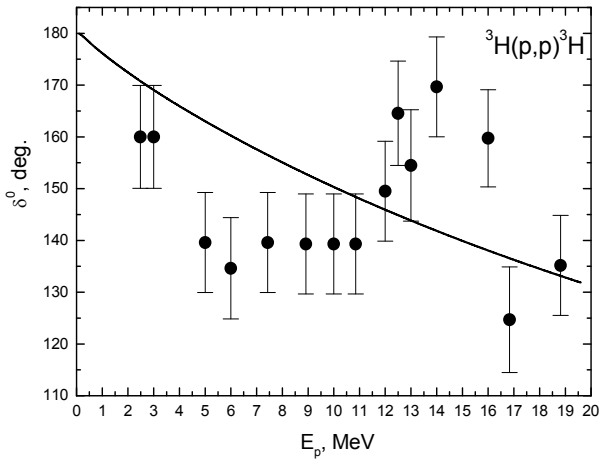

Fig. 3 - Singlet pure according to Young tableau ^1S phase shift of p^3H elastic scattering

Then, using expression (1), for the pure p^3H potential with $T = 0$ in the ^1S wave in [17] at $V_1 = 0$ the following parameters have been found:

$$V_0 = -63.1 \text{ MeV}, \quad \alpha = 0.17 \text{ fm}^{-2}. \qquad (3)$$

Fig. 3 shows the pure with respect to Young tableau singlet ^1S phase of p^3H elastic scattering (dotted line) and the results of calculation of this phase with potential (3) (solid line). Thus-obtained pure (according to Young tableau) interactions can be used for calculation of different characteristics of the bound ground state ^4He in p^3H channel. The degree of agreement of the results obtained in this case with experiment now depends only on the degree of clusterization of this nucleus in the considered channel and here one supposes that this degree is high enough and the spectroscopic factor of such channel will be close to unit.

The interaction potential (3) obtained in [17] on the whole correctly describes the channel binding energy of p^3H system (to several kiloelectronvolts) and the root-mean-square radius of ^4He. With this potential and potential of the ^1P scattering wave from Table 2 with the point-like coulomb term for p^3H system were carried out the calculations of differential [18] and total [17] cross sections of the proton radiative capture on ^3H and the astrophysical *S*-factors at energies down to 10 keV. It should be noted that at that time experimental data for the *S*-factor only was known in the energy region above 700–800 keV [33]. Subsequently, new experimental data were obtained [5] and [6]. Therefore, it is of interest to elucidate whether the potential cluster model with the singlet ^1P potential obtained earlier and refined interaction of the pure ground ^1S state of ^4He is capable of describing this new more accurate data.

Our preliminary results [17,18] have shown that for calculation of the *S*-factor at energies of the order of 1 keV the same conditions as in p^2H system [11] should be satisfied – first of all, the accuracy of finding the binding energy of ^4He in p^3H channel should be increased. New modified programs [16] were used here in order to improve parameters of the potential of the ground state for p^3H system of ^4He (see Table 3), which differ from those presented in [17] by approximately 0.2 MeV. This difference is mainly connected with the application in new calculations of more accurate values of masses of p and ^3H particles [34] and more accurate description of the binding energy of ^4He in p^3H channel.

For this energy based on more accurate values of particle masses [9,34], a value of –19.813810 MeV was obtained; the calculation with the potential considered here gives –19.81381000 MeV. The accuracy of determination of the energy value in this potential using our program based on the finite-difference method (FDM) [16] is 10^{-8} MeV. This accuracy of obtaining the binding energy in p^3H channel of ^4He in the given potential with parameters from Table 3 is confirmed by the calculations on the basis of the variational method (VM), the obtained results are given below.

Table 3 - Pure with respect to isospin of $T = 0$ potentials of form (3) for p^3H interactions in a singlet channel. Here, E_{GS} is the calculated bound ground state energy and E_{exp} is the experimental value of this energy [35]

System	^{2S+1}L	V_0 (MeV)	α (fm^{-2})	E_{GS} (MeV)	E_{exp} (MeV)
p^3H	^1S	-62.906841138	0.17	-19.81381000	-19.813810
	^1P	+8.0	0.03	–	–

The behavior of the "tail" of the numerical wave function (WF) $\chi_L(R)$ for p^3H system bound state at large distances was verified using asymptotic constant (AC) [36,37]

$$\chi_L(r) = \sqrt{2k_0}\ C_W W_{-\eta L+1/2}(2k_0 r), \tag{4}$$

which turned out to be equal to $C_W = 4.52(1)$ at an interval of 5–10 fm for the potential with GS parameters from Table 3. Here $\mu Z_1 Z_2 e^2/(q\hbar^2)$ is the coulomb parameter, where q is the wave number determined by the energy of interacting particles in the initial channel, *L* is the orbital moment, $W_{-\eta L+1/2}(2k_0R)$ is the Whittaker function [37], $k_0 = \sqrt{2\mu\frac{m_0}{\hbar^2}E}$ is the wave number of the GS, *E* is the binding energy in p^3H channel, and the constant $\hbar^2/m_0$ is equal to 41.4686 MeV fm^2, m_0 is the atomic mass unit (amu) [16]. The reduced error of the asymptotic constant is determined by its averaging over mentioned above interval of distances, it is practically stable in the limit of this zone.

The region of the AC C_W stabilization is finding for AC determination starting from the maximum distances that were considered by us, which have order 20–30 fm. This region usually is at distances about

7–12 fm. Inside this region the AC is changed by at least the value of the given relative accuracy, which usually is equal to 10^{-3}. At distances lower than stabilization region for the WF we use its numerical values obtained from the Schrödinger equation solution. At long distances WF $\chi_L(R)$ is calculated from its asymptotic (4) determined by the Whittaker function $W_{-\eta L+1/2}(2k_0r)$ taking into account the AC C_W found in the stabilization region.

Known results on extraction of the asymptotic constant from experimental data give a value of 5.16(13) for p^3H channel [37]. For the asymptotic constant of n^3He system in [37], a value of 5.10(38) has been obtained that is very close to the constant of p^3H channel for our GS potential from Table 3. At the same time, in [36] a value of 4.1 was given for the constant of n^3He system, a value of 4.0 for p^3H. The average value between the results of works [36] and [37] is in a quite agreement with our results for the GS potential from Table 3. Apparently, there is a considerable difference between the data of asymptotic constants. For n^3He system, the constant is in the interval of 4.1–5.5, whereas for p^3H channel it may assume values from 4.0 to 5.3.

We should note here the results of work [38] where the average spectroscopic S_f factor that is equal to 1.59, and the average value of the asymptotic normalizing coefficient A_{NC} (ANC) that is equal to 6.02 $fm^{-1/2}$, were obtained on the basis of calculations with different potentials. Use the known relationship between ANC and dimensional AC C [21,39]:

$$A_{NC}^2 = S \times C^2.$$

Meanwhile, this expression is used for dimensional AC C

$$\chi_L(r) = CW_{-\eta L+1/2}\left(2k_0r\right).$$

This dimensional constant is related with the used by us non-dimensional C_W constant by the following way: $C = \sqrt{2k_0}C_W$. Then, using the given in [38] values of ANC and S_f for dimensional AC C we have found the value of 4.77 $fm^{-1/2}$. In this case $\sqrt{2k_0}$ = 1.30, therefore for dimensionless AC C_W we obtain the value of 3.67, which, nevertheless, slightly less than values obtained here and given in works [36,37]. However, if the spectroscopic factor determines the possibility of certain two-body channel, so scarcely this possibility can be more than unit. Therefore, if one assumes that the value $S_f = 1.0$, so for C_W at $\sqrt{2k_0}$ = 1.30 we obtain 4.63 that agrees acceptably with the given above dimensionless value of 4.52 for the ^1S potential of the ground state from Table 3.

For the charge radius of ^4He, with the potential from Table 3, we have obtained value of 1.78 fm (calculation methods of such radius are described in [16-18]) at the experimental value of ^4He radius 1.671(14) fm [35]. For these calculations we have used the values of the tritium radius of 1.73 fm from [9] and the proton radius of 0.8775 fm from data base [34].

The variational method with the independent variation of parameters with the expansion of the cluster wave function of the p^7Li system in non-orthogonal Gaussian basis [16] is used for an additional control of the accuracy of determination the binding energy in the S potential of the GS from Table 3.

$$\Phi_L(R) = \frac{\chi_L(R)}{R} = R^L \sum_i C_i \exp(-\beta_i r^2), \quad (5)$$

where β – variational parameters and C – expansion coefficients [16]. This method at the basis dimension equals 10 and at independent parameter variation enabled us to obtain the binding energy of -19.81380998 MeV. The asymptotic constant C_W specified by the expression (4) of variational wave function at distances 5–10 fm was survived at level of 4.52(2), and the value of residuals is not more than 10^{-11} [16].

It is known that the variational energy decreases with increasing of the basis dimensionality and gives the upper limit for the true binding energy [40], while the finite-difference energy increases with decreasing of step and increasing of number of steps [16]. Therefore, in the given GS potential in Table 3 for the actual binding energy an average value of –19.81380999(1) MeV can be taken. Thereby, the error of determination of the binding energy in the known GS potential by two methods presented above (FDM

and VM) and based on two different computer programs [16] is ±0.01 eV = ±10 meV or $\pm 10^{-8}$ MeV. Meanwhile it coincides with the initially given accuracy of the FDM, that is equal to 10^{-8} MeV [16].

It can be seen from the given results that the simple two-cluster p^3H model with classification of orbital states according to Young tableaux makes it possible to obtain a quite reasonable values for such characteristics of the bound state of ^{4}He as binding energy, charge radii and asymptotic constants. These results can testify in favor of a relatively high degree of clusterization of this nucleus in p^3H channel. Therefore, such model is completely able to bring us to reasonable results at the calculations of the astrophysical *S*-factors at low and astrophysical energy range.

Acknowledgments

This work was supported by the Grant of Ministry of Education and Science of the Republic of Kazakhstan through the program No. AP05130104 “Studying of the radiative capture reactions in stars and controlled thermonuclear fusion” through the Fesenkov Astrophysical Institute of the National Center for Space Research and Technology of the Ministry of Defence and Aerospace Industry of the Republic of Kazakhstan (RK).

УДК 52-48, 524, 539.14, 539.17

А.В. Джазаиров-Кахраманов[1], Л.Т. Карипбаева[1]

[1]Астрофизический институт В.Г. Фесенкова “НЦКИТ” АКК МИР РК, 050020,
Обсерватория 23, Каменское плато, Алматы, Казахстан

РАДИАЦИОННЫЙ ЗАХВАТ ПРОТОНОВ НА ^{3}H ПРИ АСТРОФИЗИЧЕСКИХ ЭНЕРГИЯХ И ЕГО РОЛЬ В НАЧАЛЬНОМ ФОРМИРОВАНИИ ЗВЕЗД

Аннотация. В рамках модифицированной потенциальной кластерной модели (МПКМ) с классификацией орбитальных состояний ядерных частиц по схемам Юнга и изоспину выполнены расчеты астрофизического *S*-фактора реакции радиационного p^3H захвата при энергиях от 1 кэВ до 10 МэВ. Дано объяснение используемой феноменологической модели МПКМ. Приведена классификация p^3H состояний по схемам Юнга. Найдены потенциалы p^3H взаимодействия и фазы p^3H упругого рассеяния.

Ключевые слова: ядерная астрофизика; первичный нюклеосинтез; легкие атомные ядра; астрофизические энергии; радиационный захват; термоядерные процессы; потенциальная кластерная модель; запрещенные состояния, p^3H система.

А.В. Джазаиров-Кахраманов[1], Л.Т. Карипбаева[1]

[1] В.Г. Фесенков атындағы Астрофизикалық институт “ҰҒЗТО” ҚР ҚАӨМ АҒК, 050020,
Обсерватория 23, Каменское плато, Алматы, Қазақстан

АСТРОФИЗИКАЛЫҚ ЭНЕРГИЯ КЕЗІНДЕГІ ^{3}H ПРОТОНДАРДЫҢ РАДИАЦИЯЛЫҚ БАСЫП АЛУ ЖӘНЕ ОНЫҢ ЖҰЛДЫЗДАРЫНЫҢ БАСТАПҚЫ ҚАЛЫПТАСУЫНДАҒЫ РӨЛІ

Аннотация. Түрленген әлеуетті кластерлік модель (ТӘКМ) шеңберінде Юнг сызбалары және изоспин бойынша ядролық бөлшектердің орбиталық жағдайының жіктеуімен 1 кэВ-дан 10 МэВ-ға дейінгі энергия кезінде радиациялық p^3H басып алу реакциясының астрофизикалық S-факторының есептері орындалды. ТӘКМ пайдаланылатын феноменологиялық моделіне түсініктеме берілді. Юнг схемалары бойынша p^3H жағдайының жіктелуі келтірілген. Өзара әрекеттесудің p^3H шамалары және серпінді шашылаудың p^3H фазалары табылды

Түйін сөздер: Ядролық астрофизика; бастапқы нюклеосинтез; жеңіл атом ядролар; астрофизикалық энергия; радиациялық басып алу; термоядролық процесстер; әлеуетті кластерлік модель; тыйым салынған жағдай, p^3H жүйе.

REFERENCES

[1] Barnes C.A., Clayton, D.D., Schramm D.N. Essays in Nuclear Astrophysics. Presented to William A. Fowler. UK, Cambridge: Cambridge University Press. 1982. 562p.

[2] Gorbunov D.S., Rubakov V.A. Introduction to theory of early Universe. Hot Big Bang theory. Singapore: World Scientific. 2011. 488p.

[3] Zeldovich Ya.B., Novikov I.D. The Structure and Evolution of the Universe. USA: University of Chicago Press. 1983. 751p.

[4] Penionzhkevich Yu.E. Exotic nuclei in astrophysics // Phys. Part. Nucl. 2012. V.43. P.452-473.

[5] Hahn K. et al. ^{3}H(p,γ)^{4}He cross section // Phys. Rev. C 1995. V.51. P. 1624-1632.

[6] Canon R. et al. ^{3}H(p,γ)^{4}He reaction below E_p = 80 keV // Phys. Rev. C 2002. V.65. P. 044008.1-044008.7.

[7] Bednyakov V.A. About Creation of the Chemical Elements // Phys. Part. Nucl. 2002. V.33. №4. P.915-963.
[8] Kramarovskii Ya.M., Chechev V.P. The puzzle of the lightest elements: observations, predictions, hypotheses // Phys. Uspekhi 1999. V.42. P.563-573 (http://ufn.ru/en/articles/1999/6/d/)
[9] Purcell J.E. et al. Energy levels of light nuclei A = 3 // Nucl. Phys. A 2010. V.848. P.1-74.
[10] Greene S.L. Maxwell averaged cross sections for some thermonuclear reactions on light isotopes // UCRL-70522. 67.
[11] Dubovichenko S.B., Dzhazairov-Kakhramanov A.V. Astrophysical S-factor of the radiative p^2H capture // Euro. Phys. Jour. A 2009. V.39. P.139-143.
[12] Dubovichenko S.B., Dzhazairov-Kakhramanov A.V., Burtebaev N., Alimov D. Radiative $p^{14}C$ capture at astrophysical energies // Mod. Phys. Lett. A 2014. V.29. P.1450125(1-16).
[13] Dubovichenko S.B., Dzhazairov-Kakhramanov A.V. Radiative n^7Li capture at Astrophysical Energies // Annalen der Physik 2012. V.524. P.850-861.
[14] Dubovichenko S.B., Dzhazairov-Kakhramanov A.V. Neutron radiative capture by ^{10}B, ^{11}B and proton radiative capture by ^{11}B, ^{14}C and ^{15}N at thermal and astrophysical energies // Int. Jour. Mod. Phys. E 2014. V.23. P.1430012(1-55).
[15] Dubovichenko S.B., Dzhazairov-Kakhramanov A.V. $^8Li(n,\gamma)^9Li$ reaction at astrophysical energies and its role in primordial nucleosynthesis // Astrophys. Jour. 2016. V.819. №1. P.78(8p.).
[16] Dubovichenko S.B. Thermonuclear processes in Stars and Universe. Second English edition, revised and expanded. Germany, Saarbrucken: Scholar's Press. 2015. 332p.; https://www.scholars-press.com/catalog/details/store/gb/book/978-3-639-76478-9/Thermonuclear-processes-in-stars
[17] Dubovichenko S.B. Photonuclear processes in the channels p^3H and n^3He of the ^4He nucleus in potential cluster models // Phys. Atom. Nucl. 1995. V.58. P.1295-1302.
[18] Neudatchin V.G., Sakharuk A.A., Dubovitchenko S.B. Photodisintegration of ^4He and the supermultiplet potential model of cluster-cluster interactions // Few-Body Systems 1995. V.18. P.159-172.
[19] Neudatchin V.G. et al. Generalized potential model description of mutual scattering of the lightest p^2H, $^2H^3He$ nuclei and the corresponding photonuclear reactions // Phys. Rev. C 1992. V.45. P.1512-1527.
[20] Angulo C. et al. A compilation of charged-particle induced thermonuclear reaction rates // Nucl. Phys. A 1999. V.656. P.3-183.
[21] Adelberger E.G. et al. Solar fusion cross sections. II. The pp chain and CNO cycles // Rev. Mod. Phys. 2011. V.83. P.195-245.
[22] Itzykson C., Nauenberg M. Unitary groups: Representations and decompositions // Rev. Mod. Phys. 1966. V.38. P. 95-101.
[23] Bohr A., Mottelson B.R. Nuclear structure Vol.I. Single particle motion. Singapore: World Scientific Publ. Co. Ldt. 1998. 471p.
[24] Tombrello T.A. Phase shift analysis for $^3He(p,p)^3He$ // Phys. Rev. 1965. V.138. P. B40-B47.
[25] Yoshino Y. et al. Phase shift of p^3He scattering at low energies // Prog. Theor. Phys. 2000. V.103. P. 107-125.
[26] McSherry D.H., Baker S.D. ^3He polarization measurements and phase shifts for p^3He elastic scattering // Phys. Rev. C 1970. V.1. P. 888-892.
[27] Drigo L., Pisent G. Analysis of the p^3He low energy interaction // Nuovo Cim. 1967. V.BLI. P. 419-436.
[28] Szaloky G., Seiler F. Phase shift analysis of $^3He(p,p)^3He$ elastic scattering // Nucl. Phys. A 1978. V.303. P. 57-66.
[29] Tombrello T.A. et al. The scattering of protons from ^3He // Nucl. Phys. 1962. V.39. P. 541-550.
[30] McIntosh J.S., Gluckstern R.L., Sack S. Proton triton interaction // Phys. Rev. 1952. V.88. P. 752-759.
[31] Frank R.M., Gammel J.L. Elastic scattering of proton by ^3He and ^3H // Phys. Rev. 1955. V.99. P. 1406-1410.
[32] Kankowsky R. et al. Elastic scattering of polarized protons on tritons between 4 and 12 MeV // Nucl. Phys. A 1976. V.263. P. 29-46.
[33] Arkatov Yu.M. et al. Study of the reaction $^4He(\gamma,p)^3H$ at maximum energy of gamma radiation 120 MeV // Sov. Jour. Nucl. Phys. 1970. V.12. P.227-233.
[34] Constants in the category "Atomic and nuclear constants" http://physics.nist.gov/cgi-bin/cuu/Category?view=html&Atomic+and+nuclear.x=87&Atomic+and+nuclear.y=12
[35] Tilley D.R., Weller H.R., Hale G.M. Energy levels of light nuclei A = 4 // Nucl. Phys. 1992. V. A541. P. 1-157.
[36] Lim T.K. 3He-n vertex constant and structure of 4He // Phys. Lett. B 1975. V.55. P. 252-254; Lim T.K. Normalization of the p-3H and n-3He tails of 4He and the 4He charge from factor // Phys. Lett. B 1973. V.44. P. 341-342.
[37] Plattner G.R., Viollier R.D. Coupling constants of commonly used nuclear probes // Nucl. Phys. A 1981. V.365. P. 8-12.
[38] Timofeyuk N.K. Overlap functions, spectroscopic factors, and asymptotic normalization coefficients generated by a shell-model source term// Phys. Rev. C 2010. V.81. P.064306(1-21).
[39] Mukhamedzhanov A.M., Blokhintsev L.D., and Irgaziev B. F. Reexamination of the astrophysical S factor for the $\alpha+d\rightarrow{}^6Li+\gamma$reaction // Phys. Rev. C 2011. V.83. P.055805(1-9).
[40] Mott N., Messey H. The theory of atomic collisions. UK: Clarendon Press. 1965. 858 p.

N E W S
OF THE NATIONAL ACADEMY OF SCIENCES OF THE REPUBLIC OF KAZAKHSTAN
PHYSICO-MATHEMATICAL SERIES
ISSN 1991-346X **https://doi.org/10.32014/2019.2518-1726.20**
Volume 3, Number 325 (2019), 22 – 31

UDC 52-48, 524, 539.14, 539.17

A.V. Dzhazairov-Kakhramanov[1], L.T. Karipbayeva[1]

[1]V.G. Fesenkov Astrophysical Institute "NCSRT" NSA RK, 050020, Observatory 23,
Kamenskoe plato, Almaty, Kazakhstan
albert-j@yandex.ru; larisa_karipbaeva@mail.ru

ASTROPHYSICAL S-FACTOR AND REACTION RATE OF THE RADIATIVE ^{3}H(p,γ)^{4}He CAPTURE

Abstract. Calculations of the astrophysical S-factor of the proton radiative capture on ^{3}H at energies from 1 keV to 10 MeV in the frame of Modified Potential Cluster Model with classification of orbital states of nuclear particles according to Young tableaux and isospin were carried out and the possibility of description of available experimental data in the energy range from 50 keV to 5 MeV is shown. We calculated rate of this reaction from 0.05 to 2 T_9, because it can play certain role in the primordial nucleosynthesis of the Universe.

Key words: Nuclear astrophysics; primordial nucleosynthesis; light atomic nuclei; astrophysical energies; radiative capture; thermonuclear processes; potential cluster model; forbidden states, p^3H system.

1. Introduction

The proton capture on ^{3}H reaction is of interest from both theoretical and experimental points of view for understanding the dynamics of photonuclear processes involving the lightest atomic nuclei at low and ultralow, i.e., astrophysical energies [1]. It also plays a role in the nucleosynthesis of primordial elements in the early Universe [1-3] leading to the pre-stellar formation of ^{4}He nuclei. Therefore, experimental studies of this reaction continue. New data for the total cross section of proton radiative capture on ^{3}H and the astrophysical *S*-factor in the energy range from 50 keV to 5 MeV [4] and at 12 and 39 keV [5] in the center of mass system (c.m.) have been obtained. These data will be used by us for further comparison with the calculation results. In addition, we ought to note other experimental studies of the photodisintegration of ^{4}He carried out, for example, in works [6]. Also, interesting theoretical results for photodisintegration of this nucleus into the p^{3}H channel were published in [7], including, on the basis of *ab initio* studies (see, for example, [8]).

Upon cooling to a temperature of ~0.8 MeV, the processes of the primordial nucleosynthesis became possible [9,10] with the formation of stable ^{2}H, ^{3}He and ^{4}He nuclei and, also stable in the first minutes of the Universe, the ^{3}H nucleus. These reactions are shown in Table 1 – the processes of the radiative capture are marked by italic. In table also the data of the *S*-factors and total cross sections at low energies in the energy range 10 – 20 keV were given with references to original works with these results. Table 1 shows that only one of these reactions, No.4, results in energy absorption Q<0. All of the others lead to energy release Q>0. Some inverse nuclear reactions, for example, photodisintegration of ^{3,4}He and ^{2,3}H by gamma-quantum cannot occur because of their extremely low energies at which weak processes cannot keep the balance [10]. Therefore the constant synthesis of stable nuclei without their further disintegration to lighter nuclei becomes possible.

Table 1 - Basic reaction of the primordial nucleosynthesis with light nuclei

No.	Process	Released energy in MeV	Astrophysical *S*-factor in keV b at 10 – 20 keV in center of mass – the accurate energy is stated in square brackets	The total cross section σ_t in μb for the given energy	Reference
1.	$p+n \rightarrow {}^2H+\gamma$	2.225	$3.18(25)\cdot10^{-3}$ [10.0]	$3.18(25)\cdot10^{2}$ [10.0]	[11]
2.	${}^2H+p \rightarrow {}^3He+\gamma$	5.494	$3.0(6)\cdot10^{-4}$ [10.4]	$1.0(2)\cdot10^{-2}$ [10.4]	[12]
3.	${}^2H+n \rightarrow {}^3H+\gamma$	6.257	$1.2\cdot10^{-5}$ [10.5]*	1.1 [10.5]*	[13]
4.	^{3}H+p → ^{3}He+n	–0.763 (see [14])	2536 [12]***	81537 [roughly at 12 keV above the threshold or 1.03354 MeV in l.s.]	[15]
5.	^{3}He+n → ^{3}H+p	0.764	63.2 [10.3]	$6.14(16)\cdot10^{6}$ [10.3]	[16]
6.	${}^3H+p \rightarrow {}^4He+\gamma$	19.814	$2.2\cdot10^{-3}$ [10.0]	$4.0\cdot10^{-2}$ [10.0]	[5]
7.	${}^3He+n \rightarrow {}^4He+\gamma$	20.578	$1.7\cdot10^{-4}$ [18.4]	9.2(2.0) [18.4]	[17]
8.	^{2}H+^{2}H → ^{3}He+n	3.269	51.4(2.0) [9.94]	241.3(9.4) [9.94]**	[18]
			53.05(0.55) [10.0]***	255.1(2.9) [10.0]	[19]
9.	^{2}H+^{2}H → ^{3}H+p	4.033	56.1(1.6) [9.97]	270.4(7.6) [9.97]	[20]
10.	^{2}H+^{3}He→^{4}He+p	18.353	7480(200) [10.7]	0.5(1) [10.7]**	[21]
11.	^{2}H+^{3}H→^{4}He+n	17.589	12328.4 [9]***	14200 [9]	[22]
12.	${}^2H+{}^2H \rightarrow {}^4He+\gamma$	23.847	$5.7(2.4)\cdot10^{-6}$ [10.0]	$2.9(1.2)\cdot10^{-5}$ [10.0]	[23]
13.	${}^2H+{}^3He \rightarrow {}^5Li+\gamma$	16.66	0.41 [111]***	5.3 [111]	[24]
14.	${}^2H+{}^3H \rightarrow {}^5He+\gamma$	16.792	0.17 [90]***	50 [90]	[24]

* - theoretical value calculated on the basis of the Modified Potential Cluster Model
** - the value calculated on the basis of the *S*-factor
*** - the value calculated on the basis of the total cross section

This was the situation when the Universe was about 100 sec old and the number of protons and neutrons was comparable – approximately 0.2 neutrons to each proton. The epoch of primordial nucleosynthesis finished at approximately 200 sec [9] by which time practically all neutrons are bound into ^{4}He nuclei and the number of ^{4}He is about 25% of the number of ^{1}H nuclei. At that point the content of ^{2}H and ^{3}He relative to ^{1}H was about 10^{-4}–10^{-6} [1–3,10].

Thus ^{4}He was the last nucleus to emerge at the initial stage of nucleosynthesis because heavier nuclei such as C and O could only be synthesized in the process of nuclear reactions in stars. The reason for this is the existence of some an instability gap for light nuclei (A = 5), which, apparently, cannot be bridged in the process of initial nucleosynthesis. In principle, ^{4}He could have given rise to heavier nuclei (A = 7) in the $^4\text{He} + {}^3\text{H} \rightarrow {}^7\text{Li} + \gamma$ and $^4\text{He} + {}^3\text{He} \rightarrow {}^7\text{Be} + \gamma$ reactions. However the Coulomb barrier for these reactions is about 1 MeV while the kinetic energy of the nuclei at temperatures of ~1 T_9 is of the order of 0.1 MeV and probability of such reactions will be negligible [25]. The mechanism of synthesis of ^{4}He explains its abundance in the Universe confirms its origin at the pre-stellar stage and corroborates the Big Bang theory.

It is important to estimate the *S*-factors of reactions 1–14. For example, as will be seen further, the astrophysical *S*-factor of proton capture on ^{2}H at an energy of 1 keV is in 5–10 times lower than the *S*-factor of the proton capture on ^{3}H at the same energy [13]. This means that the latter process, which contributes to the formation of ^{4}He in primordial nucleosynthesis, is much more likely, in spite of the lower abundance of ^{3}H relative to ^{2}H [9,10,26]. Most data available in the literature [1–4,13,25] relate to the abundance of elements such as ^{3}He at present time. This is generally confirmed by modern astrophysical observations [9,26]. However, the abundance of ^{3}H for the first 100–200 s after the Big Bang cannot be much smaller than that of ^{2}H since the neutron capture reaction, in spite of the reduction of neutron numbers down to 0.2 of the proton numbers, can go on deuteron at any energy. In addition, the half-life of ^{3}H is 4500(8) days [27] and do not make a real contribution to the decrease of the number of ^{3}H at the first few minutes after the Big Bang.

The quantity of tritium, additionally to process No.3, also increases due to reactions No.5 and No.9, but can decrease due to processes No.6 and 11. At energies lower than 0.8 MeV reaction No.4 makes

virtually no contribution to reductions in tritium. Meanwhile, the total cross section of reaction No.11 is about 14.2 mb at 9 keV [22] and of the reaction No.6 is about $4 \cdot 10^{-2}$ □b at 10 keV [5] show their small relative contributions to the formation of ^{4}He. However the number of deuterons available for reaction No.11 is approximately 4–5 orders of magnitude less than the number of protons taking part in reaction No.6. Therefore the overall contribution of the two reactions in pre-stellar formation of ^{4}He will be similar.

Reaction No.12 proceeds with comparatively low probability, since the $E1$ process is forbidden by the isospin selection rules. This leads to the factor $\left(Z_1 / m_1^J + (-1)^J Z_2 / m_2^J\right)$ at multipolarity of γ-quantum of $J = 1$ [13]. This product defines the value of the total cross sections of the radiative capture and $E1$ processes with the same Z/m ratio, for particles of the initial channel leads to zero cross sections. The probability of the allowed $E2$ transitions in such processes is usually nearly 1.5 to 2.0 orders of magnitude less [28] that was noted earlier in reviews [9,10].

Let us show furthermore the reaction rates given in work [29] in the form of parametrizations. Shape of these rates for first reactions, leading to the formation of ^{4}He or nuclei with mass of 3, is shown in Fig. 1. One can see that considered in this work reaction is at the third level for rate of forming ^{4}He and its rate in some times lower, for example, that the reaction rates of ^{3}H(d,n)^{4}He or ^{3}He(d,p)^{4}He. However, at the energy about 10 T_6 the rate of the last reaction equals the reaction rate of the proton radiative capture on ^{3}H.

All these results and more new data from works [30,31] show that the contribution of the ^{3}H(p,γ)^{4}He capture reaction into the processes of primordial nucleosynthesis is relatively small. However, it makes sense to consider this process for making the picture complete of the formation of prestellar ^{4}He and clearing of mechanisms of this reaction. In addition, as it was shown furthermore, our calculations of this reaction rate, based on the modern data of the astrophysical S-factors [5], lays slightly lower from the results of works [29,32-34]. The latest works do not take into account new data [4,5], which were taken into account by us in this work, and our results can be considered as an improved data on the rate of the considered reaction.

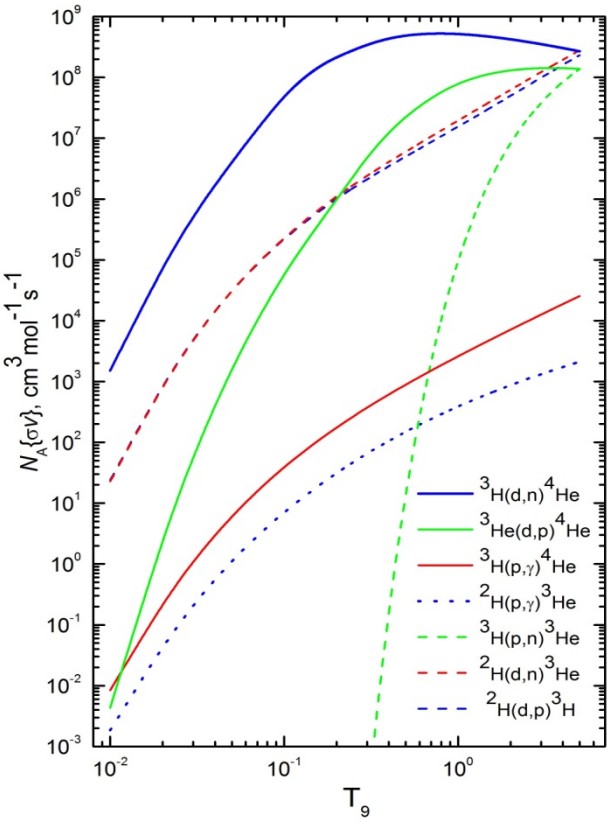

Figure 1 - Reaction rates from [29]

Moreover it should be noted that our understanding of the different stages in the formation of the Universe, of the processes of nucleosynthesis occurring in it and of the properties of new stars, is still developing. Therefore there is a pressing need to acquire new information on primordial nucleosynthesis and on the mechanisms of the Universe's formation and this is one of the main tasks for the construction of a unified cosmological model. All of this directly applies to the detailed study of the ^{3}H(p,γ)^{4}He capture reaction in the astrophysical energy region on the basis of the modern nuclear model. This model, as shown below, has already demonstrated its efficiency in the description of the characteristics of almost 30 such reactions [13,35-41].

2. Used model

Earlier in our works [13,35-37,40-42] the possibility of description of astrophysical *S*-factors or total cross-sections of the radioactive capture for three dozens of processes on the basis of two-body potential cluster model (PCM) was shown and also the preliminary results [43] for p^{3}H-capture at astrophysical energies have been obtained. The calculations of these reactions are carried out on the basis of the modified variant of PCM with forbidden states (FSs) [44] and classification of states according to Young tableaux (MPCM).

The well-defined success of the MPCM in the description of the total cross sections of this type can be explained by the fact that the potentials of the intercluster interaction in the continuous spectrum are constructed on the basis of the known elastic scattering phase shifts or structure of the resonance spectrum levels of the final nucleus, and for the discrete spectrum – on the basis of the main characteristics of the bound states (BSs) of such nuclei: the excited (ES) or the ground (GS) states. These intercluster potentials are based also on the classification of the cluster states according to Young tableaux [45], which enables one to determine the presence and quantity of the FSs in each partial wave. This means finding the number of wave function (WF) nodes in such cluster systems [35].

Furthermore, such potentials permit us to carry out the calculations of some basic characteristics of the considered particles interaction in the elastic scattering processes and reactions. For instance, these can be the astrophysical *S*-factors of the radiative capture reactions [46] or the total cross sections of these reactions [47]. Including radiative capture cross sections at the astrophysical and thermal energy range which has been considered in our previous papers [13,35-37,40-42]. On the basis of such conception we succeeded in the correct description of the total cross sections of the radiative capture processes of almost thirty reactions for light nuclei at thermal and astrophysical energies [13,35-37,40-42].

Therefore, continuing studying the thermonuclear reactions [13,35-37,40-42] on the basis of the MPCM [13,35] with separation of orbital states according to Young tableaux let us consider description of the astrophysical *S*-factor of the radiative proton capture on ^{3}H at energies of 1 keV–10 MeV and rate of this reaction from $T_9 = 0.05$ to $T_9 = 2$. Preliminary results on *S*-factor of this reaction at astrophysical energies in the frame of the MPCM were given in our previous work [43]. New results for the rate of the proton capture on ^{3}H were obtained here and comparison of our results from [43], published in 1995, and the newest experimental data also published in 1995 year too, given further and do not take into account in our work [43]. For carrying out of the present calculations the potentials of the scattering processes and bound p^{3}H states were improved and detailed classification orbital states of p^{3}H system according to Young tableaux and isospin is given. Basic methods and principles of the MPCM used here recently were partially given in [40], and more detailed in book [35].

3. Astrophysical S-factor of the proton capture on ^{3}H

Earlier in [43], based on the modified potential cluster model, the total cross sections and the astrophysical *S*-factor of the proton radiative capture process on ^{3}H were calculated. Meanwhile, it was assumed that the main contribution into the cross sections of *E*1 photodisintegration of ^{4}He in p^{3}H channel, or into the proton radiative capture on ^{3}H, was due to the isospin-flip transitions for which $\Delta T = 1$ [48]. Therefore, the $^1P_1$ potential for p^{3}He scattering in the pure with respect to isospin ($T = 1$) singlet state of this system and the ^1S potential for the ground pure with respect to the isospin $T = 0$ bound state of ^{4}He nucleus in p^{3}H channel [43] should be used in calculations.

Using these conceptions, the calculations of the *E*1 transition with refined potential of the ground state of ^{4}He (see Table 2) were carried out from the start, in comparison with [43]. The results of these calculations of the astrophysical *S*-factor at energies from 1 keV up to 10 MeV are shown in Figs. 2a and

2b by the green solid lines. In the energy region specifically from 10 keV, considered earlier in [43], and up to 10 MeV here the new results were obtained and they practically do not differ from our previous results given in [43].

Table 2 Pure with respect to isospin of $T = 0$ potentials of the Gaussian form for p^3H interactions in the singlet channel. Here, E_{GS} is the calculated bound ground state energy and E_{exp} is the experimental value of this energy [14]

System	^{2S+1}L	V_0 (MeV)	α (fm^{-2})	E_{GS} (MeV)	E_{exp} (MeV)
p^3H	^1S	-62.906841138	0.17	-19.81381000	-19.813810
	^1P	+8.0	0.03	–	–

New experimental data was taken from [4,5], and additional data from [49] not known to us earlier were also used. It can be seen from these figures that the calculations performed about 20 years ago [43] well reproduce the data on the *S*-factor obtained in [4] at energies of p^3H capture from 50 keV to 5 MeV (center of mass system). These data were published after the publication of our article [43] and have noticeably lower ambiguity at energies lower 1 MeV than do earlier results [50-53] and they more accurately determine the general behavior of the *S*-factor at low energies, practically coinciding with early data [49] in an energy range of 80–600 keV. The energy region above 1–2 MeV has been studied in many papers; therefore, for comparison, we are shown these earlier results in Fig. 2b, that demonstrate a large ambiguity of experimental measurements done in different time and works: circles [51], open squares [52], crosses (×) [53], and downward open triangles [50].

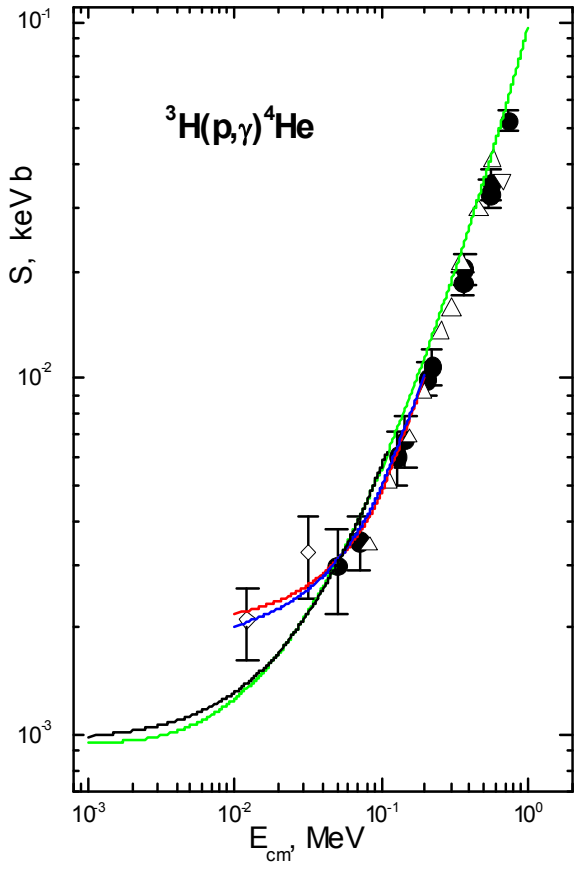

Figure 2a - Astrophysical *S*-factor of the proton radiative capture on ^3H in a range of 1 keV–1 MeV. Green line shows calculation with the GS ^1S potential given in Table 3, red line shows the results of approximation from [5], blue line shows results of approximation from [4], black line shows our approximation. Points show recalculation of total capture cross sections [4], given in [5], upward open triangles [49], rhombs [5], downward open triangles [50]

At the energy 1 keV the calculated value of the *S*-factor is equal to 0.95 eV b, and calculation results at energies less than 50 keV are slightly lower than data of [5], where for S_0 from the parametrization of the form

$$S(E_{\text{c.m.}}) = S_0 + E_{\text{c.m}}S_1 + E^2_{\text{c.m}}S_2, \quad (1)$$

the value 2.0(2) keV mb was obtained, for the S_1 parameter the value $1.6(4)\cdot10^{-2}$ mb in [5], and for the S_2 $1.1(3)\cdot10^{-4}$ mb keV^{-1} is given. The results of approximation by expression (1) with the given above parameters of experimental data [5] being in a good agreement with these data are shown in Fig. 2a by the red solid line.

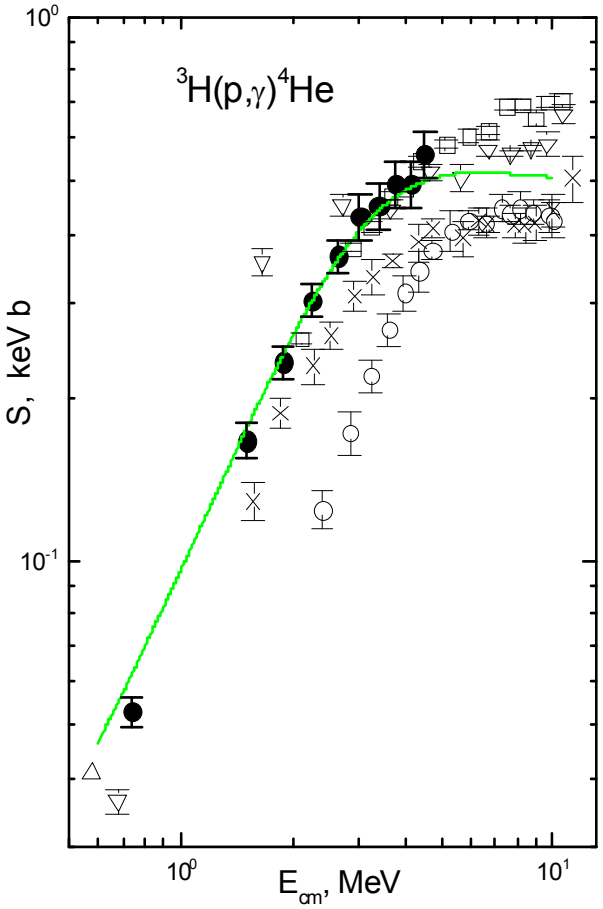

Figure 2b - Astrophysical *S*-factor of the proton radiative capture on ^{3}H in a range of 1÷10 MeV. Green line shows calculation with the GS potential given in Table 3. Points show recalculation of total capture cross sections [4] given in [5], upward open triangles [49], circles [51], open squares [52], crosses [53], and downward open triangles [50]

In [4] for the same values we found $S_0 = 1.8(1.5)$ keV mb, $S_1 = 2.0(3.4)\cdot10^{-2}$ mb and $S_2 = 1.1(1.4)\cdot10^{-4}$ mb·keV^{-1}. Results of such extrapolation are given in Fig. 2a by the blue solid line. However, the linear extrapolation of the available experimental data according to three latest points of works [4,49] to 1 keV leads to its value about 0.6(4) eV b, i.e., is three times less than it was in [5]. In addition, the data of [5] have relatively large error and, notably, are needed to be refined in future. In order to get rid of the existent data ambiguity of the *S*-factor of the proton capture on ^{3}H, we need its new measurements, even though in 2–3 points in the energy range approximately from 5–10 up to 30–50 keV.

It is seen from Fig. 2a that the calculated *S*-factor at the lowest energies, approximately at the region 1–3 keV, practically does not depend on energy. It affords ground for assumption that its value at zero energy practically does not differ from the value at 1 keV. Therefore, the difference of the *S*-factor at 0 and 1 keV, evidently will be equal not more than 0.05 eV b and this value one can consider as an error of determination of the calculated *S*-factor at zero energy, i.e., represent it in the form $S(0) = 0.95(5)$ eV b. If for parametrization of the calculated *S*-factor at the energy range 1–100 кэВ it is necessary to use quadratic form (1), so for its parameters it is possible to obtain the next values: $S_0 = 0.9530$ eV b, $S_1 = 3.497\ 10^{-2}$ eV b keV^{-1}, $S_2 = 1.216\ 10^{-4}$ eV b keV^{-2} at the value of $\chi^2 = 0.049$ at 10% errors of *S*-factor.

The results of such interpolation are shown in Fig. 2a by the black solid line. It is clear that expression (1) doesn't fit very well for interpolation of the calculated *S*-factor, especially lower 10–12 keV, since leads to the other shape of the line at low energies.

4. Reaction rate of the ^{3}H(p, γ)^{4}He radiative capture

Furthermore, in Fig. 3, the reaction rate $N_A\langle\sigma v\rangle$ of the proton capture on ^{3}H is shown by the solid green line, which corresponds to the solid green line in Figs. 2a and 2b and is presented in the form [46]

$$N_A\langle\sigma v\rangle = 3.7313\cdot 10^4\,\mu^{-1/2}T_9^{-3/2}\int_0^\infty \sigma(E)E\exp(-11.605E/T_9)dE\,, \qquad (2)$$

where $N_A\langle\sigma v\rangle$ is the reaction rate in cm^{3}mole^{-1}sec^{-1}, E is in MeV, the cross section σ (E) is measured in μb, μ is the reduced mass in amu, T_9 is the temperature in 10^9 K [46], which specifies in our calculations in the range from 0.05 to 2.0 T_9. Integration of the cross sections was carried out in the range 1 keV–2 MeV for 2000 steps with the step value of 1 keV. The expansion of this interval into the large side, for example, up to 3 MeV from 3000 steps at the same step led to a change of the reaction rate of about 1%.

We can see in Fig. 3 the sharp increase of the reaction rate value at low T_9 in the range 0.05–0.5. However, at larger T_9, approximately 1.5–2.0, $N_A\langle\sigma v\rangle$ almost reaches its saturation, tending to the value on the order of 10^4 cm^{3}mole^{-1}sec^{-1}. Finally note that we do not succeed to find other results on the rate of this reaction, obtained by using other methods, in order to make a comparison with our calculations.

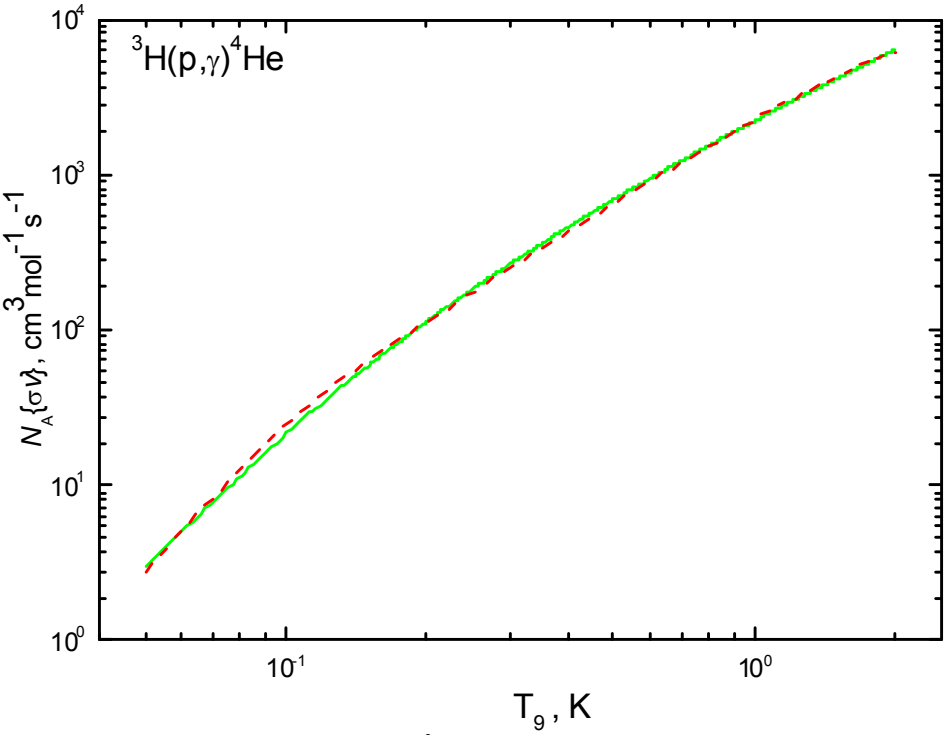

Figure 3 - Reaction rate of the proton radiative capture on ^{3}H. Green line is the calculation results for the GS potential from the Table 2, which correspond to cross sections shown in Fig. 2 by the green solid line. Dashed red line is reaction rate approximation by (3)

The resulting shape of the reaction rate in the range of 0.05–2.0 T_9 can be approximated by a general polynomial

$$N_A\langle\sigma v\rangle = \sum_{k=1}^{5} a_k T_9^{k-1} \qquad (3)$$

with parameters given in Table 3.

Table 3 - Expansion parameters for the reaction rate of the form (3)

k	1	2	3	4	5
a_k	-9.0	105.5	2628.0	-313.0	-130.0

The result of the rate calculation with such parameters is shown in Figure 3 by dashed red line at the average value $\chi^2 = 1.33$ at 1% errors of the reaction rate. The increasing of the series dimension up to 7 leads to unessential improvement in the description of the theoretical curve. However, the reduction of dimension up to 4 leads to a sharp increasing of χ^2 up to a value of about 100.

5. Conclusion

Thereby, in the frame of considered modified potential cluster model based on the intercluster potentials describing elastic scattering phase shifts and characteristics of the binding state with the potential parameters suggested about 20 years ago [43], on the basis of only the $E1$ transition we succeeded in description of the general behavior of the S-factor of the proton capture on ^{3}H at energies from 50 to 700 keV. Really, on the basis of analysis of the experimental data above 700 keV [50] about 20 years ago we have done calculations of the S-factor for energies down to 10 keV [43]. As we can see it now, the results of these calculations reproduce well new data on the S-factor, obtained in [4] (points in Figs. 2a and 2b) at energies in the range 50 keV to 5 MeV.

However, the available experimental data on the S-factor at 50 keV and lower energies have a low enough accuracy and significant ambiguity, as it seen from Figure 2a. To avoid these ambiguities, it needs new additional and independent measurements of S-factor in the energy range from about 5–10 to 30–50 keV with minimal errors. The experimenters did not return to this problem for more than 10 years [5], while reliable measurements of S-factor at energies of 50 keV–5.0 MeV have been made more than 20 years ago [4]. Evidently, modern measurement techniques could reduce error value and obtain more reliable data, especially at the lowest energies. And this, in turn, will get rid of the existing ambiguities in determining the reaction rate.

The magnitude of p^3H capture reaction rate calculated in this paper at temperatures from 0.01 T_9 up to 5 T_9 leads to the conclusion that this reaction might make some contribution to the formation of ^{4}He nuclei in the primordial nucleosynthesis of elements in the Universe, especially at higher temperatures of order 3–5 T_9. The results obtained for the reaction rate due to their simple numerical approximation can be used later for the comparative evaluation of yield of ^{4}He produced in this reaction, and, perhaps, in order to determine their contribution to the abundance of helium nuclei formed in the primordial nucleosynthesis of the Universe.

We emphasize once again that we could not find the results of other papers with calculations of the astrophysical S-factor or the considerable reaction rate obtained by other methods, in spite of the appreciable interest that this reaction represents in terms of some astrophysical problems. Currently available errors of measurements of the astrophysical S-factor [5] may significantly affect the value of the reaction rate of radiation p^3H capture leading to ambiguities in calculations of ^{4}He yield and, ultimately, affect the results obtained for its abundance. Perhaps it is time to eliminate the existing problems in measuring the astrophysical S-factor of the considerable reaction and obtain, eventually, more accurate results for the reaction rate.

Acknowledgments

This work was supported by the Grant of Ministry of Education and Science of the Republic of Kazakhstan on the program No. AP05130104 “Studying of the radiative capture reactions in stars and controlled thermonuclear fusion” through the Fesenkov Astrophysical Institute of the National Center for Space Research and Technology of the Ministry of Defence and Aerospace Industry of the Republic of Kazakhstan (RK).

А.В. Джазаиров-Кахраманов[1], Л.Т. Карипбаева[1]

[1] В.Г. Фесенков атындағы Астрофизикалық институт “ҰҒЗТО” ҚР ҚАӨМ АҒК, 050020, Обсерватория 23, Каменское плато, Алматы, Қазақстан

АСТРОФИЗИКАЛЫҚ S-ФАКТОР ЖӘНЕ ^{3}H(p, γ)^{4}He РАДИАЦИЯЛЫҚ БАСЫП АЛУ РЕАКЦИЯЛАРЫНЫҢ ЖЫЛДАМДЫҒЫ

Аннотация. Түрленген әлеуетті кластерлік модель (ТӘКМ) шеңберінде Юнг сызбалары және изоспин бойынша ядролық бөлшектердің орбиталық жағдайының жіктеуімен 1 кэВ-дан 10 МэВ-ға дейінгі энергия кезінде радиациялық p^3H басып алу реакциясының астрофизикалық S-факторының есептері орындалды және 50 кэВ-дан 5 МэВ-ға дейінгі энергия аумағында қолда бар эксперименттік мәліметтерді сипаттау мүмкіндігі көрсетілді. Бұл реакция Әлемнің бастапқы нуклеосинтезінде белгілі бір рөл атқара алатындықтан, оның жылдамдығы 0.05-ден 2 T_9. дейінгі температураларда есептелген

Түйін сөздер: Ядролық астрофизика; бастапқы нюклеосинтез; жеңіл атом ядролар; астрофизикалық энергия; радиациялық басып алу; термоядролық процесстер; әлеуетті кластерлік модель; тыйым салынған жағдай, p^3H жүйе.

А.В. Джазаиров-Кахраманов, Л.Т. Карипбаева

Астрофизический институт им. В.Г. Фесенкова «НЦКИТ» АКК МИР РК, Алматы

АСТРОФИЗИЧЕСКИЙ S-ФАКТОР И СКОРОСТЬ РЕАКЦИИ РАДИАЦИОННОГО 3H(p, γ)^{4}He ЗАХВАТА

Аннотация. В рамках модифицированной потенциальной кластерной модели с классификацией орбитальных состояний ядерных частиц по схемам Юнга и изоспину выполнены расчеты астрофизического *S*-фактора реакции радиационного *p*3H захвата при энергиях от 1 кэВ до 10 МэВ и показана возможность описания имеющихся экспериментальных данных в области энергий от 50 кэВ до 5 МэВ. Поскольку эта реакция может играть определенную роль в первичном нуклеосинтезе Вселенной, рассчитана ее скорость при температурах от 0.05 до 2 Т9.

Ключевые слова: Ядерная астрофизика; первичный нюклеосинтез; легкие атомные ядра; астрофизические энергии; радиационный захват; термоядерные процессы; потенциальная кластерная модель; запрещенные состояния, *p*3H система.

REFERENCES

[1] Barnes C.A., Clayton, D.D., Schramm D.N. Essays in Nuclear Astrophysics. Presented to William A. Fowler. UK, Cambridge: Cambridge University Press. 1982. 562p.

[2] Gorbunov D.S., Rubakov V.A. Introduction to theory of early Universe. Hot Big Bang theory. Singapore: World Scientific. 2011. 488p.

[3] Zeldovich Ya.B., Novikov I.D. The Structure and Evolution of the Universe. USA: University of Chicago Press. 1983. 751p.

[4] Hahn K. et al. 3H(p,γ)4He cross section // Phys. Rev. C 1995. V.51. P.1624-1632.

[5] Canon R. et al. 3H(p,γ)4He reaction below Ep = 80 keV // Phys. Rev. C 2002. V.65. P.044008.1-044008.7.

[6] Shima T. et al. Simultaneous measurement of the photodisintegration of 4He in the giant dipole resonance region // Phys. Rev. C 2005. 72. P.044004; Nilsson B. et al. Measurement of the 4He(γ,n) reaction from 23<Eγ<70 MeV // Phys. Rev. C 2007. 75. P.014007.

[7] Halderson D. σ(γ,p)⁄σ(γ,n) ratio, current conservation, and nucleon scattering in 4He // Phys. Rev. C 2004. 70. P.034607; Dinur Nir Nevo, Barnea Nir, Leidemann Winfried Theoretical Study of the 4He(γ, p)3H and 4He(γ, n)3He Reactions // Few-Body Systems 2014. 55. P.997; Nollett K.M., Burles S. Estimating reaction rates and uncertainties for primordial nucleosynthesis // Phys. Rev. D 2000. 61. P.123505.

[8] Horiuchi W., Suzuki Y., Arai K. Ab initio study of the photoabsorption of 4He // Phys. Rev. C 2012. 85. P.054002; Quaglioni S. et al. Two-body photodisintegration of 4He with full final state interaction // Phys. Rev. C 2004. 69. P.044002.

[9] Bednyakov V.A. About Creation of the Chemical Elements // Phys. Part. Nucl. 2002. V.33. №4. P.915-963.

[10] Kramarovskii Ya.M., Chechev V.P. The puzzle of the lightest elements: observations, predictions, hypotheses // Phys. Uspekhi 1999. V.42. P.563-573 (http://ufn.ru/en/articles/1999/6/d/).

[11] Suzuki T.S. et al. First measurement of a p(n,γ)d reaction cross section between 10 and 80 keV // Astroph. J. Lett. 1995. 439. P.L59.

[12] Casella C. et al. First measurement of the d(p,γ)3He cross section down to the solar Gamow peak // Nucl. Phys. A 2002. 706. P.203.

[13] Dubovichenko S.B., Dzhazairov-Kakhramanov A.V. Thermonuclear processes for three body system in the potential cluster model // Nucl. Phys. A 2015. 941. P.335.

[14] Tilley D.R., Weller H.R., Hale G.M. Energy levels of light nuclei A = 4 // Nucl. Phys. A 1992. 541. P.1.

[15] Brune C.R. et al. Total cross section of the 3H(p,n)3He reaction from threshold to 4.5 MeV // Phys. Rev. C 1999. 60. P.015801.

[16] Borzakov S.B. et al. // Sov. J. Nucl. Phys. 1982. 35. P.307.

[17] Wervelman R. et al. Cross-Section Measurement of the 3He(n, γ) Reaction at En = 24.5 keV // Nucl. Sci. & Eng. (NSE) 1989. 102. P.428.

[18] Krauss A. et al. Low-energy fusion cross sections of D + D and D + 3He reactions // Nucl. Phys. A 1987. 465. P.150.

[19] Greene S.L. Maxwell averaged cross sections for some thermonuclear reactions on light isotopes // UCRL-70522. 67.
[20] Brown R.E., Jarmie N. Differential cross sections at low energies for 2H(d,p)3H and 2H(d,n)3He // Phys. Rev. C 1990. 41. P.1391.
[21] Aliotta M. et al. Electron screening effect in the reactions 3He(d,p)4He and d(3He,p)4He // Nucl. Phys. A 2001. 690. P.790.
[22] Stewart L., Hal G.M. T(d,n)He-4 and T(t,2n) cross sections at low energies // LA-5828-MS. 1975.
[23] Jing Zhou et al. Measurement of the astrophysical S-factor for the low energy 2H(d,γ)4He reaction // Chin. Phys. C 2009. 33. P.350.
[24] Buss W. et al. Deuteron capture in 3He // Nucl. Phys. A 1968. 112. P.47.
[25] Penionzhkevich Yu.E. Exotic nuclei in astrophysics // Phys. Part. Nucl. 2012. 43. P.452.
[26] Table of Isotopic Masses and Natural Abundances. 1999; https://www.ncsu.edu/ncsu/pams/chem/msf/pdf/IsotopicMass_NaturalAbundance.pdf
[27] Purcell J.E. et al. Energy levels of light nuclei A = 3 // Nucl. Phys. A 2010. 848. P.1.
[28] Eisenberg J.M., Greiner W. Excitation mechanisms of the nucleus. Amsterdam: North Holland. 1976. 421p.
[29] Caughlan G.R., Fowler W.A. Thermonuclear reaction rates V // Atom. Dat. & Nucl. Dat. Tab. 1988. 40. P.283.
[30] Serpico P.D. et al. Nuclear reaction network for primordial nucleosynthesis: a detailed analysis of rates, uncertainties and light nuclei yields // Journal of Cosmology and Astroparticle Physics (JCAP) 2004. 12. P.010.
[31] Bertulani C.A., Kajino T. Frontiers in nuclear astrophysics // Prog. Part. Nucl. Phys. 2016. 89. P.56.
[32] Fowler W.A., Caughlan G.R., Zimmerman B.A. Thermonuclear Reaction Rates, II // Annu. Rev. Astron. Astrophys (ARA&A) 1975. 13. P.69.
[33] Harris M.J., Fowler W.A., Caughlan G.R., Zimmerman B.A. Thermonuclear Reaction Rates, III // Annu. Rev. Astron. Astrophys (ARA&A) 1983. 21. P.165.
[34] Caughlan G.R., Fowler W.A., Harris M.J., Zimmerman B.A. Tables of thermonuclear reaction rates for low-mass nuclei ($1 \le Z \le 14$) // Atom. Dat. & Nucl. Dat. Tab. 32 197 (1985).
[35] Dubovichenko S.B. Thermonuclear processes in Stars and Universe. Second English edition, revised and expanded. Germany, Saarbrucken: Scholar's Press. 2015. 332p.; https://www.scholars-press.com/catalog/details/store/gb/book/978-3-639-76478-9/Thermonuclear-processes-in-stars
[36] Dubovichenko S.B., Dzhazairov-Kakhramanov A.V. Astrophysical S-factor of the radiative p2H capture // Euro. Phys. Jour. 2009. V.A39. P.139-143.
[37] Dubovichenko S.B., Dzhazairov-Kakhramanov A.V. Radiative n7Li capture at Astrophysical Energies // Annalen der Physik 2012. V.524. P.850-861.
[38] Dubovichenko S.B., Dzhazairov-Kakhramanov A.V. Study of the nucleon radiative captures 8Li(n,γ)9Li, 9Be(p,γ)10B, 10Be(n,γ)11Be, 10B(p,γ)11C, and 16O(p,γ)17F at thermal and astrophysical energies // Int. J. Mod. Phys. E 2017. 26. 1630009(1-56).
[39] Dubovichenko S.B., Dzhazairov-Kakhramanov A.V. Radiative 10Be(n,γ)11Be capture at thermal and astrophysical energies // J. Phys. G 2016. V.43. P.095201(14pp.).
[40] Dubovichenko S.B., Dzhazairov-Kakhramanov A.V. 8Li(n,γ)9Li reaction at astrophysical energies and its role in primordial nucleosynthesis // Astrophys. Jour. 2016. V.819. №1. P.78(8p.).
[41] Dubovichenko S.B., Dzhazairov-Kakhramanov A.V., Burtebaev N., Alimov D. Radiative p14C capture at astrophysical energies // Mod. Phys. Lett. A 2014. V.29. 1450125(1-16).
[42] Dubovichenko S.B., Dzhazairov-Kakhramanov A.V. Neutron radiative capture by 10B, 11B and proton radiative capture by 11B, 14C and 15N at thermal and astrophysical energies // Int. J. Mod. Phys. E 2014. V.23. 1430012(1-55).
[43] Dubovichenko S.B. Photonuclear processes in the channels p3H and n3He of the 4He nucleus in potential cluster models // Phys. Atom. Nucl. 1995. V.58. P.1295-1302.
[44] Neudatchin V.G., Sakharuk A.A., Dubovitchenko S.B. Photodisintegration of 4He and the supermultiplet potential model of cluster-cluster interactions // Few-Body Systems 1995. V.18. P.159-172.
[45] Neudatchin V.G. et al. Generalized potential model description of mutual scattering of the lightest p2H, 2H3He nuclei and the corresponding photonuclear reactions // Phys. Rev. C 1992. V.45. P.1512-1527.
[46] Angulo C. et al. A compilation of charged-particle induced thermonuclear reaction rates // Nucl. Phys. A 1999. V.656. P.3-183.
[47] Adelberger E.G. et al. Solar fusion cross sections. II. The pp chain and CNO cycles // Rev. Mod. Phys. 2011. V.83. P.195-245.
[48] Gibson B.F. Electromagnetic disintegration of the A = 3 and A = 4 nuclei // Nucl. Phys. A 1981. V.353. P. 85-98.
[49] Perry J.E., Bame S.J. 3H(p,γ)4He reaction // Phys. Rev. 1955. V.99. P. 1368-1375.
[50] Arkatov Yu.M. et al. Study of the reaction 4He(γ,p)3H at maximum energy of gamma radiation 120 MeV // Sov. J. Nucl. Phys. 1970. V.12. P.227-233.
[51] Balestra F. et al. Photodisintegration of 4He in Giant-Resonance Region // Nuovo Cim. A 1977. V.38. P.145-166.
[52] Meyerhof W. et al. 3He(p,γ)4He reaction from 3 to 18 MeV // Nucl. Phys. A 1970. V.148. P. 211-224.
[53] Feldman G. et al. 3H(p,γ)4He reaction and the (γ,p)/(γ,n) ratio in 4He // Phys. Rev. C 1990. V.42. P.R1167- R1170.

N E W S
OF THE NATIONAL ACADEMY OF SCIENCES OF THE REPUBLIC OF KAZAKHSTAN
PHYSICO-MATHEMATICAL SERIES
ISSN 1991-346X **https://doi.org/10.32014/2019.2518-1726.21**
Volume 3, Number 325 (2019), 32 – 37

UDC 524.54

L.N. Kondratyeva, E.K. Denissyuk, I.V. Reva, M.A. Krugov

Fesenkov Astrophysical Institute, Almaty, Kazakhstan
lu_kondr@mail.ru, eddenis@mail.ru, alfekka@list.ru, mkrugov@astroclub.kz

SPECTRAL AND PHOTOMETRIC STUDY OF THE OBJECT IRAS20462 + 3416

Abstract. RAS20462 + 3416 belongs to low-mass post-AGB stars with a dense compact envelope, which was formed in the process of the mass loss by the star at the end of the pulsating AGB phase. The spectrum of the object consists of the HI, [NII], [SII] emission lines and of HeI, which is mainly observed in absorbtion.

The temperature of the central star corresponds to the value Teff = 19500 ± 500K, the electron density is 10^4 cm^{-3}. Several episodes of gas ejection from the atmosphere of the central star were recorded. So, in 1993 - 1994, PCygni profiles appeared in the UV and optical spectral lines. The stellar wind velocity was ~ 800 - 990 km/s. The photometric variability of the object was noted by many authors. In particular, quasi-periodic oscillations of brightness in the optical range with an amplitude of $0.^m1$ - $0.^m2$ and a period of ~ 4 days were detected. Rapid fluctuations in brightness can be caused by stellar pulsations and continuing mass loss.

In this paper, we present new spectral and photometric data obtained mainly in 2015–2018. Irregular brightness variations were detected in B, V, and R filters with an amplitude of ~ $0^m.4$. The results of spectral observations indicate a gradual increase in emission line fluxes. Thus, absolute fluxes in Hβ, Hα, [NII] lines increased by about 30 – 40%.

In terms of its physical parameters and the nature of the spectrum, the object is similar to a young planetary nebula of low excitation. However, the irregular variability of brightness and fluxes in emission lines, as well as the observed episodes of the matter ejection, indicate that the shell formation has not finishhed. Most likely this object can be considered as a protoplanetary nebula.

Key words: protoplanetary nebulae, emission lines; B V R values; individual: IRAS20462 + 3416.

Introduction The object IRAS20462 + 3416 = LSII + 34 26 = V1853 Cyg belongs to the low massive post-AGB stars with a dense compact envelope of gas and dust [1, 2]. The envelope was formed in the process of mass loss by the star at the end of the pulsating AGB phase. According to the radio observations [3], the image of the nebula in the Brγ line has dimensions 2.0″ x 1.5", with the 49º position angle. The object is located at a distance of 2.9 - 4.6 kpc [4]. The emission lines of HI, [NII], and [SII] are observed on the background of the continuum. HeI lines are mainly observed in absorption. In addition, numerous metal absorption lines have been recorded. The temperature of the central star according to the observations of 1991 corresponds to the value Teff = 19500 ± 500K [2]. The variability of the intensities and profiles of emission lines is noted. So, in the early spectrograms of 1977 and 1981, only a weak Hβ emission line was observed, while Hγ and Hδ were in absorption. Optical observations of the object in 1991-1995 showed the presence of strong Balmer emission and the weaker forbidden lines. The electron density calculated from the ratio of the intensities of the lines [SII], 6717, 6731Å is 10^4 cm^{-3}. The presence of SiII, CII, FeII emission lines in the spectrum of the object indicates that there is an internal zone which is located near the central star and has the even higher density. During the observation of the object, several episodes of gas ejection from the atmosphere of the central star were recorded. So, in 1993 - 1994, PCygni profiles appeared in the UV and optical spectral lines. The stellar wind velocity about 800 - 990 km/s was determined from the SiIV, 1400 Å and C IV, 1550Å line profiles,. Observations on September

1997 showed the presence of the PCygni profile in the optical and UV lines, and the broad wings of the Hα line [5]. On the IRAS 20462 + 3416 spectrograms (June 4, 2003) the blue wing in the Hα profile is weaker than the red — a sign of P Cygni with absorption filled with emission, since the wings are very wide [6].

The photometric variability of an object is noted by many authors. Thus, quasi-periodic brightness variations in the optical range with amplitude of $0.^m1$ - $0.^m2$ and a period of ~ 4 days were detected [7]. Information on rapid brightness fluctuations with an amplitude of $0.^m3$ in filters B and V is given in [8]. They may be due to stellar pulsations and ongoing mass loss.

Observations and processing

The first spectral observations of the object IRAS20462 + 3416 in the Fesenkov Astrophysical Institute were carried out in 2006-2007. Those spectra contained only the Balmer hydrogen lines. That time an absolute calibration of the spectra was not carried out, only equivalent widths of emission lines and the shape of profiles were obtained. Later, in 2015–2018 spectral and photometric observations of the object were performed. The star HD 198183 with a known energy distribution [9] was used as a standard for the absolute calibration of the spectra.

Photometric observations of the object were carried out with the telescope AZT-8, the 1-meter telescope at the Assy-Turgen Observatory, and the 1-meter telescope at the Tian Shan Observatory (TSHAO). The following CCDs: SBIG ST-8 (1530x1020, 9μ) (AZT-8), SBIG ST-7 (756x510, 9μ) (Assy-Turgen), Alta F16M (4096x4096, 9μ) of Apogee (TShAO) and a set of Johnson B V R filters were used.

The initial processing of an image consists of standard operations using the Bias, Dark and Flat service files. Image measurements are performed using the standard software packages MaximDl 6 and IRAF. Correction for atmospheric extinction and transformation of the obtained brightness to the standard system B V R is carried out using a system of corresponding equations.

Spectral observations were carried out using diffraction spectrographs mounted on the already mentioned telescopes. The following CCD: ST-8 (1530x1020, 9μ) and SBIG STT-3200 (2184x1472, 6.8μ) were used. The spectral range available for observations is ~ 3500Å (4000Å -7500Å).

Recent years, additional spectral observations were carried out on a 1-meter telescope installed at the Tian Shan Observatory. The telescope is equipped with a new diffraction spectrograph. At the output of the spectrograph, SBIG STT-3200 (2184x1472, 6.8μ) is installed.

During observations, the spectrograms of an object with a narrow (2"- 3") and a wide (7"- 10") entrance slit are obtained. Observations of a standard star with a known energy distribution are performed with a wide slit, which guarantees the pass and registration of the full radiation flux. File processing consists of subtracting the dark background, taking into account field errors and taking into account atmospheric absorption.

The spectral sensitivity of the equipment is determined by comparing the observed energy distribution in the standard spectrum with the Catalog data. After taking into account all corrections, the values of fluxes are determined in absolute energy units. Spectrograms obtained with a narrow slit and with a resolution of 0.25 - 0.5Å/pc are used to study the structure of emission profiles. Log of observations of IRAS20462+3416 is presented in Table 1.

Obtained results

The data obtained from photometric observations are given in Table 2 and in Figure 1. Rapid brightness fluctuations with amplitudes of $0.^m4$, $0.^m1$ and $0.^m1$ were recorded in 2016, in B V R filters, respectively.

The overall picture of the behavior of the object brightness is as follows: at first, its decrease was observed in all three filters, the minimum was in the middle of 2017. Then the reverse process began, and by mid-2018 the brightness increased by about $0.^m15$ (Figure 1).

Table 1 – Log of observations of IRAS20462+3416

Date of observations	Type of observations	Wavelength range (Å)	Spectral resolution	Telescope, Observatory
10.10.2007	Spectral	4400 - 5100 6100 - 6800	9800 13000	1-м. Assy-Turgen
18.07.2015	Spectral Spectral Photometric	4400 - 5100 6100 – 6800 B V R	9800 13000	1-м. Assy-Turgen
12.08.2015	Spectral Spectral Photometric	4400 - 5100 6100 – 6800 B V R	9800 13000	1-м. Assy-Turgen
01.08.2016	Spectral Photometric	6100 – 6800 B V R	13000	1-м. Assy-Turgen
03.08.2016	Photometric	B V R		1-м. Assy-Turgen
06.08.2016	Spectral Photometric	4400-5100 B V R	9800	1-м. Assy-Turgen
26.06.2017	Spectral	4400 -5100 6100 - 6800	9800 13000	1-м. Assy-Turgen
21.07.2017	Spectral	4400 - 5100 6100 - 6800	9800 13000	1-м. Assy-Turgen
15.09.2017	Spectral	6100 - 6800	13000	1-м. TShAO
19.09.2017	Spectral	6100 - 7100	9000	0.7м. AZT-8
22.06.2018	Spectral	4400 - 5100	7500	0.7м. AZT-8
09.07.2018	Photometric	B V R		1-м. TShAO
18.07.2018	Spectral	4400 - 5100	7500	0.7м. AZT-8

Table 2 - B V R magitudes of the object IRAS20462+3416

Date of observations	JD-2400000	B mag	V mag	R mag
18.07.2015	57222.330	11.28±0.01	11.07±0.01	11.02±0.01
12.08.2015	57247.268	11.26±0.05	11.10±0.04	10.97±0.04
01.08.2016	57602.306	11.39±0.01	11.20±0.01	11.14±0.02
03.08.2016	57604.267	11.80±0.06	11.15±0.05	11.13±0.04
06.08.2016	57607.278	11.53±0.01	11.25±0.01	11.04±0.03
21.07.2017	58048.348	11.46±0.01	11.29±0.01	11.23±0.01
09.07.2018	58309.330	11.38±0.01	11.09±0.01	11.14±0.01

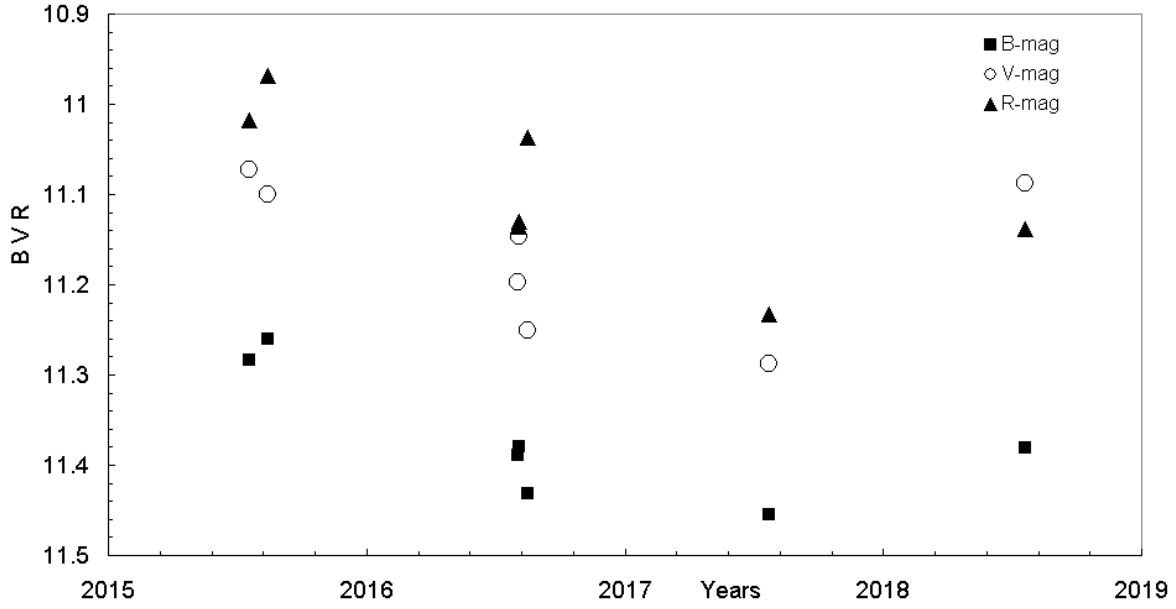

Figure 1 –Change of brightness of the object IRAS20462+3416 in 2015 – 2018

Only emission lines Hβ, Hα, [NII],6548,6583Å and HeI, 4921,6678Å in absorption are registered on our spectrograms. Absolute fluxes and equivalent widths of lines are given in Table 3. The figure 2 illustrates the behavior of radiation fluxes in hydrogen lines. The results of spectral observations indicate a gradual increase of emission line fluxes during 2015-2018 (Fig 2). A similar trend is observed in the behavior of the forbidden lines [NII], 6548, 6583Å.

Table 3 – Characteristics of emission lines in spectrum of IRAS20462+3416

Date of observations	Hβ		Hα		[NII],6583	
	$F \cdot 10^{13}$	EW	$F \cdot 10^{12}$	EW	$F \cdot 10^{13}$	EW
11.09.2006		1.2±0.2				
12.10.2007		1.3±0.3		13±0.6		0.51±0.09
18.07.2015	2.66±0.07	0.9±0.3	1.45±0.15	6.9±0.3	0.98±0.15	0.43±0.06
12.08.2015	3.06±0.23	1.0±0.1	1.40±0.04	7.3±0.2	1.10±0.02	0.58±0.01
06.08.2016	3.34±0.28	1.2±0.1				
21.07.2017	3.84±0.27	1.4±0.1	1.57±0.01	9.7±0.7	1.00±0.19	0.63±0.18
15.09.2017			1.38±0.12	6.9±0.2	1.09±0.12	0.58±0.11
19.09.2017			1.75±0.11	8.0±0.2		
22.06.2018	4.04±0.16	1.5±0.1				
18.07.2018	3.78±0.31	1.2±0.1	1.45±0.07	7.2±0.3	0.98±0.21	0.49±006

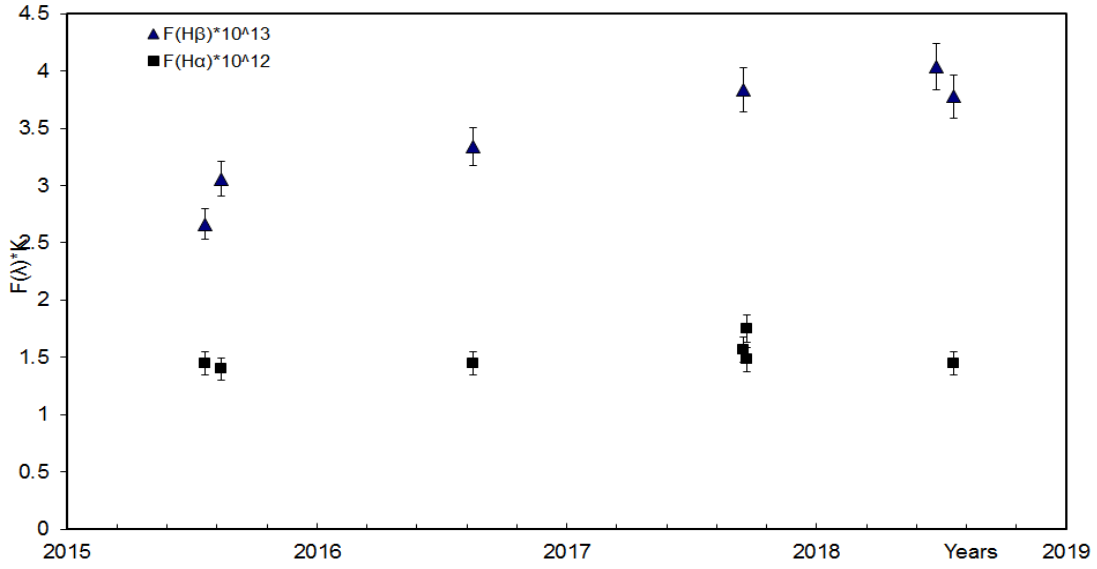

Figure 2 – Change of Hβ and Hα emission line fluxes

Due to its physical parameters:(Teff=19500K, Ne=10^4cm^{-3}) and the spectrum, the object is similar to a young low excitation planetary nebula. However, the irregular variability of brightness and emission fluxes, as well as the observed episodes of matter outflow, indicate that the shell formation was not finished, and the object is now in a transitional stage from post-AGB stars to planetary nebulae. Most likely, it can be considered as a protoplanetary nebula.

The work was carried out within the framework of Project No. BR05236322, financed by the Ministry of Education and Science of the Republic of Kazakhstan.

УДК 524.54

Л.Н. Кондратьева,Э.К. Денисюк, И.В. Рева, М.А. Кругов

«В.Г.Фесенков атындағы Астрофизика институты» ЕЖШС, Алматы, Қазақстан

IRAS20462+3416 ОБЪЕКТІСІНЕ СПЕКТРЛІК ЖӘНЕ ФОТОМЕТРЛІК ЗЕРТТЕУЛЕР

Аннотация. IRAS20462 + 3416 объектісі, лүпілдеу кезеңінің соңында масса жоғалту нәтижесінде қалыптасқан, тығыз, шағын қабықшалы post-AGB аз массивті жұлдыздарға жатады. Объектінің спектрінде HI, [NII], [SII] және HeI эмиссиялық сызықтары көбіне жұтылу кезінде байқалады. Орталық жұлдыздың температурасы Teff = 19500 ± 500К шамаға сәйкес, электрондық тығыздық 10^4см$^{-3}$ құрайды.

Орталық жұлдыз атмосферасынан газ бөлшектер жарқылының бірнеше эпизодттары тіркелді. 1993-1994 жылдарда УК профилінде және оптикалық сызықтарда Pcygni құраушылары пайда болды. Жұлдыздық желдің сәйкес мәні ~ 800 - 990 км/сек құрайды.

Көптеген авторлар объектінің фотометрлік айнымалылығы туралы атап өтті. Соның ішінде, периоды ~ 4 күн болатын және $0.^m1$ - $0.^m2$ амплитудалы жарқырауының квазипериодты тербелісі тіркелді. Объектінің жылдам өзгеруі зат ағынының жалғасуы және жұлдысдық лүпүлмен байланысты болуы мүмкін.

Бұл жұмыста 2015-2018 жылдар аралығында алынған спектрлік және фотометрлік жаңа бақылаулар келтірілген. Амплитудасы ~0^m.4 болатын, B, V және R фильтрларында дұрыс емес жарқырау тербелістері табылды. Спектрлік бақылаулар кезінде эмиссиялық сызықтардың сәулеленуінің біртіндеп өсуі байқалады. Біздің бақылаулар кезінде Hβ, Hα, [NII] эмиссиялық сызықтардағы сәулеленудің абсолюттік ағыны шамамен 20-40 % артты.

Спектрлік және физикалық сипаттамалары бойынша IRAS20462+3416 объектісі белсенді емес жас планеталық тұмандыққа тән. Эмиссиялық сызықтардағы жарқырау ағыны және жарқырау айнымалылығының дұрыс еместігі қабықшаның қалыптасуының жалғасуын көрсетеді. Мүмкін, бұл объектіні протопланеталық тұмандыққа жатқызуға болады.

Түйін сөздер: планеталық тұмандықтар, эмиссиялық сызықтар, ионды сызықтар, жеке объектілер: IRAS20462+3416.

УДК 524.54

Л.Н. Кондратьева, Э.К. Денисюк, И.В. Рева, М.А. Кругов

Астрофизический Институт им Фесенкова, Алматы, Казахстан

СПЕКТРАЛЬНЫЕ И ФОТОМЕТРИЧЕСКИЕ ИССЛЕДОВАНИЯ ОБЪЕКТА IRAS20462+3416

Аннотация. Объект IRAS20462 + 3416 относится к маломассивным post-AGB звездам с плотной компактной оболочкой, которая сформировалась, благодаря процессам потери массы в конце пульсационной стадии. В спектре объекта представлены эмиссионные линии HI, [NII], [SII] и линии HeI, которые в основном наблюдаются в поглощении.

Температура центральной звезды соответствует значению Teff = 19500 ± 500К, электронная плотность составляет 10^4см$^{-3}$.

Зарегистрировано несколько эпизодов выброса фрагментов газа из атмосферы центральной звезды. Так, в 1993 – 1994гг в профилях УФ и оптических линий появились Pcygni компоненты. Соответствующее значение звездного ветра составляет ~ 800 - 990 км/сек.

Фотометрическая переменность объекта отмечена многими авторами. В частности, были зафиксированы квазипериодические колебания блеска с амплитудой $0.^m1$ - $0.^m2$ и периодом ~ 4 дней. Быстрые флуктуации блеска объекта могут быть вызваны звездными пульсациями и продолжающимся истечением вещества.

В данной работе приводятся новые спектральные и фотометрические данные, полученные, в основном, в 2015 – 2018 гг. Обнаружены нерегулярные колебания блеска в B, V и R фильтрах с амплитудой ~0^m.4. В процессе спектральных наблюдений выявлено постепенное усиление излучения в эмиссионных линиях. Так, абсолютные потоки излучения в эмиссионных линиях Hβ, Hα, [NII] увеличились примерно на 20 – 40%.

По своим физическим и спектральным характеристикам объект IRAS20462 + 3416 похож на молодую планетарную туманность низкого возбуждения. Однако нерегулярная переменность блеска и потоков излучения в эмиссионных линиях, так же как и выбросы материи, указывают на то, что формирование оболочки продолжается. Вероятнее всего, данный объект можно классифицировать, как протопланетарную туманность.

Ключевые слова: протопланетарные туманности, эмиссионные линии; B V R величины; индивидуальные объекты: IRAS20462+3416

Information about authors:
Kondratyeva L.N. - Doctor of Physical and Mathematical Sciences, Fesenkov Astrophysical Institute. lu_kondr@mail.ru;
Denissyuk E.K. - Doctor of Physical and Mathematical Sciences, Fesenkov Astrophysical Institute. eddenis@mail.ru;
Reva I.V. – Junior resecher, Fesenkov Astrophysical Institute. alfekka@list.ru;
Krugov M.A. - Engineer , Fesenkov Astrophysical Institute. mkrugov@astroclub.kz

REFERENCES

[1] Parthasarathy M. Post-Asymptotic-Giant-Branch Supergiants //ASPC. 1993. V 60. P. 265. [2] Garcia-Lario P., Parthasarathy M., de Martino D., et al. A multiwavelength study of LS II+34026: a hot post-AGB star in the process of becoming a planetary nebula// A&A. 1997. V. 326. P.1103.

[3] Gledhill T., Forde K., Imaging the transition between pre-planetary and planetary nebulae: Integral Field Spectroscopy of hot post-AGB stars with NIFS// MNRAS. 2015. V.447. P.1080.

[4] Parthasarathy M. LS II +34 deg 26 is a low-mass post-asymptotic giant branch B supergiant and not a massive Population I B star located near the outer edge of the galaxy// ApJ. 1993. V. 414. P. L 109.

[5] Arrieta A., Torres-Peimbert S. Broad Ha wings in nebulae around evolved stars and in young planetary nebulae// ApJS. 2003. V. 147. - P.97.

[6] Contreras S. C., Sahai R., Gil de Pas A., et al. Echelle long-slit optical spectroscopy of evolved stars// ApJS. 2008. V.179. P.166.

[7] Turner D., Drilling J. LSII + 34 deg 26, an unusual B supergiant located near the outer edge of the galaxy// PASP. 1984. V.96. - P.292.

[8] Arkhipova V., Ikonnikova N., Noskova R Photometric variability and spectral features of the preplanetary nebula LSII+34 26==V1853Cyg.// Astron Letters. 2001. V. 27. – P. 719.

[9] Kharitonov A.V., Tereschenko V.M., Knyazeva L.N. Spectrophotometric Catalog of stars. Almaty. 1988.

N E W S
OF THE NATIONAL ACADEMY OF SCIENCES OF THE REPUBLIC OF KAZAKHSTAN
PHYSICO-MATHEMATICAL SERIES
ISSN 1991-346X **https://doi.org/10.32014/2019.2518-1726.22**
Volume 3, Number 325 (2019), 38 – 41

UDK 524.386

L.A. Pavlova

Fesenkov Astrophysical Institute, Almaty, Kazakhstan
lapavlova44@mail.ru

FEATURES OF X-RAY RADIATION IN SYMBIOTIC STARS

Abstract. Modern observations of X-ray radiation from individual symbiotic stars are given to clarify their nature. Thus, the spectral features in a wide range of X-rays, optical and ultraviolet, and the rapid UV variability found in SU Lyn are consistent with the assumption that this is a symbiotic star with an accreting white dwarf. RT Cru is a prototype of symbiotics without burning shell on a dwarf with a hard type of x-ray radiation, providing an idea of the most internal structures of accretion. The X-ray type of radiation from the symbiotic star V1329 Cyg indicates that some of the high-energy radiation may occur as a result of strikes in the jet and beyond the symbiotic nebula. In the symbiotic recurrent new T CrB, a sharp increase in the rate at which the material reaches the innermost part of the accretion disk, that is, the boundary layer, is found, this can dramatically change its structure. X-ray satellite Suzaku investigated symbiotics in which X-rays exceed 10 keV (T CrB, CH Cyg, V648 Car). Suzaku CD-28 3719, Hen 3-1591, Hen 3-461, EG And and 4 Dra were observed, in which the models are compatible with X-rays emitted in the boundary layer between the accretion disk and the white dwarf. This paper discusses the various observable properties of individual symbiotic stars on space telescopes to identify common features that can explain the nature of symbiotic stars.

Keywords: symbiotic stars, the nature of X-ray radiation.

Introduction Spectral observations of symbiotic stars in optics have shown a complex spectrum, which is associated with duality. The hot compact component (usually a white dwarf, WD) contributes to the blue UV region of the spectrum, while the cold red giant dominates the spectrum on longer waves. Optical, infrared and ultraviolet spectral regions are rich in radiation lines from forbidden and allowed transitions, which arise mainly as a result of photoionization and recombination of a nebular plasma heated by a hot component. Radio, optical and X-ray observations show jets with velocities from several hundred to 1000 km / s and the thermal radiation from the red giant's ionized wind can even generate γ rays during eruptions. This paper discusses the various observable properties of individual symbiotic stars in the x-ray range, obtained by space telescopes, to identify common features that can explain the nature of X-ray radiation from symbiotic stars.

The results of modern observations on space telescopes

Observations from space telescopes XMM-Newton, Swift / XRT, Suzaku and others have made it possible to detect new sources of X-ray radiation in symbiotic stars. X-ray spectra with energies above 2 keV, obtained using Swift / XRT, are consistent with thermal radiation and are divided into three different groups. They allow us to understand the place of the formation of X-ray radiation: 1 group-associated with the boundary layer of the accretion disk. 2- consists of sources with a single, soft X-ray spectral component, which is associated with the region of collision of winds, 3- consists of sources with hard and soft X-ray spectral components, which exhibit UV-blink, which is a common property of symbiotic stars. The physical interpretation of the two spectral components of x-ray radiation and simultaneous ultraviolet photometry of Swift show that symbiotic stars with more intense x-rays tend to have more UV flicker, which is usually associated with disk accretion. [1]

Studies on symbiotic stars usually rely on low-resolution optical spectroscopy. Observations from Swift and ground-based optical spectroscopy made it possible to detect a hard x-ray source 4PBC J0642.9 + 5528, which was identified with the poorly studied red giant SU Lyn. The X-ray spectra, from optical to

ultraviolet, and the fast UV variability of SU Lyn are in good agreement with the assumption that this is a symbiotic star containing an accreting white dwarf. The symbiotic nature of SU Lyn has so far remained unnoticed, since it did not detect strong emission lines in low-resolution spectra. Mukai et al. (2016) discovered that the red giant SU Lyn is the optical analog of a hard, thermal x-ray source and that it is a symbiotic containing an accreting white dwarf. [2] Its properties, including excess in UV, compared with non-interacting red giants and variability in the optical lines of the Balmer series, [NeIII] and Ca II, are consistent with the accretion onto a white dwarf without burning the shell. In general, observations confirmed that, in the X-ray range, optically thin plasma dominates in emission, which can be hot 2 × 108 K (kT 17 keV) and reach a maximum at 3 × 108 K with the assumption of cooling flux in the model. An analysis of the hard X-ray radiation properties of the SU Lyn allowed us to identify strong and variable internal X-ray absorption with rapid variability, suggesting that the absorber is located next to the accreting white dwarf. [3]

Luna G.J.M. et.al. [4] showed that the RT Cru object is a prototype of symbiotics without burning the shell on a dwarf; its hard type of X-ray radiation gives an idea of its most internal accretion structures. Over the past 20 years, RT Cru has experienced two similar events of increasing brightness, separated by an interval of 4000 days and with an amplitude of ΔV = 1.5 mag. Swift detected an increase in X-ray brightness, near the second optical peak. Spectral and temporal analysis of multiwave observations indicate that accretion continues through a disk that reaches the surface of a white dwarf. Moreover, the similarity of ultraviolet and x-ray fluxes indicate that the boundary layer of the accretion disk remained optically thin with respect to its own radiation during the increase in brightness when the accretion rate on WD increased to 6.7 × 10 -9 Mo / yr. [4]

Among symbiotics, there are also white dwarfs with quasi-stable burning of the shell on their surface, although the origin of this burning is not yet clear. Probably in slow symbiotic, it is associated with past thermonuclear release. So in June 2015, the symbiotic slow new AG Peg was seen only in its second optical flash since 1850. This recent outbreak had a much shorter duration and lower amplitude than the previous outburst, and it contained multiple peaks — similar outbreaks were seen in classic symbiotic stars such as Z And. Between June 2015 and January 2016, fast Peg X-ray and UV observations were obtained. The X-ray flux was noticeably altered in time scale, especially during the four days near the optical maximum, when the X-rays became bright and soft. This strong X-ray variability continued for another month, after which the X-rays became hard when the optical flux decreased. The UV flux was high throughout the flash, which is consistent with the quasistationary burning of the shell on a white dwarf. Considering that accretion disks around white dwarfs with shell burning usually do not produce noticeable X-rays (due to Compton-cooling of the boundary layer), X-rays are likely to have originated from blows in the emissions. Since the photoelectric absorption of x-rays has not changed significantly, the variability of x-rays can be directly attributed to the properties of the discarded material. This is how AG Peg transitioned from a slow symbiotic one (which supplanted the outbreak of 1850) to the classic symbiotic star. [5]

In another case, the X-rays of the symbiotic star V1329 Cyg detected with XMM-Newton showed a spectrum consisting of plasma with two temperature peaks: kT = 0.11 keV and kT = 0.93 keV. The impact velocities corresponding to the observed temperatures are about 300 km / s and about 900 km / s. No periodic or aperiodic X-ray variations were detected; the upper limits of the amplitudes of such changes were 46% and 16%, respectively (rms value). The nature of the soft component of the X-ray spectrum suggests that some of the high-energy radiation may occur as a result of impacts in the jet and outside the symbiotic nebula. Lower speed in HST observations corresponds to the speed of the expanding structure. Higher velocity may be associated with an internal impact at the base of the jet or with impacts in the area of accretion. [6]

According to the work of Luna G.J.M. et.al. [7] The symbiotic recurrent new T CrB showed a sharp increase in the rate at which the material reaches the innermost part of the accretion disk, i.e., the boundary layer, which can drastically change its structure. From data analysis from X-ray, ultraviolet and optical telescopes and the American Association of Variable Star Observers (AAVSO) in the V and B-bands, it was found that during the optical set, which began in early 2014 (Δ V≈ 1.5): 1 - hard X-rays, as seen from BAT, almost disappeared; 2- XRT X-ray flux decreased significantly, while the optical flux remained high; 3- The UV flux increased 40 times the dormancy value; and 4-x-ray spectrum has become

much softer, and a bright, new, blackish component has appeared. Probably, the optical brightness event, similar to the one observed approximately 8 years before the most recent thermonuclear flash in 1946, is associated with disk instability. [7]

X-rays from five symbiotic stars observed from the Suzaku satellite were recorded. These objects were selected for deeper observations after their first detection using ROSAT and Swift. It turned out that X-ray spectra can be adequately adapted to the absorbed optically thin different thermal plasma models. Such models are compatible with X-rays in the innermost area of the accretion disk, that is, in the boundary layer. Based on the large amplitude of blinking (only detected in 4 Da), high plasma temperature and previous measurements of UV variability and brightness, it was assumed that all five sources are accretion-active due to the optically thick boundary layer. Considering the time interval between the previous and these observations, the long-term variability of X-ray was studied and it was found that its own X-ray flux and intermediate absorption column may vary depending on three or more factors. However, the location of the source of absorption and how changes in the rate of accretion and absorption are still elusive are still elusive. [8]

Currently, symbiotics are recognized as objects with X-rays. Of the 220 known systems, 45 were detected on X-ray waves, most of them with radiation in the range 0.3–10 keV. However, some of them were detected at energies up to 100 keV. X-ray satellite Suzaku investigated symbiotics in which X-rays exceed 10 keV (T CrB, CH Cyg, V648 Car). Suzaku CD-28 3719, Hen 3-1591, Hen 3-461, EG And and 4 Dra were observed with higher quality X-ray spectra. It was found that the X-ray spectra of all five sources can adequately correspond to the absorbed, optically thin thermal plasma models with a multi-temperature plasma. These models are compatible with X-rays that occur in the boundary layer between the accretion disk and the white dwarf. High plasma temperatures kT> 3 keV for all objects were higher than expected for headwinds. Based on these high temperatures, as well as on previous measurements of UV variability and UV brightness and on a large X-ray reflection amplitude, it was concluded that all five sources belong to objects with accretion, with mostly optically thick boundary layers. X-ray data allow us to observe only a small optically thin part of the radiation of these boundary layers. Considering the time between previous observations and observations, it was found that its own X-ray flux and intermediate absorbing medium can vary over three years or more. But the location of the absorber and the relationship between changes in the rate of accretion and absorption are still unknown. [9]

Conclusion

Thus, the region of formation of X-ray radiation at high plasma temperatures of about kT> 3 keV is most likely associated with the boundary layer between the accretion disk and the surface of the white dwarf, and a soft X-ray can form in the region of wind collision. X-ray spectra can be adequately adapted to the absorbed optically thin multi-temperature thermal plasma models. Such models can explain the formation of X-ray radiation in the innermost region of the accretion disk, that is, in the boundary layer. Sources with hard and soft X-ray spectral components, which are accompanied with UV blinking, are most likely associated with accretion into predominantly optically thick boundary layers.

The work is supported by the Targeted Financing Program № BR05336383 Aerospace Committee of the Ministry of Defense and Aerospace Industry of the RK.

УДК 524.386

Л.А. Павлова

«В.Г.Фесенков атындағы Астрофизика институты» ЕЖШС, Алматы, Қазақстан

СИМБИОТИКАЛЫҚ ЖҰЛДЫЗДАРДЫҢ РЕНТГЕН СӘУЛЕЛЕНУІНДЕГІ ЕРЕКШЕЛІГІ

Аннотация. Жеке симбиотикалық жұлдыздардың табиғатын түсіндіруге, X-ray сәулеленуінің заманауи бақылау мәліметтері келтірілген. SULyn объектісінің спектрлік ерекшеліктері кең диапазонды рентгеннен, оптикалық және ультракүлгін және тез УК-айнымалылық табылды, бұл симбиотикалық жұлдыз ақ ергежей RTCru мен аккрецияланады, ергежейде қатаң рентгенсәулеленуі, қабықшаның жануы болмайды, бұл дегеніміз аккрецияның түпкі ішкі құрылымына жалпы тұжырымдама береді. Симбиотикалық жұлдыз V1329

Cyg X-ray сәулеленуінің кейбір бөлігі жоғары энергиялы сәулеленудің болу себебін симбиотикалық тұмандықтан тыс ағын соққыларының нәтижесінде болуы сүмкін. TCrB реккурентті жаңа симбиотикалық жұлдызда жылдамдықтың кенеттен өсуі, шекаралық қабат яғни аккрециялық дисктің түпкі ішкі бөлігіне материяның жетуі оның құрылымының өзгерісіне әкеледі. Suzaku рентген серігі сәулеленуі 10 кэВ асатын (TCrB, CHCyg, V648 Car) симбиотикалық жұлдыздарды зерттеді. Шекаралық қабатта аккрециалық диск және ақ ергежейдің рентген сәулеленуінде модельдері сәйкес келетін SuzakuCD-28 3719, Hen 3-1591, Hen 3-461, EGAnd және 4 Dra объектілеріне бақылаулар жүргізілді. Бұл жұмыста, симбиотикалық жұлдыздардың табиғатын түсіндіруге ғарыштық телескоптар көмегімен бағыланған жеке симбиотикалық жұлдыздардың жалпы ұқсас жеке қасиеттерін табу болып табылады.

Түйін сөздер: симбиотикалық жұлдыздар, табиғат X-ray сәулелену.

УДК 524.386

Л.А. Павлова

Астрофизический Институт им Фесенкова, Алматы, Казахстан

ОСОБЕННОСТИ РЕНТГЕНОВСКОГО ИЗЛУЧЕНИЯ В СИМБИОТИЧЕСКИХ ЗВЕЗДАХ

Аннотация. Приведены современные данные наблюдений X-ray излучения отдельных симбиотических звезд для выяснения их природы. Так, спектральные особенности в широком диапазоне от рентгена, оптического и ультрафиолета и быстрая УФ-изменчивость, обнаруженная у SU Lyn, согласуются с предположением, что это симбиотическая звезда с аккрецирующим белым карликом. RT Cru является прототипом симбиотиков без горения оболочки на карлике с жестким типом рентгеновского излучения, обеспечивающим представление о самых внутренних структурах аккреции. Тип X-ray излучения симбиотической звезды V1329 Cyg показывает, что некоторая часть излучения высокой энергии может возникать в результате ударов в струе и за пределами симбиотической туманности. У симбиотической рекуррентная новой T CrB обнаружено резкое увеличение скорости, с которой материал достигает самой внутренней части аккреционного диска, т. е. пограничного слоя, это может резко изменить его структуру. Рентгеновский спутник Suzaku исследовал симбиотики, у которых рентгеновское излучение превышает 10 кэВ (T CrB, CH Cyg, V648 Car). Проведены наблюдения Suzaku CD-28 3719, Hen 3-1591, Hen 3-461, EG And и 4 Dra, у которых модели совместимы с рентгеновским излучением, возникающим *в пограничном слое между аккреционным диском и* белым карликом. В данной работе рассматриваются разнообразные наблюдаемые свойства отдельных симбиотических звезд на космических телескопах для выявления общих признаков, способных объяснить природу симбиотических звезд.

Ключевые слова: симбиотические звезды, природа X-ray излучения.

Information about author:
Pavlova L.A. - Doctor of Physical and Mathematical Sciences, Fesenkov Astrophysical Institute. lapavlova44@mail.ru.

REFERENCES

[1] Luna G.J.M., Sokoloski J.L., Mukai K., Nelson T. arXiv:1211.6082v3 A&A2013.V.559.p.6L DOI: 0.1051/0004-6361/201220792

[2] Mukai K, Luna G.J.M., Cusumano G., Segreto A.,et.al. arXiv:1604.08483v1 *MNRAS: Lett 2016.*, Vol.461, P.L1-L

[3] Raimundo Lopes de Oliveira , Sokoloski J., Luna G.L.M., Mukai K., Nelson T. arXiv:1807.04280v1)

[4] Luna G. J. M., Mukai K., Sokoloski J.l., A. B. Lucy A.B.et.al. arXiv:1801.02492v2 A&A.2018. 616, A53.

[5] Ramsay G., Sokoloski J.l., Luna G. J. M., Nuñez N.E., MNRAS 2016.V.461.P.3599-3606 DOI: 10.1093/mnras/stw1546

[6] M., Luna G.L.M., Sokoloski J.L. arXiv:1102.1976 v1 Ap.J.V.731.N1.P.12. DOI: 10.1088/0004-637X/731/1/12

[7] Luna G.J.M., Mukai K., Sokoloski J.L., Nelson T, et.al arXiv:1807.01304 A&A 619, A61 (2018). DOI: 10.1051/0004-6361/201833747

[8] Nuñez N.E., Nelson T., Mukai K., Sokoloski J.L., Luna G.L.M. arXiv:1505.00633v1

[9] Nuñez N.E., Nelson T., Mukai K., Sokoloski J.L., Luna G.L.M. arXiv:1604.05980v1 Ap.J.2016.V.824.N1

N E W S
OF THE NATIONAL ACADEMY OF SCIENCES OF THE REPUBLIC OF KAZAKHSTAN
PHYSICO-MATHEMATICAL SERIES
ISSN 1991-346X **https://doi.org/10.32014/2019.2518-1726.23**
Volume 3, Number 325 (2019), 42 – 55

UDC 524.31

V. M. Tereschenko

Fesenkov Astrophysical Institute

THE ESTIMATION OF THE RELIABILITY OF THE DATA FROM THE SHAMAKHA SPECTROPHOTOMETRIC CATALOGUE

Abstract. On the basis of existing spectrophotometric catalogues and individual articles we plan to create a joint uniform catalogue of stars with known distributions of energy in their spectra. As original catalogues we intend to use catalogues which were created in the Fesenkov astrophysical institute, Sternberg astronomical institute, Main astronomical observatory RAS, Odessa astronomical and Shamakha astrophysical observatories. At the preliminary stage of the proposed project, it is necessary to assess the reliability of the data of initial catalogues. The first three catalogues are already investigated in this respect. In this paper, we analyze the data of the Shamakha catalogue. The reliability of the data is estimated by indirect means – according to the similarity of magnitudes calculated from the energy distribution with the directly observed star magnitudes using the most accurate photometric WBVR-system. Calculations of the magnitudes and color-indexes are made using standard formulas for synthetic photometry. Then, the difference (residuals) between calculated and directly observed stellar magnitudes was computed. The results of calculations are presented in the table. On their basis the dependencies of residuals from the V- magnitudes and color-indexes were plotted. From them follows that noticeable systematic errors in Shamakha spectrophotometric catalogue are absent. However, there are a significant number of accidental residuals reaching 0.20^m and higher. The results of the calculations will be used for creating joint catalogue and for the selection of standard stars from it.

Key words: stars, energy distribution, Shamakha spectrophotometric catalogue, catalogue WBVR-magnitudes, comparison.

Introduction. Since the astronomical observations are performed on different instruments and at different conditions, they must be standardized. Standardization of spectrophotometric observations are carried out by binding the observations of the studied bodies to the B-G-stars with a known distribution of energy in their spectra. We intend to create the joint spectrophotometric catalogue, which covers all existing catalogues and articles in which the absolute energy distributions are represent. Similar catalogues were created previously as well, see, for example [1, 2]. The catalogue planned by us is similar to the compile catalogue [2], but is more complete. In addition, its data will be reduced in more common calibration of Vega - main spectrophotometric standard.

In the joint catalogue the stars will be marked that can be used for the purposes of standardization and calibration of receiving-recording equipment. At present, the most frequently used three spectrophotometric catalogues, which were created in FAI [3], SAI [4] and MAO RAS [5]. All three catalogues are detailed investigated. There are still three analogues catalogue, created in Odessa Astronomical Observatory [6,7] and Shamakha Astrophysical Observatory [8]. It is obvious that the joint catalogue will greatly facilitate users to find suitable standards.

The method of calculations. The present paper is a first step in creating the joint catalogue. It is devoted to the estimation of the reliability of the data of the Shamakha catalogue. Analysis carried out by indirect means, namely, by comparing the magnitudes and color-indexes calculated from the distribution of energy with directly observed indexes. Such comparison is necessary because the authors of Shamakha directory used as standards, in addition to the 8 primary standards, 20 other stars being zonal standards [9]. Accuracy of zonal standards is lower than primary. In addition, some of them are suspected of variability. Note that due to the lack of spectrophotometric data other authors' method of comparison with photometric data is used quite often. In this comparison, of course, information about errors and faults of

energy distribution in narrow spectral intervals is lost. Comparison with photometric data helps to identify only big errors in the spectral energy distribution of the stars under investigation. Such an analysis is made by the authors of Shamakha catalogue in the UBV-system. Photometric data were taken from the compile catalogue Nikolet [10]. The accuracy and homogeneity of the data of this catalogue is relatively low. We, however, took the most precision photometric catalogue WBVR-magnitudes [11]. Magnitude in band V and color-indexes W-B and B-V calculated with the next formulas [12]:

$$V = -2.5\ \lg\Sigma E(\lambda)\times S_V(\lambda)\times\Delta\lambda + C_V; \quad (1)$$

$$W\text{-}B = -2.5\ \lg\ [\Sigma E(\lambda)\times S_W(\lambda)\times\Delta\lambda] / [\Sigma\ E(\lambda)\times S_B(\lambda)\times\Delta\lambda] + C_{U\text{-}B}; \quad (2)$$

$$B\text{-}V = -2.5\ \lg\ [\Sigma E(\lambda)\times S_B(\lambda)\times\Delta\lambda] / [\Sigma\ E(\lambda)\times S_V(\lambda)\times\Delta\lambda] + C_{B\text{-}V}; \quad (3)$$

where $E(\lambda)$ - monochromatic illumination on wavelength λ; S_W, S_B and S_V - response curves photometric bands W, B and V; $\Delta\lambda$ - length averaging interval energy distribution curves, histogram step.

Reaction curves of the corresponding bands were taken from the directory [11]. Numerical values of the constants depend on the adopted zero-point scale of magnitudes, absolute calibration of primary standards and physical units. Note that in Shamakha catalogue the "old" Vega-calibration was used, which was obtained in FAI in 1968. [9]. The constants in equations (1-3) are defined using the star HD221525, which served as the primary standard in catalogues [3, 11]. For bands W, B and V they respectively amount to 1.285^m, 2.629^m and 2.039^m. Then residuals $\delta V = V_{cal} - V_{obs}$, $\delta(B\text{-}V) = (B\text{-}V)_{cal} - (B\text{-}V)_{obs}$ и $\delta(W\text{-}B) = (W\text{-}B)_{cal} - (W\text{-}B)_{obs}$ were calculated. The numeric values of the residuals are put into table (see annex).

Results and discussion. The table shows that for some stars the residuals reach 0.2^m or more, which is much larger than the errors of observation listed in the Shamakha catalogue. Large values of residuals can be explained both with variability of studied stars and with errors of observations. One of the reasons for significant differences can be used as primary standards for variable stars, or stars, for which the energy distribution in their spectra is erroneous. Each case requires special consideration. This was not intended in this work. For visualization of results our calculations the different dependencies for residuals were formed (figures 1-4). The graphs were constructed according to date for stars of first half of catalogue (number from 1 to 212). The stars with residuals > 0.30^m (in table they by asterisk marked) on graphs are not represent.

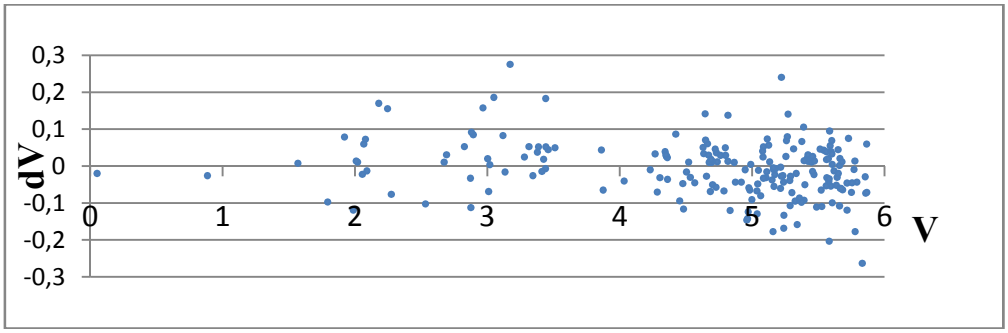

Figure 1 - The dependence of the residuals δV from magnitude V

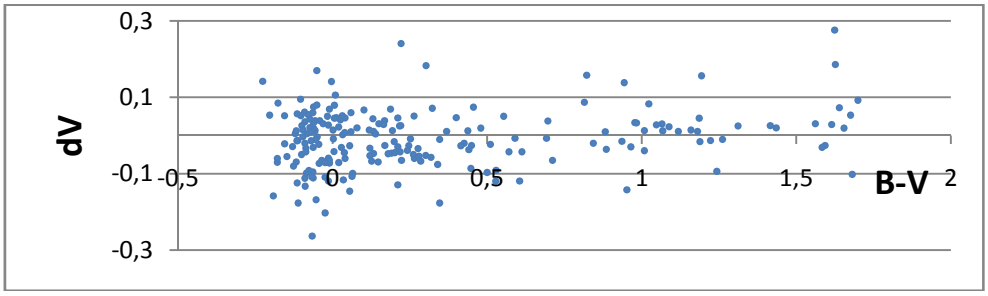

Figure 2 - The dependence of the residuals δV from color-indexes B-V

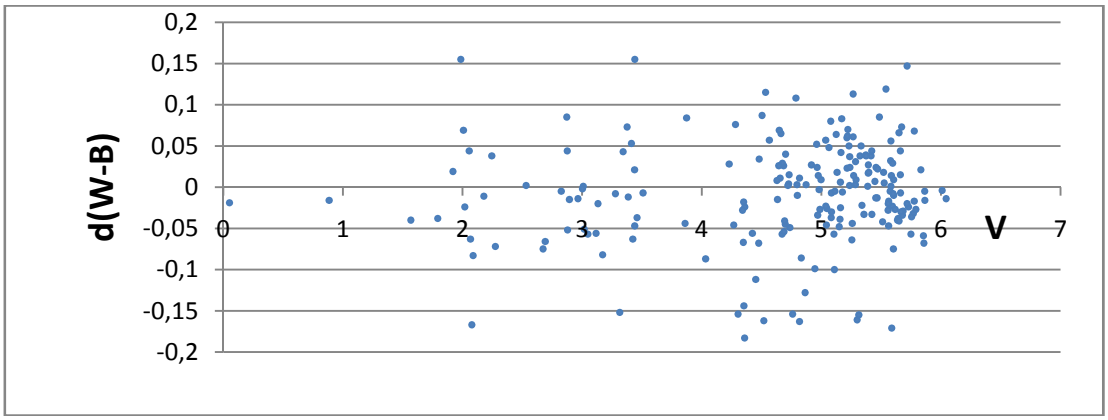

Figure 3 - The dependence of the residuals δ(W-B) from V

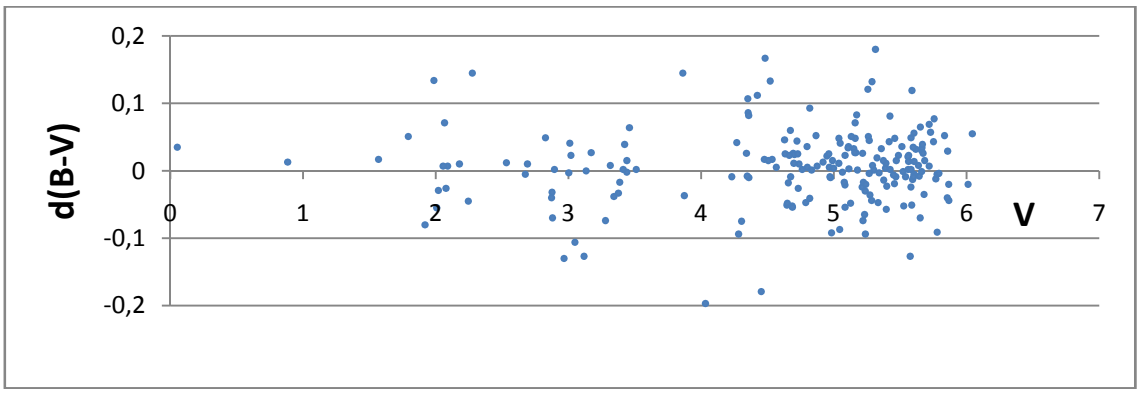

Figure 4 - The dependence of the residuals δ(B-V) from V

The results of our calculations might be used by other observers in case of choosing the spectrophotometric standards from Shamakha catalog. For the standardization of observations it is advisable to use standard stars with residuals less than 0.03^m-0.04^m.

Table 1 - The values V, (W-B) and (B-V) and residuals δV, δ (W-B) and δ (B-V)

№	HD	Sp	V	δV	W-B	δ(W-B)	B - V	δ(B-V)
1	3	7	4	5	6	7	8	9
1	144	B9IIIe	5.582	-0.203	-0.225	0.056	-0.024	0.049
2	358	B8IVp	2.067	0.060	-0.566	-0.063	-0.064	0.071
3	432	F2III-IV	2.275	-0.076	0.068	-0.072	0.34	0.145
4	560	B9Vn	5.541	0.043	-0.251	0.119	-0.074	-0.009
5	886	B2IV	2.826	0.053	-1.054	-0.005	-0.204	0.049
6	1976	B5IV	5.586	0.095	-0.735	0.014	-0.104	-0.051
7	2011	B9IIIe	5.388	0.106	-0.168	0.001	0.009	0.004
8	2054	B9IV	5.729	0.075	-0.380	-0.024	-0.062	0.057
9	2628	A7III	5.214	-0.060	0.071	0.060	0.264	-0.024
10	2772	B8Vn	4.731	0.036	-0.401	0.015	-0.09	-0.026
11	3240	B7III	5.085	0.052	-0.460	-0.007	-0.103	0.023
12	3546	G8IIIp	4.360	-0.036	0.295	-0.024	0.885	-0.010

13	3627	K3III	3.279	0.025	1.352	-0.008	1.311	-0.074
14	3712	K0IIIa	2.245	0.156	0.966	0.038	1.193	-0.045
15	4222	A2Vs	5.416	0.022	0.073	0.038	0.019	0.043
16	4382	B8III	5.422	0.013	-0.508	0.044	-0.057	0.081
17	4614	G0V+M	3.439	-0.007	-0.154	0.021	0.590	-0.002
18	4813	F7IV-V	5.171	-0.023	-0.154	0.083	0.510	0.083
19	5015	F8V	4.797	0.050	-0.082	0.003	0.553	0.036
20	5112	M0III	4.761	0.029	1.795	-0.154	1.614	0.002
21	5394	B0IVe	2.179	0.170	-1.315	-0.011	-0.051	0.010
22	5395	G8.5IIIb	4.634	0.034	0.481	-0.015	0.977	0.025
23	5408	B9IVn	5.563	0.018	-0.393	-0.047	-0.061	0.023
24	5848	A5V	3.861	0.044	0.152	-0.044	0.130	0.145
25	6186	K0IIIa	4.268	0.033	0.528	-0.046	0.983	0.042
26	6582	G5Vp	5.177	-0.007	-0.092	-0.006	0.692	0.001
27	6676	B8Vn	5.769	-0.009	-0.355	-0.032	0.002	-0.012
28	6805	K1.5III	3.46	0.045	1.040	-0.037	1.186	0.064
29	6860	M0IIIa	2.078	0.073	1.888	-0.167	1.639	-0.026
30	6960	B9.5V	5.564	-0.031	-0.151	-0.017	-0.063	0.014
31	6961	A7V	4.342	0.039	0.143	-0.028	0.168	0.026
32	6972	B9IV	5.576	0.020	-0.374	-0.005	0.079	-0.127
33	7034	F0V	5.161	-0.009	0.261	-0.025	0.252	0.071
34	7106	K0IIIb	4.520	0.011	0.845	-0.162	1.118	0.133
35	7318	K0III	4.672	0.030	0.680	-0.057	1.065	0.060
36	7439	F5V	5.150	-0.037	-0.168	-0.048	0.441	0.033
37	7927	F0Ia	4.982	-0.065	0.597	-0.003	0.711	-0.092
38	8374	A1m	5.594	-0.054	0.085	-0.023	0.279	-0.013
39	8491	K0III	4.737	0.012	0.777	-0.049	1.068	0.010
40	8538	A5III-IV	2.674	0.011	0.179	-0.075	0.132	-0.005
41	8890	F7Ib-IIv	1.986	-0.119	0.332	0.155	0.605	0.134
42	9408	G9IIIb	4.699	0.013	0.578	-0.045	1.008	0.011
43	10204	sgA9	5.643	-0.030	0.138	-0.038	0.211	-0.008
44	10221	A0pSi	5.560	0.039	-0.295	-0.020	-0.057	0.002
45	10425	B8IIIn	5.777	0.014	-0.381	-0.017	0.001	-0.005
46	10982	B9.5V	5.858	-0.073	-0.146	-0.068	-0.044	0.029
47*	11415	B3III	3.351	1.577	-0.722	0.163	-0.125	0.083
48	11443	F6IV	3.424	0.019	-0.063	-0.063	0.479	0.039
49	11502/3	B9V+A1p	3.874	-0.065	-0.135	0.084	-0.035	-0.037
50	11857	B5III	6.011	0.027	-0.508	-0.004	-0.014	-0.020
51	11909	K1Vp	5.110	-0.015	0.539	-0.100	0.936	0.036
52	11946	A0Vn	5.300	-0.072	-0.001	-0.161	-0.010	0.001
53	11973	0.239	4.788	-0.067	0.064	0.108	0.285	-0.047
54	12471	A2V	5.513	0.046	0.094	-0.042	0.040	0.036
55	12533/4	K3IIb+B8	2.089	-0.013	0.778	-0.083	1.222	0.007
56	12573	A5III	5.423	0.031	0.185	-0.033	0.150	0.002

57	12869	A2m	5.037	-0.067	0.098	0.057	0.126	0.048
58	12929	K2IIIab	2.019	0.011	0.953	-0.024	1.180	-0.029
59	13161	A5III	3.018	0.004	0.154	-0.051	0.139	0.023
60	13869	A0V	5.259	0.069	-0.059	-0.044	-0.011	0.051
61	13974	G0V	4.873	-0.043	-0.144	0.003	0.612	0.007
62	14191	A1Vn	5.580	-0.042	0.049	0.032	0.004	-0.024
63	15089	A5pSr	4.477	-0.047	0.040	-0.068	0.132	0.017
64	16161	G8III	4.865	0.010	0.382	-0.128	0.882	0.052
65	16739	F9V	4.918	-0.043	-0.025	0.027	0.570	0.013
66	17584	F2III	4.230	-0.010	0.057	0.028	0.346	-0.009
67	17904	F4IV	5.333	-0.020	-0.056	0.050	0.425	-0.047
68	18411	A2Vn	4.694	0.010	0.157	-0.041	0.059	0.026
69	18449	K2III	4.947	-0.010	1.142	-0.099	1.261	0.022
70	18604	B6III	4.702	-0.050	-0.549	0.040	-0.101	0.024
71	18883	B7V	5.618	-0.013	-0.511	-0.027	-0.113	0.032
72	18884	M1.5IIIa	2.532	-0.102	1.875	0.002	1.681	0.012
73	19058	M4II	3.315	0.053	1.731	-0.152	1.675	0.008
74	19787	K2IIIv	4.351	0.028	0.750	-0.018	1.047	0.107
75	20315	B8V	5.486	-0.111	-0.437	0.085	-0.063	0.023
76	20365	B3V	5.160	-0.004	-0.724	0.006	-0.050	0.048
77	20418	B5V	5.047	-0.011	-0.694	-0.026	-0.055	0.041
78	20677	A3V	4.961	-0.146	0.067	0.052	0.055	0.025
79	20809	B5V	5.324	-0.095	-0.683	0.038	-0.064	0.019
80	20902	F5Ib	1.793	-0.097	0.398	-0.038	0.500	0.051
81	21278	B5V	4.989	0.005	-0.689	-0.027	-0.083	0.015
82	21362	B6Vn	5.597	0.039	-0.583	0.029	-0.042	0.035
83	21428	B3V	4.663	0.061	-0.735	0.065	-0.091	0.023
84	21447	A1V	5.106	-0.031	0.069	-0.057	0.028	0.034
85	21552	K3III	4.353	0.026	1.429	-0.144	1.416	0.086
86	21699	B8IIIpMn	5.458	0.026	-0.724	0.024	-0.100	0.048
87	21770	F4III	5.314	0.047	-0.125	-0.155	0.400	0.180
88	22780	B7Vne	5.589	0.055	-0.528	-0.171	-0.079	0.119
89	22928	B5III	3.010	-0.069	-0.621	0.001	-0.118	0.041
90	22951	B0.5V	4.975	-0.059	-1.041	0.014	-0.014	-0.010
91	23016	B9Vne	5.684	-0.064	-0.340	-0.029	-0.011	0.015
92	23193	A2m	5.605	-0.099	0.116	-0.010	0.065	-0.005
93	23288	B7IV	5.467	-0.023	-0.421	-0.013	-0.045	-0.009
94	23300	B6V	5.661	-0.108	-0.590	0015	-0.067	0.030
95	23324	B8V	5.663	0.021	-0.447	-0.007	-0.074	0.034
96	23630	B7IIIe	2.872	-0.033	-0.420	0.085	-0.087	-0.040
97	23753	B8V	5.456	-0.014	-0.390	-0.013	-0.070	-0.019
98	23793	B3V+F5V	5.064	-0.080	-0747	0.048	-0.127	-0.002
99*	23862	B8Vpe	5.116	0.990	-0.333	-0.115	-0.074	0.025
100	23985	A2V+A5V	5.237	-0.043	0.052	0.002	0.218	-0.030

101	24504	B6V	5.392	-0.092	-0.615	0.017	-0.077	0.011
102	24546	F5IV	5.291	-0.027	-0.127	0.009	0.415	0.008
103	24760	B0.5V+A2	2.894	0.085	-1.210	-0.015	-0.177	0.002
104	25204	B3V+A4IV	3.413	-0.014	-0.757	0.053	-0.116	0.002
105	25330	B5V	5.661	0.002	-0.551	0.044	0.032	-0.001
106	25570	F2V	5.449	0.011	-0.111	0.007	0.369	-0.006
107	25604	K0III	4.359	0.023	0.815	-0.183	1.088	0.082
108	26793	B9Vn	5.216	-0.003	-0.405	0.023	-0.096	0.026
109	26965	K1V	4.424	0.087	0.259	-0.056	0.814	0.112
110	27397	F0IV	5.582	-0.034	0.028	0.001	0.276	0.002
111	27459	F0V	5.256	0.026	0.084	-0.064	0.220	0.121
112	27749	A1m	5.637	-0.052	0.119	-0.040	0.301	0.008
113	27819	A7V	4.800	0.029	0.117	-0.010	0.165	0.005
114	28556	F0V	5.398	-0.050	0.061	0.018	0.261	-0.023
115	28910	A8V	4.656	-0.027	0.071	0.011	0.246	-0.018
116	29139	K5III	0.885	-0.026	1.834	-0.016	1.593	0.013
117	29365	B8V	5.866	-0.071	-0.454	-0.016	-0.024	-0.044
118	29479	A4m	5.085	-0.033	0.136	-0.030	0.120	-0.054
119	29488	A5Vn	4.685	-0.069	0.153	0.026	0.147	-0.052
120	30780	A7IV-V	5.083	0.025	0.103	-0.037	0.216	-0.021
121	31373	B9V	5.791	-0.043	-0.570	-0.027	-0.087	-0.004
122	31398	K3II	2.692	0.031	1.632	-0.066	1.561	0.010
123	32549	A0p	4.675	0.010	-0.100	0.029	-0.070	-0.009
124	33167	F5V	5.679	0.012	-0.079	-0.034	0.437	-0.035
125	33959	A9IV	5.038	-0.129	0.136	-0.023	0.211	0.011
126	34029	G5IIIe+G0	0.052	-0.020	0.285	-0.019	0.843	0.035
127	34203	A0V	5.526	-0.109	0.022	0.005	-0.024	-0.052
128	34557	A3V	5.471	0.014	0.102	0.022	0.118	0.015
129	34559	G8III	4.965	-0.142	0.537	0.024	0.952	0.005
130	34790	A1V	5.667	-0.060	0.064	-0.030	0.040	0.039
131	34904	A3V	5.559	-0.053	0.149	-0.028	0.121	0.021
132	34989	B1V	5.778	-0.177	-1.099	0.068	-0.112	-0.091
133	35296	F8V	4.998	-0.091	-0.140	0.009	0.529	0.004
134	35600	B9Ib	5.718	-0.046	-0.202	-0.020	0.190	0.007
135	35671	B5V	5.394	0.015	-0.684	0.027	-0.096	-0.057
136	36371	B5Iab	4.727	-0.057	-0.656	0.004	0.318	0.025
137	36653	B3V	5.605	0.005	-0.788	0.009	-0.121	0.014
138	36819	B2.5IV	5.373	-0.098	-0.795	0.039	-0.085	0.015
139	36861/2	O8e	3.386	0.052	-1.268	-0.012	-0.156	-0.017
140	36881	B9IIIp	5.601	0.069	0.143	-0.008	0.187	-0.009
141	37098	B9IV-V	5.833	-0.263	-0.477	0.021	-0.066	0.052
142	37147	F0V	5.521	-0.065	0.081	0.018	0.223	-0.001
143	37269	B9.5V+F9	5.357	-0.086	0.197	-0.033	0.447	0.033
144	37320	B8III	5.865	0.060	-0.453	-0.005	-0.059	-0.020

145	37438	B3IV	5.165	-0.055	-0.867	0.042	-0.148	0.027
146	38656	G8III	4.534	-0.030	0.513	0.115	0.965	0.017
147	38771	B0.5Iav	2.056	-0.022	-1.257	0.044	-0.155	0.007
148	39291	B2IV-V	5.340	-0.158	-1.039	-0.022	-0.192	-0.003
149	40394	B9.5p	5.718	-0.119	-0.121	0.147	-0.014	0.069
150	40536	A6m	5.043	-0.048	0.175	-0.046	0.179	-0.087
151	40967	B5III	4.970	-0.124	-0.752	-0.034	-0.115	-0.009
152	41040	B8III	5.132	0.012	-0.530	0.018	-0.118	0.051
153	41117	B2Iaev	4.629	0.051	-0.900	0.008	0.263	0.046
154	41335	B2Ven	5.238	-0.168	-1.082	0.037	-0.054	-0.094
155	42087	B2.5Ibe	5.755	-0.045	-0.813	-0.036	0.201	0.077
156	42477	A0Vnn	6.044	0.047	0.056	-0.014	0.012	0.055
157	42995	M3III	3.172	0.276	1.549	-0.082	1.624	0.027
158	44478	M3IIIab	2.879	0.092	1.914	-0.052	1.699	-0.070
159	46089	A3V	5.232	-0.026	0.107	0.050	0.169	-0.065
160	46553	A0Vnn	5.267	-0.400	-0.027	0.113	-0.019	0.045
161	47105	A0IV	1.920	0.079	0.099	0.019	0.006	-0.080
162*	47152	B9np	5.765	-0.448	-0.084	0.111	-0.003	0.050
163	47839	O7Ve+B7	4.645	0.142	-1.309	0.026	-0.226	-0.051
164	48097	A2V	5.220	-0.027	0.062	0.062	0.055	-0.074
165	48329	G8Ib	3.003	0.020	1.305	-0.002	1.435	-0.003
166	48433	K0III	4.505	-0.016	0.996	0.087	1.188	0.015
167	48737	F5III	3.343	-0.026	-0.062	0.043	0.449	-0.038
168	49606	B7III	5.854	-0.029	-0.621	-0.059	-0.130	-0.040
169	49908	A2V	5.271	0.141	0.082	0.014	-0.004	-0.036
170	50635	F0Vp	4.649	0.071	0.003	0.069	0.322	-0.048
171	58187	A5IV	5.375	0.067	0.159	0.038	0.101	-0.014
172	58715	B8Ve	2.876	-0.112	-0.318	0.044	-0.090	-0.032
173	58923	F0III	5.222	0.241	0.179	0.070	0.221	-0.017
174*	59037	A4V	5.076	-0.352	0.118	-0.043	0.121	-0.006
175	60178/9	A1V+A2Vm	1.568	0.008	-0.003	-0.040	0.039	0.017
176*	62509	K0IIIb	1.138	-0.433	0.671	-0.055	1.024	0.355
177	63975	B8II	5.125	0.057	-0.552	0.064	-0.115	-0.048
178*	64145	A3V	4.972	-0.474	0.141	-0.384	0.100	-0.114
179	65900	A1V	5.650	0.045	0.040	0.066	0.006	-0.070
180	73471	K2III	4.452	-0.094	1.123	-0.112	1.243	-0.179
181	74280	B3V	4.283	-0.070	-0.928	0.076	-0.179	-0.094
182	74521	A1p	5.651	-0.020	-0.309	-0.041	-0.090	0.065
183	74738/9	A3V+G7.5III	4.033	-0.040	0.612	-0.087	1.008	-0.197
184	74874	G5III+A8IV	3.377	0.038	0.230	0.073	0.696	-0.033
185	75137	A0Vn	4.348	0.031	-0.019	-0.067	-0.031	-0.008
186	76294	G9II-III	3.117	0.083	0.616	-0.056	1.023	-0.127
187	76644	A7IV+dM1	3.133	-0.016	0.045	-0.020	0.199	0.000
188	77309	A2V	5.750	-0.071	0.080	-0.057	0.020	0.043

189	78316	B8IIIp	5.240	-0.133	-0.549	0.024	-0.089	-0.020
190	78556	B9.5III	5.603	0.033	-0.164	-0.075	-0.062	0.056
191	79439	A5V	4.818	0.013	0.068	0.011	0.193	0.093
192	80586	G8III+F5V	4.818	0.138	0.501	-0.163	0.943	-0.041
193*	81797	K3II-III	1.988	0.386	1.591	-0.022	1.491	-0.091
194	82308	K5III	4.304	-0.031	1.819	-0.154	1.583	-0.075
195	82621	A2V	4.481	-0.116	0.094	0.034	0.035	0.167
196	84441	G1III	2.966	0.158	0.317	-0.014	0.822	-0.130
197	85235	A3IV	4.566	-0.045	0.121	0.057	0.038	0.005
198	85376	A5IV	5.285	-0.039	0.032	0.003	0.242	-0.044
199	85558	A1V+A4V	5.079	0.041	0.050	0.080	0.025	-0.017
200	85795	A3III	5.287	-0.107	0.095	0.031	0.063	0.132
201	86146	F6Vs	5.114	0.074	-0.121	-0.005	0.455	0.003
202	86360	B9IV	5.267	0.080	-0.114	0.061	-0.051	-0.004
203	96663	M2IIIab	4.688	0.019	1.909	-0.054	1.654	-0.054
204	87015	B2.5IV	5.672	-0.060	-0.905	0.073	-0.179	0.026
205	87737	A0Ib	3.510	0.050	-0.225	-0.007	-0.017	0.002
206	89021	A2IV	3.441	0.052	0.108	0.155	0.031	0.015
207	89025	F0III	3.440	0.183	0.181	-0.047	0.302	-0.202
208	89484/5	K1IIIb+G7	2.008	0.014	0.795	0.069	1.159	-0.055
209	89758	M0III	3.048	0.186	1.816	-0.057	1.626	-0.106
210	90839	F8V	4.833	-0.120	-0.166	-0.086	0.527	0.001
211	91312	A7IV	4.721	0.046	0.052	0.002	0.211	0.044
212	91480	F1V	5.157	-0.177	-0.114	-0.039	0.346	0.027
213	94334	A1Vs	4.672	0.026	-0.033	-0.022	-0.039	0.069
214	95128	G0V	5.037	0.005	-0.056	-0.018	0.622	-0.024
215	95418	A1V	2.345	0.126	0.026	-0.050	-0.012	0.053
216	95608	A1m	4.406	0.035	0.075	-0.019	0.046	-0.018
217	95689	K0IIIa	1.793	-0.071	0.748	-0.042	1.093	-0.022
218	96738	A3IV	5.703	0.017	0.152	0.042	0.068	0.004
219	96833	K1III	3.016	0.039	0.963	-0.111	1.177	0.028
220	97603	A4V2	2.547	0.225	0.133	0.008	0.127	-0.032
221	98230/1	G0V	3.762	0.121	-0.153	-0.067	0.595	-0.019
222	98262	K3IIIp	3.478	0.082	1.434	-0.183	1.442	-0.031
223*	100203	F6V+G3V	5.466	-0.331	-0.171	0.016	0.507	0.048
224	102212	M1IIIab	4.031	0.007	1.754	-0.059	1.561	-0.062
225	102647	A3V	2.123	0.054	0.085	0.080	0.102	0.009
226	108283	F0p	4.920	-0.016	0.203	0.089	0.266	-0.025
227	110423	A2V	5.578	0.011	-0.017	0.018	-0.008	0.031
228	112413	A0p	2.904	0.047	-0.419	0.013	-0.098	0.068
229	113797	B9V	5.198	0.045	-0.224	-0.043	-0.069	0.122
230	115004	K0III	4.949	0.041	0.757	-0.094	1.079	0.085
231	115271	A7V	5.786	0.010	0.113	-0.052	0.195	0.114
232	115604	F3III	5.718	0.014	0.203	-0.063	0.307	0.116

233	116656/7	A1Vp+A1m	2.033	0.099	0.040	0.012	0.032	0.060
234	116842	A5V	3.999	-0.001	0.074	0.065	0.171	0.002
235	118022	A1p	4.929	0.085	-0.011	-0.001	0.028	-0.002
236	118098	A3V	3.377	0.197	0.091	0.042	0.119	-0.035
237	118232	A5V	4.669	0.014	0.144	-0.085	0.141	0.072
238	119228	M2IIIab	4.649	0.019	1.901	-0.023	1.686	0.073
239	120136	F6IV	4.489	0.053	-0.101	-0.041	0.488	0.092
240	124897	K1IIIb	-0.089	-0.087	1.096	0.172	1.270	0.099
241	125161	A9V	4.753	-0.166	0.033	-0.070	0.213	-0.010
242	126661	F0m	5.412	0.070	0.190	-0.068	0.229	0.108
243	128167	F2V	4.465	0.058	-0.195	-0.050	0.373	0.082
244	129174/5	B9p+A6V	4.504	0.055	-0.365	0.034	-0.008	0.022
245	129988/9	A2V+K0II	2.371	0.137	0.600	-0.104	0.986	0.091
246	133582	K2III	4.528	0.086	1.187	-0.136	1.293	0.051
247	134083	F5V	4.928	0.071	-0.161	-0.089	0.443	0.123
248	135722	G8III	3.479	0.144	0.492	-0.056	0.977	0.041
249	136849	B9Vn	5.384	-0.005	-0.219	0.000	-0.053	0.000
250	137391	F0V	4.313	0.028	0.003	0.034	0.315	0.006
251	137759	K2III	3.311	-0.036	1.066	-0.004	1.195	0.043
252	137909	F0p	3.669	-0.042	0.070	-0.042	0.279	0.012
253	138917/8	F0IV	3.797	0.035	0.095	-0.068	0.257	0.026
254	139006	A0V	2.219	0.071	0.007	-0.027	-0.019	0.055
255	140573	K2IIIb	2.631	0.098	1.107	-0.099	1.200	0.083
256	140775	A0V	5.568	0.034	0.077	-0.069	0.032	0.205
257	141004	G0V	4.419	0.003	-0.064	-0.075	0.611	0.079
258	141653	A2IV	5.197	-0.042	0.082	0.013	0.052	0.031
259	141714	G3.5III-IV	4.652	0.018	0.192	-0.091	0.805	0.031
260	146926	B8V	5.49	0.048	-0.453	0.022	-0.096	0.027
261	1476777	K0III	4.861	-0.010	0.638	-0.148	0.993	0.122
262	148387	G8IIIab	2.730	-0.018	0.468	0.083	0.922	-0.018
263	148856	G7IIIa	2.783	-0.009	0.494	0.088	0.945	0.006
264	150680	G0IV	2.811	-0.033	0.032	0.002	0.654	-0.013
265	151525	B9p	5.229	0.065	0.017	0.111	-0.017	0.050
266	151956	A3m	5.479	0.147	0.116	0.071	0.110	0.072
267	153210	K2III	3.195	0.145	1.026	0.140	1.181	0.060
268	154029	A3IV	5.279	0.053	0.069	-0.106	0.015	0.089
269	154494	A4IV	4.871	-0.039	0.111	-0.052	0.137	-0.013
270	155103	A5m	5.408	-0.103	-0.002	0.031	0.310	0.022
271	156014/5	M5Ib-IIa	2.933	0.115	0.948	-0.133	1.507	0.007
272	156164	A3IV	3.118	0.036	0.072	0.106	0.085	0.057
273	156729	A2V	4.615	-0.081	0.055	-0.011	0.039	0.010
274	157087	A3III	5.372	0.046	0.148	0.100	0.051	0.004
275	157198	A2V	5.131	0.001	0.079	0.112	-0.004	0.053
276	157728	F0IV	5.714	0.043	0.021	0.094	0.226	0.004
277	157778/9	B9.5III+	4.154	-0.088	0.019	0.032	-0.029	0.022
278	158352	A8V	5.415	0.074	0.087	-0.025	0.242	0.046

279	159139	A1V	5.652	0.068	-0.010	0.064	-0.002	0.005
280	159181	G2Ib-IIa	2.795	-0.140	0.465	-0.089	0.980	0.001
281	160181	A2Vn	5.754	-0.002	0.052	0.070	0.119	0.001
282	161797	G5IV	3.416	0.280	0.208	0.016	0.761	0.006
283	161858	A0V	3.743	0.011	0.066	0.057	0.040	0.004
284	163472	B2IV-V	5.821	0.025	-0.845	0.068	0.098	-0.006
285	163506	F2Ibe	5.416	0.026	0.383	0.007	0.332	0.065
286	164136	F2II	4.403	-0.102	0.168	-0.010	0.379	0.051
287	164284	B2Ve	4.610	-0.070	-1.068	0.111	-0.001	0.000
288	164577	A2Vn	4.436	0.056	0.036	0.147	0.031	-0.013
289	165908	F7V	5.059	-0.124	-0.213	-0.018	0.529	0.079
290	166045	A3V	5.857	-0.083	0.092	0.014	0.129	0.058
291	166046	A3V	5.878	-0.155	0.039	0.056	0.142	0.029
292*	167006	M3III	4.967	-0.089	1.912	-0.377	1.685	0.009
293	168723	K2IIIab	3.251	-0.018	0.478	-0.086	0.955	0.050
294	169702	A3IVn	5.127	-0.151	0.123	-0.009	0.040	0.036
295	174044	B8II-IIIp	5.408	0.074	-0.611	-0.074	-0.095	0.074
296	173417	F1III-IV	5.688	-0.066	-0.037	0.014	0.353	0.025
297	173582/3	A4V+F1V	4.681	-0.054	0.073	-0.007	0.174	0.039
298	173607/8	A8Vn+F0Vn	4.604	-0.107	0.084	0.021	0.185	0.046
299	173648	Am	4.344	0.009	0.178	-0.025	0.201	0.041
300	174602	A3V	5.226	-0.129	0.136	-0.052	0.098	0.066
301	175426	B2.5V	5.584	-0.035	-0.823	-0.016	-0.133	0.042
302	175588	M4II	4.316	-0.094	1.614	-0.073	1.726	-0.020
303*	175751	K2III	4.835	-0.121	0.841	-0.570	1.111	0.008
304	176051	F9V+K1V	5.220	0.003	-0.110	0.000	0.601	0.058
305	176318	B7IV	5.890	-0.028	-0.521	-0.037	-0.090	0.101
306	176437	B9III	3.246	-0.031	-0.005	0.007	-0.041	0.042
307*	176524	K0III	4.829	-0.409	0.935	-0.022	1.176	0.386
308	176678	K1III	4.017	0.075	0.846	0.095	1.131	0.052
309	176984	A1V	5.394	0.006	0.025	-0.037	0.013	0.061
310	177178	A4V	5.824	-0.044	0.067	0.021	0.194	0.017
311	177756	B9Vn	3.419	0.036	-0.310	-0.075	-0.081	0.082
312	178125	B8III	5.068	-0.127	-0.480	-0.016	-0.054	0.105
313	178475	B6IV	5.246	0.081	-0.652	-0.023	-0.105	0.040
314	178596	F0III-IV	5.239	-0.055	-0.050	0.028	0.344	-0.010
315	180482	A3IV	5.583	-0.042	0.219	0.209	0.091	-0.087
316	180868	F0IV	5.289	-0.095	0.210	-0.039	0.191	0.084
317	181276	G9III	3.803	-0.026	0.559	0.012	0.966	0.054
318	181333	F0III	5.5228	-0.148	0.170	0.012	0.270	0.083
319	182568	B3IV	4.985	0.039	-0.893	0.133	-0.107	-0.049
320	182572	G8IV	5.179	-0.075	0.244	0.009	0.777	-0.052
321	182640	F3IV	3.368	-0.040	-0.031	0.038	0.338	0.035
322	182835	F2Ib	4.678	-0.026	0.657	0.078	0.593	-0.047
323	183912/4	K3II+B0.5V	3.067	0.009	0.456	0.059	1.163	-0.028
324	184406	K3IIIb	4.460	-0.025	1.101	-0.013	1.204	0.071

325	184759	A0V+F8III	5.415	0.027	0.268	0.107	0.581	0.001
326	184875	A2V	5.342	0.085	0.151	0.030	0.066	0.029
327	184905	A0p	6.632	-0.088	-0.320	-0.105	-0.023	0.002
328	185351	G9IIIb	5.183	0.065	0.513	0.053	0.954	-0.031
329	185507	B3V+B3V	5.148	0.001	-0.784	0.031	0.047	0.052
330	185734	G8III-IV	4.692	0.798	0.613	-0.032	0.994	-0.849
331	185758	G1IIab	4.386	-0.014	0.273	-0.086	0.789	0.006
332	185762	A3IV	5.640	-0.047	0.110	0.125	0.115	-0.043
333	185872	B9III	5.409	0.081	-0.218	0.047	-0.060	0.035
334	186155	F5II/III	5.067	0.054	0.103	0.008	0.413	0.013
335	186203	dF3+A3	5.291	-0.039	-0.155	-0.055	0.604	0.076
336	186791	K3II	2.718	-0.002	1.589	-0.191	1.567	0.066
337	186882	B9.5IV+F1V	2.869	0.102	-0.074	0.016	-0.028	0.002
338	187691	F8V	5.121	-0.049	-0.080	0.032	0.564	0.067
339	187879	B1III+B3V	5.655	0.086	-0.996	0.106	-0.029	0.046
340	188209	O9.5Ib	5.634	0.056	-1.210	0.075	-0.063	0.049
341	188252	B2III	5.906	0.115	-1.080	0.068	-0.163	-0.001
342	188260	B9.5III	4.581	-0.070	-0.142	0.042	-0.041	-0.012
343	188310	K0IIIb	4.721	-0.015	0.730	0.033	1.071	0.038
344	188728	A1IV	5.278	-0.039	0.017	0.009	0.009	0.059
345	189319	M0III	3.508	-0.036	1.857	-0.050	1.617	0.011
346	190940	K3III	4.522	-0.041	1.370	-0.038	1.363	-0.017
347	191610	B2.5Ve	4.942	0.047	-0.971	0.080	-0.141	0.050
348	191692	B9.5III	3.232	-0.033	-0.121	0.029	-0.061	0.004
349	192640	A2V	4.945	-0.058	0.031	-0.005	0.160	0.062
350	192806	K3III	4.511	-0.087	0.995	-0.218	1.302	-0.006
351	193237	B2pe	4.752	0.001	-0.826	0.013	0.416	0.059
352	193495	F8V+A0	3.089	0.076	0.159	0.035	0.814	0.041
353	194093	F8Ib	2.233	-0.069	0.469	0.049	0.674	0.066
354	195050	A3V	5.642	0.010	0.104	-0.030	0.066	0.064
355	195556	B2.5IV	4.944	-0.106	-0.805	0.094	-0.065	0.011
356	196178	B9p	5.785	-0.122	-0.664	0.086	-0.141	0.084
357	196502	A0p	5.207	0.007	0.132	-0.089	0.085	-0.026
358	196524	F5IV	3.627	-0.064	-0.039	-0.643	0.448	0.004
359	196662	B7III	-	-	-	-	-	-
360	197345	A2Iae	1.267	-0.045	-0.243	0.044	0.102	0.055
361	197392	B8II-III	5.677	-0.049	-0.534	0.018	-0.094	0.021
362	197963/4	K1IV+A2Ia	3.890	-0.046	0.372	-0.104	0.863	0.043
363	198149	K0IV	3.430	0.085	0.420	-0.041	0.929	-0.032
364	198183	B5Ve	4.526	0.062	-0.616	0.052	-0.098	0.007
365	198478	B3Iae	4.834	-0.027	-0.640	0.061	0.382	0.063
366	198639	A4m	5.064	-0.033	0.103	0.002	0.205	0.015
367	198809	G7III	4.570	-0.058	0.302	-0.119	0.866	0.039
368	199081	B5V	4.778	-0.033	-0.725	0.073	-0.123	0.023
369	199629	A1Vn	3.943	-0.104	0.046	0.019	0.017	0.036
370	200120	B1nne	4.765	-0.065	-1.186	0.060	-0.051	0.084

371	200310	D1Ve	5.365	0.032	-1.172	0.120	-0.176	0.022
372	202275	F5V+G0V	4.488	-0.036	-0.158	-0.013	0.512	-0.003
373	202444	F2IV	3.731	-0.045	-0.068	0.006	0.409	0.059
374	202850	B9Iab	4.260	-0.024	-0.455	0.069	0.127	-0.027
375	202904	B2Vne	4.225	0.045	-0.978	0.114	-0.087	0.016
376	203467	B3IVe	5.122	0.183	-0.827	0.070	0.004	-0.037
377	204724	M1III	4.524	-0.047	1.874	-0.125	1.650	0.113
378	204770	B7V	5.431	-0.048	-0.534	0.008	-0.112	0.058
379	204867	G0Ib	2.885	0.168	0.446	0.029	0.852	0.035
380	205021	B2IIIev	3.241	0.033	-1.181	0.026	-0.213	0.030
381	206267	O6f+B0V	5.629	-0.034	-0.979	0.017	0.208	0.046
382	206672	B3IV	4.682	-0.003	-0.836	0.015	-0.106	-0.006
383	206778	K2Ib	2.376	0.028	1.532	0.125	1.581	0.001
384	206952	K0III	4.550	-0.022	0.954	-0.004	1.124	0.012
385	207330	B3III	4.235	-0.066	-0.889	-0.018	-0.117	0.026
386	208057	B3Ve	5.094	0.040	-0.826	-0.046	-0.150	0.082
387	208565	A2Vnn	5.536	0.004	0.091	0.033	0.057	0.009
388	209409	B7IVe	4.695	0.129	-0.538	0.083	-0.084	0.004
389	209459	B9.5V	5.831	0.014	-0.111	0.078	-0.050	0.005
390	209481	O8.5III+O9	5.555	0.074	-1.096	0.012	0.075	0.003
391	209750	G2Ib	2.938	0.144	0.579	-0.030	0.996	0.077
392	209790	F3III/IV	4.273	-0.060	0.030	-0.044	0.351	0.083
393	209975	O9Ib	5.112	0.000	-1.090	0.013	0.079	0.030
394	210418	A2V	3.519	0.003	0.114	0.041	0.085	-0.014
395	210745	K1.5Ib	3.343	0.010	1.549	0.037	1.611	-0.022
396	210855	F8V	5.258	-0.039	-0.055	0.034	0.522	-0.061
397	210884	F2V	5.480	0.002	-0.115	-0.017	0.399	0.022
398	212097	B9III	4.798	-0.050	-0.240	0.071	-0.011	-0.033
399	212120	B6V	4.556	-0.036	-0.651	-0.019	-0.099	0.003
400	212710	B9.5Vn	5.276	0.079	--0.069	-0.088	-0.033	0.084
401	212943	K0III	4.789	0.068	0.708	0.076	1.076	0.022
402	213323	B9.5V	5.643	0.107	-0.090	-0.036	-0.033	-0.003
403*	213798	A3V	5.469	0.440	0.105	-0.001	0.072	0.032
404	214035	A2V	5.705	0.074	0.107	-0.001	0.009	0.049
405	214994	A1IV	4.802	0.094	0.039	-0.037	-0.012	0.015
406	215182	G2II+F0V	2.936	0.140	0.423	0.038	0.874	-0.006
407	215648	F6III/IV	4.207	0.002	-0.146	-0.008	0.502	0.020
408	216131	G8III	3.511	-0.021	0.496	0.023	0.951	-0.004
409	216228	K0III	3.513	0.072	0.763	-0.092	1.064	0.095
410	217906	M2.5IIIe	2.365	0.151	1.921	0.001	1.730	-0.027
411	218376	B0.5IV	4.850	0.053	-1.070	0.026	-0.045	0.099
412	218634	M4III+A2V	5.052	-0.022	1.161	0.180	1.541	0.160
413	218658	G2III+F3V	4.404	0.032	0.323	0.080	0.808	-0.038
414	219485	A0V	5.901	0.038	0.011	0.078	-0.020	0.071
415	219615	K0III	3.701	0.022	0.407	0.021	0.940	-0.023
416	220061	A5V	4.595	-0.068	0.110	0.011	0.181	0.130

417	220222	B6III	5.343	0.016	-0.561	0.075	-0.099	0.050
418	220954	K1III	4.280	0.044	0.825	-0.021	1.095	0.079
419	221253	B3IV	4.890	-0.024	-0.800	-0.009	-0.121	0.034
420	221525	A7IV	5.571	0.054	0.176	0.021	0.226	0.155
421	222368	F7V	4.129	0.047	-0.131	0.041	0.511	0.014
422	222404	K1III-IV	3.241	0.031	0.771	0.052	1.050	0.070
423	222439	B9IVn	4.140	-0.062	-0.258	-0.041	-0.076	0.043
424*	224427	M3III	4.678	-0.088	1.593	-0.357	1.635	0.092
425	224893	F0III	5.576	-0.091	0.536	0.049	0.402	0.052

- - numbers of stars with residuals more 0.2^m marked by asterisks;
- - star HD196692 is absent in catalogue [11].

Acknowledgement. I express sincere gratitude to T. Bobryashova for help in calculations, N. Morozova for digitizing the Shamakha catalogue and L. Usoltseva for remarks to manuscript of this article.

This work has been carry out in the frame of PGF AC MDAI RK, code BR05336383.

В. М. Терещенко

Fesenkov Astrophysical Institute

ШАМАХИН СПЕКТРОФОТОМЕТРЛІК КАТАЛОГЫНЫҢ ДҰРЫСТЫҒЫН БАҒАЛАУ

Аннотация. Жеке мақалалар және танымал спектрофотометрлік каталогының негізінде біз спектрлерінде энергияның талалуы анықталған жұлдыздардың бірыңғай және жинақталған каталогын құруды жоспарлаудамыз. Жұмыстың алғашқы сатысында берілген каталогтардың дұрыстығын бағалау. Бұл жұмыста, Шамахин обсерваториясында құрылған каталогтың мәліметтеріне талдаулар жүргізілді. Мәліметтердің дұрыстығы– WBVR фотометрлік жүйесінің тікелей бақыланатын және энергияның таралуы бойыншаесептелген жұлдыздардық шамалармен сәйкестігін салыстыру бойынша анықталған жанама жолмен бағаланған. Жұлдыздық шамаларды есептеу белгілі синтетикалық фотометрия өрнегімен анықталған. Одан кейін, бақыланатын және есептелген шамалардың арасындағы (қателіктер) айырмасы есептелді. Түс көрсеткіштігі және V шамасы бойынша қателіктер тәуелділігінің графиктері тұрғызылды. 0.20^m шамадан асатын, айтарлықтай қателіктер саны бар. Алынған нәтижелер жұлдызды-стандарттар таңдап алуға және жинақталған каталог құруға қолданылады.

Түйін сөздер: жұлдыздар, энергияның таралуы, Шамахин спектрофотометрлік каталогы, WBVR-шамаларының каталогы, тенеу.

В. М. Терещенко

Fesenkov Astrophysical Institute

ОЦЕНКА ДОСТОВЕРНОСТИ ШАМАХИНСКОГО СПЕКТРОФОТОМЕТРИЧЕСКОГО КАТАЛОГА

Аннотация. На базе существующих спектрофотометрических каталогов и отдельных статей мы планируем создать сводный и однородный каталог звезд с известным распределением энергии в их спектрах. В качестве исходных каталогов мы намерены использовать каталоги, созданные в Астрофизическом институте им. В.Г. Фесенкова, Государственном астрономическом институте им. П.К. Штернберга, главной астрономической обсерватории РАН, Одесской астрономической и Шамахинской астрофизической обсерваториях. На первом этапе работы необходимо оценить достоверность данных исходных каталогов. В настоящей работе мы анализируем данные каталога, созданного в Шамахинской обсерватории. Достоверность данных оценивается косвенным путем - по сходимости вычисленных из распределения энергии звездных величин с непосредственно наблюдаемыми величинами в фотометрической системе WBVR. Вычисления звездных величин выполнены по известным формулам синтетической фотометрии. Затем были вычислены разности между вычисленными и наблюдаемыми величинами (невязки). Результаты вычислений представлены в таблице. По ним были построены зависимости невязок от звездной величины V и показателей цвета. Из них следует, что заметные систематические ошибки в Шамахинском каталоге отсутствуют. Однако, имеется значительное число случайных невязок, достигающих 0.20^m и более. Полученные результаты будут использованы при создании сводного каталога и при выборке из него звезд-стандартов.

Ключевые слова: звезды, распределение энергии, Шамахинский спектрофотометрический каталог, каталог WBVR-величин, сравнение.

Information about author:
Tereschenko Vladimir Mikhaylovich – candidate of phys.-math. sciences, leading science collaborator of Fesenkov Astrophysical Institute. volter2307@mail.ru

REFERENCES

[1] Breger M. Second spectrophotometric catalogue // Astrophys. J. Suppl. Vol. 32. **1976.** P. 1-86.

[2] Burnashev V. I. Spectrophotometry of 1588 stars // SIMBAD. **1985.** http://vizier.u-strasb.fr./ III/126/stars

[3] Tereschenko V. M., Kharitonov A. V., Knyazeva L. N. // Spectrofotometricheskiy catalog zvezd. Alma-Ata. "Kazak University". **2011**. 304p. (in Russ.)

[4] Voloshina I.B., Glushneva I.N., Doroshenko V.T,. Kolotilov E.A,. Mossakovskaya K.I., Ovchinnikov S.L., Fetisova T.S. pod red. I. N. Glushnevoy // Spektrofotometriya yarkikh zvezd. M. Nauka. **1982.** 256 p. (in Russ.)

[5] Alekseeva G. A., Arkharov A. A., Galkin V. D., Hagen-Thorn E. I., Nikanorova I. N., Novikov V. V., Novopashenny V. B., Pakhomov V. P., Ruban E. V., Shchegolev D. E. The Pulkovo spectrophotometric catalog of bright stars in the range from 320 to 1080nm // Baltic astronomy. **1996.** Vol. 5, № 4. P. 603-838.

[6] Komarov N.S., Pozigun V.A., Belik S.I., Dragunova A.V., Gopka V.F., Zakozhurnikova N.N., Kantsen L.E., Karamysh V.F., Mishenina T.V., Orlova L.F., Pereverzentsev A.F., Russo T.A., Cherkass A.G. Spektrofotometriya zvezd v diapazone λλ 550 - 900 nm // Kiev. Naukova dumka. **1983.** 312 p. (in Russ.)

[7] Komarov N. S., Arkhipov M.G., Basak N.Yu., Belik S. I., Cherkass A.G., Chuprina R. I., Depenchuk E. A., Dragunova A. V., Dulapchi I. F., Gorbaneva T. I., Karamysh V. F., Kantsen L.E., Korotin S.A., Kovtyukh V.V., Orlova L.F., Motrich V.D., Pereverzentsev A.F., Shevchuk T.V., Zakozhurnikova N.N. The New Spectrophotometric Star Catalogue // Odessa Astronomical Publication. Vol. 11. **1998.** P. 3–48.

[8] Omarov S.Z., Gadzhiev M.S., Goldberg E.P., Omarova G.P., Shestopalov D.I., Shustarev P.N. Raspredelenie energii v spektrakh 425 yarkikh zvezd // Tsirkulyar Shamakhinskoy astrofiz. observ. im. Tusi. № 104. **2002,** P. 3-174. (in Russ.)

[9] Tereschenko V. M., Kharitonov A. V. Zonalnie spectrophotometricheskie standarty // Alma-Ata. "Nauka Kaz SSR". **1972** . 126 p. (in Russ.)

[10] Nicolet B. Astron. and Astrophys. Suppl. Ser. // Vol.34. **1978**, P.1.

[11] Kornilov V.G., Volkov I.M., Zakharov A.I., Kozyreva V. C., Kornilova L.N., Krutyakov A.N., Krylov A.V., Kusakin A.V., Leontyev S.E., Mironov A.V., Moshkalev V.G., Pogrosheva T.M., Sementsov V.N., Khaliullin Kh. F. Katalog WBVR-velichin yarkikh zvezd severnogo neba // Trudy Gos. astron. in-ta im. P.K. Shternberga. Vol. 63. **1991.** 400 p. (in Russ.)

[12] Mironov A.V. Osnovy astrofotometrii. M. Fizmatlit. **2008.** 260 p. (in Russ.)

N E W S
OF THE NATIONAL ACADEMY OF SCIENCES OF THE REPUBLIC OF KAZAKHSTAN
PHYSICO-MATHEMATICAL SERIES
ISSN 1991-346X **https://doi.org/10.32014/2019.2518-1726.24**
Volume 3, Number 325 (2019), 56 – 63

UDC 523.62

G.S. Minasyants, T.M. Minasyants, V.D. Vdovichenko, A. G. Bibossinov

Fesenkov Astrophysical Institute, Almaty, Kazakhstan
gennadii_minasya@mail.ru, gennadii_minasya@mail.ru,
vdv1942@mail.ru, bibossinov@gmail.com

PROPERTIES OF ULTRAVIOLET EMISSION AT DEVELOPMENT OF SOLAR FLARES

Abstract. By means of processing photoheliograms in the λ1700Å ultraviolet emission (temperature minimum, upper photosphere) obtained on the Solar Dynamics Observatory (SDO) spacecraft, the behavior of the relative intensity of bright plasma at the level of the photosphere during the development of impulsive phase of solar flares was studied. The interrelation of the course of change in flare ultraviolet emission with the profile of time derivative of the X-ray flux (1–8) Å and with the value of enhancement in the density of electrons arising at development of flares has been revealed.

Keywords: Solar flares, photometry, emission of flares, gamma rays.

Introduction

With the help of modern space observations of the Sun with high temporal, spatial and spectral resolution, it is possible to study in detail the process of direct flare enhancement during the development of its impulsive phase. As a result of the effect of magnetic reconnection in the active regions of the corona, from areas of primary energy release, there are fluxes of rapidly moving plasma flows, heat waves and high-energy charged particles, some of which propagate downward through magnetic flux tubes. When interacting with a denser plasma at the footpoints of loops, X-rays, gamma rays are generated and the plasma is heated. The rapid and significant heating of plasma in the photosphere and the chromosphere leads to “evaporation” and raising it up and filling of all volume of the magnetic arches. During this period the greatest increase of soft X-ray radiation is observed. All this relates to the development of the impulsive phase. This is followed the main phase at which heated plasma in the system of arches radiates a long time in the soft X-ray range, gradually losing energy [1].

For powerful flares at a maximum of impulsive phase at photoheliograms λ1700 Å there are bright thin vertical rays located in opposite directions from sites of hot plasma (bluming) that indicates to the excess brightness of radiation, overflowing of a charge in photomatrix pixels and its further redistribution.

At the same time, different flares have their own current sheet structure, as well as the underlying magnetic power tubes, which in each case leads to a unique direct flare energy enhancement, both in structural and in time dimension. Our purpose - to find regularities in properties of impulsive phase at development of various flares.

Processing of observational data

For each of the flares presented for consideration, the profiles of the change with time of the intensity of X-ray 1-8Å (GOES), its derivative and the change in brightness of ultraviolet emission were compared. Temporal values of derivative X-ray (resolution 1 min) for flares events are taken in the SDO spacecraft database.

The VLAD program by means of which temporary changes of brightness of ultraviolet emission of flare concerning the center of a disk (figure 1) are received was developed for photometric processing of photoheliograms of SDO. The intensity of undisturbed photosphere was accepted for 1.00.

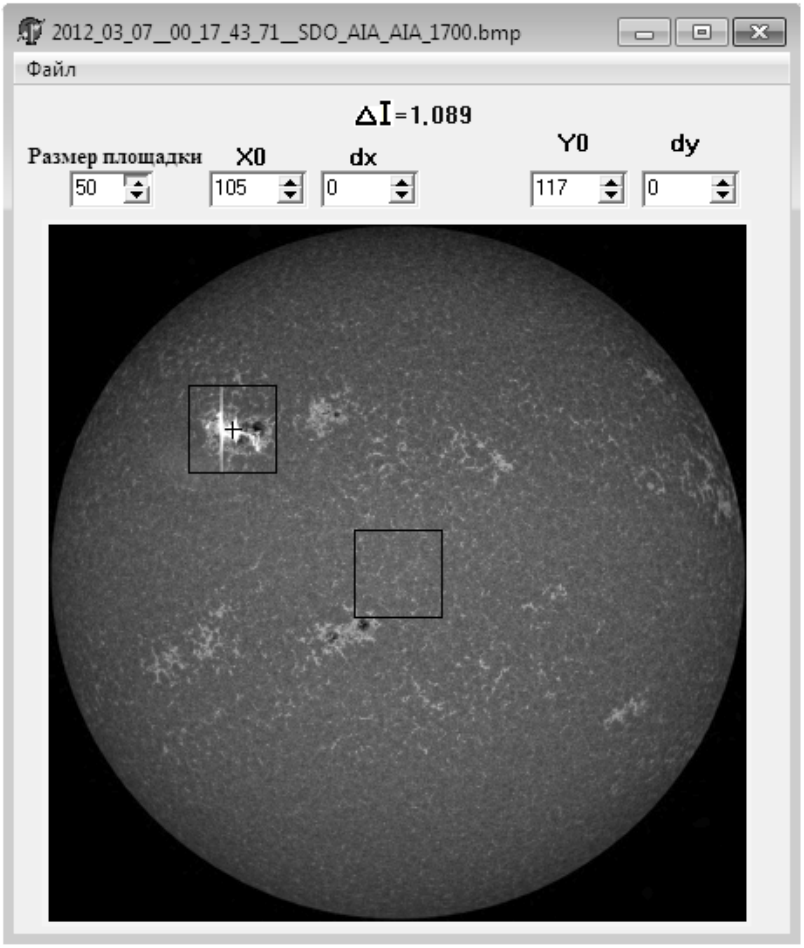

Figure 1 - A screenshot of process of photometric processing of photoheliogram λ1700 Å with the image of flare on March 7, 2012 at 00:17:43 UT

In total 12 flare events in the development of which were followed by bright areas of ultraviolet emission (table 1) are analyzed. Flares of various X-ray power from C2.5 to X6.9 and according to different classes are presented: impulsive and gradual.

Table I - Characteristics of the flares used in work, results of photometric processing and data on enhancement of density of electrons in flare plasma

№	Data and Onset Flares UT	Power X-ray Class of Flares	ΔImax λ1700Å	ΔN_{e^-} e^-/cm^3
1	07.03.2011 19:43	M3.7 Gradual	1.125	3.02
2	09.08.2011 07:48	X6.9 Gradual	1.236	3.00
3	06.09.2011 22:12	X2.1 Gradual	1.155	4.97
4	23.01.2012 03:38	M8.7 Gradual	1.099	2.50
5	07.03.2012 00:02	X5.4 Gradual	1.312	7.02
6	09.03.2012 03:22	M6.3 Gradual	1.141	2.98
7	06.07.2012 23:01	X1.1 Gradual	1.246	4.01
8	02.05.2013 04:58	M1.1 Impulsive	1.054	0.72
9	25.02.2014 00:39	X4.9 Gradual	1.253	4.03
10	16.05.2014 20:11	C2.5 Impulsive	1.020	0.51
11	20.10.2014 16:00	M4.5 Impulsive	1.051	1.03
12	24.10.2014 21:07	X3.1 Gradual	1.216	5.05

For three events in the figure 2 results of processing of observation data are presented. On geometrical arrangement and the sizes of bright areas of ultraviolet emission we can assume possible the structure of coronal loops in which flare radiation during the impulsive phase gets. Each of the flares shown in fig. 2, had a different number of flare nuclei at the level of the photosphere - from one to three. This was it corresponded in the number of peaks in the changes in the intensity of ultraviolet emission, in changes in the X-ray flux, as well as in the derivative of profile of this flux. Moreover, each peak is associated with changes in the brightness of an individual region, it indicates the discrete manifestation of sources of energy release during the development of flare in different parts of the corona.

Since the steady period of presence of negative values of a derivative on time of a flux of soft X-ray radiation, action of a source of flare enhancement – the end of impulsive phase actually comes to end. Further the main phase of development of flare begins. Between a maximum of impulsive phase and the beginning of the main phase there is a period of possible raising up of the heated plasma of photosphere and chromosphere (process of "evaporation" - an explosive stage) and fillings of all volume of coronal arches – an interval of maximum brightness of flare loops.

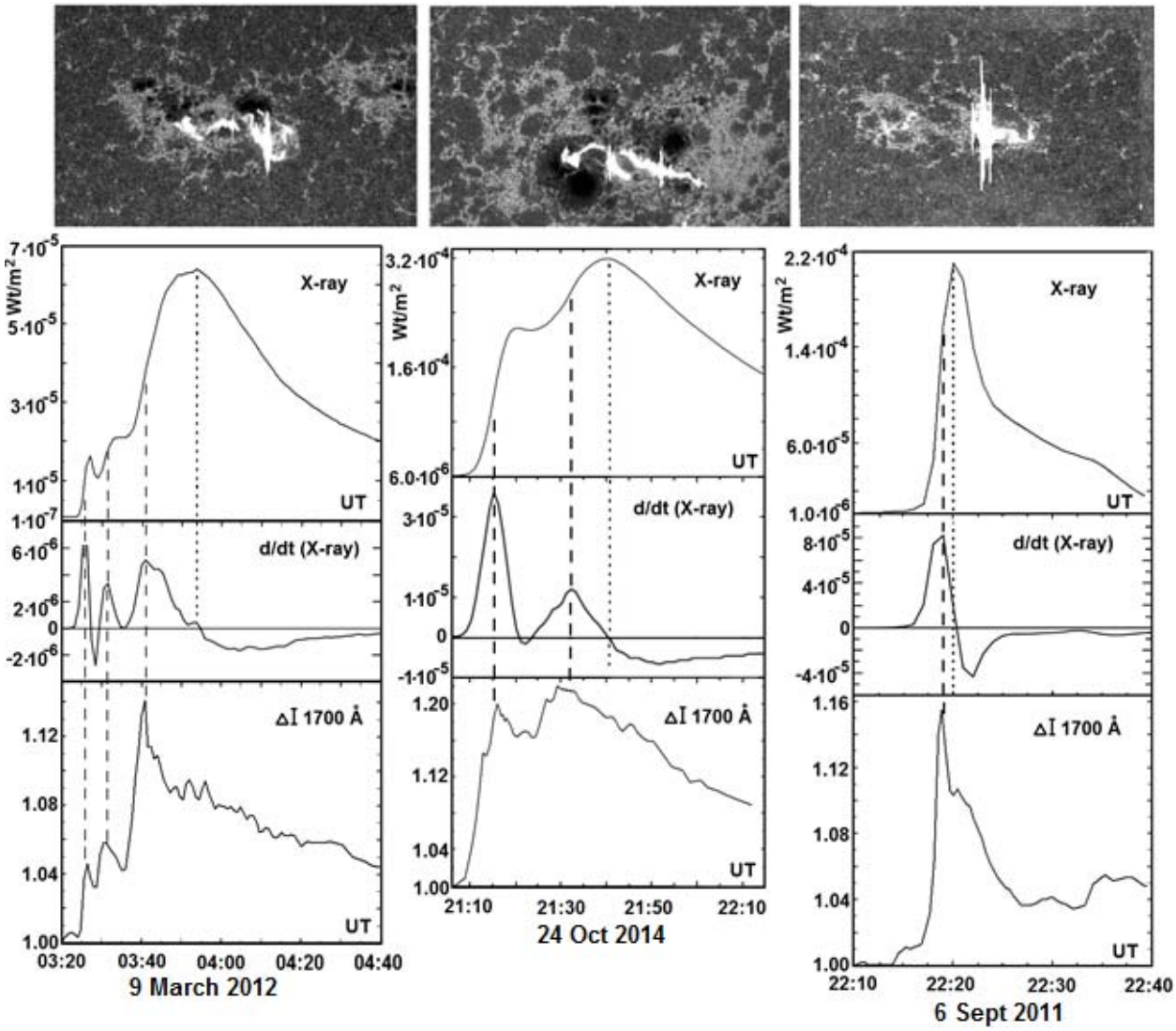

Figure 2 - Top panel: images of ultraviolet emission in a maximum of development of impulsive phase of flares: March 9, 2012 03:40:55 UT, M6.3; October 24, 2014 21:16:06 UT X3.1: September 6, 2011 22:18:55 UT, X2.1. Below - comparison of profiles of change fluxes X-ray intensity with its derivative on time and relative intensity of ultraviolet emission of flare plasma. Vertical dash lines are the moments of the greatest values of ultraviolet emission ΔI λ1700 Å; the dot line – maximum X-ray intensity

All the boundaries of the existing phases in development of flares are determined by the moments of the maximum values the intensity of ultraviolet emission λ1700Å, the X-ray flux and its derivative. Including the position of the explosive stage, which is shown on figure 3.

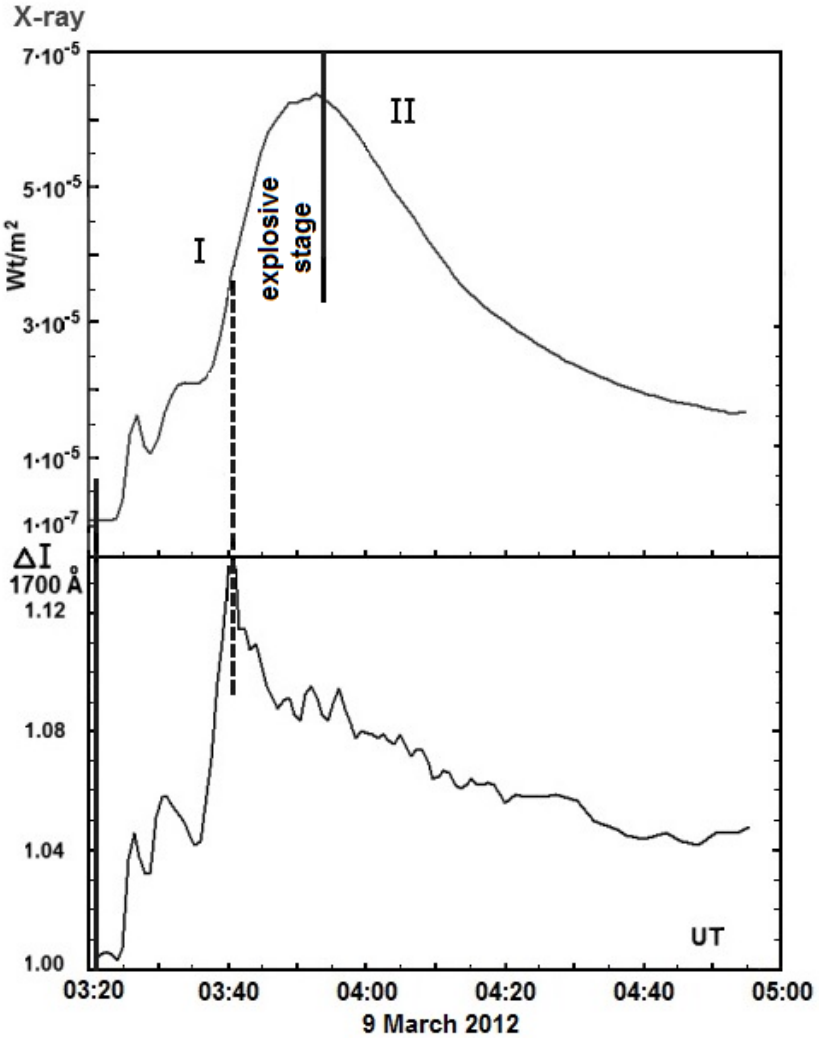

Figure 3 - Flare on March 9, 2012 M6.3 N15W03. Phases in flare development: I - impulsive phase (two vertical solid lines), II – the main phase. An interval between a maximum of impulsive phase and the beginning of the main phase – is explosive stage. The top curve - profile X-ray intensity and lower - relative intensity of ultraviolet emission of flare plasma

The change in the intensity of bright plasma at the level of photosphere λ1700Å is a good index characterizing the direct flash strengthening, including the emission of flare gamma-ray fluxes. The materials of the telegram on the results of observations of the X6.9 flare on August 9, 2011 on FERMI spacecraft [2] reported that gamma radiation in the range energy >500 keV (the GBM tool, BGO device in period 08:02:05 - 08:03:43 UT) and LAT tool (20MeV – 1GeV, 08:01:40 - 08:05:00 UT) was recorded. It is remarkable that all these time intervals of enhancement fluxes of gamma radiation with emission peaks, coincide with a profile of maximum stage of development of ultraviolet emission flare plasma (fig. 4). At the same time the visibility period on photoheliograms of bright narrow rays with an excess brightness (08:01:43 - 08:03:43 UT), practically coincides with time of flare fluxes of high-energy gamma radiation. The flare on August 9, 2011 represents an exceptional case when at development of a gradual event the power prevalence of radiation in the period of impulsive phase, over main was observed.

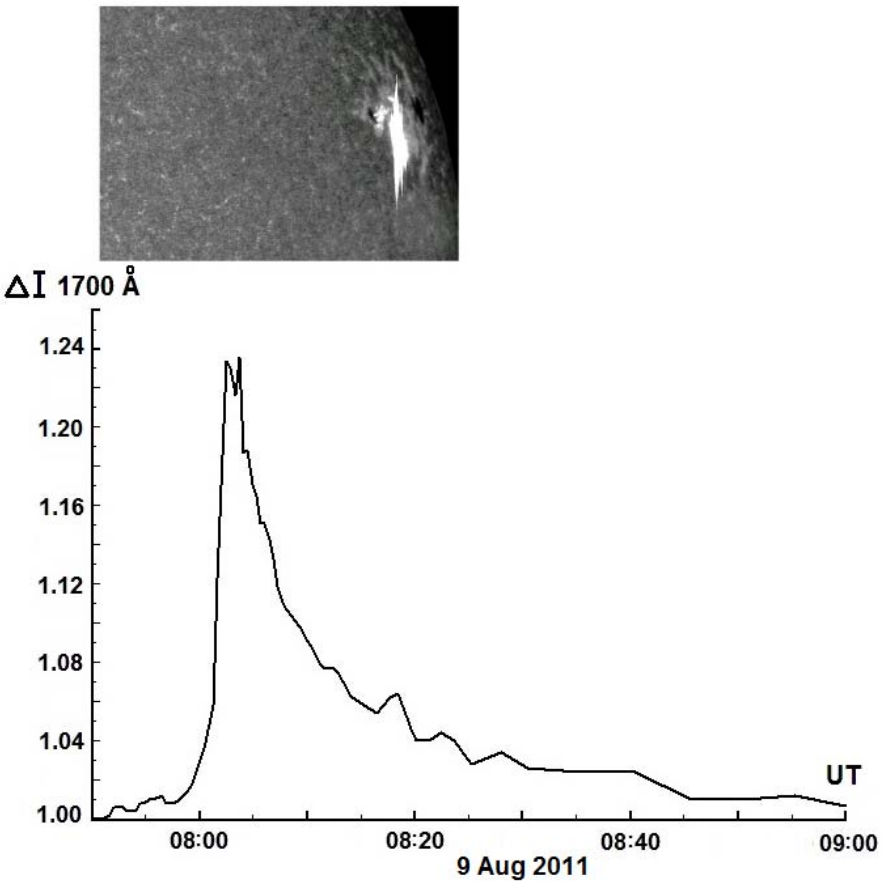

Figure 4 - Change of relative intensity of ultraviolet emission of flare plasma August 9, 2011 X6.9 N14 W69 and its look in the period of the maximum brightness - 08:03:43 UT (top picture)

Results of observations on the FERMI telescope for the period of impulsive phase were published also for flare on September 6, 2011 [3]. Significant increase in intensity of gamma radiation (~ 5 MeV) on the BGO device was observed from 22:18 till 22:23 UT, radiation peak at 22:19 UT. At the same time on images of the photosphere the increased flare brightness in the form of narrow rays is visible during the 22:18:07 – 22:23:19 UT, with a maximum at 22:18:55 UT (see fig.2). That is, there is a coincidence on time of the enhancement of gamma radiation with the maximum ultraviolet emission of flare.

As for development of gradual flares during the main phase, all of them were followed by joint influence of coronal mass ejections (CME). An additional source of proton acceleration associated with the development of high-velocity CME may be the occurrence of shock waves in the upper layers of the corona and in the interplanetary space. The flare protons accelerated on the shock front of emissions to energy E_k >500 MeV, became a source of gamma radiation of very high energy: (100 MeV-10 GeV) which was registered on the FERMI telescope. Only gradual events on August 9, 2011 and on October 24, 2014 showed the maximum values of energy of gamma radiation of smaller values.

The important parameter connected with relative intensity of flare emission at the level of photosphere the values of enhancement of density of electrons during flare development is represented. In figure 5 comparison of temporary change of relative intensity of flare brightness in the photosphere λ1700 Å and enhancement density of electrons of Ne^- in $1/cm^3$ (SC WIND) is shown. Coincidence of the course of these profiles for two flares of an event on March 7, 2012 indicates relationship of the considered parameters.

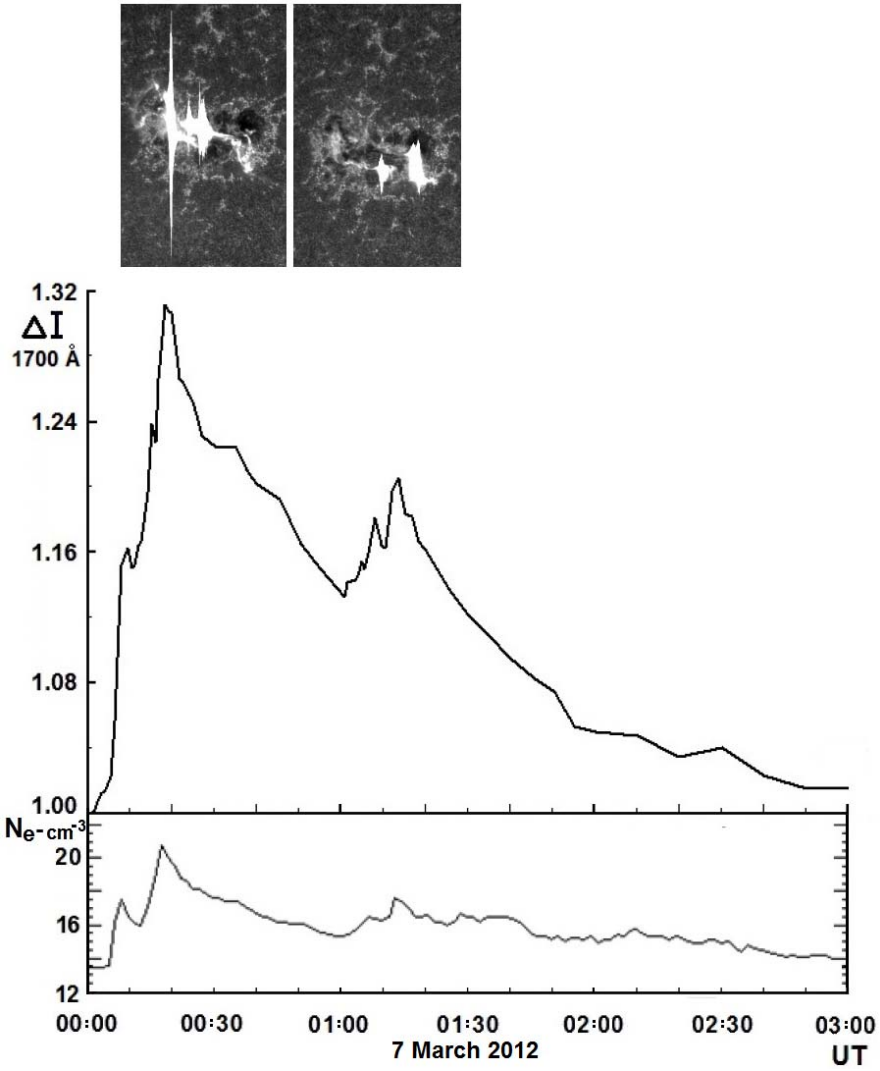

Figure 5 - Comparison of the relative intensity of the ultraviolet emission λ1700Å with the electron density of Ne^- during the development of flares on March 7, 2012. At the top: photoheliograms of flares March 7, 2012 00:17:43 UT X5.4 N18 E31 and March 7, 2012 01:13:43 UT X1.3 N15 E26 in the periods of maximum ultraviolet emission

The similar picture is observed for all events used in our work. Satellite observations show of enhancement of density of flare electrons practically simultaneous registration with gamma radiation of ultraviolet flare emission. To explain this fact, it is necessary to allow an exit of fluxes of high-energy flare electrons through open magnetic structures of active regions in interplanetary space and, in the minimum interaction with plasma of solar wind, before arrival to Earth orbit. So for flares on March 7, 2012 considerable raising of an integrated fluxes of electrons > 4 MeV from background value $1.7 \cdot 10^1$ to $2.9 \cdot 10^3$ $e^-/(cm^2\ s\ sr)$ was registered on the GOES spacecraft.

At development of three considered impulsive flares (table 1): on May 2, 2013, ΔNe^-=0.7 ($1/cm^3$), on May 16, 2014, ΔNe^-=0.5 ($1/cm^3$) and on October 20, 2014 ΔNe^-=1.0 ($1/cm^3$), are registered only insignificant enhancement of density of electrons, in limits by ΔNe^-= 1.0 ($1/cm^3$). While the gradual flares led to more significant enhancement of density of electrons: ΔNe^-=2.5-7.0 ($1/cm^3$).

Thus, it is possible to claim about existence of relationship between the values of the maximum intensity ΔI λ1700 Å and enhancement of density of electrons ΔNe^- the arising from development of flares (fig. 6).

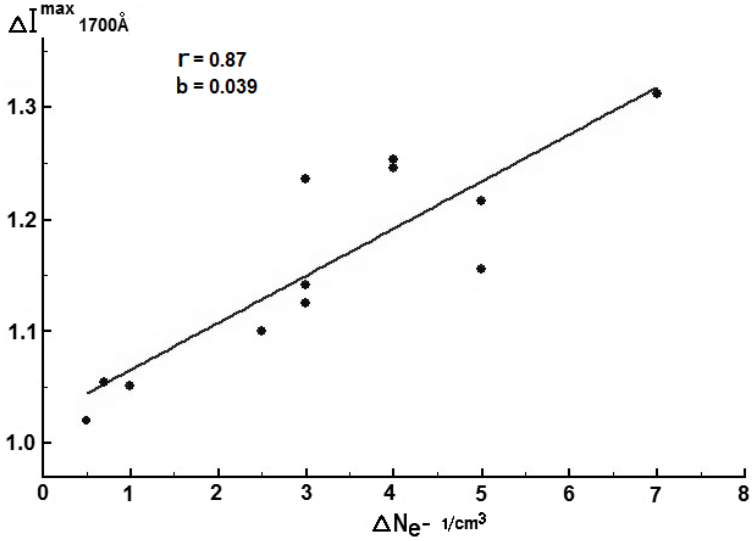

Figure 6 - Comparison of maximum relative intensity of ultraviolet emission λ1700 Å and values of enhancement of density of electrons ΔNe^- for the considered flare events. Averaging of dependence is shown on condition of minimum mean squared deviations of values from an average. A coefficient of correlation according to Pearson r=0.87 and a regression coefficient of b=0.039 are calculated

Discussion of the results and conclusion

12 flare events of different classes from C2.5 to X6.9 (March, 2011 – October, 2014) are analysed in which development bright ultraviolet emission (λ1700 Å), were observed. The program by means of which temporary changes of brightness of ultraviolet flare emission concerning the center of a disk are received is developed for photometric processing of photoheliograms (temporary resolution ~ 50 sec.). For each flares change profiles intensity X-ray (1-8 Å) were compared with its derivative on time and relative brightness of an ultraviolet emission. The maximum X-ray emission of flares, which coincides with the zero value of its derivative, corresponds to the end of the impulsive phase and the beginning of the main phase of the development of flares. The explosive stage of flares connected with "evaporation" of the chromosphere and fast raising of hot plasma up occurs in a period between a maximum of impulsive phase and the beginning of the main phase.

A quite satisfactory relationship was found between the values of the maximum intensity of bright regions of ultraviolet emission at λ1700Å and the magnitude of the enhancement of the electron density, ΔNe^-, arising during the development of flares.

The course of the relative intensity of bright flare plasma at the level of the photosphere coincides with the profile of the derivative of the X-ray flux, and its values are a good index of direct flare enhancement, including the emission of gamma-ray fluxes in the impulsive phase of flare development.

Acknowledgements

Authors express gratitude to groups of the scientists supervising carrying out observations on SDO, GOES, WIND, FERMI spacecrafts for providing the experimental data published on the Internet.

Work is supported by the Program of target financing BR05336383 of Space committee of MOAP of the Republic of Kazakhstan.

Г. Минасянц, Т. Минасянц, В. Вдовиченко, А.Ж. Бибосинов

В.Г. Фесенков атындағы Астрофизикалық институт, Обсерватория-23, Алматы, Қазақстан

КҮН ЖАРҚЫЛЫНЫҢ ДАМУ КЕЗІНДЕГІ УЛЬТРАКҮЛГІН ЭМИССИЯНЫҢ ҚАСИЕТТЕРІ

Аннотация. Solar Dynamics Observatory (SDO) ғарыш аппаратынан алынған, ультракүлгін эмиссиялы λ1700Å, фотогелиограмм көмегімен (температура минимумын, жоғарғы фотосфера) өңдеу, күн жарқылының

импульсті фазаның дамуында фотосфера деңгейіндегі жарық плазманың салыстырмалы интенсивтілігінің ерекшелігі зерттелді. Уақыт бойынша туынды профильді рентген сәулеленуінің (1-8) Å ағынын, ультракүлгінді эмиссиялы жарқылмен өзара байланыстыратын және жарқылдың даму кезіндегі пайда болатын, электрондар тығыздығының күшею шамасының өзгеру жолдары анықталды.

Түйін сөздер: күн жарқылы, фотометрия, эммисиялық жарқыл, гамма сәулелену.

УДК 523.62

Г.С. Минасянц, Т. М. Минасянц, В.Д. Вдовиченко, А.Ж. Бибосинов

Астрофизический институт им. В.Г. Фесенкова, Обсерватория-23, Алматы, Казахстан

СВОЙСТВА УЛЬТРАФИОЛЕТОВОЙ ЭМИССИИ ПРИ РАЗВИТИИ СОЛНЕЧНЫХ ВСПЫШЕК

Аннотация. С помощью обработки фотогелиограмм с ультрафиолетовой эмиссией λ1700Å (температурный минимум, верхняя фотосфера), полученных на космическом аппарате Solar Dynamics Observatory (SDO), проведено изучение поведения относительной интенсивности яркой плазмы на уровне фотосферы при развитии импульсной фазы солнечных вспышек. Выявлена взаимосвязь хода изменения вспышечной ультрафиолетовой эмиссии с профилем производной по времени потока рентгеновского излучения (1-8) Å и с величиной усиления плотности электронов, возникающих при развитии вспышек.

Ключевые слова: солнечные вспышки, фотометрия, эмиссия вспышек, гамма излучение.

.

Information about authors:
1. Minasyants Gennady Sergeevich, Fesenkov Astrophysical Institute, Leading Researcher, gennadii_minasya@mail.ru;
2. Minasyants Tamara Mihailovna, Fesenkov Astrophysical Institute, Senior Researcher, gennadii_minasya@mail.ru;
3. Vdovichenko Vladimir Dementjevich, Fesenkov Astrophysical Institute, Leading Researcher, vdv1942@mail.ru;
4. Bibossinov Assylkhan, AALR «Fesenkov Astrophysical Institute» (AALR «FAI»), director, bibossinov@gmail.com

REFERENCES

[1] Livshits M.A. Solnechnyye vspyshki: rezul'taty nablyudeniy i gazodinamicheskiye protsessy. Plazmennaya geliogeofizika. Pod red. L.M. Zelenogo i I.S. Veselovskogo. M.: Nauka, Tom 1. 60-81. 2008.

[2] Omodei N., Vianello G., Perse-Rollins M. et al. Fermi LAT and GBM detection of the X6.9 Solar Flare of August 9 2011// The Astronomer's Telegram 3552. P.1. 12 Aug 2011.

[3] Ohno M., Takahashi H., Tanaka Y.T., et al. Fermi LAT and GBM detection of the X2.1 Solar Flare of September 6 2011// The Astronomer's Telegram 3635. P.1. 7 Sep 2011.

N E W S
OF THE NATIONAL ACADEMY OF SCIENCES OF THE REPUBLIC OF KAZAKHSTAN
PHYSICO-MATHEMATICAL SERIES
ISSN 1991-346X **https://doi.org/10.32014/2019.2518-1726.25**
Volume 3, Number 325 (2019), 64 – 70

UDC 524.7

S. Shomshekova, E. Denissyuk, R. Valiullin, A. Kusakin, I. Reva, Ch.Omarov

Fesenkov Astrophysical Institute, Almaty, Kazakhstan
shmshekva-saule@mail.ru, eddenis@mail.ru, rashit_valiullin@mail.ru, un7gbd@gmail.com, reva@aphi.kz, chingis.omarov@gmail.com

PHOTOMETRIC RESEARCH OF SEYFERT GALAXIES MRK 766, MRK 6, MRK 1040, MRK 1513

Abstract. The paper presents the results of the photometric observations of the Seyfert galaxies from the Markarian list: MRK 766, MRK 6, MRK 1040, MRK 1513. The observations were carried out on "the Eastern" 1-meter telescope, located at the Tien-Shan Astronomical Observatory of the Fesenkov Astrophysical Institute. The observational data were processed using the MaximDL6 software package. The brightness was estimated by differential photometry, using standard stars in the vicinity of galaxies. This paper presents the light curves of the galaxies: Mrk 766, Mrk 6, Mrk 1040, Mrk 1513. It has been noted, that in Mrk 766, there is a tendency to a gradual weakening of the brightness in the three filters. Photometric changes of the galaxy Mrk 6 during 2016-2019 occurred synchronously in all three filters. The weakening of its brightness began in 2017and by 2019 it reached ~ $0^m.9$. During the investigation period, irregular brightness fluctuations were registered in galaxies Mrk 1040 and Mrk 1513 with amplitudes of ~ 1^m 0 and $0^m.8$, respectively.

Key words: Seyfert galaxies, photometry, B V R values.

Introduction

The regular observations of active galactic nuclei (AGNs) from the list of Markaryan galaxies are carried in Fesenkov Astrophysical Institute since 1971. Variability is the main feature of AGNs. Its maximum manifestations are recorded in the X-ray region [1,2]. It is believed that their brightness variability is associated with inhomogeneities of their accretion disks, flashes, and jets. The study of variability allows to understand the structure of the nuclear regions and to identify the processes responsible for certain observable characteristics. Photometric studies of AGNs in the BVR photometric system have been conducted at AFIF over the past ten years.

The Mrk 766, Mrk 6, Mrk 1040, Mrk 1513 galaxies belong to the Seyfert galaxies (SG) of the NLSy1 class (Seyfert 1 galaxy with narrow emission lines). This subclass of SG, discovered by Osterbrok, is distinguished by the following properties: relatively narrow lines of the Balmer series (FWHM (Hβ) <2000 km / s), strong FeII lines and weak forbidden lines [3].

1. Observations and research methods. Photometric observations of the galaxies from the Markaryan list were carried out on the "Eastern" 1-meter telescope of the Richie-Chretien system (focal length 6.5 m) using the Apogee Alta F16M CCD camera and the Astrodon BVR filter set. The angular scale of the frame with the image of the object corresponds to 0.563 "/ pixel. The MaximDL6 software package was used to process the observational data. The standard procedure of processing consists of correction with the Dark, Bias and Flat field files. The brightness was estimated using differential photometry, standard stars were used located in the vicinity of galaxies. The obtained instrumental data were transferred to the international Johnson-Morgan system using the following equations transition:

$$(B-V)_{calc} = 1,035 \cdot (B-V)_{obs} - 0,013 - 0.0512 \cdot \sec Z$$
$$(V-R)_{calc} = 1.009 \cdot (V-R)_{obs} - 0.0021 - 0.0881 \cdot \sec Z$$
$$V_{calc} = V_{obs} - 0.014 \cdot (B-V)calc - 0.016 - 0.2627 \cdot \sec Z \quad (1)$$
$$B_{calc} = V_{calc} + (B-V)_{calc}$$
$$R_{calc} = V_{calc} - (V-R)_{calc}$$

Typical errors of brightness measurements do not exceed ± $0^m.01$, the real accuracy of the results is limited by the accuracy of the standards [4].

2. Processing and analysis of results.

Mrk766 = NGC4253 refers to the Seyfert galaxies of the Sy1 class with supermassive central body (SMBH). The mass of the central body is 1.29×10^6 M_{Sun} [7]. Equatorial coordinates of the galaxy: α(2000)=$12^h18^m26^s,51552$; δ(2000)=+$29^048'46,5187''$. Red shift z= 0.01271±0.00005.

A star with coordinates α(2000)=$12^h18^m17^s,75547$; δ(2000) = + $29^053'00,4561''$

B=14.72; V=14.2; R=13.0 was used as the photometric standard. The following two stars were chosen as check stars:

- Pul-3-920040 with coordinates α(2000)=$12^h18^m19^s,495$; δ(2000)=+$29^050'53,8036''$, B=16,14; V=15,2;

- GPM 184.6072220+29.83269 with coordinates α(2000)=$12^h18^m25^s,765$; δ(2000)=+$29^049'47,9247''$, B=15,7.

As a rule, such galaxies are characterized by the rapid variability in the X-ray range, the source of which is usually considered to be dynamical processes in the nearest vicinity of the central body (CB) [5, 6].

Table 1 - The light curves of the Sy Mrk 766 in filters B, V, R for 2015-2019.

Date of observation	JD-2440000	B	V	R
10.04.2015	17122	14,57	13,837	12,412
11.04.2015	17123	14,564	13,798	12,351
04.04.2016	17482	14,543	13,813	12,358
15.12.2016	17737	14,745	13,983	12,576
09.02.2017	17793	14,769	13,979	12,571
05.03.2017	17817	14,737	13,973	12,568
08.03.2017	17820	14,728	13,964	12,563
11.06.2017	17915	14,774	14,021	12,615
18.04.2017	17861	14,718	13,961	12,571
11.04.2018	18219	14,894	14,116	12,701
12.04.2018	18220	14,861	14,165	12,686
24.01.2018	18142	14,878	14,108	12,707
05.05.2018	18243	14,818	14,063	12,657
05.06.2018	18274	14,858	14,102	12,68
11.03.2019	18553	14,792	14,047	12,608

Figure 1 shows the light curves of Sy Mrk 766 in BVR filters for the period 2015- 2019

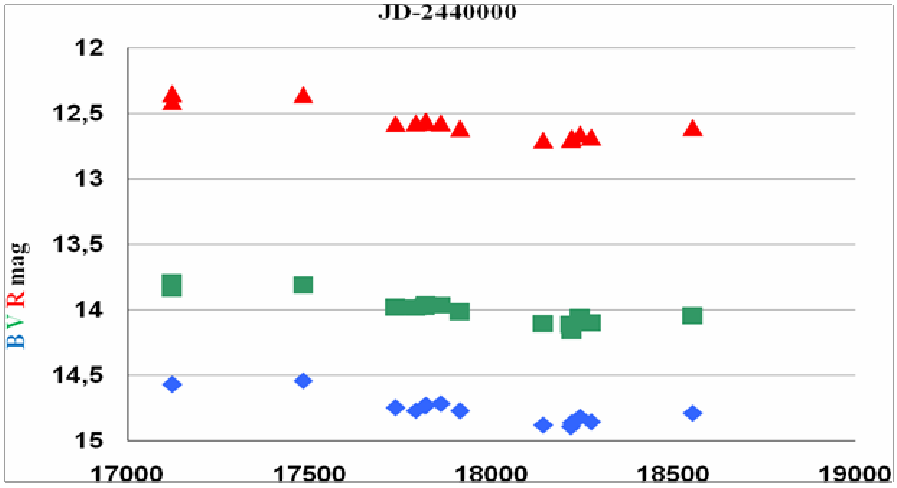

Figure 1 – the light curves of the Sy Mrk 766 in filters B (rhombus), V (square), R (triangle). The X-axis is the Julian date scale, the Y-axis is the magnitudes

Figure 1 shows a tendency to decrease the brightness of the Sy Mrk 766 in the three (BVR) filters.

Mrk 6 = IC450 – Seyfert galaxy with equatorial coordinates: $\alpha(2000)=06^h52^m12^s,323$; $\delta(2000) = +74^0 25' 37,2376''$, red shift $z = 0.018676 \pm 0.000834$.

Distance to the galaxy 79 Mpc. This object belongs to the Sy 1.0-1.5 class. The mass of the central body (CB) of the galaxy is $(1-2) \times 10^8 M_{Sun}$ [8]. In AFIF, observations of Mrk6 in the BVR photometric system have been carried out since 2016.

The star GSC04371-00113 with coordinates $\alpha(2000)=06^h51^m54^s,31965$; $\delta(2000)=+74^0 21' 37,6672''$, B=15,06; V=14,44; R=14,33 was used as the photometric standard. The following two stars were used as the check stars:

- TYC 4771-167-1 with coordinates $\alpha(2000)=06^h51^m02^s,63561$; $\delta(2000)=+74^0 27' 37,7407''$, B=12,81; V=11,32;

- TYC 4371-867-1 with coordinates $\alpha(2000)=06^h52^m01^s,02391$; $\delta(2000)=+74^0 22' 46,0150''$, B=12,07; V=11,16.

Table 2 - Light curves of Sy Mrk 6 in filters B, V, R for 2016-2019.

Date observation	JD-2440000	B	V	R
05.04.2016	17483	14,102	13,477	13,158
24.11.2016	17716	14,153	13,503	13,14
15.12.2016	17737	14,068	13,438	13,097
17.01.2017	17770	14,065	13,433	13,086
27.02.2017	17811	14,272	13,595	13,29
28.03.2017	17840	14,554	13,823	13,411
14.12.2017	18101	15,178	14,301	13,883
27.01.2018	18145	15,123	14,278	13,858
07.01.2019	18490	15,287	14,458	14,029
23.01.2019	18506	15,189	14,375	13,975
29.01.2019	18512	15,081	14,297	13,911
18.03.2019	18560	14,97	14,163	13,756

Figure 2 shows the light curves of Sy Mrk 6 in BVR filters for a specified period of time.

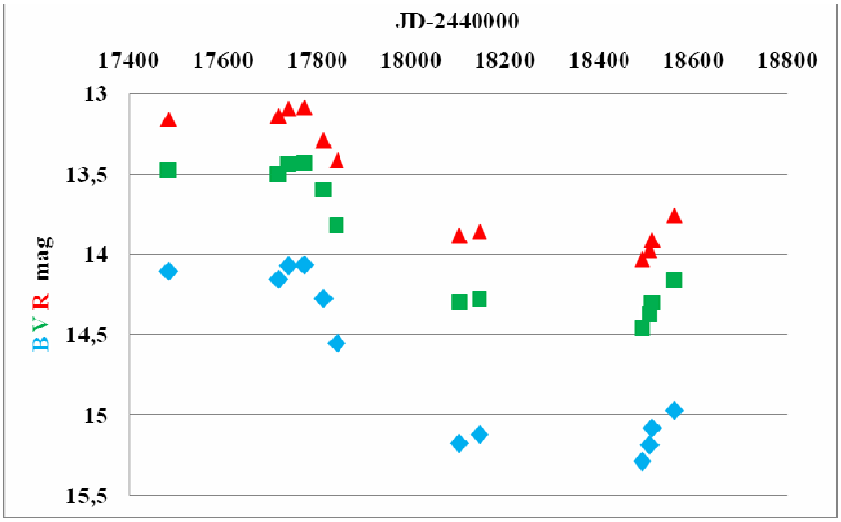

Figure 2 - light curves of the Sy Mrk 6 in filters B (rhombus), V (square), R (triangle).
The X axis is the Julian date scale, the Y axis is the stellar magnitudes

It can be seen from Figure 2 that the weakening of brightness started in early 2017 and by 2019 it reached ~ $0^m.9$. A slight increase of brightness is observed at the end of our observation period. In general, it should be noted that all changes occur synchronously in the three filters (Fig.2).

Mrk1040 = NGC931 – the bright spiral galaxy of Sy1 type. Equatorial coordinates of the galaxy: $\alpha(2000)=02^h28^m14^s,469$; $\delta(2000)=+31^0 18' 41'',467$, red shift $z = 0.016338 \pm 0.000314$. Distance to the galaxy 340 Mpc. The high-resolution spectral data for the Seyfert galaxy Mrk1040, obtained in the X-ray range in 2013- 2014 with the Chandra space telescope, were analyzed in [11].

The mass of the central body is $(7.64 \pm 0.40) \times 10^7 M_{Sun}$ [9]. The physical and spectral characteristics of Mrk 1040 are considered in [11].

The last photometric studies of this galaxy were carried out by Doroshenko et al. In 2005 [12]. In FAPHI Mrk 1040 observations in the BVR photometric system have been made since 2015.

The star TYC 2323-1484-1 with coordinates $\alpha(2000)=02^h27^m48^s,777$; $\delta(2000)=+31^0 21' 40,994''$, B=11,47; V=10,49; R=10,16 was used as the photometric standard The star TYC2323-282-1 with coordinates $\alpha(2000)=02^h27^m59^s,79154$; $\delta(2000)=+31^0 11' 10,4625''$, B=12,29; V=10,97; R=10,476, was chosen as the check star.

Table 3 - Light curves of the SG Mrk1040 in filters B, V, R for 2015-2019.

Date of observation	JD-2440000	B	V	R
10.09.2015	17275	15,253	13,646	13,06
11.09.2015	17276	14,977	13,314	12,861
15.12.2015	17371	15,379	13,86	13,212
20.01.2016	17407	15,527	14,143	13,532
05.09.2016	17636	15,172	13,648	12,947
24.11.2016	17716	15,369	13,852	13,237
13.12.2016	17735	15,481	14,397	13,846
27.08.2017	17992	15,269	13,943	13,357
15.10.2017	18041	15,384	14,166	13,587
13.12.2017	18100	15,408	14,044	13,469
29.01.2018	18147	15,49	14,566	14,05
08.01.2019	18491	15,471	14,37	13,79
28.01.2019	18511	15,504	14,364	13,777

Figure 3 shows the light curves of Sy Mrk1040 in BVR filters for a specified period of time.

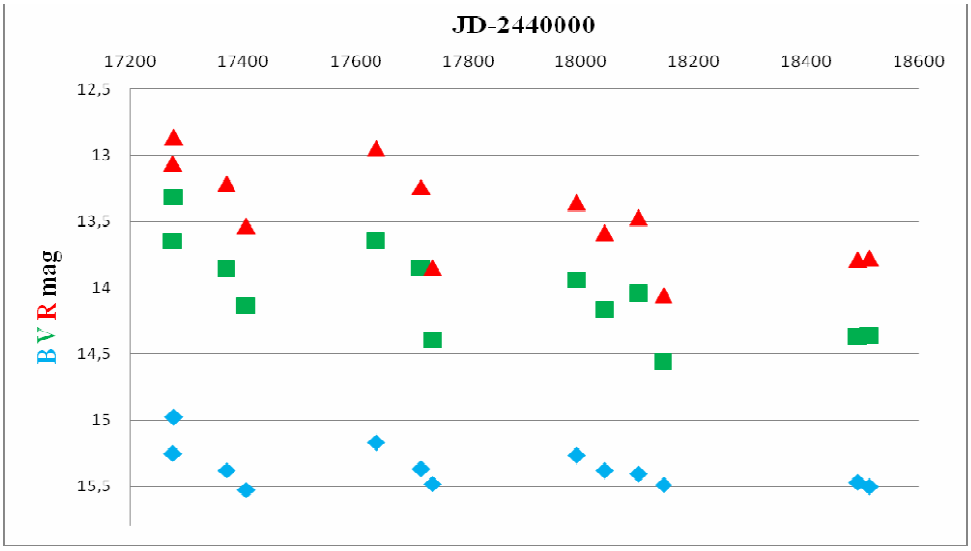

Figure 3 - light curves of the Sy Mrk 1040 in filters B (rhombus), V (square), R (triangle). The X axis is the Julian date scale, the Y axis is the stellar magnitudes

Obtained data indicate that the investigating object is constantly experiencing irregular brightness fluctuations in all three filters with an amplitude of ~ 1^m. In addition, there is a gradual decrease in the average level of brightness (Fig. 3).

2.4 Mrk 1513 = UGC 11763 = II Zw 136 = PG 2130+099. Equatorial coordinates of the galaxy: $\alpha(2000)=21^h32^m27^s,8$; $\delta(2000)=+10^0 08' 19''$, red shift z=0.061990 ±0.000947. Distance to galaxy 257 Mpc.

The bright compact galaxy Mrk 1513 was originally classified as NLSy1 (Seyfert 1 with narrow lines), but in the mid-80s it was "transferred" to the quasar group (radio-quiet, low luminosity quasar). By luminosity ($M=-22^m.9$) this object is located on the border between quasars ($M_{min}=-23^m$) и Sy [13].

In FAPHI, observations of Mrk 1513 in the BVR photometric system have been carried out since 2015.

The star BD +094836 with coordinates $\alpha(2000)=21^h32^m00^s,1017$; $\delta(2000)=+10^0 09' 31,681''$, B=11,1; V=9,98; R=9,48 was used as the photometric standard. A star with coordinates: α (2000) = $21^h32^m22^s,33$; $\delta(2000)=+10^0 07' 49,7''$, B=15,708; V=14,741; R=14,266 was selected as the check one.

Table 4 - Light curves of the Sy Mrk1513 in the B, V, R filters for 2015-2018.

Date of observation	JD-2440000	B	V	R
17.08.2015	17251	14,16	13,125	12,907
18.08.2015	17252	14,503	13,424	13,162
19.08.2015	17253	14,552	13,414	13,38
11.09.2015	17276	14,363	13,252	12,975
16.09.2015	17281	14,615	13,541	13,155
17.09.2015	17282	14,702	13,515	13,147
23.09.2015	17288	14,694	13,836	13,471
06.10.2015	17301	14,327	13,273	13,066
19.06.2016	17558	14,456	13,477	13,146
04.09.2016	17635	14,261	13,231	13
11.06.2017	17915	14,769	13,919	13,621
22.07.2017	17956	14,734	13,768	13,477
30.07.2017	17964	14,728	13,835	13,504
12.10.2017	18038	14,848	13,865	13,489
09.07.2018	18308	14,778	13,823	13,444

Figure 4 shows the light curves for the Sy Mrk 1513 in BVR filters over a specified period of time.

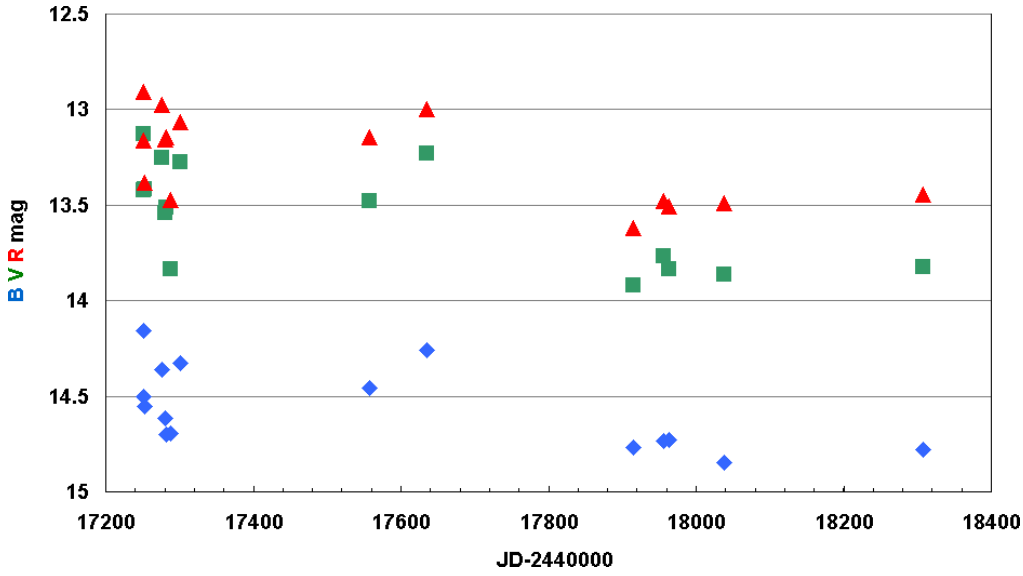

Figure 4 – The light curves of the Sy Mrk 1513 in filters B (rhombus), V (square), R (triangle).
The X axis is the Julian date scale, the Y axis is the stellar values in the BVR filters

High galaxy instability, within $0^m.6$, was observed in 2015. Since mid-2017, the level of the brightness has decreased in all three filters, by about $0^m.8$ and it is still now at a rather low level (Fig.4).

3. Conclusion. Variability of the active nuclei of galaxies from the Markarian list is manifested in a wide range of wavelengths. In particular, the optical variability of different degrees of activity is registered in the all studied objects. During observable period a gradual decrease in the level of brightness were noted in the Sy Mrk 6, Mrk766 and Mrk1513. The results of photometric observations of the Seyfert galaxies in the optical range can be used together with X-ray data to determine the physical and dynamic characteristics of individual zones near the nuclear regions of the AGN and to create adequate models of these objects.

Work is performed within the program «MDDOAT RK № BR05336383»

УДК 524.7

С. Шомшекова, Э. Денисюк, Р. Валлиулин, А. Кусакин, И. Рева, Ч. Омаров

«В.Г. Фесенков атындағы Астрофизика институты» ЕЖШС, Алматы қ.

MRK 766, MRK 6, MRK 1040, MRK 1513 ОБЪЕКТІЛЕРІНЕ ФОТОМЕТЛІК ЗЕРТТЕУЛЕР

Аннотация: Мақалада, Маркарян тізіміндегі: MRK 766, MRK 6, MRK 1040, MRK 1513 сейферт ғаламдарының фотометрлік бақылауларының нәтижелері берілген. Бақылаулар В.Г. Фесенков атындағы Астрофизика институтының Тянь-Шань астрономиялық бақылау базасында орналасқан диаметрі 1 метрлік «шығыс» телескобының көмегімен жүргізілді. Бақылау мәліметтерін өңдеуге MaximDL6 пакет бағдарламасы қолданылды. Ғаламдардың маңында орналасқан стандарт жұлдыздардың көмегімен, объектілердің жарқырауы дифференциалдық әдіс арқылы өлшенді. Жұмыста, Mrk 766, Mrk 6, Mrk 1040, Mrk 1513 жарқырау қисықтары келтірілген. Mrk 766 үш фильтрда біртіндеп жарқырауының азайғаны бақыланады. Mrk 6 ғаламының зерттеу уақыт аралығында (2016-2019жж.) фотометрлік айнымалылық үш фильтр бойынша синхронды. 2017 жылдың басында жарқырауының әлсіреуі байқалады, ~ $0^m.8$. Mrk 1040 және Mrk 1513 ғаламдарының жарқырауы дұрыс емес айнымалы болып келеді, амплитудалары ~1^m (Mrk 1040) және ~ $0^m.8$ (Mrk 1513) жұлдыздық шамаларына тең.

Түйін сөздер: стандартты жұлдыздар, фотометрия, B V R шамалары.

УДК 524.7

С. Шомшекова, Э. Денисюк, Р. Валлиулин, А. Кусакин, И. Рева, Ч. Омаров

ДТОО «Астрофизический институт им. В.Г. Фесенкова», г. Алматы

ФОТОМЕТРИЧЕСКИЕ ИССЛЕДОВАНИЯ СЕЙФЕРТОВСКИХ ГАЛАКТИК MRK 766, MRK 6, MRK 1040, MRK 1513

Аннотация. В статье приводятся результаты фотометрических наблюдений сейфертовских галактик из списка Маркаряна: MRK 766, MRK 6, MRK 1040, MRK 1513. Наблюдения проводились на «восточном» 1-метровом телескопе, расположенном на Тянь-Шаньской астрономической обсерватории Астрофизического института им. В.Г. Фесенкова. Для обработки наблюдательных данных применялся пакет программ MaximDL6. Оценка блеска выполнялось методом дифференциальной фотометрии, использовались стандартные звезды в окрестностях галактик. В работе приводятся кривые блеска галактик: Mrk 766, Mrk 6, Mrk 1040, Mrk 1513. В Mrk 766 выявлена тенденция к постепенному ослаблению блеска в трех фильтрах. Установлено, что фотометрические изменения в галактике Mrk 6 в исследуемый период (2016-2019 гг.) происходили синхронно во всех трех фильтрах. С начала 2017г. началось ослабление её блеска и к началу 2019 г. оно достигло ~ $0^m.9$. Для галактик Mrk 1040 и Mrk 1513 за исследуемый период были характерны нерегулярные колебания блеска с амплитудами ~1^m и ~ $0^m.8$, соответственно.

Ключевые слова: сейфертовские галактики, фотометрия, B V R величины.

Information about authors:

Shomshekova Saule Akhmetbekovna - Home address: Almaty, Shelikhova 163. Place of work – SLLP "V.G. Fesenkov Astrophysical Institute". Researcher lab. physics of stars and nebulae. Phone: 2607591, e-mail: shmshekva-saule @ .mail.ru;

Denissyuk Eduard Konstantinovich - Candidate of Physical and Mathematical Sciences, Associate Professor. Home Address: Almaty, Observatory, 20, ap.18. Place of work - SLLP " V.G. Fesenkov Astrophysical Institute ". Lr. lab. physics of stars and nebulae. Phone: 260-74-99, e-mail: eddenis@mail.ru;

Valiullin Rashit Ravilevich - Candidate of Physical and Mathematical Sciences. Home address: Almaty, 8-md., h.86. ap.10. Place of work – SLLP " V.G. Fesenkov Astrophysical Institute". Deputy director for science “FAPHI”. Phone: 249-69-33, e-mail: rashit_valiullin@mail.ru;

Kusakin Anatoly Vasilyevich - Candidate of Physical and Mathematical Sciences. Home address: Almaty, Kislovodskaya st., h.34.ap.1. Place of work – SLLP " V.G. Fesenkov Astrophysical Institute. ". Lr. lab. physics of stars and nebulae. Phone: 3-999-879, e-mail: un7gbd@gmail.com;

Reva Inna Vladimirovna - Home address: Almaty, Observatory, 23. Place of work - the SLLP “V.G. Fesenkov Astrophysical Institute”. Jr. lab. the physics of stars and nebulae. Phone: +7 707 531 38 55, e-mail: alfekka@list.ru;

Omarov Chingis Tukenovich - Candidate of Physical and Mathematical Sciences (PhD). Home address: Almaty, Observatory. 20. apt. 21. Place of work - SLLP "V.G. Fesenkov Astrophysical Institute". Chief Researcher lab.cosmology, stellar dynamics and computational astrophysics. Phone: +7 777 372 68 12, e-mail: chingis.omarov@gmail.com

REFERENCES

[1] Klimek E., Gaskell M., Hedrick H **2004**. ApJ. V.609. P.69.
[2] Bon, E., Zucker, S., Marziani, P. et al. **2016**. ApJS. V.225. P.29.
[3] Osterbrock D., Pogge R. 1985. ApJ. V. 297. P.166.
[4] S. A. Shomshekova, I. V. Reva, L.N. Kondrat'eva. **2017**.Izvestija NAN RK. Serija fiz.-mat, № 4, 314, C.155-161 (in Russ).
[5] Zhang P., Zhang P., Yan J., et al. **2017.** ApJ. V.849. P.9.
[6] Smith K.L., Mushotzky R., Boyd P., et al. **2018.** ApJ. V.860. L10.
[7] Yao S., Qiao E., Xue-Bing. **2018.** MNRAS. V. 477. P.1356.
[8] Freitas S., Riffel R. A., Storchi-Bergmann T., et al**. 2018**. MNRAS. V.476. P.2760.
[9] De Marco, B., Ponti, G., Cappi, M., et al. **2013.** MNRAS. V.431. P.2441.
[10] Huchra, J., Vogeley, M., Geller, M. **1999.** ApJS. V. 121. P.287.
[11] Reeves J., V. Braito V., E. Behar E., et al. **2017**. AJ. V.837. P.23.
[12] Doroshenko, V. T., Sergeev, S. G.; Merkulova, N. **2005.** Ap. V.48. P.156.
[13] Doroshenko, V. T. **2013.** PZ 33,5.

N E W S
OF THE NATIONAL ACADEMY OF SCIENCES OF THE REPUBLIC OF KAZAKHSTAN
PHYSICO-MATHEMATICAL SERIES
ISSN 1991-346X **https://doi.org/10.32014/2019.2518-1726.26**
Volume 3, Number 325 (2019), 71 – 76

UDC 539.14

A.D. Duisenbay[1], N.ZH. Takibayev[1],
V.S. Vasilevsky[2], V.O. Kurmangaliyeva[1], E.M. Akzhigitova[1]

[1]Kazakh National University named after al-Farabi, Almaty, Kazakhstan;
Bogolyubov Institute for Theoretical Physics, Kiev, Ukraine
aknurka___93@mail.ru, venera_baggi@mail.ru, kzo1994@mail.ru

FORM FACTORS AND DENSITY DISTRIBUTIONS OF PROTONS AND NEUTRONS IN ^{7}Li AND ^{7}Be

Abstract. Form factors and density distribution of protons and neutrons in ^{7}Li and ^{7}Be are investigated within a microscopic two-cluster model. The model correctly treat the Pauli principle and make use of the oscillator basis to expand wave function of two-cluster system. Dynamics of two-cluster system is totally governed by a semirealistic nucleon-nucleon potential. We demonstrate that the model used correctly reproduces form factors for the ground state of ^{7}Li and ^{7}Be.

Key words: two-cluster system, form factors, density distribution, nucleon-nucleon potential etc.

Introduction

In this paper we consider the form factor of the elastic scattering of electron and density distribution of protons and neutrons in light nuclei ^{7}Li and ^{7}Be. In previous paper [1] we have investigated properties of light nuclei ^{5}He, ^{5}Li, ^{6}Li, ^{7}Li, ^{7}Be and ^{8}Be within a microscopic two-cluster model. This model is the algebraic version of the resonating group method. In Ref. [1] main attention was paid to the spectrum and wave functions of bound and resonance states in these nuclei, and also to phase shifts of the elastic two-cluster scattering. It was shown in Ref. [1] that the two-cluster model used correctly reproduces the main properties of light nuclei ^{5}He, ^{5}Li, ^{6}Li, ^{7}Li, ^{7}Be and ^{8}Be. The aim of the present investigations is to obtain complementary information on structure of bounds states in light nuclei ^{7}Li and ^{7}Be. This

Table 1 - Main input parameters of calculations and energy of the ground state in ^{7}Li and ^{7}Be.

Nucleus	Potential	*b,fm*	*m/u*	f_{LS}	E_{GS}, *MeV*
^{7}Li	MP	1.3451	0.969	1.00	-2.468
	MHNP	1.362	0.0002	1.00	-2.467
^{7}Be	MP	1.3451	0.969	1.00	-1.630
	MHNP	1.362	0.0002	1.00	-1.588

will be done within the same two-cluster model. It is well known that the form factor provides information on distribution of charge in a nucleus. Values of the form factor in the region of small transferred momenta allows one to determine the proton root-mean-square radius.

Details of calculations and results

As in previous paper [1], we represent ^{7}Li and ^{7}Be as two-cluster system α+t and α+^{3}He, respectively. We use a common oscillator length *b* to discribe distribution of nucleons in each cluster.

Two semirealistic nucleon-nucleon interactions: the Minnesota potential (MP) [2], [3] and the modified Hasegawa-Nagata potential (MHNP) [4, 5, 6] are employed in our calculations. As in Ref. [1] we select the oscillator length *b* to minimize the two-cluster threshold. We also slightly modified the Majorana parameter *m* of MHNP and the parameter *u* of MP to reproduce the energy of the ground state accounted from the two-

cluster threshold. In Table 1 we display all input parameters of our calculations. In all our calculations we make of 200 oscillator functions. This number of functions guarantees a good precision for the energy and wave functions of bound states, even for weakly bound states. We have also checked that this number of oscillator functions provides form factors and densities distributions with acceptable precision.

Since we consider light nuclei ^{7}Li and ^{7}Be within two-cluster microscopic model, wave function of bound and continuos spectrum states is represented in the following form:

$$\Psi_{EJ^\pi} = \hat{A}\left\{\left[\Phi_1(A_1, s_1)\Phi_2\left(A_{2,}s_2\right)\right]_S \psi^{J^\pi}_{ELS}(q)Y_L(\hat{q})\right\}_J \quad (1)$$

Notations which we are using here are identical to those of Ref. [1].

Since wave functions $\Phi_1(A_1, s_1)$ and $\Phi_2\left(A_{2,}s_2\right)$, describing internal motion of nucleons inside each cluster are known and fixed, thus we have to find the inter-cluster function $\psi^{J^\pi}_{ELS}(q)$ by solving the dynamic equations of the resonating group method (RGM). In the standard version of the RGM, they are the integro-differential equation. In the algebraic version of RGM, which we employ, the dynamic equations are transformed into a set of linear algebraic equations. This is achieved by using a full set of the radial part of oscillator functions$\{\Phi_{\mathrm{nL}}(\mathrm{q},\mathrm{b})\}$. By expanding the inter-cluster function $\psi^{J}_{ELS}(q)$ over oscillator functions

$$\psi^{J}_{ELS}(q) = \sum_{n=0}^{\infty} C_{nL;SJ}\Phi_{nL}(q,b) \quad (2)$$

or the total two-cluster function Ψ_{EJ} over cluster oscillator functions $\{|\ nL;SJ\rangle\}$

$$\Psi_{\mathrm{EJ}} = \sum_{\mathrm{n}=0}^{\infty} \mathrm{C}_{\mathrm{nL;SJ}}|\ nL;SJ\rangle, \quad (3)$$

we arrive to a system of linear algebraic equations

$$\sum_{\mathrm{n}=0}^{\infty}\left\{\langle nL|\hat{H}|\tilde{n}L\rangle - E\langle nL|\tilde{n}L\rangle\right\}\mathrm{C}_{\mathrm{nL;SJ}} = 0. \quad (4)$$

In real calculations, the infinite set of equations (4) can be reduced a finite set of equations. And thus to find energies and wave functions of bound state, we need to obtain eigenvalues and corresponding eigenfunctions of the $N \times N$ matrix

$$\left\|\langle nL|\hat{H}|\tilde{n}L\rangle\right\|_N.$$

It worthwhile noticing that, by assuming that the wave function Ψ_{EJ^π} of a bound state is obtained, one has to calculate the matrix element

$$F_p(q) = \left\langle \Psi_{EJ^\pi}\middle|\hat{F_p}\middle|\Psi_{EJ^\pi}\right\rangle \quad (5)$$

$$F_n(q) = \left\langle \Psi_{EJ^\pi}\middle|\hat{F_n}\middle|\Psi_{EJ^\pi}\right\rangle \quad (6)$$

in order to determine the proton and neutron form factors, and one has also to calculate matrix elements

$$D_p(\boldsymbol{r}) = \left\langle \Psi_{EJ^\pi}\middle|\tfrac{1}{2}\sum_{i=1}^{A}(1+\hat{\tau}_{iz})\delta(\boldsymbol{r}-\boldsymbol{r_i})\middle|\Psi_{EJ^\pi}\right\rangle, \quad (7)$$

$$D_n(\boldsymbol{r}) = \left\langle \Psi_{EJ^\pi}\middle|\tfrac{1}{2}\sum_{i=1}^{A}(1-\hat{\tau}_{iz})\delta(\boldsymbol{r}-\boldsymbol{r_i})\middle|\Psi_{EJ^\pi}\right\rangle, \quad (8)$$

to obtain the density distribution of protons $D_p(\boldsymbol{r})$ and neutrons $D_n(\boldsymbol{r})$. Here the operators $\hat{F_p}$ and $\hat{F_n}$ are

$$\hat{F_p} = \tfrac{1}{2}\sum_{\mathrm{i}=1}^{\mathrm{A}}(1+\hat{\tau}_{iz})\exp\{i(\mathbf{q}\mathbf{r_i})\} \quad (9)$$

$$\hat{F_n} = \tfrac{1}{2}\sum_{\mathrm{i}=1}^{\mathrm{A}}(1-\hat{\tau}_{iz})\exp\{i(\mathbf{q}\mathbf{r_i})\} \quad (10)$$

and the operators $\frac{1}{2}(1+\hat{\tau}_{iz})$ and $\frac{1}{2}(1-\hat{\tau}_{iz})$ are projection operators on proton and neutron state, respectively. In equations (5), (6), (7) and (8), integration is carried out over all spatial, spin and isospin coordinates.

It is worth noticing that by calculating both proton and neutron form factor or densities we can easily construct the matter form factors or densities from the relations

$$F_m(q) = F_p(q) + F_n(q)$$

$$D_m(\boldsymbol{r}) = D_p(\boldsymbol{r}) + D_n(\boldsymbol{r})$$

Recall that the nucleon densities are normalized by the conditions

$$\int d\boldsymbol{r} D_p(\boldsymbol{r}) = Z, \quad \int d\boldsymbol{r} D_n(\boldsymbol{r}) = N, \quad \int d\boldsymbol{r} D_m(\boldsymbol{r}) = A,$$

where Z is the total number of protons, N is the total number of neutrons, and the mass number A=Z+N.

Form factor

In section we consider form factor of elastic scattering of electrons.

The elastic form factors for ground $3/2^-$ states of ^{7}Li and ^{7}Be are presented in Fig. 1. The form factors are calculated with MHNP.

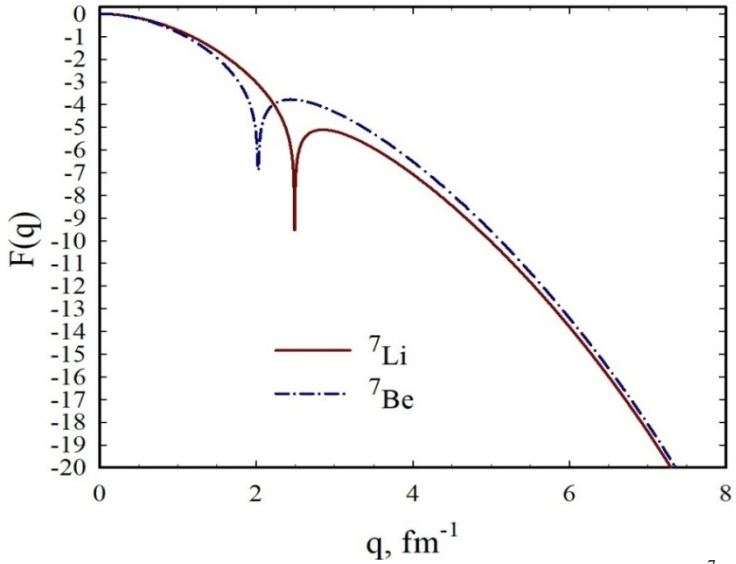

Figure 1 - Form factors of the elastic electron scattering from the ground states of ^{7}Li and ^{7}Be.

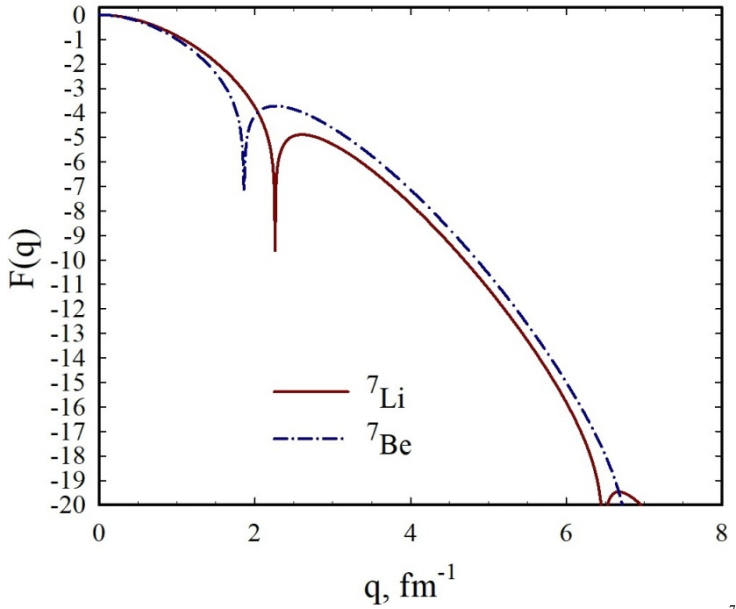

Figure 2 - Form factor F(q) of elastic electron scattering on the first excited $1/2^-$ states in ^{7}Li and ^{7}Be.

In Fig. 2 we display form factor of electron elastic scattering from the excited $1/2^-$ states in ^{7}Li and ^{7}Be. These results are also obtained with MHNP.

On both figures 1 and 2 we use the logarithmic scale and indicate only an exponent of log (F (q)). We can see that the form factors for the ground and first excited states rapidly turn to the zero with increasing of the momentum transfer q. The form factor for the ground state of ^{7}Li has a node at q=2.49 fm^{-1}, while for ^{7}Be the first node appear at q=2.03 fm^{-1}. For the first excited $1/2^-$ states, the position of a node slightly shifted to small values of the momentum transfer q and equals to q=2.26 fm^{-1} for ^{7}Li and equals to q=1.86 fm^{-1} for ^{7}Be.

The present results are in agreement with other microscopic model. For example, the form factors for the ground state of ^{7}Li and ^{7}Be, presented above, are very close to those obtained in Refs. [7], [8], [9] within the other realization of the resonating group method. There is also fairly good agreement with the experimental data Ref. [10].

Density distributions

Now we turn our attention to the density distribution of proton and neutrons. The proton and neutron density distributions for the ^{7}Li ground states are shown in Fig. 3. They are calculated with MHNP. As we see the protons are mainly concentrated at small distances, while the neutron density distribution is more dispersed in the space.

In Figure 4 we display the proton and neutron density distribution for the ground state of ^{7}Be. This nucleus is mirror to the nucleus ^{7}Li, and thus we have inverse picture for proton and neutron density distributions with respect to Fig. 3. Despite that the energy of the ^{7}Be is smaller than the ground state energy of ^{7}Li, both nuclei have similar density distributions of proton and neutron.

Conclusion

We have applied a two-cluster microscopic model to study density distribution of protons and neutrons in light atomic nuclei ^{7}Li and ^{7}Be. We also have studied the form factors of elastic electron scattering from these nuclei. The microscopic model which has been employed is the algebraic version of the resonating group method. The later is using the full set of oscillator functions to expand wave functions of bound and scattering states. Nucleon-nucleon interaction being a key ingredient of any microscopic model was represented by two semirealistic potentials which are often used in two- and three-cluster microscopic models.

It was demonstrated that the present two-cluster model reproduces fairly well the elastic form factors of ^{7}Li and ^{7}Be as a function of the momentum transfer. It was also demonstrated that our results are compatible with results of other theoretical models.

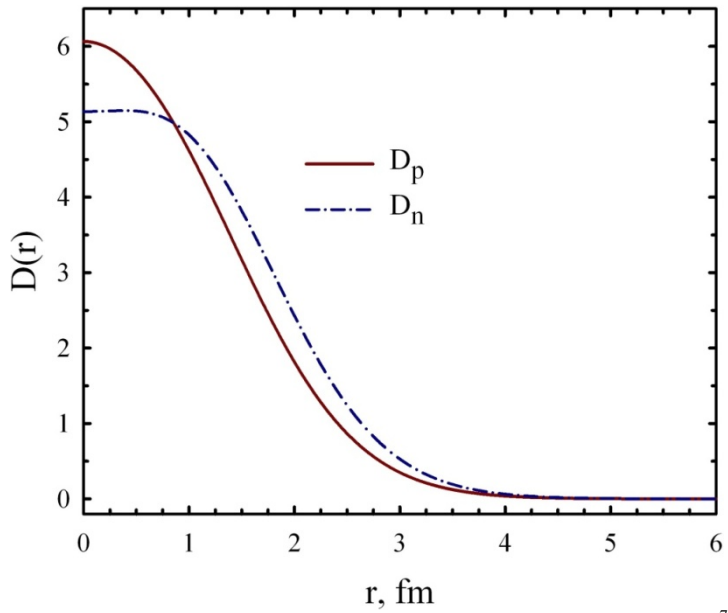

Figure 3 - The proton and neutron density distribution in the ground state of ^{7}Li.

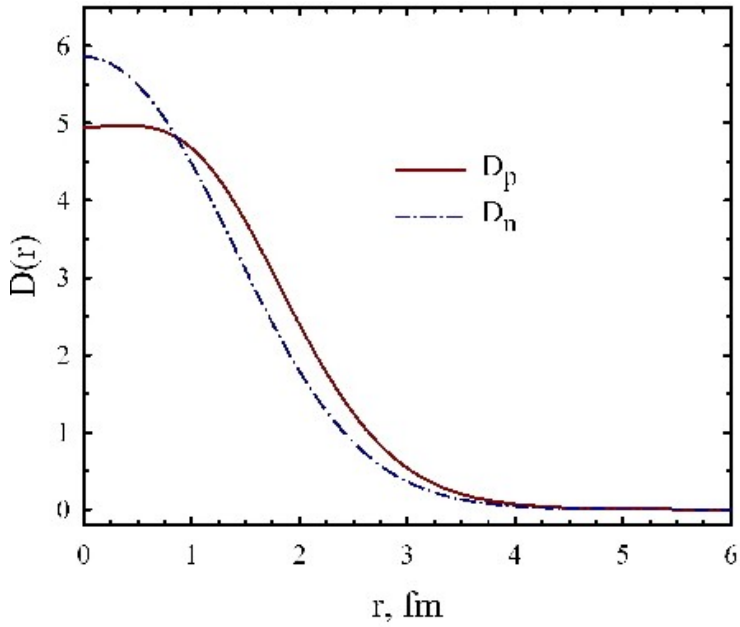

Figure 4 - The proton and neutron density distributions in the ground state of ^{7}Be

Acknowledgment

One of the authors (V.V.) is grateful to the members of the subdepartment of theoretical and nuclear physics from the Physical and Technical Department, al-Farabi Kazakh National University, Almaty, Republic of Kazakhstan, for hospitality and stimulating discussion during his stay at al-Farabi Kazakh National University.

This work was supported in part by the Program of Fundamental Research of the Physics and Astronomy Department of the National Academy of Sciences of Ukraine (Project No. 0117U000239) and by the Ministry of Education and Science of the Republic of Kazakhstan, Research Grant IRN: AP 05132476.

А.Д. Дүйсенбай[1], Н.Ж. Такибаев[1], В.С. Василевский[2], В.О. Құрманғалиева[1], Е.М. Ақжігітова[1]

[1]Әл- Фараби атындағы Қазақ Ұлттық Университеті, Алматы, Қазақстан;
[2]Боголюбов атындағы Теориялық Физика Институты, Киев, Украина

^{7}LI ЖӘНЕ ^{7}BE ЯДРОЛАРЫНДАҒЫ ПРОТОНДАР МЕН НЕЙТРОНДАР ТЫҒЫЗДЫҒЫНЫҢ ТАРАЛУЫ МЕН ФОРМ ФАКТОРЛАРЫ

Аннотация. ^{7}Li және ^{7}Be ядроларындағы нейтрондар мен протондар тығыздығының таралуы мен форм факторлары микроскопиялық екі кластерлік модель ретінде зерттелінді. Бұл модель Паули принципін ескере отырып, екі кластерлік жүйенің толқындық функциясын жіктеу үшін осцилляторлық негізді қолданады. Екі кластерлік жүйенің динамикасы толығымен жартылай реалистік нуклон-нуклондық потенциалымен анықталады. Қолданылып отырған модель ^{7}Li және ^{7}Be ядроларының негізгі күйлері үшін форм-факторды дұрыс беретіндігін көрсетеміз.

Түйін сөздер: екі кластерлік жүйе, форм факторлар, тығыздықтың таралуы, нуклон-нуклондық потенциал және т.б.

А.Д. Дуйсенбай[1], Н.Ж. Такибаев[1], В.С. Василевский[2], В.О. Курмангалиева [1], Э.М. Акжигитова[1]

[1]Казахский национальный университет имени аль-Фараби, Алматы, Казахстан;
[2]Институт Теоретической Физики имени Боголюбова, Киев, Украина

ФОРМ ФАКТОРЫ И РАСПРЕДЕЛЕНИЕ ПЛОТНОСТИ ПРОТОНОВ И НЕЙТРОНОВ В ЯДРАХ ^{7}LI И ^{7}BE

Аннотация. Форм факторы и распределение плотности протонов и нейтронов в ядрах ^{7}Li и ^{7}Be исследованы в рамках микроскопической двухкластерной модели. Модель правильно учитывает принцип Паули и использует осцилляторную основу для разложения волновой функции двухкластерной системы. Динамика двухкластерной системы полностью определяется полуреалистическим нуклон-нуклонным потенциалом. Мы показываем, что используемая модель правильно воспроизводит форм-факторы для основного состояния ^{7}Li и ^{7}Be.

Ключевые слова: двухкластерная система, форм факторы, распределение плотности, нуклон-нуклонный потенциал и т.д.

Information about authors:

Duisenbay A.D. - al-Farabi Kazakh National University, Almaty, Kazakhstan, 1st course PhD student, aknurka___93@mail.ru, ORCID: https://orcid.org/0000-0003-3881-3958;

Takibayev N.Zh. - al-Farabi Kazakh National University, Almaty, Kazakhstan, d.ph.-m.sc., professor, academic of NAS RK, takibayev@gmail.com, ORCID: https://orcid.org/0000-0002-2604-6838;

Vasilevsky V.S. - Bogolyubov Institute for Theoretical Physics, Kiev, Ukraine, professor, vsvasilevsky@gmail.com, ORCID: https://orcid.org/0000-0003-0417-5978;

Kurmangalieva V.O. - al-Farabi Kazakh National University, Almaty, Kazakhstan, c.ph.-m.sc., docent, venera_bagg@mail.ru, ORCID: https://orcid.org/0000-0001-8046-8508;

Akzhigitova E.M. - al-Farabi Kazakh National University, Almaty, Kazakhstan, 1st course PhD student, kzo1994@mail.ru, ORCID: https://orcid.org/0000-0002-8544-1248

REFERENCES

[1] V.S. Vasilevsky, K. Kato, V. Kurmangaliyeva, A.D. Duisenbay, N. Kalzhigitov, N. Takibayev, Investigation of discrete and continuous spectrum states in two-cluster system. Sapporo, Japan: Hokkaido University, 2017

[2] D.R. Thompson, M. LeMere, and Y.C. Tang, Systematic investigation of scattering problems with the resonating-group method, Nucl. Phys., vol. A286, no. 1, pp. 53-66, 1977.

[3] I. Reichstein and Y.C. Tang, Study of N+α system with the resonating group method Nucl. Phys. A, vol. 158, pp. 529-545, Dec. 1970.

[4] A. Hasegawa and S. Nagata, Ground state of ^{6}Li, Prog. Theor. Phys., vol. 45, pp. 1786-1807, 1971.

[5] F. Tanabe, A. Tohsaki and R. Tamagaki, αα scattering at intermediate energies, Prog. Theor. Phys., vol. 53, pp. 677-691, 1975.

[6] M. Odsuren, A.T. Sarsembayeva, G. Khuukhenkhuu, S. Davaa, K. Kato, B. Usukhbayar , Higher excited states of α+α system // News of the National Academy of Sciences of the Republic of Kazakhstan, series of physical-mathematical series. Vol. 2, №324. – 2019. – P.5-8, ISSN 2518-1726, https://doi.org/10.32014/2019.2518-1726.6

[7] T. Kaneko, M. Shirata, H. Kanada, and Y.C. Tang, Neutron and proton form factors of ^{7}Li and ^{7}Be, Phys. Lett. B, vol. 192, pp. 259-262, July 1987.

[8] H. Kanada, Q.K.K. Liu and Y.C. Tang, Charge form factor of ^{7}Li with resonating-group wave function, Phys. Rev. C, vol. 22, pp. 813-822, Aug. 1980.

[9] T. Kajino, T. Matsuse and A. Arima, Electromagnetic properties of ^{7}Li and ^{7}Be in a cluster model, Nucl. Phys. A, vol. 413, p. 323, Jan. 1984.

[10]L.R. Suelzle, M.R. Yearian, and H.Crannell, Elastic Electron Scattering from Li^6 and Li^7, Phys. Rev., vol. 162, pp. 992-1004, Oct. 1967.

N E W S
OF THE NATIONAL ACADEMY OF SCIENCES OF THE REPUBLIC OF KAZAKHSTAN
PHYSICO-MATHEMATICAL SERIES
ISSN 1991-346X **https://doi.org/10.32014/2019.2518-1726.27**
Volume 3, Number 325 (2019), 77 – 84

UDC 517.62/64, 517.968.7, 517.977.1/5
MRNTI 27.33.19; 27.37.17; 27.41.19

A.T.Assanova[1,2], E.A.Bakirova[1,2,3], Zh.M.Kadirbayeva[1,2,4]

[1] Institute of Mathematics and Mathematical Modeling, Almaty, Kazakhstan;
[2]Institute of Information and Computational Technologies, Almaty, Kazakhstan;
[3]Kazakh National Women's Teacher Training University, Almaty, Kazakhstan;
[4]International Information Technology University, Almaty, Kazakhstan
assanova@math.kz, bakirova1974@mail.ru, zh.kadirbayeva@gmail.com

NUMERICAL IMPLEMENTATION OF SOLVING A BOUNDARY VALUE PROBLEM FOR A SYSTEM OF LOADED DIFFERENTIAL EQUATIONS WITH PARAMETER

Abstract. A linear two-point boundary value problem for the loaded differential equations with parameter is considered. This problem is investigated by parameterization method. We offer algorithm for solving to boundary value problem for the system of loaded differential equations with parameter. In first, original problem is reduced to equivalent problem consisting the Cauchy problems for system of ordinary differential equations with parameters in subintervals and functional relations with respect to introduced additional parameters. At fixed values of parameters the Cauchy problem for system of ordinary differential equations in subinterval has a unique solution. This solution is represented with fundamental matrix of system. Using these representations we compile a system of linear algebraic equations with respect to parameters. We proposed algorithm for finding of numerical solution to the equivalent problem. This algorithm includes of the numerical solving of the Cauchy problems for system of the ordinary differential equations and solving of the linear system of algebraic equations. For numerical solving of the Cauchy problem we apply the Runge–Kutta method of 4th order. The proposed numerical implementation is illustrated by example.

Key words: boundary value problem with parameter, loaded differential equation, numerical method, algorithm.

Funding: The work was supported by grants (№№ AP05132486, AP05131220, AP05132455) of Ministry of Education and Science of the Republic of Kazakhstan (2018-2020).

As well-known, the problem of constructing effective models finds its solution in many areas of science and technology. The active development of computer technology in recent decades, the emergence of new software tools designed to automate professional activity, has significantly affected the methods for solving the problems of identification of parameters. The application of software tools specialized in the field of scientific, technical and engineering calculations provides an opportunity for a deeper study of the investigated area, transferring the main burden of solving the problems from the development, debugging of algorithms and programs to the study of qualitative and numerical characteristics of the problem. Therefore, a modern approach in the theory of control and identification of parameters should be directed to the development of new constructive methods and modifications of known methods for solving boundary value problems for loaded differential equations with parameters. The theory of boundary value problems for the loaded differential equations with parameters is rapidly developing and is used in various fields of applied mathematics, biophysics, biomedicine, chemistry, etc. [1-10]. In spite of this, the questions of finding the effective criterions of unique solvability and constructing the numerical algorithms for finding the solutions of boundary value problems for the system of loaded differential equations with parameters still remain open. One of the constructive

methods for investigating and solving the boundary value problems with parameters for the system of ordinary differential equations is the parameterization method [11]. The parameterization method was developed for the investigating and solving the boundary value problems for the system of ordinary differential equations. On the basis of this method, coefficient criteria for the unique solvability of linear boundary value problems for the system of ordinary differential equations were obtained. Algorithms for finding the approximate solutions were also proposed and their convergence to the exact solution of the problem studied was established. Later, the parameterization method was developed for the two-point boundary value problems for the Fredholm integro-differential equations [12-16]. Necessary and sufficient conditions for the solvability and unique solvability are established, the algorithms for finding the approximate solutions of the problems considered are constructed. In [17], methods for investigating and solving the linear boundary value problems for the linear Fredholm integro-differential equation on the basis of new algorithms of parameterization method are constructed. In [18] this algorithm is used for solve boundary value problem for system of ordinary differential equations with parameter.

In present paper the proposed new algorithms of parameterization method are extended to boundary value problem for loaded differential equations with parameters. We offer the numerical implementation of these algorithms to solve boundary value problem for the loaded differential equations with parameters.

So, we consider the linear boundary value problem for the loaded differential equations with parameter

$$\frac{dx}{dt} = A(t)x + \sum_{j=0}^{N} K_j(t)x(\theta_j) + A_0(t)\mu + f(t), \quad x \in R^n, \quad \mu \in R^m, \ t \in (0,T), \quad (1)$$

$$Bx(0) + Cx(T) + B_0\mu = d, \quad d \in R^{n+m}, \quad (2)$$

where the $(n \times n)$-matrices $A(t), K_j(t), \quad j = \overline{0,N}$, $(n \times m)$-matrix $A_0(t)$, and n-vector-function $f(t)$ are continuous on $[0,T]$, the $((n+m) \times n)$ - matrices B, C, the $((n+m) \times m)$ - matrix B_0 are constants.

Let $C([0,T],R^n)$ denote the space of continuous functions $x:[0,T] \to R^n$ with the norm $\|x\|_1 = \max\limits_{t \in [0,T]} \|x(t)\|$. A solution to problem (1), (2) is a pair $(\mu^*, x^*(t))$, with $x^*(t) \in C([0,T],R^n)$, $\mu^*(t) \in R^m$, where the function $x^*(t)$ is continuously differentiable on $(0,T)$ and satisfies the loaded differential equation (1) and boundary condition (2) with $\mu = \mu^*$.

Given the points: $\theta_0 = 0 < \theta_1 < \theta_2 < \ldots < \theta_{N-1} < \theta_N = T$, and let $\Delta_N(\theta)$ be the partition of interval $[0,T)$ into N subintervals: $[0,T) = \bigcup\limits_{r=1}^{N} [\theta_{r-1}, \theta_r)$.

By $C([0,T],\Delta_N,R^{nN})$ we denote the space of function systems $x[t] = (x_1(t), x_2(t), \ldots, x_N(t))$, where $x_r : [\theta_{r-1}, \theta_r) \to R^n$ are continuous and have finite left-hand limits $\lim\limits_{t \to \theta_r - 0} x_r(t)$ for all $r = \overline{1,N}$, with the norm $\|x\|_2 = \max\limits_{r=\overline{1,N}} \sup\limits_{t \in [\theta_{r-1}, \theta_r)} \|x_r(t)\|$.

Denote by $x_r(t)$ the restriction of function $x(t)$ to the r-th interval $[\theta_{r-1}, \theta_r)$ and reduce problem (1), (2) to the equivalent multipoint boundary value problem with parameter for the loaded differential equations

$$\frac{dx_r}{dt} = A(t)x_r + \sum_{j=0}^{N-1} K_j(t)x_{j+1}(\theta_j) + K_N(t)x(\theta_N) + A_0(t)\mu + f(t), \quad (3)$$

$$t \in (\theta_{r-1}, \theta_r), r = \overline{1,N},$$

$$Bx_1(0) + Cx_N(T) + B_0\mu = d, \quad (4)$$

$$\lim_{t\to\theta_s-0} x_s(t) = x_{s+1}(\theta_s), \quad s=\overline{1,N-1}, \tag{5}$$

$$\lim_{t\to\theta_N-0} x_N(t) = x(\theta_N), \tag{6}$$

where (5), (6) are conditions for matching the solution at the interior points of partition $\Delta_N(\theta)$ and at the point $t=\theta_N$.

The solution of problem (3) - (6) is the triple $(\mu^*, x^*(\theta_N), x^*[t])$ with elements $\mu^* \in R^m$, $x^*(\theta_N) \in R^n$, $x^*[t] = (x_1^*(t), x_2^*(t), \ldots, x_N^*(t)) \in C([0,T], \Delta_N, R^{nN})$, where functions $x_r^*(t)$, $r=\overline{1,N}$, are continuously differentiable on $[\theta_{r-1}, \theta_r)$, which satisfies system of loaded differential equations (3) and boundary condition (4) with $\mu = \mu^*$ and continuity conditions (5), (6).

We introduce additional parameters $\lambda_r = x_r(\theta_{r-1})$, $r=\overline{1,N}$, and $\lambda_{N+1} = x(\theta_N)$, $\lambda_{N+2} = \mu$. Making the substitution $u_r(t) = x_r(t) - \lambda_r$, on every $r-$th interval $[\theta_{r-1}, \theta_r)$, $r=\overline{1,N}$, we obtain multipoint boundary value problem with parameters

$$\frac{du_r}{dt} = A(t)(u_r + \lambda_r) + \sum_{j=0}^{N} K_j(t)\lambda_{j+1} + A_0(t)\lambda_{N+2} + f(t), \quad t \in [\theta_{r-1}, \theta_r), \quad p=\overline{1,N}, \tag{7}$$

$$u_r(\theta_{r-1}) = 0, \quad p=\overline{1,N}, \tag{8}$$

$$B\lambda_1 + C\lambda_{N+1} + B_0\lambda_{N+2} = d, \tag{9}$$

$$\lambda_s + \lim_{t\to\theta_s-0} u_s(t) = \lambda_{s+1}, \quad s=\overline{1,N}. \tag{10}$$

A pair $(\lambda^*, u^*[t])$ with elements $\lambda^* = (\lambda_1^*, \lambda_2^*, \ldots, \lambda_{N+1}^*, \lambda_{N+2}^*) \in R^{nN+m}$, $u^*[t] = (u_1^*(t), u_2^*(t), \ldots, u_N^*(t)) \in C([0,T], \Delta_N, R^{nN})$, is said to be a solution to problem (7)-(10) if the functions $u_r^*(t)$, $r=\overline{1,N}$ are continuously differentiable on $[\theta_{r-1}, \theta_r)$, and satisfy (7) and additional conditions (9), (10) with $\lambda_j = \lambda_j^*$, $j=\overline{1,N+2}$, and initial conditions (8).

Problem (1), (2) is equivalent to problem (7)-(10) in the following sense. If a pair $(\lambda^*, u^*[t])$ is a solution to problem (7)-(10), then the pair $(x^*[t], \mu^*)$ with function $x^*(t)$ defined by the equalities $x^*(t) = \lambda_r^* + u_r^*(t)$, $t \in [\theta_{r-1}, \theta_r)$, $r=\overline{1,N}$, $x^*(T) = \lambda_{N+1}^*$, $\mu^* = \lambda_{N+2}^*$, is a solution to problem (1), (2). Conversely, if a pair $(\tilde{x}(t), \tilde{\mu})$ is a solution to problem (1), (2) and $\tilde{\lambda}_r = \tilde{x}(\theta_{r-1})$, $\tilde{\lambda}_{N+1} = \tilde{x}(\theta_N)$, $\tilde{\lambda}_{N+2} = \tilde{\mu}$, $\tilde{u}_r(t) = \tilde{x}(t) - \tilde{x}(\theta_{r-1})$, $t \in [\theta_{r-1}, \theta_r)$, $r=\overline{1,N}$, then the pair $(\tilde{\lambda}, \tilde{u}[t])$ with $\tilde{\lambda} = (\tilde{\lambda}_1, \tilde{\lambda}_2 \ldots, \tilde{\lambda}_{N+1}, \tilde{\lambda}_{N+2}) \in R^{nN+m}$, and $\tilde{u}[t] = (\tilde{u}_1(t), \tilde{u}_2(t), \ldots, \tilde{u}_N(t))$, is a solution to problem (7)- (10).

Let $X(t)$ be a fundamental matrix to the differential equation $\frac{dx}{dt} = A(t)x$ on $[\theta_{r-1}, \theta_r)$, $r=\overline{1,N}$.

Then the unique solution to the Cauchy problem for the system of ordinary differential equations (7), (8) at the fixed values $\lambda = (\lambda_1, \lambda_2 \ldots, \lambda_{N+1}, \lambda_{N+2})$ has the following form

$$u_r(t) = X(t)\int_{\theta_{r-1}}^{t} X^{-1}(\tau)A(\tau)d\tau\cdot\lambda_r + X(t)\int_{\theta_{r-1}}^{t} X^{-1}(\tau)\sum_{j=0}^{N} K_j(t)d\tau\lambda_{j+1} +$$

$$+ X(t)\int_{\theta_{r-1}}^{t} X^{-1}(\tau)A_0(\tau)d\tau\lambda_{N+2} + X(t)\int_{\theta_{r-1}}^{t} X^{-1}(\tau)f(\tau)d\tau,\ \ t\in(\theta_{r-1},\theta_r),\ \ r=\overline{1,N}. \quad (11)$$

Substituting (11) into continuity conditions (10) and taking into account (9), we get the system of algebraic equations with respect to unknown parameters $\lambda=(\lambda_1,\lambda_2,\ldots,\lambda_{N+1},\lambda_{N+2})\in R^{nN+m}$:

$$B\lambda_1 + C\lambda_{N+1} + B_0\lambda_{N+2} = d, \quad (12)$$

$$\lambda_s + X(\theta_s)\int_{\theta_{s-1}}^{\theta_s} X^{-1}(\tau)A(\tau)d\tau\cdot\lambda_r + X(\theta_s)\int_{\theta_{s-1}}^{\theta_s} X^{-1}(\tau)\sum_{j=0}^{N} K_j(\tau)d\tau\lambda_{j+1} - \lambda_{s+1} +$$

$$+ X(\theta_s)\int_{\theta_{s-1}}^{\theta_s} X^{-1}(\tau)A_0(\tau)d\tau\cdot\lambda_{N+2} + X(\theta_s)\int_{\theta_{s-1}}^{\theta_s} X^{-1}(\tau)f(\tau)d\tau = 0, \quad s=\overline{1,N}. \quad (13)$$

Denoting by $Q_{\bullet}(\Delta_N)$ the matrix corresponding to the left-hand side of system (12), (13) which is consist of the coefficients at the parameters λ_r, $r=\overline{1,N+2,}$ and then introducing the vector

$$F_*(\Delta_N)=\left(-d, X(\theta_1)\int_{\theta_0}^{\theta_1} X^{-1}(\tau)f(\tau)d\tau,\ldots, X(\theta_N)\int_{\theta_{N-1}}^{\theta_N} X^{-1}(\tau)f(\tau)d\tau\right),$$

we write the system (12), (13) as:

$$Q_*(\Delta_N)\lambda = -F_*(\Delta_N), \quad \lambda\in R^{nN+m}. \quad (14)$$

The boundary value problem (1), (2) is solved by the following algorithm:

As can be seen from the equations (12), (13), the coefficients and right-hand side of the system (14) are composed of solutions to the Cauchy problems

$$\frac{dz}{dt} = A(t)z + A(t), \quad z(\theta_{r-1})=0, \quad r=\overline{1,N}, \quad (15)$$

$$\frac{dz}{dt} = A(t)z + K_j(t), \quad z(\theta_{r-1})=0, \quad r=\overline{1,N}, \quad (16)$$

$$\frac{dz}{dt} = A(t)z + A_0(t), \quad z(\theta_{r-1})=0, \quad r=\overline{1,N}, \quad (17)$$

$$\frac{dz}{dt} = A(t)z + f(t), \quad z(\theta_{r-1})=0, \quad r=\overline{1,N}. \quad (18)$$

Construct the following algorithm for the numerical solving of two-point boundary value problem for the systems of loaded differential equations with parameter by applying the Runge–Kutta method of 4th order for numerical solving of the Cauchy problem (15) – (18).

Suppose we have a partition $\theta_0 = 0 < \theta_1 < \ldots < \theta_{N-1} < \theta_N = T$. Divide each subinterval $[\theta_{i-1},\theta_i),\ i=\overline{1,N}$, into N_i parts. Define the approximate values of coefficients and right-hand side of (14) via solutions to the Cauchy matrix and vector problems obtained using the Runge–Kutta method of 4th order with step $h_i=(\theta_i-\theta_{i-1})/N_i,\ i=\overline{1,N}$. Then we obtain the following approximate system of algebraic equations with respect to parameters λ:

$$Q_*^{\tilde{h}}(\Delta_N)\lambda = -F_*^{\tilde{h}}(\Delta_N), \quad \lambda\in R^{nN+m}. \quad (19)$$

Solving the system of linear algebraic equations (19) we find $\lambda^{\tilde{h}} \in R^{nN+m}$.

As noted above, $\lambda^{\tilde{h}} = \left(\lambda_1^{\tilde{h}}, \lambda_2^{\tilde{h}}, ..., \lambda_{N+2}^{\tilde{h}}\right) \in R^{nN+m}$ components are the values of approximate solution to problem (1), (2) at the initial points of subintervals:

$$x^{\tilde{h}_r}(\theta_0) = \lambda_1^{\tilde{h}},\ x^{\tilde{h}_r}(\theta_1) = \lambda_2^{\tilde{h}},\ ...,\ x^{\tilde{h}_r}(\theta_N) = \lambda_{N+1}^{\tilde{h}},\ \mu^{\tilde{h}_r} = \lambda_{N+2}^{\tilde{h}}.$$

Applying the Runge–Kutta method of 4th order for numerical solving of Cauchy problem

$$\frac{dx}{dt} = A(t)x + \sum_{j=0}^{N} K_j(t)\lambda_{j+1}^{\tilde{h}} + A_0\lambda_{N+2}^{\tilde{h}} + f(t),$$

$$x(\theta_{r-1}) = \lambda^{\tilde{h}},\ t \in [\theta_{r-1}, \theta_r), \quad r = \overline{1, N},$$

we determine the numerical solution to problem (1), (2). To illustrate the proposed approach of the numerical solving of two-point boundary value problem for systems of loaded differential equations with parameter (1), (2) based on the parametrization method, let us consider the following example

Example. Consider on $[0,T]$ the linear two-point boundary value problem for the systems of loaded differential equations with parameter:

$$\frac{dx}{dt} = A(t)x + K_0(t)x(\theta_0) + K_1(t)x(\theta_1) + K_2(t)x(\theta_2) + A_0(t)\mu + f(t),$$

$$t \in [0,T],\ x \in R^2,\ \mu \in R^3, \tag{20}$$

$$Bx(0) + Cx(T) + B_0\mu = d,\ d \in R^5, \tag{21}$$

where $A(t) = \begin{pmatrix} t^2 & t+1 \\ 2 & 3t \end{pmatrix}$, $K_0(t) = \begin{pmatrix} t & 2 \\ t^2 & t-4 \end{pmatrix}$, $K_1(t) = \begin{pmatrix} 8 & t^2+1 \\ t & 3t \end{pmatrix}$, $K_2(t) = \begin{pmatrix} t^3 & 0 \\ t & 4 \end{pmatrix}$,

$$A_0(t) = \begin{pmatrix} 1 & t & t^2 \\ t+3 & 2 & t^3 \end{pmatrix}, \quad f(t) = \begin{pmatrix} -2t^4 - 2t^3 - \frac{59}{8}t^2 + 7t + \frac{101}{8} \\ -3t^4 - 12t^3 + 2t^2 + \frac{117}{8}t - 5 \end{pmatrix},$$

$$B = \begin{pmatrix} 1 & 0 \\ 2 & 1 \\ 3 & -2 \\ 0 & 4 \\ 7 & 9 \end{pmatrix},\ C = \begin{pmatrix} 5 & -2 \\ 0 & 4 \\ 5 & 3 \\ 8 & 11 \\ 7 & 8 \end{pmatrix},\ B_0 = \begin{pmatrix} 1 & 3 & -5 \\ 0 & 2 & 4 \\ 4 & -2 & 3 \\ -1 & 3 & 8 \\ 4 & -2 & 0 \end{pmatrix},\ d = \begin{pmatrix} -51 \\ 28 \\ 36 \\ 57 \\ -17 \end{pmatrix}.$$

In this example, the matrix of differential part is variable and the construction of fundamental matrix fails. We use a numerical implementation of algorithm of the parametrization method. Below we provide the results of numerical implementation of the algorithm by partitioning the subintervals [0,0.5], [0.5,1] with step $h_1 = h_2 = 0.05$.

Solving the system of equations (19) we obtain the numerical values of the parameters:

$$\lambda_1^{\tilde{h}} = \begin{pmatrix} -0.99999562 \\ -2.00000517 \end{pmatrix},\ \lambda_2^{\tilde{h}} = \begin{pmatrix} -0.74999836 \\ -1.62499829 \end{pmatrix},\ \lambda_3^{\tilde{h}} = \begin{pmatrix} 0.00000017 \\ 0.00000511 \end{pmatrix}.$$

We find the numerical solutions at the other points of the subintervals applying the Runge-Kutta method of the 4th order to the following Cauchy problems:

$$\frac{dx_1}{dt} = A(t)x_1 + K_0(t)\lambda_1^{\tilde{h}} + K_1(t)\lambda_2^{\tilde{h}} + K_2(t)\lambda_3^{\tilde{h}} + B(t)\lambda_4^{\tilde{h}} + f(t), \quad t \in \left[0, \frac{1}{2}\right), \quad x_1(0) = \lambda_1^{\tilde{h}},$$

$$\frac{dx_2}{dt} = A(t)x_2 + K_0(t)\lambda_1^{\tilde{h}} + K_1(t)\lambda_2^{\tilde{h}} + K_2(t)\lambda_3^{\tilde{h}} + B(t)\lambda_4^{\tilde{h}} + f(t), \quad t \in \left[\frac{1}{2}, 1\right), \quad x_2\left(\frac{1}{2}\right) = \lambda_2^{\tilde{h}}.$$

The exact solution of the problem (20)-(21) is a pair $(\mu^*, x^*(t))$, where $\mu^* = \begin{pmatrix} 1 \\ -2 \\ 9 \end{pmatrix}$,

$x^*(t) = \begin{pmatrix} t^2 - 1 \\ t^3 + t^2 - 2 \end{pmatrix}, \quad t \in [0,1].$

The results of calculations of numerical and exact solutions at the partition points are presented in the following table:

t	$\tilde{x}_1(t)$ (numerical solution)	$x_1^*(t)$	$\tilde{x}_2(t)$ (numerical solution)	$x_2^*(t)$
0	-0.99999562	-1	-2.00000517	-2
0.05	-0.99749604	-0.9975	-1.99737924	-1.997375
0.1	-0.98999643	-0.99	-1.98900339	-1.989
0.15	-0.97749678	-0.9775	-1.97412762	-1.974125
0.2	-0.9599971	-0.96	-1.9520019	-1.952
0.25	-0.93749739	-0.9375	-1.92187622	-1.921875
0.3	-0.90999764	-0.91	-1.88300059	-1.883
0.35	-0.87749786	-0.8775	-1.83462498	-1.834625
0.4	-0.83999805	-0.84	-1.7759994	-1.776
0.45	-0.79749822	-0.7975	-1.70637383	-1.706375
0.5	-0.74999836	-0.75	-1.62499829	-1.625
0.55	-0.69749848	-0.6975	-1.53112275	-1.531125
0.6	-0.63999858	-0.64	-1.42399724	-1.424
0.65	-0.57749867	-0.5775	-1.30287174	-1.302875
0.7	-0.50999875	-0.51	-1.16699627	-1.167
0.75	-0.43749884	-0.4375	-1.01562083	-1.015625
0.8	-0.35999893	-0.36	-0.84799544	-0.848
0.85	-0.27749906	-0.2775	-0.66337012	-0.663375
0.9	-0.18999923	-0.19	-0.46099489	-0.461
0.95	-0.09749948	-0.0975	-0.2401198	-0.240125
1	0.00000017	0	0.00000511	0

$\tilde{\mu}_1 = \lambda_{41}^{\tilde{h}}$ (numerical solution)	μ_1^*	$\tilde{\mu}_2 = \lambda_{42}^{\tilde{h}}$ (numerical solution)	μ_2^*	$\tilde{\mu}_3 = \lambda_{43}^{\tilde{h}}$ (numerical solution)	μ_3^*
0.9999919	1	-2.00000308	-2	8.99999553	9

For the difference of the corresponding values of the exact and constructed solutions of the problem the following estimate is true:

$$\max \left\| \mu^* - \tilde{\mu} \right\| < 0.0000081,$$

$$\max_{j=0,20} \left\| x^*(t_j) - \tilde{x}(t_j) \right\| < \varepsilon, \quad \varepsilon = 0.000005.$$

УДК 517.62/64, 517.968.7, 517.977.1/5
МРНТИ 27.33.19; 27.37.17; 27.41.19

А.Т. Асанова[1,2], Э.А. Бакирова[1,2,3], Ж.М. Кадирбаева[1,2,4]

[1]Математика және математикалық модельдеу институты, Алматы, Қазақстан
[2]Ақпараттық және есептеуіш технологиялар институты, Алматы, Қазақстан
[3]Қазақ Ұлттық қыздар педагогикалық университеті, Алматы, Қазақстан
[4]Халықаралық ақпараттық технологиялар университеті, Алматы, Қазақстан

ПАРАМЕТРІ БАР ЖҮКТЕЛГЕН ДИФФЕРЕНЦИАЛДЫҚ ТЕҢДЕУЛЕР ЖҮЙЕСІ ҮШІН ШЕТТІК ЕСЕПТІ ШЕШУДІҢ САНДЫҚ ЖҮЗЕГЕ АСЫРЫЛУЫ

Аннотация. Параметрі бар жүктелген дифференциалдық теңдеулер үшін сызықты екі нүктелі шеттік есеп қарастырылады. Аталған есеп параметрлеу әдісі арқылы зерттеледі. Параметрі бар жүктелген дифференциалдық теңдеулер жүйесі үшін шеттік есептің шешімін табудың алгоритмі ұсынылады. Алдымен бастапқы есеп ішкіаралықтардағы параметрлері бар жәй дифференциалдық теңдеулер жүйесі үшін Коши есебін және енгізілген параметрлерге қатысты функционалдық қатынастарды қамтитын пара-пар есепке келтіріледі. Параметрлердің бекітілген мәнінде ішкіаралықтағы жәй дифференциалдық теңдеулер жүйесі үшін Коши есебінің жалғыз шешімі бар болады. Бұл шешім жүйенің фундаменталдық матрицасы арқылы кейіптеледі. Осы кейіптемелерді пайдалана отырып параметрлерге қатысты сызықты алгебралық теңдеулер жүйесін құрамыз. Пара-пар есептің сандық шешімін табуға арналған алгоритм ұсынылады. Бұл алгоритм жәй дифференциалдық теңдеулер жүйесі үшін Коши есептерін сандық шешуді және алгебралық теңдеулер жүйесін шешуді қамтиды. Коши есептерін сандық түрде шешу үшін төртінші ретті Рунге-Куттаның әдісі қолданылады. Ұсынылып отырған сандық жүзеге асырылу мысалмен көрнектеледі.

Кілттік сөздер: параметрі бар шеттік есеп, жүктелген дифференциалдық теңдеу, сандық әдіс, алгоритм.

УДК 517.62/64, 517.968.7, 517.977.1/5
МРНТИ 27.33.19; 27.37.17; 27.41.19

А.Т. Асанова[1,2], Э.А. Бакирова[1,2,3], Ж.М. Кадирбаева[1,2,4]

[1]Институт математики и математического моделирования, Алматы, Казахстан;
[2]Институт информационных и вычислительных технологий, Алматы, Казахстан;
[3]Казахский Национальный Женский Педагогический Университет, Алматы, Казахстан;
[4]Международный Университет Информационных Технологий, Алматы, Казахстан

ЧИСЛЕННАЯ РЕАЛИЗАЦИЯ РЕШЕНИЯ КРАЕВОЙ ЗАДАЧИ ДЛЯ СИСТЕМЫ НАГРУЖЕННЫХ ДИФФЕРЕНЦИАЛЬНЫХ УРАВНЕНИЙ С ПАРАМЕТРОМ

Аннотация. Рассматривается линейная двухточечная краевая задача для системы нагруженных дифференциальных уравнений с параметром. Данная задача исследуется методом параметризации. Предлагается алгоритм нахождения решения краевой задачи для системы нагруженных дифференциальных уравнений с параметром. Вначале исходная задача сводится к эквивалентной задаче, состоящей из задач Коши для системы обыкновенных дифференциальных уравнений с параметрами на подинтеравалах и функциональных соотношений относительно введенных дополнительных параметров. При фиксированных значениях параметров задача Коши для системы обыкновенных дифференциальных уравнений на подинтервале имеет единственное решение. Это решение представляется через фундаментальную матрицу системы. Используя эти представления составляется система линейных алгебраических уравнений относительно параметров. Предлагается алгоритм нахождения численного решения эквивалентной задачи. Данный алгоритм включает численное решение задач Коши для системы обыкновенных дифференциальных уравнений и решение линейной системы алгебраических уравнений. Для численного решения задачи Коши применяется метод Рунге-Кутта четвертого порядка. Предлагаемая численная реализация иллюстрируется примером.

Ключевые слова: краевая задача с параметром, нагруженное дифференциальное уравнение, численный метод, алгоритм.

Information about authors:

Assanova Anar Turmaganbetkyzy**,** the member of Editorial Board of journal "News of the NAS RK. Physico-Mathematical Series",

Institute of Mathematics and Mathematical Modeling, Institute of Information and Computational Technologies, chief scientific researcher, Doctor of Physical and Mathematical Sciences, professor, assanova@math.kz; https://orcid.org/0000-0001-8697-8920;

Bakirova Elmira Ainabekovna,

Institute of Mathematics and Mathematical Modeling, Institute of Information and Computational Technologies, leading scientific researcher, Candidate of Physical and Mathematical Sciences, ass. professor, Kazakh National Women's Teacher Training University, associated professor, bakirova1974@mail.ru; https://orcid.org/0000-0002-3820-5373;

Kadirbayeva Zhazira Muratbekovna,

Institute of Mathematics and Mathematical Modeling, Institute of Information and Computational Technologies, leading scientific researcher, Candidate of Physical and Mathematical Sciences, International Information Technology University, head teacher, zh.kadirbayeva@gmail.com; https://orcid.org/0000-0001-8861-4100

REFERENCES

[1] Nakhushev A.M. Equations of mathematical biology. M.: Vyshaiya shkola, 1995. (in Russ.)

[2] Dzhenaliev M.T. To the theory linear boundary value problems for loaded differential equations. Almaty: Computenryi centr ITPM, 1995. (in Russ.)

[3] Nakhushev A.M. Problems with replacement for partial differential equations. M.: Nauka, 2006. (in Russ.)

[4] Dzhenaliev M.T., Ramazanov M.I. Loaded equations as perturbations of differential equations. Almaty: Gylym, 2010. (in Russ.)

[5] Nakhushev A.M. Loaded equations and their applications. M.: Nauka, 2012. (in Russ.)

[6] Bakirova E.A. About of a criteria of unique solvability of two-point boundary value problem for system of loaded differential equations, Izvestiya NAN RK. Ser.phyz.-matem. 2005. No 1. P.95-102. (in Russ.)

[7] Bakirova E.A. About of a necessary and sufficient conditions of unique solvability of two-point boundary value problem for loaded differential equations, Mathematical journal. 2005. Vol. 5. No 3. P.25-34. (in Russ.)

[8] Kadirbayeva Zh.M.About of one algorithm for finding solution of linear two-point boundary value problem for loaded differential equations, Mathematical journal. 2009. Vol.9. No 2(32). P.64-70. (in Russ.)

[9] Kadirbayeva Zh.M. About of a necessary and sufficient conditions of unique solvability of two-point boundary value problem for loaded differential equations, Mathematical journal. 2009. Vol.9. No 4(34). P.63-71. (in Russ.)

[10] Assanova A.T., Kadirbayeva Zh.M. On the numerical algorithms of parametrization method for solving a two-point boundary-value problem for impulsive systems of loaded differential equations, Computational and Applied Mathematics. 2018. - Vol. 37, No. 4. -P. 4966-4976. DOI: https://doi.org/ 10.1007/s40314-018-0611-9

[11] Dzhumabayev D.S. Criteria for the unique solvability of a linear boundary-value problem for an ordinary differential equation, USSR Comp. Math. & Math. Phys. 1989. V.29, No. 1. P. 34-46.

[12] Dzhumabaev D.S. A method for solving the linear boundary value problem for an integro-differential equation, Comp. Math. & Math. Phys. 2010. V.50, No. 7. P. 1150-1161.
DOI: https://doi.org/10.1134/S0965542510070043

[13] Dzhumabaev D.S. An algorithm for solving a linear two-point boundary value problem for an integrodifferential equation, Comp. Math. & Math. Phys. 2013. V.53, No. 6. P. 736-758. DOI: https://doi.org/10.1134/S0965542513060067

[14] Dzhumabaev D.S., Bakirova E.A. Criteria for the unique solvability of a linear two-point boundary value problem for systems of integro-differential equations, Differ. Equ. 2013. V.49, No. 9. P. 1087-1102. DOI: https://doi.org/10.1134/S0012266113090048

[15] Dzhumabaev D.S. Necessary and sufficient conditions for the solvability of linear boundary-value problems for the Fredholm integrodifferential equations, Ukranian Math. J. 2015. V.66, No. 8. P. 1200-1219. DOI: https://doi.org/10.1007/s11253-015-1003-6

[16] Dzhumabaev D.S. Solvability of a linear boundary value problem for a Fredholm integro-differential equation with impulsive inputs, Differ. Equ. 2015. V. 51, No. 9. P. 1180-1196. DOI: https://doi.org/10.1134/S0012266115090086

[17] Dzhumabaev D.S. On one approach to solve the linear boundary value problems for Fredholm integro-differential equations, J. Comp. Appl. Math. 2016. V. 294, P. 342-357. DOI: https://doi.org/10.1016/j.cam.2015.08.023

[18] Dzhumabaev D.S., Bakirova E.A., Kadirbayeva Zh.M. An algorithm for solving a control problem for a differential equation with a parameter, News of the NAS RK. Phys.-Math. Series. 2018. Volume 5, Number 321. P.25-32. DOI: https://doi.org/10.32014/2018.2518-1726.4

N E W S
OF THE NATIONAL ACADEMY OF SCIENCES OF THE REPUBLIC OF KAZAKHSTAN
PHYSICO-MATHEMATICAL SERIES
ISSN 1991-346X **https://doi.org/10.32014/2019.2518-1726.28**
Volume 3, Number 325 (2019), 85 – 96

UDK 517.43

A.Sh. Shaldanbayev[1], A.B. Imanbayeva[2], A.Zh. Beisebayeva[3], A.A. Shaldanbayeva[4]

[1]"Silkway" International University, Shymkent;
[2,3]M.Auezov South Kazakhstan State University, Shymkent;
[4]"Regional Social-Innovative University", Shymkent.
shaldanbaev51@mail.ru, aigul_baratovna@bk.ru, akbope_a@mail.ru, altima_a@mail.ru

ON THE SQUARE ROOT OF THE OPERATOR OF STURM-LIOUVILLE FOURTH-ORDER

Abstract. In the present work found the root of the positive operator of the Sturm - Liouville problem of the fourth order, which is invertible composition operator of the Sturm - Liouville problem and its adjoint. The found root does not possess the property of positivity, but is a self-adjoint operator in the essential. One theorem of Putnam of algebraic character is used as a leading idea. It is hoped that the results will find applications in spectral operator theory and theoretical physics.

Keywords. Kato conjecture, dissipative operator, square root of operator, Putnam theorem, deviating argument, fractional powers of an operator, inverse problem, spectrum, unitary operator, self-adjoint operator, positive operator, functional differential operator, spectral theory.

1. Introduction.

Definition. Let H be a Hilbert space. A linear bounded operator B is called positive if $(Bx, x) \geq 0$ for all $x \in H$. We write $B \geq 0$ if B is positive.

Lemma1.1 (On the square root). Let A be a linear bounded operator and $A \geq 0$. Then there is a single operator $B \gg 0$ and $B^2 =$ A. Moreover, B commutes with any bounded operator commuting with A. [1. p.219] .

When extending the concept of root to dissipative operators, the hypothesis of Kato [3] arose, consisting in the fact that the domain of the root definition from the operator always coincides with the domain of the root definition from the conjugate operator. But in 1972 A. Macintosh [4] built a counterexample, since then the hypothesis has been slightly reformulated: to find the largest class of operators that satisfies this condition, and is now given very active research in this direction [5-57].

Many operators of theoretical physics have square roots [57–64]; in particular, the square root of an operator in a Banach space was found in [65, pp.169-176]. We give an excerpt from this work.

Consider a generating operator A in a Banach space $\mathcal{B}$ with the following properties:

1) The operator $(I + \gamma^2 A)^{-1}$ exists, is defined everywhere in $\mathcal{B}$ and is bounded by one;

2) The operator A^{-1} exists;

3) $\left\|e^{iAt}\right\| \leq M, \ -\infty < t < +\infty.$

Under these conditions, the following lemmas are valid.

Lemma 1.1. Operator

$$T = \frac{2e^{-i\pi/4}}{\sqrt{\pi}} A \int_0^\infty e^{iAx^2} dx$$

exists as an operator in B on the area $D(A)$.

Lemma 1.2. For any $y \in D(A)$ the equality is true

$$T^2 g = Ag.$$

In connection with these results, the following problem arises.

Formulation of the problem. Let a reversible Sturm-Liouville operator L

$$Ly = -y''(x), \qquad x \in (0,1)$$

$$\begin{cases} a_{11}y(0) + a_{12}y'(0) + a_{13}y(1) + a_{14}y'(1) = 0, \\ a_{21}y(0) + a_{22}y'(0) + a_{23}y(1) + a_{24}y'(1) = 0, \end{cases}$$

where a_{ij} $(i = 1,2; j = 1,2,3,4)$ $-$ are complex numbers. Then it takes the following form:

$$Ly = -y''(x), \ x \in (0,1) \tag{1}$$

$$\begin{cases} \Delta_{13}y(0) - (\Delta_{12} + \Delta_{32})y'(0) - \Delta_{13}y(1) - \\ \quad -(\Delta_{14} + \Delta_{34})y'(1) = 0; \\ (\Delta_{12} + \Delta_{13} + \Delta_{14})y(0) - (\Delta_{32} + \Delta_{42})y'(0) + \\ \quad +(\Delta_{32} + \Delta_{34})y(1) - (\Delta_{34} + \Delta_{24})y'(1) = 0; \end{cases} \tag{2}$$

conjugate which has the form:

$$L^+ z = -z''(x), \ x \in (0,1), \tag{1}^+$$

$$\begin{cases} \bar{\Delta}_{13}z(0) - (\bar{\Delta}_{34} + \bar{\Delta}_{32})z'(0) - \bar{\Delta}_{13}z(1) - \\ \quad -(\bar{\Delta}_{14} + \bar{\Delta}_{12})z'(1) = 0; \\ (\Delta_{12} + \Delta_{13} + \Delta_{14})y(0) - (\Delta_{32} + \Delta_{42})y'(0) + \\ \quad +(\Delta_{32} + \Delta_{34})y(1) - (\Delta_{34} + \Delta_{24})y'(1) = 0. \end{cases} \tag{2}^+$$

The question is whether there is a unitary operator.

$$T = i\cos\varphi\, I + \sin\varphi \cdot S,$$

such that the formula takes place

$$TL = L^+ T^*, \tag{3}$$

where $I -$ is an identical operator and S is:

$$Su(x) = u(1-x). \tag{4}$$

2. Research methods.

As a suggestive idea, we take the following theorem of Putnam.

Theorem [2. p.337]. $M, N, T \in \mathcal{B}(H)$ Suppose that the operators M, N are normal and the operator T is invertible. Suppose that

$$M = TNT^{-1}. \tag{*}$$

If $T = UP -$ the polar decomposition of the operator T, then

$$M = UNU^{-1}.$$

Two operators connected by a relation (*) are called similar. If $U -$is a unitary operator and the relation (1.9) is satisfied, then the operators M and N are called unitary equivalent. Thus, this theorem establishes that such normal operators are unitary equivalent.

Our operators A, B are Hermitian (i.e, symmetric), and such operators belong to the class of normal operators; so there is a unitary operator T such that

$$AT = TB.$$

We believe that this particular operator is the solution of the equations:

$$(Tl)^2 = l^+ l = A, \qquad (lT)^2 = ll^+ = B.$$

Perhaps the operator T we need to impose additional conditions?!

From formula

$$(Tl)^2 = Tl \cdot Tl = l^* l,$$

we see that we need to require $Tl = l^* T^*$, then

$$Tl \cdot Tl = l^* \underbrace{T^* T}_{I} l = l^* l = A\ ,$$

Next, from $Tl = l^* T^*$, we have

$$TlT = l^*, \qquad lT = T^{-1} l^* = T^* l^*,$$

then

$$(lT)^2 = lT \cdot lT = |lT = T^* l^*| = lT \cdot T^* l^* = ll^* = B.$$

In addition,

$$TB = Tll^* = l^* T^* l^* = l^* lT = AT.$$

We proved the following Lemma.

Lemma 2.1. If $T -$ is a unitary operator satisfying the condition

$$(Tl)^* = Tl = l^* T^*,$$

then we have the formula

a) $(Tl)^2 = l^* l = A,$

b) $(lT)^2 = ll^* = B,$

c) $AT = TB.$

Thus, the problem was reduced to finding a unitary operator T, with the property, $Tl = l^* T^*$. This Lemma forms the basis of our method.

3. Research Results.

Let$y(x) \in D(L)$, then

$$z(x) = T^* y(x) = -i \cos\varphi\, y(x) + \sin\varphi \cdot y(1-x) \in D(L^+),$$

therefore, there are formulas

$$z(x) = -i \cos\varphi\, y(x) + \sin\varphi \cdot y(1-x),$$
$$z'(x) = -i \cos\varphi\, y'(x) - \sin\varphi \cdot y'(1-x),$$
$$z(0) = -i \cos\varphi\, y(0) + \sin\varphi \cdot y(1),$$
$$z'(0) = -i \cos\varphi\, y'(0) - \sin\varphi \cdot y'(1),$$
$$z(1) = -i \cos\varphi\, y(1) + \sin\varphi \cdot y(1),$$
$$z'(1) = -i \cos\varphi\, y'(1) - \sin\varphi \cdot y'(0),$$
$$z(0) - z(1) = (i\cos\varphi + \sin\varphi)y(1) - (i\cos\varphi + \sin\varphi)y(0) =$$
$$= (i\cos\varphi + \sin\varphi)[y(1) - y(0)],$$
$$\overline{\Delta_{13}}(i\cos\varphi + \sin\varphi)[y(1) - y(0)] + (\overline{\Delta_{32}} + \overline{\Delta_{34}})$$
$$[i\cos\varphi\, y'(0) + \sin\varphi \cdot y'(1)] +$$
$$+(\overline{\Delta_{12}} + \overline{\Delta_{14}})[i\cos\varphi\, y'(1) + \sin\varphi \cdot y'(0)] = 0;$$
$$\overline{\Delta_{13}}(i\cos\varphi + \sin\varphi)[y(1) - y(0)] +$$
$$+[i\cos\varphi\,(\overline{\Delta_{32}} + \overline{\Delta_{34}}) + \sin\varphi\,(\overline{\Delta_{12}} + \overline{\Delta_{14}})]y'(0) +$$
$$+[\sin\varphi\,(\overline{\Delta_{32}} + \overline{\Delta_{34}}) + i\cos\varphi\,(\overline{\Delta_{12}} + \overline{\Delta_{14}})]y'(1) = 0;$$

$$(\overline{\Delta_{12}}+\overline{\Delta_{14}}+\overline{\Delta_{34}})[-i\cos\varphi\, y(0)+\sin\varphi\cdot y(1)]+$$
$$+(\overline{\Delta_{32}}+\overline{\Delta_{34}})[i\cos\varphi\, y'(0)+\sin\varphi\cdot y'(1)]+$$
$$+(\overline{\Delta_{12}}+\overline{\Delta_{32}})[-i\cos\varphi\, y(1)+\sin\varphi\cdot y(0)]+(\overline{\Delta_{12}}+\overline{\Delta_{24}})\cdot$$
$$\cdot[i\cos\varphi\, y'(1)+\sin\varphi\cdot y'(0)]=$$
$$=[-i\cos\varphi\,(\overline{\Delta_{13}}+\overline{\Delta_{14}}+\overline{\Delta_{34}})+(\overline{\Delta_{12}}+\overline{\Delta_{32}})\sin\varphi]y(0)+$$
$$+[\sin\varphi\,(\overline{\Delta_{13}}+\overline{\Delta_{14}}+\overline{\Delta_{34}})-i\cos\varphi\,(\overline{\Delta_{12}}+\overline{\Delta_{32}})]y(1)+$$
$$+[(\overline{\Delta_{32}}+\overline{\Delta_{42}})\sin\varphi+i\cos\varphi\,(\overline{\Delta_{12}}+\overline{\Delta_{24}})]y'(1)=0.$$

This boundary condition corresponds to the matrix

$$\begin{pmatrix} -\overline{\Delta_{13}}(\sin\varphi+i\cos\varphi) \\ -i\cos\varphi\,(\overline{\Delta_{13}}+\overline{\Delta_{14}}+\overline{\Delta_{34}})+(\overline{\Delta_{12}}+\overline{\Delta_{32}})\sin\varphi \end{pmatrix}$$

$$\begin{matrix} i\cos\varphi\,(\overline{\Delta_{32}}+\overline{\Delta_{34}})+\sin\varphi\,(\overline{\Delta_{12}}+\overline{\Delta_{14}}) \\ i\cos\varphi\,(\overline{\Delta_{32}}+\overline{\Delta_{42}})+\sin\varphi\,(\overline{\Delta_{12}}+\overline{\Delta_{24}}) \end{matrix}$$

$$\begin{matrix} \Delta_{13}(\sin\varphi+i\cos\varphi) \\ \sin\varphi\,(\overline{\Delta_{13}}+\overline{\Delta_{14}}+\overline{\Delta_{34}})-i\cos\varphi\,(\overline{\Delta_{12}}+\overline{\Delta_{32}}) \end{matrix}$$

$$\begin{pmatrix} \sin\varphi\,(\overline{\Delta_{32}}+\overline{\Delta_{34}})+i\cos\varphi\,(\overline{\Delta_{12}}+\overline{\Delta_{14}}) \\ (\overline{\Delta_{32}}+\overline{\Delta_{42}})\sin\varphi+i\cos\varphi\,(\overline{\Delta_{12}}+\overline{\Delta_{24}}) \end{pmatrix}.$$

Combining the obtained system of equations with respect to the unknowns: $y(0), y'(0), y(1), y'(1)$ with the previously known boundary conditions (2), we obtain a system of homogeneous algebraic equations. Since this resulting system of equations obviously has nontrivial solutions, its determinant is zero.

Taking advantage of this fact, we obtain one equation to determine the unknown value φ.

$$\begin{cases} 1)\ \Delta_{13}y(0)-(\Delta_{12}+\Delta_{32})y'(0)-\Delta_{13}y(1)- \\ (\Delta_{14}+\Delta_{34})y'(1)=0; \\ 2)\ (\Delta_{12}+\Delta_{13}+\Delta_{14})y(0)-(\Delta_{32}+\Delta_{42})y'(0)+ \\ (\Delta_{32}+\Delta_{34})y(1)-(\Delta_{34}+\Delta_{24})y'(1)=0; \\ 3)\ \overline{\Delta_{13}}(\sin\varphi+i\cos\varphi)y(0)+[i\cos\varphi\,(\overline{\Delta_{32}}+\overline{\Delta_{34}})+(\overline{\Delta_{12}}+\overline{\Delta_{14}})\sin\varphi]\cdot \\ \cdot y'(0)-\Delta_{13}(\sin\varphi+i\cos\varphi)y(1)+ \\ +[(\overline{\Delta_{32}}+\overline{\Delta_{34}})\sin\varphi+i\cos\varphi\,(\overline{\Delta_{12}}+\overline{\Delta_{14}})]y'(1)=0; \\ 4)\ [-i\cos\varphi\,(\overline{\Delta_{13}}+\overline{\Delta_{14}}+\overline{\Delta_{34}})+\sin\varphi\,(\overline{\Delta_{12}}+\overline{\Delta_{32}})]y(0)+ \\ +[i\cos\varphi\,(\overline{\Delta_{32}}+\overline{\Delta_{42}})+\sin\varphi\,(\overline{\Delta_{12}}+\overline{\Delta_{24}})]y'(0)+ \\ [(\overline{\Delta_{13}}+\overline{\Delta_{14}}+\overline{\Delta_{34}})\cdot\sin\varphi-i\cos\varphi\,(\overline{\Delta_{12}}+\overline{\Delta_{32}})]y(1)+ \\ +[(\overline{\Delta_{32}}+\overline{\Delta_{42}})\sin\varphi+i\cos\varphi\,(\overline{\Delta_{12}}+\overline{\Delta_{24}})]y'(1)=0. \end{cases}$$

This system of homogeneous algebraic equations is denoted by (5).

The determinant of the system of equations (5) has the following form:

$$\begin{vmatrix} \Delta_{13} \\ \Delta_{12}+\Delta_{13}+\Delta_{14} \\ \overline{\Delta_{13}}(\sin\varphi+i\cos\varphi) \\ -i\cos\varphi\,(\overline{\Delta_{13}}+\overline{\Delta_{14}}+\overline{\Delta_{34}})+\sin\varphi\,(\overline{\Delta_{12}}+\overline{\Delta_{32}}) \end{vmatrix}$$

$$
\begin{matrix}
-(\Delta_{12}+\Delta_{32}) \\
-(\Delta_{32}+\Delta_{42}) \\
i\cos\varphi\,(\overline{\Delta_{32}}+\overline{\Delta_{34}})+(\overline{\Delta_{12}}+\overline{\Delta_{14}})\sin\varphi \\
[i\cos\varphi\,(\overline{\Delta_{32}}+\overline{\Delta_{42}})+\sin\varphi\,(\overline{\Delta_{12}}+\overline{\Delta_{24}})]
\end{matrix}
$$

$$
\begin{matrix}
-\Delta_{13} \\
\Delta_{32}+\Delta_{34} \\
-\overline{\Delta_{13}}(\sin\varphi+i\cos\varphi) \\
(\overline{\Delta_{13}}+\overline{\Delta_{14}}+\overline{\Delta_{34}})\sin\varphi-i\cos\varphi\,(\overline{\Delta_{12}}+\overline{\Delta_{32}})
\end{matrix}
$$

$$
\begin{matrix}
-(\Delta_{14}+\Delta_{34}) \\
-(\Delta_{34}+\Delta_{24}) \\
(\overline{\Delta_{32}}+\overline{\Delta_{34}})\sin\varphi+i\cos\varphi\,(\overline{\Delta_{12}}+\overline{\Delta_{14}}) \\
(\overline{\Delta_{32}}+\overline{\Delta_{42}})\sin\varphi+i\cos\varphi\,(\overline{\Delta_{12}}+\overline{\Delta_{24}})
\end{matrix}
\Bigg].
$$

This determinant splits into the sum of two determinants:

$$
\begin{bmatrix}
\Delta_{13} & -(\Delta_{12}+\Delta_{32}) \\
\Delta_{12}+\Delta_{13}+\Delta_{14} & -(\Delta_{32}+\Delta_{42}) \\
-\overline{\Delta_{13}}\sin\varphi & (\overline{\Delta_{12}}+\overline{\Delta_{14}})\sin\varphi \\
(\overline{\Delta_{12}}+\overline{\Delta_{32}})\sin\varphi & (\overline{\Delta_{12}}+\overline{\Delta_{24}})\sin\varphi
\end{bmatrix}
$$

$$
\begin{bmatrix}
-\Delta_{13} & -(\Delta_{14}+\Delta_{34}) \\
\Delta_{32}+\Delta_{34} & -(\Delta_{34}+\Delta_{24}) \\
\overline{\Delta_{13}}\sin\varphi & (\overline{\Delta_{32}}+\overline{\Delta_{34}})\sin\varphi \\
(\overline{\Delta_{13}}+\overline{\Delta_{14}}+\overline{\Delta_{34}})\sin\varphi & (\overline{\Delta_{32}}+\overline{\Delta_{42}})\sin\varphi
\end{bmatrix}
+
\begin{bmatrix}
\Delta_{13} \\
\Delta_{12}+\Delta_{13}+\Delta_{14} \\
-\overline{\Delta_{13}}i\cos\varphi \\
-i\cos\varphi\,(\overline{\Delta_{13}}+\overline{\Delta_{14}}+\overline{\Delta_{34}})
\end{bmatrix}
$$

$$
\begin{bmatrix}
-(\Delta_{12}+\Delta_{32}) & -\Delta_{13} & -(\Delta_{14}+\Delta_{34}) \\
-(\Delta_{32}+\Delta_{42}) & \Delta_{32}+\Delta_{34} & -(\Delta_{34}+\Delta_{24}) \\
i\cos\varphi\,(\overline{\Delta_{32}}+\overline{\Delta_{34}}) & i\cdot\overline{\Delta_{13}}\cos\varphi & i\cos\varphi\,(\overline{\Delta_{12}}+\overline{\Delta_{14}}) \\
i\cos\varphi\,(\overline{\Delta_{32}}+\overline{\Delta_{42}}) & -i\cos\varphi\,(\overline{\Delta_{12}}+\overline{\Delta_{32}}) & i\cos\varphi\,(\overline{\Delta_{12}}+\overline{\Delta_{24}})
\end{bmatrix}.
$$

This matrix is denoted by (6).

(a) Calculate the first determinant:

$$
sin^2\varphi\begin{bmatrix}
\Delta_{13} & -(\Delta_{12}+\Delta_{32}) & -\Delta_{13} & -(\Delta_{14}+\Delta_{34}) \\
\Delta_{12}+\Delta_{13}+\Delta_{14} & -(\Delta_{32}+\Delta_{42}) & \Delta_{32}+\Delta_{34} & -(\Delta_{34}+\Delta_{24}) \\
-\overline{\Delta_{13}} & \overline{\Delta_{12}}+\overline{\Delta_{14}} & \overline{\Delta_{13}} & \overline{\Delta_{32}}+\overline{\Delta_{34}} \\
\overline{\Delta_{12}}+\overline{\Delta_{32}} & \overline{\Delta_{12}}+\overline{\Delta_{24}} & \overline{\Delta_{13}}+\overline{\Delta_{14}}+\overline{\Delta_{34}} & \overline{\Delta_{32}}+\overline{\Delta_{42}}
\end{bmatrix}=
$$

$$
=sin^2\varphi\begin{bmatrix}
0 & -\Delta & -\Delta_{13} & -(\Delta_{14}+\Delta_{34}) \\
\Delta & 0 & \Delta_{32}+\Delta_{34} & -(\Delta_{34}+\Delta_{24}) \\
0 & \bar{\Delta} & \overline{\Delta_{13}} & \overline{\Delta_{32}}+\overline{\Delta_{34}} \\
\bar{\Delta} & \bar{\Delta} & \overline{\Delta_{13}}+\overline{\Delta_{14}}+\overline{\Delta_{34}} & \overline{\Delta_{32}}+\overline{\Delta_{42}}
\end{bmatrix}=
$$

$$
=sin^2\varphi\begin{bmatrix}
0 & -\Delta & -\Delta_{13} & -(\Delta_{14}+\Delta_{34}) \\
\Delta & 0 & \Delta_{32}+\Delta_{34} & -(\Delta_{34}+\Delta_{24}) \\
0 & \bar{\Delta} & \overline{\Delta_{13}} & \overline{\Delta_{32}}+\overline{\Delta_{34}} \\
\bar{\Delta} & 0 & \overline{\Delta_{14}}+\overline{\Delta_{34}} & -(\overline{\Delta_{24}}+\overline{\Delta_{34}})
\end{bmatrix}=
$$

$$= sin^2\varphi \left\{ -\Delta \begin{vmatrix} -\Delta & -\Delta_{13} & -(\Delta_{14}+\Delta_{34}) \\ \bar{\Delta} & \overline{\Delta_{13}} & \overline{\Delta_{32}}+\overline{\Delta_{34}} \\ 0 & \overline{\Delta_{14}}+\overline{\Delta_{34}} & -(\overline{\Delta_{24}}+\overline{\Delta_{34}}) \end{vmatrix} - \bar{\Delta} \begin{vmatrix} -\Delta & -\Delta_{13} & -(\Delta_{14}+\Delta_{34}) \\ 0 & \Delta_{32}+\Delta_{34} & -(\Delta_{34}+\Delta_{24}) \\ \bar{\Delta} & \overline{\Delta_{13}} & \overline{\Delta_{32}}+\overline{\Delta_{34}} \end{vmatrix} \right\} =$$

$$= sin^2\varphi \left\{ \Delta \begin{vmatrix} \Delta & \Delta_{13} & \Delta_{14}+\Delta_{34} \\ \bar{\Delta} & \overline{\Delta_{13}} & \overline{\Delta_{32}}+\overline{\Delta_{34}} \\ 0 & \overline{\Delta_{14}}+\overline{\Delta_{34}} & -(\overline{\Delta_{24}}+\overline{\Delta_{34}}) \end{vmatrix} - \bar{\Delta} \begin{vmatrix} \Delta & \Delta_{13} & \Delta_{14}+\Delta_{34} \\ \bar{\Delta} & \overline{\Delta_{13}} & \overline{\Delta_{32}}+\overline{\Delta_{34}} \\ 0 & \Delta_{32}+\Delta_{34} & -(\Delta_{34}+\Delta_{24}) \end{vmatrix} \right\} =$$

$$= sin^2\varphi \left\{ \Delta \cdot \left[-(\overline{\Delta_{14}}+\overline{\Delta_{34}}) \begin{vmatrix} \Delta & \Delta_{14}+\Delta_{34} \\ \bar{\Delta} & \overline{\Delta_{32}}+\overline{\Delta_{34}} \end{vmatrix} - (\overline{\Delta_{24}}+\overline{\Delta_{34}}) \begin{vmatrix} \Delta & \Delta_{13} \\ \bar{\Delta} & \overline{\Delta_{13}} \end{vmatrix} \right] - \right.$$

$$\left. - \Delta \left[-(\Delta_{32}+\Delta_{34}) \begin{vmatrix} \Delta & \Delta_{14}+\Delta_{34} \\ \bar{\Delta} & \overline{\Delta_{32}}+\overline{\Delta_{34}} \end{vmatrix} - (\Delta_{34}+\Delta_{24}) \begin{vmatrix} \Delta & \Delta_{13} \\ \bar{\Delta} & \overline{\Delta_{13}} \end{vmatrix} \right] \right\} =$$

$$= sin^2\varphi \cdot \left\{ \begin{vmatrix} \Delta & \Delta_{14}+\Delta_{34} \\ \bar{\Delta} & \overline{\Delta_{32}}+\overline{\Delta_{34}} \end{vmatrix} \cdot [\bar{\Delta}(\Delta_{32}+\Delta_{34}) - \Delta(\overline{\Delta_{14}}+\overline{\Delta_{34}})] + \right.$$

$$\left. + \begin{vmatrix} \Delta & \Delta_{13} \\ \bar{\Delta} & \overline{\Delta_{13}} \end{vmatrix} \cdot [\bar{\Delta}(\Delta_{24}+\Delta_{34}) - \Delta(\overline{\Delta_{24}}+\overline{\Delta_{34}})] \right\} =$$

$$= sin^2\varphi \cdot \{[\Delta(\overline{\Delta_{32}}+\overline{\Delta_{34}}) - \bar{\Delta}(\Delta_{14}+\Delta_{34})] \cdot [\bar{\Delta}(\Delta_{32}+\Delta_{34}) - \Delta(\overline{\Delta_{14}}+\overline{\Delta_{34}})] +$$

$$+ (\Delta \cdot \overline{\Delta_{13}} - \bar{\Delta} \cdot \Delta_{13})[\bar{\Delta}(\Delta_{24}+\Delta_{34}) - \Delta(\overline{\Delta_{24}}+\overline{\Delta_{34}})]\} =$$

$$= sin^2\varphi \cdot [|\Delta|^2 \cdot |\Delta_{32}+\Delta_{34}|^2 - \Delta^2(\overline{\Delta_{32}}+\overline{\Delta_{34}})(\overline{\Delta_{14}}+\overline{\Delta_{34}}) - \bar{\Delta}^2(\Delta_{14}+\Delta_{34})(\Delta_{32}+\Delta_{34}) +$$

$$+ |\Delta|^2 \cdot |\Delta_{14}+\Delta_{34}|^2 + |\Delta|^2 \cdot \overline{\Delta_{13}}(\Delta_{24}+\Delta_{34}) - \Delta^2\overline{\Delta_{13}}(\overline{\Delta_{24}}+\overline{\Delta_{34}}) -$$

$$- \bar{\Delta}^2\Delta_{13}(\Delta_{24}+\Delta_{34}) + |\Delta|^2\Delta_{13}(\overline{\Delta_{24}}+\overline{\Delta_{34}})] =$$

$$= sin^2\varphi \cdot \{|\Delta|^2 \cdot [|\Delta_{32}+\Delta_{34}|^2 + |\Delta_{14}+\Delta_{34}|^2] -$$

$$- \Delta^2 \cdot [(\overline{\Delta_{32}}+\overline{\Delta_{34}})(\overline{\Delta_{14}}+\overline{\Delta_{34}}) + \overline{\Delta_{13}}(\overline{\Delta_{24}}+\overline{\Delta_{34}})] -$$

$$- \bar{\Delta}^2[(\Delta_{14}+\Delta_{34})(\Delta_{32}+\Delta_{34}) + \Delta_{13}(\Delta_{24}+\Delta_{34})] +$$

$$+ |\Delta|^2[\overline{\Delta_{13}}(\Delta_{24}+\Delta_{34}) + \Delta_{13}(\overline{\Delta_{24}}+\overline{\Delta_{34}})]\};$$

Using the obvious formula $\Delta_{13}\Delta_{24} + \Delta_{14}\Delta_{32} = \Delta_{12}\Delta_{34}$ transform the coefficients of the resulting expression

$$(\Delta_{14}+\Delta_{34})(\Delta_{32}+\Delta_{34}) + \Delta_{13}(\Delta_{24}+\Delta_{34}) = \Delta_{14}\Delta_{32} + \Delta_{14}\Delta_{34} + \Delta_{34}\Delta_{32} +$$

$$+ \Delta_{34}^2 + \Delta_{13}\Delta_{24} + + \Delta_{13}\Delta_{34} = \Delta_{12}\Delta_{34} + \Delta_{14}\Delta_{34} + \Delta_{34}\Delta_{32} + \Delta_{34}^2 + \Delta_{13}\Delta_{34} =$$

$$= \Delta_{34}(\Delta_{12}+\Delta_{13}+\Delta_{14}+\Delta_{32}+\Delta_{34}) = \Delta_{34} \cdot \Delta.$$

Thus, the value of the first determinant will be

$$sin^2\varphi \cdot \{|\Delta|^2 \cdot [|\Delta_{32}+\Delta_{34}|^2 + |\Delta_{14}+\Delta_{34}|^2] -$$

$$- \Delta^2 \cdot \overline{\Delta_{34}} \cdot \bar{\Delta} - \bar{\Delta}^2 \cdot \Delta_{34} \cdot \Delta + |\Delta|^2[\overline{\Delta_{13}}(\Delta_{24}+\Delta_{34}) + \Delta_{13}(\overline{\Delta_{24}}+\overline{\Delta_{34}})]\} =$$

$$sin^2\varphi \cdot \{|\Delta|^2 \cdot [|\Delta_{32}+\Delta_{34}|^2 + |\Delta_{14}+\Delta_{34}|^2] - [|\Delta|^2\Delta \cdot \overline{\Delta_{34}} + \bar{\Delta} \cdot \Delta_{34}|\Delta|^2] +$$

$$+|\Delta|^2[\overline{\Delta_{13}}(\Delta_{24}+\Delta_{34})+\Delta_{13}(\overline{\Delta_{24}}+\overline{\Delta_{34}})]\}$$

$$=|\Delta|^2\cdot sin^2\varphi\cdot\{[|\Delta_{32}+\Delta_{34}|^2+|\Delta_{14}+\Delta_{34}|^2]-$$

$$-\left[\Delta\cdot\overline{\Delta_{34}}+\bar{\bar{\Delta}}\cdot\Delta_{34}\right]+[\overline{\Delta_{13}}(\Delta_{24}+\Delta_{34})+\Delta_{13}(\overline{\Delta_{24}}+\overline{\Delta_{34}})]\}.$$

Thus, the coefficient at $sin^2\varphi$ turned out to be a real value.
Now we calculate the second determinant from formula (6).
b)

$$-cos^2\varphi\begin{bmatrix}\Delta_{13} & -(\Delta_{12}+\Delta_{32}) & -\Delta_{13} & -(\Delta_{14}+\Delta_{34})\\ \Delta_{12}+\Delta_{13}+\Delta_{14} & -(\Delta_{32}+\Delta_{42}) & \Delta_{32}+\Delta_{34} & -(\Delta_{34}+\Delta_{24})\\ -\overline{\Delta_{13}} & \overline{\Delta_{32}}+\overline{\Delta_{34}} & \overline{\Delta_{13}} & \overline{\Delta_{12}}+\overline{\Delta_{14}}\\ -(\overline{\Delta_{13}}+\overline{\Delta_{14}}+\overline{\Delta_{34}}) & \overline{\Delta_{32}}+\overline{\Delta_{42}} & -(\overline{\Delta_{12}}+\overline{\Delta_{32}}) & \overline{\Delta_{12}}+\overline{\Delta_{24}}\end{bmatrix}=$$

$$=-cos^2\varphi\begin{bmatrix}0 & -\Delta & -\Delta_{13} & -(\Delta_{14}+\Delta_{34})\\ \Delta & 0 & \Delta_{32}+\Delta_{34} & -(\Delta_{34}+\Delta_{24})\\ 0 & \bar{\Delta} & \overline{\Delta_{13}} & \overline{\Delta_{12}}+\overline{\Delta_{14}}\\ -\bar{\Delta} & 0 & -(\overline{\Delta_{12}}+\overline{\Delta_{32}}) & \overline{\Delta_{12}}+\overline{\Delta_{24}}\end{bmatrix}=$$

$$=-cos^2\varphi\left\{-\Delta\begin{vmatrix}-\Delta & -\Delta_{13} & -(\Delta_{14}+\Delta_{34})\\ \bar{\Delta} & \overline{\Delta_{13}} & \overline{\Delta_{12}}+\overline{\Delta_{14}}\\ 0 & -(\overline{\Delta_{12}}+\overline{\Delta_{32}}) & \overline{\Delta_{12}}+\overline{\Delta_{24}}\end{vmatrix}+\bar{\Delta}\begin{vmatrix}-\Delta & -\Delta_{13} & -(\Delta_{14}+\Delta_{34})\\ 0 & \Delta_{32}+\Delta_{34} & -(\Delta_{34}+\Delta_{24})\\ \bar{\Delta} & \overline{\Delta_{13}} & \overline{\Delta_{12}}+\overline{\Delta_{14}}\end{vmatrix}\right\}=$$

$$=-cos^2\varphi\left\{\Delta\cdot\begin{vmatrix}\Delta & \Delta_{13} & \Delta_{14}+\Delta_{34}\\ \bar{\Delta} & \overline{\Delta_{13}} & \overline{\Delta_{12}}+\overline{\Delta_{14}}\\ 0 & -(\overline{\Delta_{12}}+\overline{\Delta_{32}}) & \overline{\Delta_{12}}+\overline{\Delta_{24}}\end{vmatrix}+\bar{\Delta}\cdot\begin{vmatrix}\Delta & \Delta_{13} & \Delta_{14}+\Delta_{34}\\ \bar{\Delta} & \overline{\Delta_{13}} & \overline{\Delta_{12}}+\overline{\Delta_{14}}\\ 0 & \Delta_{32}+\Delta_{34} & -(\Delta_{24}+\Delta_{34})\end{vmatrix}\right\}=$$

$$=-cos^2\varphi\left\{\Delta\cdot\left[(\overline{\Delta_{12}}+\overline{\Delta_{32}})\begin{vmatrix}\Delta & \Delta_{14}+\Delta_{34}\\ \bar{\Delta} & \overline{\Delta_{12}}+\overline{\Delta_{14}}\end{vmatrix}+(\overline{\Delta_{12}}+\overline{\Delta_{24}})\begin{vmatrix}\Delta & \Delta_{13}\\ \bar{\Delta} & \overline{\Delta_{13}}\end{vmatrix}\right]+\right.$$

$$\left.+\overline{\bar{\Delta}\left[-(\Delta_{32}+\Delta_{34})\begin{vmatrix}\Delta & \Delta_{14}+\Delta_{34}\\ \bar{\Delta} & \overline{\Delta_{12}}+\overline{\Delta_{14}}\end{vmatrix}-(\Delta_{24}+\Delta_{34})\begin{vmatrix}\Delta & \Delta_{13}\\ \bar{\Delta} & \overline{\Delta_{13}}\end{vmatrix}\right]}\right\}=$$

$$=cos^2\varphi\cdot\left\{\begin{vmatrix}\Delta & \Delta_{14}+\Delta_{34}\\ \bar{\Delta} & \overline{\Delta_{12}}+\overline{\Delta_{14}}\end{vmatrix}\cdot[\Delta(\overline{\Delta_{12}}+\overline{\Delta_{32}})-\bar{\Delta}(\Delta_{32}+\Delta_{34})]+\right.$$

$$\left.+\begin{vmatrix}\Delta & \Delta_{13}\\ \bar{\Delta} & \overline{\Delta_{13}}\end{vmatrix}\cdot[\Delta(\overline{\Delta_{12}}+\overline{\Delta_{24}})-\bar{\Delta}(\Delta_{24}+\Delta_{34})]\right\}=$$

$$=cos^2\varphi\cdot\{[\Delta(\overline{\Delta_{12}}+\overline{\Delta_{14}})-\bar{\Delta}(\Delta_{14}+\Delta_{34})]\cdot[\Delta(\overline{\Delta_{12}}+\overline{\Delta_{32}})-\bar{\Delta}(\Delta_{32}+\Delta_{34})]+$$

$$+(\Delta\cdot\overline{\Delta_{13}}-\Delta_{13}\cdot\bar{\Delta})[\Delta(\overline{\Delta_{12}}+\overline{\Delta_{24}})-\bar{\Delta}(\Delta_{24}+\Delta_{34})]\}.$$

Using the obvious formula $\Delta_{13}\Delta_{24}+\Delta_{14}\Delta_{32}=\Delta_{12}\Delta_{34}$, we transform the expression under the curly bracket.

$$\Delta^2\cdot(\overline{\Delta_{12}}+\overline{\Delta_{14}})(\overline{\Delta_{12}}+\overline{\Delta_{32}})-|\Delta|^2(\overline{\Delta_{12}}+\overline{\Delta_{14}})(\Delta_{32}+\Delta_{34})-|\Delta|^2(\Delta_{14}+\Delta_{34})(\overline{\Delta_{12}}+\overline{\Delta_{32}})+$$
$$+\bar{\Delta}^2(\Delta_{14}+\Delta_{34})(\Delta_{32}+\Delta_{34});\qquad(7)$$

$$\Delta^2\cdot\overline{\Delta_{13}}(\overline{\Delta_{12}}+\overline{\Delta_{24}})-|\Delta|^2\overline{\Delta_{13}}(\Delta_{24}+\Delta_{34})-$$
$$|\Delta|^2\Delta_{13}(\overline{\Delta_{12}}+\overline{\Delta_{24}})+\bar{\Delta}^2\Delta_{13}(\Delta_{24}+\Delta_{34});\qquad(8)$$

$$(\overline{\Delta_{12}}+\overline{\Delta_{14}})(\overline{\Delta_{12}}+\overline{\Delta_{32}})+\overline{\Delta_{13}}(\overline{\Delta_{12}}+\overline{\Delta_{24}})=\bar{\Delta}_{12}^2+\overline{\Delta_{12}}\cdot\overline{\Delta_{32}}+\overline{\Delta_{14}}\cdot\overline{\Delta_{12}}+$$
$$\overline{\Delta_{14}}\cdot\overline{\Delta_{32}}+\overline{\Delta_{13}}\cdot\overline{\Delta_{12}}+\overline{\Delta_{13}}\cdot\overline{\Delta_{24}}=$$
$$\bar{\Delta}_{12}^2+\overline{\Delta_{12}}\cdot\overline{\Delta_{32}}+\overline{\Delta_{14}}\cdot\overline{\Delta_{12}}+\overline{\Delta_{12}}\cdot\overline{\Delta_{34}}+\overline{\Delta_{13}}\cdot\overline{\Delta_{12}}=\overline{\Delta_{12}}\cdot\bar{\Delta}. \quad (9)$$

Similarly, we have

$$(\Delta_{14}+\Delta_{34})(\Delta_{32}+\Delta_{34})+\Delta_{13}(\Delta_{24}+\Delta_{34})=\Delta_{14}\Delta_{32}+\Delta_{14}\Delta_{34}+$$
$$\Delta_{34}\Delta_{32}+\Delta_{34}^2+\Delta_{13}\Delta_{24}++\Delta_{13}\Delta_{34}=\Delta_{14}\Delta_{34}+\Delta_{34}\Delta_{32}+\Delta_{34}^2+$$
$$+\Delta_{12}\Delta_{34}+\Delta_{13}\Delta_{34}=\Delta_{34}\cdot\Delta. \quad (10)$$

Adding formulas (7), (8) and considering (9) and (10), we have

$$|\Delta|^2\cdot\Delta\cdot\bar{\Delta}_{12}+|\Delta|^2\bar{\Delta}\cdot\Delta_{34}-$$
$$-|\Delta|^2[(\overline{\Delta_{12}}+\overline{\Delta_{14}})(\Delta_{32}+\Delta_{34})+(\Delta_{14}+\Delta_{34})(\overline{\Delta_{12}}+\overline{\Delta_{32}})+$$
$$+\overline{\Delta_{13}}(\Delta_{24}+\Delta_{34})+\Delta_{13}(\overline{\Delta_{12}}+\overline{\Delta_{24}})]. \quad (11)$$

Now convert the expression under the square bracket.

$$(\overline{\Delta_{12}}+\overline{\Delta_{14}})(\Delta_{32}+\Delta_{34})+(\Delta_{14}+\Delta_{34})(\overline{\Delta_{12}}+\overline{\Delta_{32}})+\overline{\Delta_{13}}(\Delta_{24}+\Delta_{34})+\Delta_{13}(\overline{\Delta_{12}}+\overline{\Delta_{24}})=$$
$$=(\bar{\Delta}-\overline{\Delta_{13}}-\overline{\Delta_{32}}-\overline{\Delta_{34}})(\Delta_{32}+\Delta_{34})+(\Delta-\Delta_{12}-\Delta_{32}-\Delta_{13})(\overline{\Delta_{12}}+\overline{\Delta_{32}})+$$
$$+\overline{\Delta_{13}}(\Delta_{24}+\Delta_{34})+\Delta_{13}(\overline{\Delta_{12}}+\overline{\Delta_{24}})=\bar{\Delta}(\Delta_{32}+\Delta_{34})-|\Delta_{32}+\Delta_{34}|^2-\overline{\Delta_{13}}(\Delta_{32}+\Delta_{34})+$$
$$+\Delta(\overline{\Delta_{12}}+\overline{\Delta_{32}})-|\overline{\Delta_{12}}+\overline{\Delta_{32}}|^2-\Delta_{13}(\overline{\Delta_{12}}+\overline{\Delta_{32}})+\overline{\overline{\Delta_{13}}}(\Delta_{24}+\Delta_{34})+\Delta_{13}(\overline{\Delta_{12}}+\overline{\Delta_{24}})=$$
$$-|\Delta_{32}+\Delta_{34}|^2-|\overline{\Delta_{12}}+\overline{\Delta_{32}}|^2+\overline{\overline{\Delta_{13}}}(\Delta_{24}-\Delta_{32})+\Delta_{13}(\overline{\Delta_{24}}-\overline{\Delta_{32}})+\bar{\Delta}(\Delta_{32}+\Delta_{34})+$$
$$\Delta(\overline{\Delta_{12}}+\overline{\Delta_{32}})=\bar{\Delta}\Delta_{32}+\Delta\bar{\Delta}_{32}+\bar{\Delta}\Delta_{34}+\Delta\bar{\Delta}_{12}+$$
$$+\bar{\Delta}_{13}(\Delta_{24}-\Delta_{32})+\Delta_{13}(\overline{\Delta_{24}}-\overline{\Delta_{32}})-|\Delta_{32}+\Delta_{34}|^2-|\overline{\Delta_{12}}+\overline{\Delta_{32}}|^2; \quad (12)$$

Substituting (12) into (1), we obtain

$$|\Delta|^2\cdot\{|\Delta_{32}+\Delta_{34}|^2+|\overline{\Delta_{12}}+\overline{\Delta_{32}}|^2-$$
$$-[\bar{\Delta}\Delta_{32}+\Delta\bar{\Delta}_{32}+\bar{\Delta}_{13}(\Delta_{24}-\Delta_{32})+\Delta_{13}(\overline{\Delta_{24}}-\overline{\Delta_{32}})]\}.$$

Thus, the second determinant has the form:

$$-cos^2\varphi\{|\Delta_{32}+\Delta_{34}|^2+|\overline{\Delta_{12}}+\overline{\Delta_{32}}|^2-$$
$$-[\bar{\Delta}\Delta_{32}+\Delta\bar{\Delta}_{32}+\bar{\Delta}_{13}(\Delta_{24}-\Delta_{32})+\Delta_{13}(\overline{\Delta_{24}}-\overline{\Delta_{32}})]\}|\Delta|^2.$$

Adding this formula to the first determinant, we obtain the equations for determining φ.

$$|\Delta|^2sin^2\varphi\{[|\Delta_{32}+\Delta_{34}|^2+|\Delta_{14}+\Delta_{34}|^2]-$$
$$-\left[\Delta\cdot\overline{\Delta_{34}}+\bar{\bar{\Delta}}\cdot\Delta_{34}\right]+[\overline{\Delta_{13}}(\Delta_{24}+\Delta_{34})+\Delta_{13}(\overline{\Delta_{24}}+\overline{\Delta_{34}})]\}-|\Delta|^2\cdot cos^2\varphi\{|\Delta_{32}+\Delta_{34}|^2+$$
$$+|\overline{\Delta_{12}}+\overline{\Delta_{32}}|^2-[\bar{\Delta}\Delta_{32}+\Delta\bar{\Delta}_{32}+\bar{\Delta}_{13}(\Delta_{24}-\Delta_{32})+\Delta_{13}(\overline{\Delta_{24}}-\overline{\Delta_{32}})]\}=0.$$

According to our assumption $\Delta\neq 0$, so we can reduce this value, and as a result we have

$$sin^2\varphi-\{|\Delta_{32}+\Delta_{34}|^2+|\overline{\Delta_{12}}+\overline{\Delta_{32}}|^2-$$
$$-[\bar{\Delta}\Delta_{32}+\Delta\bar{\Delta}_{32}+\bar{\Delta}_{13}(\Delta_{24}-\Delta_{32})+\Delta_{13}(\overline{\Delta_{24}}-\overline{\Delta_{32}})]\}\cdot cos^2\varphi=0.$$

Theorem 3.1. If φ is the solution to the equation

$$\{[|\Delta_{32}+\Delta_{34}|^2+|\Delta_{14}+\Delta_{34}|^2]-\left[\Delta\cdot\overline{\Delta_{34}}+\bar{\bar{\Delta}}\cdot\Delta_{34}\right]+$$
$$+[\overline{\Delta_{13}}(\Delta_{24}+\Delta_{34})+\Delta_{13}(\overline{\Delta_{24}}+\overline{\Delta_{34}})]\}\cdot sin^2\varphi-$$
$$\{|\Delta_{32}+\Delta_{34}|^2+|\overline{\Delta_{12}}+\overline{\Delta_{32}}|^2+$$
$$+[\bar{\Delta}\Delta_{32}+\Delta\bar{\Delta}_{32}+\bar{\Delta}_{13}(\Delta_{24}-\Delta_{32})+\Delta_{13}(\overline{\Delta_{24}}-\overline{\Delta_{32}})]\}\cdot cos^2\varphi=0, \quad (13)$$

that is the formula

$$TL=L^+T^*,$$

where

$$T = i\cos\varphi\, I + \sin\varphi\, S,\ \ Sy(x) = y(1-x), \tag{14}$$

and $I -$ is the identity operator.

Theorem 3.2.

If $\varphi -$is the solution of equation (13), then there are formulas

1) $(TL)^2$=L^*L;

2) $(LT)^2$ = LL^*;

where $L -$ is the Sturm-Liouville operator,

$$T = i\cos\varphi\, I + \sin\varphi\, S,\ \ Sy(x) = y(1-x), \tag{14}$$

and $I -$ is the identity operator.

4. Discussions.

If

a) $\{[|\Delta_{32}+\Delta_{34}|^2 + |\Delta_{14}+\Delta_{34}|^2]\left[\Delta\cdot\overline{\Delta_{34}} + \bar{\bar{\Delta}}\cdot\Delta_{34}\right] + [\overline{\Delta_{13}}(\Delta_{24}+\Delta_{34}) + \Delta_{13}(\overline{\Delta_{24}}+\overline{\Delta_{34}})]\} = 0,$

$$\{|\Delta_{32}+\Delta_{34}|^2 + +|\overline{\Delta_{12}}+\overline{\Delta_{32}}|^2 -$$

$$-[\bar{\Delta}\Delta_{32} + \Delta\bar{\Delta}_{32} + \bar{\Delta}_{13}(\Delta_{24}-\Delta_{32}) + \Delta_{13}(\overline{\Delta_{24}}-\overline{\Delta_{32}})]\} \neq 0,$$

that $cos\varphi = 0$ and the operator T takes the form $T = S$, where

$Sy(x) = y(1-x)$;

b) $\{[|\Delta_{32}+\Delta_{34}|^2 + |\Delta_{14}+\Delta_{34}|^2]\left[\Delta\cdot\overline{\Delta_{34}} + \bar{\bar{\Delta}}\cdot\Delta_{34}\right] + [\overline{\Delta_{13}}(\Delta_{24}+\Delta_{34}) + \Delta_{13}(\overline{\Delta_{24}}+\overline{\Delta_{34}})]\} \neq 0$,

$\{|\Delta_{32}+\Delta_{34}|^2 + +|\overline{\Delta_{12}}+\overline{\Delta_{32}}|^2 - [\bar{\Delta}\Delta_{32} + \Delta\bar{\Delta}_{32} + \bar{\Delta}_{13}(\Delta_{24}-\Delta_{32}) + \Delta_{13}(\overline{\Delta_{24}}-\overline{\Delta_{32}})]\} = 0,$ то $\sin\varphi = 0$, and the operator T takes the form T=il, where $I -$is the unit operator.

In the first case, the closure of the SL operator is self-adjoint, and in the second case, the operator L is skew-symmetric, therefore its closure is the normal operator.

5. The authors are grateful to Anton Selitsky for his advice on the Kato hypothesis.

УДК 517.43

А.Ш. Шалданбаев[1], А.Б. Иманбаева[2], А.Ж. Бейсебаева[3], А.А. Шалданбаева[4]

[1]"Silkway" Халықаралық Университеті, Шымкент;
[2,3]М.Әуезов атындағы Оңтүстік Қазақстан Мемлекеттік Университеті, Шымкент;
[4]Аймақтық әлеуметтік - инновациялық университеті, Шымкент.

ТӨРТІНШІ РЕТТІ ШТУРМ-ЛИУВИЛЛ ОПЕРАТОРЫНЫҢ КВАДРАТ ТҮБІРІ ТУРАЛЫ

Аннотация. Бұл еңбекте Штурм-Лиувиллдің оң төртінші ретті операторынан квадрат түбір табылды. Ол қайтымды Штурм-Лиувилл операторы мен оның сыңарының композициясы немесе көбейтіндісі. Табылған түбір оң емес, бірақ тегі жалқы операторлар санатына жатады. Бағдарлаушы ретінде Путнамның бір алгебралық теоремасы қолданылды. Зерттеу нәтиежелері операторлардың спектрәлді теортясы мен теориялық физикада қолданыс табады деп күтілуде.

Түйін сөздер. Катоның гипотезасы, диссипативті оператор, операторлардың квадрат түбірі, Путнамның теоремасы, ауытқыған аргумент, операторлардың бөлшек түбірлері, кері есептер, спектр, жалқы оператор, оң операторлар, функционәл-дифференциал оператор, спектрәлді теория.

УДК 517.43

А.Ш. Шалданбаев[1], А.Б. Иманбаева[2], А.Ж. Бейсебаева[3], А.А. Шалданбаева[4]

[1]Международный университет “Silkway”, Шымкент;
[2,3]Южно-Казахстанский государственный университет имени М.Ауезова, Шымкент;
[4]Региональный социально-инновационный университет, Шымкент.

О КВАДРАТНОМ КОРНЕ ИЗ ОПЕРАТОРА ШТУРМА-ЛИУВИЛЛЯ ЧЕТВЁРТОГО ПОРЯДКА

Аннотация. В настоящей работе найден корень из положительного оператора Штурма - Лиувилля четвертого порядка, являющегося композицией обратимого оператора Штурма - Лиувилля и его сопряженного. Найденный корень не обладает свойством положительности, но является самосопряженным оператором в существенном. В качестве наводящей идеи использована одна теорема Путнама алгебраического характера. Можно надеяться, что результаты работы найдут приложения в спектральной теории операторов и теоретической физике.

Ключевые слова: гипотеза Като, диссипативный оператор, квадратный корень из оператора, теорема Путнама, отклоняющиеся аргумент, дробные степени оператора, обратная задача, спектр, унитарный оператор, самосопряженный оператор, положительный оператор, функционально-дифференциальный оператор, спектральная теория.

Information about authors:

Shaldanbayev A.Sh. – doctor of physico-mathematical Sciences, Professor, head of the center for mathematical modeling «Silkway» International University, Shymkent; http://orcid.org/0000-0002-7577-8402;

Imanbayeva A.B. - M.Auezov South Kazakhstan State University, Shymkent, Candidate of physical and mathematical Sciences, associate Professor; https://orcid.org/0000-0002-8203-7637;

Beisebayeva A.Zh. - M.Auezov South Kazakhstan State University, Shymkent; https://orcid.org/0000-0003-4839-9156;

Shaldanbayeva A.A. - Regional Social-Innovative University, Shymkent; https://orcid.org/0000-0003-2667-3097

REFERENCES

[1] U. Rudin, Functional Analysis, M.: Mir, **1975**.

[2] C.R. Putnam, Amer.Math., 73 (**1951**), 357-362.

[3] T. Kato, Fractional powers of dissipative operators, II, J. Math. Soc. Japan, 14 (**1962**), pp. 242–248.

[4] A. McIntosh, On the compatibility of A1/2 and A*1/2, Proc. Amer. Math. Soc., 32:2 (**1972**), pp. 430–434.

[5] A.M. Selitskiy, Initial data space of the second boundary value problem for a parabolic differential-difference equation, Scientific Bulletin of BelSU, Series: Mathematics. Physics. (**2011**). № 23(118). Issue 25, pp. 102-112.

[6] M.S. Agranovich and A.M. Selitskiy, Fractional degrees of operators corresponding to coercive problems in Lipschitz domains, Funct. Analysis and its Appl., (**2013**), volume 47, issue 2, pp.2–17.

[7] V. Balakrishnan (**1960**), Fractional powers of closed operators and the semi-groups generated by them. Pacific J. Math., 10:419–437.

[8] Andreas Axelsson, Stephen Keith, and Alan McIntosh (**2006**), The Kato square root problem for mixed boundary value problems. J. London Math. Soc. (2), 74(1):113–130.

[9] Andrea Bonito and Joseph E. Pasciak (**2015**), Numerical approximation of fractional powers of elliptic operators. Math. Comp., 84(295):2083–2110.

[10] Luis Caffarelli and Luis Silvestre (**2007**), An extension problem related to the fractional Laplacian.Comm. Partial Differential Equations, 32(7-9):1245–1260.

[11] Alan McIntosh (**1989**), The square root problem for elliptic operators: a survey. In Functional analytic methods for partial differential equations, Tokyo, volume 1450 of Lecture Notes in Math., pages 122–140. Springer, Berlin, 1990.

[12] M. S. Agranovich (**2012**), Remarks on strongly elliptic second-order systems in Lipschitz domains, Russian J. Math. Phys., 20:4, 405–416.

[13] M.S. Agranovich (**2013**), Sobolev spaces, their generalization and elliptic problems in domains with smooth and Lipschitz bound, M., Izd. MSNMO.

[14] Mihoko Matsuki and Teruo Ushijima (**1993**), A note on the fractional powers of operators approximating a positive definite selfadjoint operator. J. Fac. Sci. Univ. Tokyo Sect. IA Math.,40(2):517–528.

[15] Y. Berg and Y. Lefstrem (**1980**), Interpolation Spaces, Mir, M.

[16] T. Kato (**1972**), Perturbation Theory of Linear Operators, Mir, M.

[17] M.A. Krasnoselsky, P.P. Zabreiko, E.I. Pumulnik and P.E. Sobolevsky (**1966**), Integral operators in spaces of summable functions, Nauka, M.

[18] J.-L. Lyons and E. Madjenes (**1971**), Nonhomogeneous Boundary Value Problems and their Applications, Mir, M.

[19] A. M. Selitsky, Space of initial data of the 3rd boundary value problem for parabolic differential-difference equation in one-dimensional case, Math.Notes, 92: 4 (**2012**), 636–640.

[20] A.M. Selitsky, Modeling of some optical systems on the basis of a parabolic differential-difference equation, Math. Modeling, 24:12 (**2012**), 38–42.

[21] A. L. Skubachevsky and R.V. Shamin, Second-order parabolic differential-difference equations, Dokl. RAN, 379:5 (**2001**), 595–598.

[22] H. Triebel, Theory of Functional Spaces, Mir, M., 1986.

[23] I. Ya. Shneiberg, Spectral properties of linear operators in interpolational families of Banach spaces, Math. investig. 9:2 (**1974**), 214–229.

[24] Sh. Agmon, On the eigenfunctions and on the eigenvalues of general elliptic boundary value problems, Comm. Pure Appl. Math., 15:2 (**1962**), 119–147.

[25] W. Arendt, Semigroups and evolution equations: functional calculus, regularity and kernel estimates, in: Handbook of Differential Equations, Evolutionary Differential Equations, vol. 1, Elsevier/North-Holland, Amsterdam, **2004**, 1–85.

[26] P. Auscher, N. Badr, R. Haller-Dintelmann, J. Rehberg, The square root problem for second order, divergence form operators with mixed boundary conditions on Lp, http://arxiv.org/abs/1210.0780v1.

[27] P. Auscher, S. Hofmann, M. Lacey, J. Lewis, A. McIntosh, P. Tchamitchian, The solution of Kato's conjectures, C. R. Acad. Sci. Paris, S´er. 1, 332:7 (**2001**), 601–606.

[28] P. Auscher, A. McIntosh, A. Nahmod, Holomorphic functional calculi of operators, quadratic estimates and interpolation, Indiana Univ. Math. J., 46:2 (**1997**), 375–403.

[29] P. Auscher, S. Hofmann, A. McIntosch, P. Tchamitchian, The Kato square root problem for higher order elliptic operators and systems on Rn, J. Evol. Equ., 1:4 (**2001**), 361–385.

[30] P. Auscher, P. Tchamitchian, Square root problem for divergence operators and related topics, Ast´erisque, 249 (**1998**), 1–171.

[31] P. Auscher, P. Tchamitchian, Square roots of elliptic second order divergence operators on strongly Lipschitz domains: L2 theory, J. Anal. Math., 90 (**2003**), 1–12.

[32] P. Auscher, P. Tchamitchian, Square roots of elliptic second order divergence operators on strongly Lipschitz domains: Lp theory, Math. Ann., 320:3 (**2001**), 577–623.

[33] A. Axelsson, S. Keith, A. McIntosh, The Kato square root problem for mixed boundary value problems, J. London Math. Soc., 74:1 (**2006**), 113–130.

[34] S. Blunck, P. Kunstmann, Calderron–Zygmund theory for non-integral operators and the H∞ functional calculus, Rev. Mat. Iberoamericana, 19:3 (**2003**), 919–942.

[35] A.F. M. ter Elst, D.W. Robinson, On Kato's square root problem, Hokkaido Math. J., 26:2 (**1997**), 365–376.

[36] J. Griepentrog, K. Gr¨oger, H.-Ch.Kaiser, J. Rehberg, Interpolation for function spaces related to mixed boundary value problems, Math. Nachr., 241 (**2002**), 110–120.

[37] D. Grisvard, Caractrerisation de quelques espaces d'interpolation, Arc. Rational Mech. Anal., 25 (**1967**), 40–63.

[38] M. Haase, (**2006**), The Functional Calculus for Sectorial Operators, Birkh¨auser, Basel.

[39] S. Hoffmann, A short course on the Kato problem, Contemp. Math., 289 (**2001**), 61–67.

[40] T. Hyt¨onen, A. McIntosh and P. Portal, Kato's square root problem in Banach spaces, J.Funct. Anal., 254:3 (**2008**), 675–726.

[41] S. Janson, P. Nilsson, J. Peetre, Notes on Wolff's note on interpolation spaces, Proc. London Math. Soc. (3), 48:2 (**1984**), 283–299.

[42] H. Komatsu, Fractional powers of operators, Pacif. J. Math., 19 (**1966**), 285–346.

[43] J. L. Lions (**1961**), r Equations diffrerentielles operationelles et probl`emes aux limites, Springer-Verlag, Berlin etc.

[44] J. L. Lions, Espaces d'interpolation et domaines de puissances fractionaires d'operrateurs, J. Math. Soc. Japan, 14 (**1962**), 233–241.

[45] A. McIntosh, Square roots of elliptic operators, J. Funct. Anal., 61:3 (**1985**), 307–327.

[46] A. McIntosh, Operators which have an H∞functional calculus, in: Miniconference on Operator Theory and Partial Differential Equations, Proc. Centre Math. Anal.Austral. Nat. Univ., vol. 14, Austral. Nat. Univ., Canberra, (**1986**), 210–231.

[47] A. McIntosh (**1990**), Square Root Problem for Elliptic Operators: a Survey, Lecture Notes in Math., vol. 1450, Springer-Verlag, Berlin.

[48] W. McLean (**2000**), Strongly Elliptic Systems and Boundary Integral Equations, Cambridge Univ. Press, Cambridge, UK.

[49] J. Ne˘cas (**2012**), Les mrethodes directes en threorie des erquations elliptiques, Masson, Paris, 1967; Direct Methods in the Theory of Elliptic Equations, Springer-Verlag, Berlin–Heidelberg.

[50] L. Nirenberg, Remarks on strongly elliptic partial differential equations, Comm. Pure Appl. Math., 8 (**1965**), 649–675.

[51] R.T. Seeley, Norms and domains of the complex powers Az B, Amer. J. Math., 93:2(**1971**), 299–309.

[52] R.T. Seeley, Interpolation in Lp with boundary conditions, Studia Math., 44 (**1972**),47–60.

[53] A.L. Skubachevskii and R. V. Shamin, Mixed boundary value problem for parabolic differential-difference equation, Funct. Differ. Eq., 8:3–4 (**2001**), 407–424.

[54] T.W. Wolff, A note on interpolation spaces, in: Lecture Notes in Math., vol. 918, Springer-Verlag, Berlin–New York, (**1982**), 199–204.

[55] A. Yagi, Coincidence entre des espaces d'interpolation et des domaines de puissances fractionaires d'oprreateurs, C. R. Acad. Sci. Paris, S´er. 1, 299:6 (**1984**), 173–176.

[56] L. Hörmander (**1965**), Linear Partial Differential Operators, Mir, M.

[57] M.I. Vishik, On strongly elliptic systems of differential equations, Math. Sb., 29(71), 3(**1951**), 615–676.

[58] R.V. Shamin, On spaces of initial data for differential equations in a Hilbert space, Math. Sb., 194:9 (**2003**), 141-156.

[59] H. Namsrai, Square Kleino-Gordon operator and physical interpretation, International Journal of Theoretical Physics, (**1998**). T. 37. №5. pp.1531-1540.

[60] R. Putsio (**1994**), On square root of Laplace – Beltrami operator as Hamiltonian, Classical and Quantum Gravity. Vol. 11. No.3. Pp. 609-620.

[61] T.L. Gill and V.V. Zakhari, Analytical representation of square operator, Physical Journal A: Mathematics and general. (**2005**). Vol. 38. №11. Pp. 2479-2496.

[62] P.N. Vabishchevich, Numerical solution of non-stationary spatial-fractional problems with square root of an elliptic operator, Mathematical Modeling and Analysis. (**2016**). Vol. 21. No.2. Pp. 220-238.

[63] A. Bzdak and L. Hadash, Square root of a dirac operator on superspace and Maxwell equations, Physical Letters. Section B: Nuclear Physics, Elementary Particle and High Energy Physics. (**2004**). vol. 582. №1-2. Pp. 113-116.

[64] H.T. Ito, Resonances of square root of the Pauli operator, Publications of Research Institute of Mathematical Sciences. (**2017**). Vol. 53. No.4. Pp. 517-549.

[65] H. Namsray and H.V. Von Geramb, Quantization and nonlocality of square body: Review of International Journal of Theoretical Physics. (**2001**). vol. 40. № 11. pp. 1929-2010.

[66] V.P. Maslov (**1988**), Asymptotic Methods and Perturbation Theory, M.: Mir.

[67] V.A. Marchenko (**1977**), Sturm-Liouville Operators and Their Applications, Kiev, Naukova Dumka.

[68] T.Sh. Kalmenov, S.T. Akhmetova and A.Sh. Shaldanbaev, To spectral theory of equation with deviating arguments, Mathematical Journal, Almaty, (**2004**), vol.4., No.3, pp.41-48.

[69] M.I. Akylbayev, A.Zh. Beysebayeva and A.Sh. Shaldanbayev, News of the National Academy of Sciences of the Republic of Kazakhstan, Physico-mathematical Series,Volume 1, Number 317 (**2018**), 34 – 50.

[70] T.Sh. Kal'menov and A.Sh. Shaldanbaev, On a criterion of solvability of the inverse problem of heat conduction, Journal of Inverse and Ill-Posed Problems 18, 352-369 (**2010**).

[71] I. Orazov, A. Shaldanbayev and M. Shomanbayeva, About the Nature of the Spectrum of the Periodic Problem for the Heat Equation with a Deviating Argument,Abstract and Applied Analysis №:128363 DOI: 10.1155/2013/128363 Published: (**2013**),WOS:000325557100001.

N E W S
OF THE NATIONAL ACADEMY OF SCIENCES OF THE REPUBLIC OF KAZAKHSTAN
PHYSICO-MATHEMATICAL SERIES
ISSN 1991-346X **https://doi.org/10.32014/2019.2518-1726.29**
Volume 3, Number 325 (2019), 97 – 113

UDK 517.43

A.Sh. Shaldanbayev[1], A.A. Shaldanbayeva[2], B.A. Shaldanbay[3]

[1]"Silkway" International University, Shymkent;
[2]"Regional Social-Innovative University", Shymkent;
[3]M.Auezov South Kazakhstan State University, Shymkent
shaldanbaev51@mail.ru, altima_a@mail.ru, baglan.shaldanbayev@bk.ru

ON SQUARE ROOT OF STURM-LIUVILLE OPERATOR

Abstract. In this paper, we find square root of the Sturm – Liouville operator and show that this root is a functional-differential operator of first-order. Form of the corresponding boundary problem of this functional - differential equation is found. As a suggestive idea, we use one Putnam theorem. Boundary value conditions of the Sturm-Liouville operator have a very special form, and they are dictated by the method of investigation. The found unitary operator generalizes the known momentum operator.

Keywords. Sturm-Liouville operator, square root of operator, functional differential operator, equations with deviating argument, Kato hypothesis, Macintosh example, Gours operator, inverse problem, spectrum, eigenvalues, eigenfunctions, unitary operator, similarity operator.

1. Introduction. It is known [1.p.393], that if A is a self-adjoint and non-negative operator in a Hilbert space H, then there exists unit self-adjoint operator $B \geq 0$ such that $B^2 = A$. The following theorem from the same source says that not every operator has a square root.

Theorem 1.1 [1.p.357]. Let D be a bounded open set in $\mathbb{C}$ such that the set

$$\Omega = \{\alpha \in \mathbb{C}: \alpha^2 \in D\}$$

is connected and the point 0 does not belong to the closure of the set D. Let H be a set of all holomorphic functions f in D such that

$$\int_D |f|^2 dm_2 < \infty$$

(where m_2 is a Lebesgue flat measure). We give in H scalar product by the formula:

$$(f, g) = \int_D f\bar{g} dm_2.$$

Then H is a Hilbert space. We define the product operator $M \in \mathcal{B}(H)$, assuming

$$(Mf)(z) = zf(z), \qquad (f \in H, z \in D).$$

Then the operator M is invertible in $\mathcal{B}(H)$, but it does not have a square root.

Extending the concept of a root to dissipative operators, Kato hypothesis has been arisen, consisting in the fact that the domain of a root from an operator always coincides with the domain of a root from an adjoint operator. However, in 1972 A.Makintosh [3] built a counterexample, since then the hypothesis was slightly reformulated: find the largest class of operators that satisfies this condition, and very active research in this direction is currently cited [4-57].

Many operators of theoretical physics have square roots [57–64]; in particular, the square root of operator A in a Banach space was found in [65, pp.169-176]. We give an excerpt from this work.

We consider a generating operator A in a Banach space $\mathcal{B}$, that has the following properties:

1) Operator $(I+\gamma^2 A)^{-1}$ exists, is defined everywhere in $\mathcal{B}$ and bounded by one;
2) Operator A^{-1} exists;
3) $\left\|e^{iAt}\right\| \le M,\ -\infty < t < +\infty.$

In these conditions the following lemmas hold.

Lemma 1.1. Operator

$$T = \frac{2e^{-i\pi/4}}{\sqrt{\pi}} A \int_0^{\infty} e^{iAx^2} dx$$

exists as an operator in $\mathcal{B}$ in the domain $D(A)$.

Lemma 1.2. For any $y \in D(A)$ the following equality is true

$$T^2 g = Ag.$$

Due to these results, the following problem arises.

1. Formulation of the problem. Find a square root of the Sturm - Liouville operator

$$Ly = -y''(x),\ x \in (0,1), \tag{1.1}$$

$$\begin{cases} \alpha y(0) + \beta y(1) = 0, \\ \alpha y'(1) + \beta y'(0) = 0, \end{cases} \tag{1.2}$$

where $\alpha,\ \beta$ are arbitrary (yet) complex numbers, satisfying the condition

$$|\alpha| + |\beta| \ne 0. \tag{1.3}$$

2. Research methods.

Calculate minors of the boundary matrix

$$\begin{pmatrix} \alpha & 0 & \beta & 0 \\ 0 & \beta & 0 & \alpha \end{pmatrix},$$

$$J_{12} = \alpha\beta, \quad J_{13} = 0, \quad J_{14} = \alpha^2, \quad J_{23} = -\beta^2, \quad J_{24} = 0, \quad J_{34} = \alpha\beta.$$

If $J_{14} + J_{32} = \alpha^2 + \beta^2 \ne 0$, then the Sturm - Liouville problem (1.1) - (1.3) has a complete system of eigen and associated functions, see [66., p.41].

Find eigenfunctions of the Sturm-Liouville problem (1.1) - (1.2). General solution of the equation (1.1) has the form:

$$y(x,\lambda) = A\cos\lambda x + B\frac{\sin\lambda x}{\lambda}, \tag{1.4}$$

where $A,\ B$ are arbitrary constants. Putting (1.4) into (1.2), we have

$$y'(x,\lambda) = -\lambda A\sin\lambda x + B\cos\lambda x,$$

$$y(0) = A, \quad y'(0) = B, \quad y(1) = A\cos\lambda + B\frac{\sin\lambda}{\lambda}, \quad y'(1) = -\lambda A\sin\lambda + B\cos\lambda;$$

$$\begin{cases} A\cdot\alpha + \beta\left(A\cos\lambda + B\dfrac{\sin\lambda}{\lambda}\right) = 0, \\ \alpha(-\lambda A\sin\lambda + \beta\cos\lambda) + B\cdot\beta = 0; \end{cases}$$

$$\begin{cases} A(\alpha + \beta\cos\lambda) + B\cdot\dfrac{\beta\sin\lambda}{\lambda} = 0, \\ A(-\lambda\alpha\sin\lambda) + B(\alpha\cos\lambda + \beta) = 0. \end{cases}$$

Therefore, we obtained the system of equations

$$\begin{cases} A(\alpha + \beta\cos\lambda) + B\cdot\dfrac{\beta\sin\lambda}{\lambda} = 0, \\ A(-\lambda\alpha\sin\lambda) + B(\alpha\cos\lambda + \beta) = 0. \end{cases}$$

determinant of which has the form

$$\Delta(\lambda)=\begin{vmatrix}\alpha+\beta\cos\lambda & \frac{\beta\sin\lambda}{\lambda}\\ -\lambda\alpha\sin\lambda & \alpha\cos\lambda+\beta\end{vmatrix}=(\alpha+\beta\cos\lambda)(\alpha\cos\lambda+\beta)+\alpha\beta sin^2\lambda=$$
$$=\alpha^2\cos\lambda+\alpha\beta+\beta\alpha cos^2\lambda+\beta^2\cos\lambda+\alpha\beta sin^2\lambda=$$
$$=\alpha^2\cos\lambda+\beta^2\cos\lambda+2\alpha\beta=(\alpha^2+\beta^2)\cos\lambda+2\alpha\beta.$$

If $\Delta(\lambda)=0$, then $\cos\lambda=-\frac{2\alpha\beta}{\alpha^2+\beta^2}$,

$$\dot{\Delta}(\lambda)=-(\alpha^2+\beta^2)\sin\lambda=\mp(\alpha^2+\beta^2)\sqrt{1-\frac{4\alpha^2\beta^2}{(\alpha^2+\beta^2)^2}}=$$
$$=\mp(\alpha^2+\beta^2)\frac{\alpha^2-\beta^2}{\alpha^2+\beta^2}=\mp(\alpha^2-\beta^2).$$

Consequently, if $\alpha^2-\beta^2\neq 0$, then the associated functions of the Sturm – Liouville operator are absent, so the eigenfunctions of the boundary value problem (1.1) - (1.2) are complete in the space $L_2(0,1)$.

Assuming,

$$A=\frac{\beta\sin\lambda}{\lambda},\ B=-(\alpha+\beta\cos\lambda)$$

and taking into account that

$$\cos\lambda=-\frac{2\alpha\beta}{\alpha^2+\beta^2}$$

we have

$$B=-(\alpha+\beta\cos\lambda)=-\left(\alpha-\frac{2\alpha\beta^2}{\alpha^2+\beta^2}\right)=-\alpha\left(1-\frac{2\beta^2}{\alpha^2+\beta^2}\right)=$$
$$=-\alpha\cdot\frac{\alpha^2+\beta^2-2\beta^2}{\alpha^2+\beta^2}=-\alpha\cdot\frac{\alpha^2-\beta^2}{\alpha^2+\beta^2};$$
$$A=\pm\frac{\beta}{\lambda}\sqrt{1-\frac{4\alpha^2\beta^2}{(\alpha^2+\beta^2)^2}}=\pm\frac{\beta}{\lambda}\cdot\frac{\alpha^2-\beta^2}{\alpha^2+\beta^2}.$$

If $\lambda=0$, then $\Delta(0)=\alpha^2+\beta^2+2\alpha\beta=(\alpha+\beta)^2$, consequently, if $\alpha^2-\beta^2\neq 0$, then $\Delta(0)\neq 0$.

If $|A|+|B|=0$, then $|\alpha|\cdot|(\alpha^2-\beta^2)|+|\beta|\cdot|(\alpha^2-\beta^2)|=0,=>$

$(|\alpha|+|\beta|)|\alpha^2-\beta^2|=0$, hence by the condition (1.3) it follows that

$$\alpha^2-\beta^2=0.$$

Therefore, when $\alpha^2-\beta^2\neq 0$ the solution (eigenfunction)

$$y(x,\lambda)=A\cos\lambda x+B\frac{\sin\lambda x}{\lambda}$$

is not degenerate, i.e. $y(x,\lambda)\not\equiv 0$.

Further, we transform the eigenfunction:

$$y(x,\lambda)=\pm\frac{\beta}{\lambda}\cdot\frac{\alpha^2-\beta^2}{\alpha^2+\beta^2}\cos\lambda x-\frac{\alpha(\alpha^2-\beta^2)}{\lambda(\alpha^2+\beta^2)}\sin\lambda x=$$
$$=\frac{\alpha^2-\beta^2}{\lambda(\alpha^2+\beta^2)}(\pm\beta\cos\lambda x-\alpha\sin\lambda x);$$
$$y(1-x,\lambda)=\frac{\alpha^2-\beta^2}{\lambda(\alpha^2+\beta^2)}[\pm\beta\cos\lambda(1-x)-\alpha\sin\lambda(1-x)]=$$

$$= \frac{\alpha^2 - \beta^2}{\lambda(\alpha^2 + \beta^2)}(\pm\beta \cos\lambda \cos\lambda x \pm \beta \sin\lambda \sin\lambda x - \alpha \sin\lambda \cos\lambda x +$$

$$+\alpha \cos\lambda \sin\lambda x) = \frac{\alpha^2 - \beta^2}{\lambda(\alpha^2 + \beta^2)}[(\pm\beta \cos\lambda - \alpha \sin\lambda) \cos\lambda x +$$

$$+(\alpha \cos\lambda \pm \beta \sin\lambda) \cdot \sin\lambda x];$$

Further,

$$\pm\beta \cos\lambda - \alpha \sin\lambda = \mp\frac{2\alpha\beta^2}{\alpha^2 + \beta^2} \mp \frac{\alpha(\alpha^2 - \beta^2)}{\alpha^2 + \beta^2} = \frac{\mp\alpha^3 \pm \alpha\beta^2 \mp 2\alpha\beta^2}{\alpha^2 + \beta^2} =$$

$$= \frac{\mp\alpha^3 \mp \alpha\beta^2}{\alpha^2 + \beta^2} = \mp\frac{\alpha(\alpha^2 + \beta^2)}{\alpha^2 + \beta^2} = \mp\alpha$$

$$\alpha \cos\lambda \pm \beta \sin\lambda = -\frac{2\alpha^2\beta}{\alpha^2 + \beta^2} \pm \beta\left(\pm\frac{\alpha^2 - \beta^2}{\alpha^2 + \beta^2}\right) =$$

$$= \frac{\beta(\alpha^2 - \beta^2) - 2\alpha^2\beta}{\alpha^2 + \beta^2} = \frac{\beta\alpha^2 - \beta^3 - 2\alpha^2\beta}{\alpha^2 + \beta^2} = \frac{-\beta^3 - \alpha^2\beta}{\alpha^2 + \beta^2} =$$

$$= -\frac{\beta(\alpha^2 + \beta^2)}{\alpha^2 + \beta^2} = -\beta.$$

Consequently,

$$y(1 - x, \lambda) = \frac{\alpha^2 - \beta^2}{\lambda(\alpha^2 + \beta^2)}(\mp\alpha \cos\lambda x - \beta \sin\lambda x) =$$

$$= \mp\frac{\alpha^2 - \beta^2}{\lambda(\alpha^2 + \beta^2)}(\alpha \cos\lambda x \pm \beta \sin\lambda x); \quad (1.5)$$

$$y'(x, \lambda) = \frac{\alpha^2 - \beta^2}{\lambda(\alpha^2 + \beta^2)} \cdot \lambda(\mp\beta \sin\lambda x - \alpha \cos\lambda x) =$$

$$-\lambda\frac{\alpha^2 - \beta^2}{\lambda(\alpha^2 + \beta^2)}(\alpha \cos\lambda x \pm \beta \sin\lambda x) =$$

$$= -\frac{\alpha^2 - \beta^2}{\alpha^2 + \beta^2}(\alpha \cos\lambda x \pm \beta \sin\lambda x). \quad (1.6)$$

Comparison of the formulas (1.5) - (1.6) shows that

$$y'(x, \lambda) = \pm\lambda y(1 - x, \lambda). \quad (1.7)$$

We consider the case $\alpha^2 - \beta^2 = 0$ separately.

If $\alpha^2 - \beta^2 = 0$, then $\beta = \pm\alpha$,

$$\Delta(\lambda) = 2\alpha^2 \cos\lambda \pm 2\alpha^2 = 2\alpha^2(\cos\lambda \pm 1), => \cos\lambda \pm 1 = 0.$$

In this case,

$$B = -(\alpha + \beta \cos\lambda) = -(\alpha \pm \alpha \cos\lambda) = -\alpha(1 \pm \cos\lambda) = 0,$$

$$A = \beta \frac{\sin \lambda}{\lambda} = 0.$$

In this case we should choose the coefficients by using another method.

Let

$y(x,\lambda) = \cos \lambda x + \sin \lambda x$, where $\cos \lambda \pm 1 = 0$, then

$$W[y(x,\lambda), y(1-x,\lambda)] = \begin{vmatrix} \cos \lambda x + \sin \lambda x & \cos \lambda x - \sin \lambda x \\ \lambda(\cos \lambda x - \sin \lambda x) & -\lambda(\cos \lambda x + \sin \lambda x) \end{vmatrix} =$$

$$= -\lambda[(\cos \lambda x + \sin \lambda x)^2 + (\cos \lambda x - \sin \lambda x)^2] =$$

$$= -\lambda(1+1) = -2\lambda \neq 0.$$

$$y(1-x,\lambda) = \cos \lambda (1-x) + \sin \lambda (1-x) = \cos \lambda \cos \lambda x + \sin \lambda \sin \lambda x +$$

$$+ \sin \lambda \cos \lambda x - \cos \lambda \sin \lambda x = \cos \lambda (\cos \lambda x - \sin \lambda x);$$

$$y'(x,\lambda) = \lambda(-\sin \lambda x + \cos \lambda x) = \lambda(\cos \lambda x - \sin \lambda x) = \frac{\lambda}{\cos \lambda} y(1-x,\lambda),$$

where $\cos \lambda = \pm 1$, consequently,

$$y'(x,\lambda) = \pm \lambda y(1-x,\lambda). \tag{1.7}$$

Let's check the boundary conditions:

$$y(x,\lambda) = \frac{\alpha^2 - \beta^2}{\lambda(\alpha^2+\beta^2)}(\mp\beta \cos \lambda x - \alpha \sin \lambda x) =$$

$$= \frac{K}{\lambda}(\mp\beta \cos \lambda x - \alpha \sin \lambda x).$$

$$y(x,-\lambda) = \frac{\alpha^2 - \beta^2}{-\lambda(\alpha^2+\beta^2)}(\mp\beta \cos \lambda x + \alpha \sin \lambda x) =$$

$$= \frac{K}{-\lambda}(\mp\beta \cos \lambda x + \alpha \sin \lambda x),$$

$$y'(x,\lambda) = K(\mp\beta \sin \lambda x - \alpha \cos \lambda x),$$

$$y'(x,-\lambda) = K(\pm \sin \lambda x - \alpha \cos \lambda x),$$

$$W[y(x,\lambda), y(x,-\lambda)] = \begin{vmatrix} \pm\beta \frac{K}{\lambda} & \mp\beta \frac{K}{\lambda} \\ -\alpha K & -\alpha K \end{vmatrix} = -\alpha K \begin{vmatrix} \pm\beta & \mp\beta \\ 1 & 1 \end{vmatrix} \frac{K}{\lambda} =$$

$$= -\frac{\alpha K^2}{\lambda}(\pm\beta \pm \beta) = \mp \frac{2\alpha\beta K^2}{\lambda} = \mp \frac{2\alpha\beta}{\lambda}\left[\frac{\alpha^2-\beta^2}{\alpha^2+\beta^2}\right]^2.$$

Lemma 2.1. If

$$\frac{\alpha\beta}{\lambda} \cdot \frac{\alpha^2-\beta^2}{\alpha^2+\beta^2} \neq 0$$

then any eigenfunction of the Sturm-Liouville boundary value problem (1.1) - (1.2)

$$Ly = -y''(x) = \lambda^2 y(x), \ x \in (0,1), \tag{1.1}$$

$$\begin{cases} \alpha y(0) + \beta y(1) = 0, \\ \alpha y'(1) + \beta y'(0) = 0, \end{cases} \tag{1.2}$$

is an eigenfunction of the boundary value problem

$$ly = y'(1-x) = \lambda y(x),$$

$$\alpha y(0) + \beta y(1) = 0;$$

i.e. the formula

$$l^2 y = \left(S\frac{d}{dx}\right)^2 y = Ly = -y''(x)$$

holds, where the operator S has the following form

$$Su(x) = u(1-x), \qquad \forall u(x) \in L^2(0,1).$$

In this sense, the operator L is the square root of the Sturm-Liouville operator.

The case $\alpha \cdot \beta(\alpha^2 - \beta^2) = 0$ requires separate study.

We find the operator $\sqrt{L}$, where

$$Ly = -y''(x), \ x \in (0,1),$$

$$y(0) - y(1) = 0, \ y'(0) - y'(1) = 0.$$

General idea of the solution is as follows: first, we represent the operator L in the form

$$L = l^+ l$$

the product of two mutually conjugate operators, then we find the similarity operator T such that

$$Tl^+ l = ll^+ T.$$

From Putnam's theorem [1. p.337] it follows that such an operator will certainly be unitary, that is, there is the equality

$$T^* T = TT^* = I,$$

where I is unit operator. In our observation [67], our desired operator has the form Tl, where

$$ly(x) = y'(x), \qquad y(0) - y(1) = 0.$$

We solve these problems step by steps, and more in detail.

Let $$ly(x) = y'(x), \ x \in (0,1),$$

$$\alpha y(0) + \beta y(1) = 0, \ |\alpha| + |\beta| \neq 0. \tag{1.8}$$

We find formal conjugate operator l^+.

Let $y \in D(l)$ and $z \in D(l^+)$, then the formula

$$(ly, z) = (y, l^+ z),$$

holds, where the scalar product has the form

$$(u,v)=\int_0^1 u(x)\overline{v(x)}\,dx.$$

$$(ly,z)=\int_0^1 y'(x)\bar{z}(x)dx=\int_0^1 \bar{z}(x)\,dy=\overline{z(x)}y(x)\Big|_0^1-\int_0^1 y(x)\bar{z}'(x)dx,$$

thus, we have $\overline{z(1)}y(1)-\overline{z(0)}y(0)=0$. Combining this condition with the boundary condition (1.8), we obtain the system of equations

$$\begin{cases}\overline{z(0)}y(0)-\overline{z(1)}y(1)=0,\\ \alpha y(0)+\beta y(1)=0,\end{cases}$$

which has nontrivial solution, therefore

$$\Delta=\begin{vmatrix}\overline{z(0)} & -\overline{z(1)}\\ \alpha & \beta\end{vmatrix}=\beta\overline{z(0)}+\alpha\overline{z(1)}=0,$$

then

$$\bar{\beta}z(0)+\bar{\alpha}z(1)=0.$$

Therefore,

$$l^+z=-z'(x),\qquad x\in(0,1),$$
$$\bar{\beta}z(0)+\bar{\alpha}z(1)=0.$$

Remark. If $D(l)=D(l^+)$,

then

$$\begin{cases}\alpha y(0)+\beta y(1)=0,\\ \bar{\beta}y(0)+\bar{\alpha}y(1)=0;\end{cases}\Rightarrow\ |\alpha|^2-|\beta|^2=0,\qquad |\alpha|=|\beta|.$$

We find the operator l^+l , and research its spectral properties.

Assuming $A=l^+l$, we have

$$Ay=l^+ly=l^+y'=-y''(x),\qquad x\in(0,1);$$
$$\alpha y(0)+\beta y(1)=0,\qquad \bar{\beta}y'(0)+\bar{\alpha}y'(1)=0.$$

We construct the boundary matrix

$$\begin{pmatrix}\alpha & 0 & \beta & 0\\ 0 & \bar{\beta} & 0 & \bar{\alpha}\end{pmatrix}$$

and calculate minors:

$$J_{12}=\alpha\bar{\beta},\qquad J_{13}=0,\qquad J_{14}=|\alpha|^2,\qquad J_{23}=-|\beta|^2,$$
$$J_{24}=0,\qquad J_{34}=\beta\bar{\alpha}.$$

We find the characteristic function [66, p.35].

$$\Delta(\lambda)=J_{12}+J_{34}+(J_{14}+J_{32})\cos\lambda+J_{13}\frac{\sin\lambda}{\lambda}+J_{24}\lambda\sin\lambda=$$
$$=\alpha\bar{\beta}+\beta\bar{\alpha}+(|\alpha|^2+|\beta|^2)\cos\lambda=0,$$
$$\cos\lambda=-\frac{\alpha\bar{\beta}+\beta\bar{\alpha}}{|\alpha|^2+|\beta|^2},\Rightarrow\ \lambda_n=arccos\left[-\frac{\alpha\bar{\beta}+\beta\bar{\alpha}}{|\alpha|^2+|\beta|^2}\right]+2n\pi,n=0,\pm1,\pm2,..$$

Now we find the eigenfunctions:

$$Ay=-y''(x)=\lambda^2y(x),\ x\in(0,1);$$

General solution of this equation has the form

$$y(x,\lambda) = A\cos\lambda\, x + B\frac{\sin\lambda\, x}{\lambda},$$

thus we have,

$$y(0) = A, \qquad y(1) = A\cos\lambda + B\frac{\sin\lambda}{\lambda},$$

$$\alpha A + \beta\left(A\cos\lambda + B\frac{\sin\lambda}{\lambda}\right) = 0,$$

$$A(\alpha + \beta\cos\lambda) + \beta\frac{\sin\lambda}{\lambda}\cdot B = 0;$$

Further,

$$y'(x) = -\lambda A\sin\lambda\, x + B\cos\lambda\, x,$$

$$y'(0) = B, \qquad y'(1) = -\lambda A\sin\lambda + B\cos\lambda,$$

$$\bar{\beta}B + \bar{\alpha}(-\lambda A\sin\lambda + B\cos\lambda) = 0,$$

$$-\lambda\bar{\alpha}\sin\lambda\, A + B\left(\bar{\alpha}\cos\lambda + \bar{\beta}\right) = 0.$$

We construct the system of equations:

$$\begin{cases} A(\alpha + \beta\cos\lambda) + B\cdot\beta\dfrac{\sin\lambda}{\lambda} = 0, \\ A(-\lambda\bar{\alpha}\sin\lambda) + B\left(\bar{\alpha}\cos\lambda + \bar{\beta}\right) = 0. \end{cases}$$

Calculate determinant of the system:

$$\Delta = \begin{vmatrix} \alpha + \beta\cos\lambda & \beta\dfrac{\sin\lambda}{\lambda} \\ -\lambda\bar{\alpha}\sin\lambda & \bar{\alpha}\cos\lambda + \bar{\beta} \end{vmatrix} = 0.$$

$$(\alpha + \beta\cos\lambda)\left(\bar{\alpha}\cos\lambda + \bar{\beta}\right) + \bar{\alpha}\beta\sin^2\lambda = |\alpha|^2\cos\lambda + \alpha\bar{\beta} + \beta\bar{\alpha}\cos^2\lambda +$$

$$+|\beta|^2\cos\lambda + \bar{\alpha}\beta\sin^2\lambda = (|\alpha|^2 + |\beta|^2)\cos\lambda + \alpha\bar{\beta} + \bar{\alpha}\beta = 0,$$

$$\cos\lambda = -\frac{\alpha\bar{\beta} + \bar{\alpha}\beta}{|\alpha|^2 + |\beta|^2}, => \ \lambda_n = arccos\left[-\frac{\alpha\bar{\beta} + \bar{\alpha}\beta}{|\alpha|^2 + |\beta|^2}\right] + 2n\pi, n = 0, \pm1, \pm2, ..$$

Assuming

$$A_n = \beta\frac{\sin\lambda_n}{\lambda_n}\cdot K_n, \qquad B_n = -(\alpha + \beta\cos\lambda_n)\cdot K_n,$$

we construct the eigenfunctions:

$$y_n(x) = \frac{K_n}{\lambda_n}[\beta\sin\lambda_n\ \cos\lambda_n\, x - (\alpha + \beta\cos\lambda_n)\sin\lambda_n\ x] =$$

$$= \frac{K_n}{\lambda_n}(\beta\sin\lambda_n\cos\lambda_n\, x - \beta\cos\lambda_n\sin\lambda_n\, x - \alpha\sin\lambda_n\, x) =$$

$$= \frac{K_n}{\lambda_n}[\beta\sin(\lambda_n - \lambda_n x) - \alpha\sin\lambda_n\, x] =$$

$$= \frac{K_n}{\lambda_n}[\beta\sin\lambda_n\,(1 - x) - \alpha\sin\lambda_n x];$$

We formulate the obtained result in the form of Lemma 2.2.

Lemma 2.2. Eigenvalues and eigenfunctions of the operator A have the following form:

a) $\lambda_n = arccos\left[-\frac{\alpha\bar{\beta}+\bar{\alpha}\beta}{|\alpha|^2+|\beta|^2}\right] + 2n\pi, n = 0, \pm1, \pm2, \dots;$

b) $y_n(x) = \frac{K_n}{\lambda_n}[\beta \sin\lambda_n (1-x) - \alpha \sin\lambda_n x],$

where K_n are arbitrary constants.

We find the operator $B = ll^+$, and study its spectral properties.

$$ly = y'(x),\ x \in (0,1);$$

$$\alpha y(0) + \beta y(1) = 0,$$

$$l^+z = -z'(x), \qquad x \in (0,1),$$

$$\bar{\beta}z(0) + \bar{\alpha}z(1) = 0.$$

$$l^+z = -z'(x) \in D(l), => \ \alpha[-z'(0)] + \beta[-z'(1)] = 0,$$

$$Bz = ll^+z = -z''(x), \qquad x \in (0,1),$$

$$\bar{\beta}z(0) + \bar{\alpha}z(1) = 0, \qquad \alpha z'(0) + \beta z'(1) = 0.$$

We find eigenvalues and eigenfunctions of the operator B:

$$Bz = -z''(x) = \mu^2 z(x), \qquad x \in (0,1);$$

$$\begin{cases} \bar{\beta}z(0) + \bar{\alpha}z(1) = 0, \\ \alpha z'(0) + \beta z'(1) = 0. \end{cases}$$

General solution of the equation $-z''(x) = \mu^2 z(x)$ has the following form:

$$z(x) = A\cos\mu x + B\frac{\sin\mu x}{\mu},$$

where A, B are arbitrary constants, hence we have

$$z(0) = A, \qquad z(1) = A\cos\mu + B\frac{\sin\mu}{\mu},$$

$$\bar{\beta}A + \bar{\alpha}\left(A\cos\mu + B\frac{\sin\mu}{\mu}\right) = 0,$$

$$A\left(\bar{\beta} + \bar{\alpha}\cos\mu\right) + \alpha\frac{\sin\mu}{\mu}\cdot B = 0;$$

In a similar way we get:

$$z'(x) = -\mu A\sin\mu x + B\cos\mu x,$$

$$z'(0) = B, \qquad z'(1) = -\mu A\sin\mu + B\cos\mu,$$

$$\alpha B + \beta(-\mu A\sin\mu + B\cos\mu) = 0,$$

$$A(-\beta\mu\sin\mu) + B(\alpha + \beta\cos\mu) = 0.$$

We construct the system of equations:

$$\begin{cases} \left(\bar{\beta} + \bar{\alpha}\cos\mu\right)A + \bar{\alpha}\dfrac{\sin\mu}{\mu}\cdot B = 0, \\ (-\beta\mu\sin\mu)A + (\alpha + \beta\cos\mu)B = 0. \end{cases}$$

Calculate determinant of this system of equations:

$$\Delta = \begin{vmatrix} \bar{\beta} + \bar{\alpha}\cos\mu & \bar{\alpha}\dfrac{\sin\mu}{\mu} \\ -\beta\mu\sin\mu & \alpha + \beta\cos\mu \end{vmatrix} = \left(\bar{\beta} + \bar{\alpha}\cos\mu\right)(\alpha + \beta\cos\mu) +$$

$$+\bar{\alpha}\beta sin^2\mu = \bar{\beta}\alpha + |\beta|^2\cos\mu + |\alpha|^2\cos\mu + \bar{\alpha}\beta\cos^2\mu + \bar{\alpha}\beta\sin^2\mu =$$

$$= (|\alpha|^2 + |\beta|^2)\cos\mu + \alpha\bar{\beta} + \bar{\alpha}\beta = 0,$$

$$\cos\mu = -\frac{\alpha\bar{\beta} + \bar{\alpha}\beta}{|\alpha|^2 + |\beta|^2}, => \ \mu_n = arccos\left[-\frac{\alpha\bar{\beta} + \bar{\alpha}\beta}{|\alpha|^2 + |\beta|^2}\right] + 2n\pi, n = 0, \pm1, \pm2, ..$$

We find the eigenfunctions:

$$A_n = K_n\cdot(\alpha + \beta\cos\mu_n), \qquad B_n = K_n\beta\cdot\mu_n\sin\mu_n,$$

$$z_n(x) = K_n(\alpha + \beta\cos\mu_n)\cos\mu_n x + K_n\beta\cdot\mu_n\sin\mu_n\cdot\frac{\sin\mu}{\mu} =$$

$$= K_n(\alpha\cos\mu_n x + \beta\cos\mu_n\cos\mu_n x + \beta\sin\mu_n\sin\mu_n x) =$$

$$= K_n[\alpha\cos\mu_n x + \beta\cos(\mu_n - \mu_n x)] =$$

$$= K_n[\alpha\cos\mu_n x - \beta\cos\mu_n(1 - x)].$$

Lemma 2.3. Spectrum of the operator

$$Bz = -z''(x), \qquad x \in (0,1);$$

$$\begin{cases} \bar{\beta}z(0) + \bar{\alpha}z(1) = 0, \\ \alpha z'(0) + \beta z'(1) = 0, \end{cases}$$

consists of eigenvalues:

$$\mu_n = arccos\left[-\frac{\alpha\bar{\beta} + \bar{\alpha}\beta}{|\alpha|^2 + |\beta|^2}\right] + 2n\pi, n = 0, \pm1, \pm2, ...$$

which correspond to the eigenfunctions:

$$z_n(x) = K_n[\alpha\cos\mu_n x - \beta\cos\mu_n(1 - x)],$$

where K_n are arbitrary constants.

We note that there is the following equality

$$\lambda_n = \mu_n, \qquad n = 0, \pm1, \pm2, ...$$

i.e. spectrums of the operators A and B coincide, and this happens when operators A and B are similar to each other, i.e. there is the equality

$$TA = BT,$$

where $T,\ T^{-1}$ are linear bounded operators.

We find the similarity operator T. We note that

$$l^+l = A, \qquad ll^+ = B$$

thus

$$ll^+l = lA, \qquad ll^+l = Bl,$$

i.e. $lA = Bl$, but the operator l is unbounded, therefore it is not suitable for our purposes.

As a suggestive idea, we take the following Putnam theorem.

Theorem [1. p.337]. Let $M, N, T \in \mathcal{B}(H)$, moreover the operators M, N are normal, and the operator T is invertible. We suppose that

$$M = TNT^{-1}. \tag{1.9}$$

If $T = UP$ is a polar decomposition of the operator T, then

$$M = UNU^{-1}.$$

Two operators, connected by the relation (1.9), are called similar. If U is a unitary operator and the relation (1.9) holds, then the operators M and N are called unitarily equivalent. Thus, in this theorem we establish that similar normal operators are unitarily equivalent.

Our operators A, B are Hermitian (i.e., symmetric), and such operators belong to the class of normal operators; therefore, there exists a unitary operator T such that

$$AT = TB.$$

We assume that exactly this operator is a solution of the equations:

$$(Tl)^2 = l^+l = A, \qquad (lT)^2 = ll^+ = B.$$

Perhaps, it is necessary to impose additional conditions to the operator T?!

From the formula

$$(Tl)^2 = Tl \cdot Tl = l^*l,$$

we see that it is necessary to require $Tl = l^*T^*$, then

$$Tl \cdot Tl = l^* \underbrace{T^*T}_{I} l = l^*l = A,$$

Further, from $Tl = l^*T^*$, we get

$$TlT = l^*, \qquad lT = T^{-1}l^* = T^*l^*,$$

then

$$(lT)^2 = lT \cdot lT = |lT = T^*l^*| = lT \cdot T^*l^* = ll^* = B.$$

Moreover,

$$TB = Tll^* = l^*T^*l^* = l^*lT = AT.$$

We have proved the following lemma.

Lemma 2.4. If T is an unitary operator satisfying the condition

$$(Tl)^* = Tl = l^*T^*,$$

then the following formulas hold:

a) $(Tl)^2 = l^*l = A$,

b) $(lT)^2 = ll^* = B$,

c) $AT = TB$.

Therefore, the problem has come down to finding a unitary operator T, with the property $Tl = l^*T^*$.

We build an unitary operator T, satisfying the condition:

$$Tl = l^*T^*.$$

If $y \in D(l)$, then $z(x) = T^*y(x) \in D(l^*)$. We look for the operator T as follows

$$T = i\cos\varphi\, I + \sin\varphi \cdot S,$$

where $Su(x) = u(1-x)$, I is unit operator, φ is unknown (yet) angle, then

$$T^* = -i\cos\varphi\, I + \sin\varphi \cdot S,$$

$$TT^* = \cos^2\varphi \cdot I + i\cos\varphi \cdot \sin\varphi \cdot S - i\cos\varphi \sin\varphi \cdot S + \sin^2\varphi \cdot I = I,$$

$$y \in D(l),\ z(x) = T^*y(x) \in D(l^*)$$

$$z(x) = T^*y(x) = -i\cos\varphi\, y(x) + \sin\varphi\, y(1-x),$$

$$\bar{\beta}[-i\cos\varphi\, y(0) + \sin\varphi\, y(1)] + \bar{\alpha}[-i\cos\varphi\, y(1) + \sin\varphi\, y(0)] =$$

$$\left(-i\cos\varphi \cdot \bar{\beta} + \bar{\alpha}\sin\varphi\right)y(0) + \left(\bar{\beta}\sin\varphi - i\bar{\alpha}\cos\varphi\right)y(1) = 0.$$

Let's make the equation scheme:

$$\begin{cases} \left(-i\cos\varphi \cdot \bar{\beta} + \bar{\alpha}\sin\varphi\right)y(0) + \left(\bar{\beta}\sin\varphi - i\bar{\alpha}\cos\varphi\right)y(1) = 0, \\ \alpha y(0) + \beta y(1) = 0. \end{cases}$$

Calculate the determinant of this system of equations

$$\Delta = \begin{vmatrix} -i\cos\varphi \cdot \bar{\beta} + \bar{\alpha}\sin\varphi & \bar{\beta}\sin\varphi - i\bar{\alpha}\cos\varphi \\ \alpha & \beta \end{vmatrix} = 0,$$

$$-i\cos\varphi \cdot |\beta|^2 + \beta\bar{\alpha}\sin\varphi - \alpha\bar{\beta}\sin\varphi + i|\alpha|^2\cos\varphi = 0;$$

$$i(|\alpha|^2 - |\beta|^2)\cos\varphi + \left(\beta\bar{\alpha} - \alpha\bar{\beta}\right)\sin\varphi = 0.$$

a) If $\alpha\bar{\beta} - \bar{\alpha}\beta \neq 0$, then

$$tg\varphi = \frac{i(|\alpha|^2 - |\beta|^2)}{\alpha\bar{\beta} - \bar{\alpha}\beta};$$

b) If $|\alpha|^2 - |\beta|^2$, then

$$ctg\varphi = \frac{\alpha\bar{\beta} - \bar{\alpha}\beta}{i(|\alpha|^2 - |\beta|^2)}.$$

c) If $|\alpha|^2 - |\beta|^2 = 0$ and $\alpha\bar{\beta} - \bar{\alpha}\beta = 0$, then

$$\begin{cases}\alpha\bar{\alpha} - \beta\bar{\beta} = 0,\\ \alpha\bar{\beta} - \bar{\alpha}\beta = 0,\end{cases} => \begin{vmatrix}\bar{\alpha} & -\bar{\beta}\\ \bar{\beta} & -\bar{\alpha}\end{vmatrix} = -(\bar{\alpha})^2 + \left(\bar{\beta}\right)^2 = 0, => \alpha^2 - \beta^2 = 0,$$

the converse is also true.

In our case the case c) holds, therefore the operator T has the form:

$$T = i\cos\varphi\, I + \sin\varphi \cdot S,$$

where $0 \le \varphi \le 2\pi$ is an arbitrary angle.

3. Research Results.

Theorem 3.1. The following formulas hold:

a) $(Tl)^2 = l^*l = A$,

b) $(lT)^2 = ll^* = B$,

where

$$Ay = -y''(x),\ x \in (0,1);$$

$$\alpha y(0) + \beta y(1) = 0,\ \bar{\beta}y'(0) + \bar{\alpha}y'(1) = 0;$$

$$Bz = -z''(x) = \mu^2 z(x),\ x \in (0,1);$$

$$\bar{\beta}z(0) + \bar{\alpha}z(1) = 0, \alpha z'(0) + \beta z'(1) = 0;$$

$$ly = y'(x),\ x \in (0,1); \tag{1.10}$$

$$\alpha y(0) + \beta y(1) = 0, |\alpha| + |\beta| \ne 0; \tag{1.11}$$

$$l^+ z = -z'(x),\ x \in (0,1), \tag{1.10}^+$$

$$\bar{\beta}z(0) + \bar{\alpha}z(1) = 0; \tag{1.11}^+$$

$$T = i\cos\varphi\, I + \sin\varphi \cdot S, \tag{1.12}$$

$$Su(x) = u(1-x);$$

The angle φ is defined by the following way:

If $\alpha\bar{\beta} - \bar{\alpha}\beta \ne 0$, Then

$$tg\varphi = \frac{i\left(|\alpha|^2 - |\beta|^2\right)}{\alpha\bar{\beta} - \bar{\alpha}\beta}; \tag{1.13}$$

If $|\alpha|^2 - |\beta|^2 \neq 0$, then

$$ctg\varphi = \frac{\alpha\bar{\beta} - \bar{\alpha}\beta}{i(|\alpha|^2 - |\beta|^2)}; \quad (1.14)$$

If $\alpha^2 - \beta^2 = 0$, then φ is an arbitrary angle, belonging to $0 \leq \varphi \leq 2\pi$.

4. Discussion.

If $\alpha\bar{\beta} - \bar{\alpha}\beta \neq 0$ and $|\alpha|^2 - |\beta|^2 \neq 0$, then from (1.13) we obtain $tg\varphi = 0$, thus $\varphi = 0$, then (1.12) implies that

$$Tly = iy'(x), \ x \in (0,1), \quad (1.14)$$

$$\alpha y(0) + \beta y(1) = 0,$$

where $|\alpha|^2 - |\beta|^2 = 0$.

If $|\alpha|^2 - |\beta|^2 \neq 0$ and $\alpha\bar{\beta} - \bar{\alpha}\beta = 0$, then from the formula (1.14) we have $ctg\varphi = 0$, then $\varphi = \frac{\pi}{2}$, and from the formula (1.12) we obtain that

$$Tly = Ty' = Sy'(x) = y'(1 - x), \quad (1.15)$$

$$\alpha y(0) + \beta y(1) = 0, |\alpha| + |\beta| \neq 0, \quad (1.16)$$

where $\alpha\bar{\beta} - \bar{\alpha}\beta = 0$.

This last operator (1.15) - (1.16) has been studied in detail in [67], the results of which were used in study of the Gourse problem for wave equation [68] and in solving inverse problems [69-70]. These two spectral problems are special cases of the spectral problem $Tly = \lambda y$, $\alpha y(0) + \beta y(1) = 0$, $|\alpha| + |\beta| \neq 0$, study of which is of undoubted interest in all respects.

5. Conclusion.

Square root of the Sturm-Liouville operator is a functional differential operator of the first-order that generalizes the well-known momentum operator. Results of this paper can be used to solve inverse problems of mathematical physics, as well as in the spectral theories of linear operators.

УДК 517.43

А.Ш. Шалданбаев[1], А.А. Шалданбаева[2], Б.А. Шалданбай[3]

[1]"Silkway" Халықаралық Университеті, Шымкент;
[2]Аймақтық әлеуметтік - инновациялық университеті, Шымкент;
[3]М.Әуезов атындағы Оңтүстік Қазақстан Мемлекеттік Университеті, Шымкент.

ШТУРМ - ЛИУВИЛЛ ОПЕРАТОРЫНЫҢ КВАДРАТ ТҮБІРІ

Аннотация. Бұл еңбекте Штурм-Лиувилл операторының квадрат түбірі табылды және бұл түбірдің бірінші ретті функционәл-дифференциал оператор екені көрсетілді. Бұл функционәл-дифференциал операторға сәйкес шекаралық есеп табылды. Бағдар ретінде Путнамның бір теоремасы қолданылды. Штутм-Лиувилл операторының шекаралық шарты онша кең емес, оның түр зерттеу әдісіне тәуелді. Табылған унитар оператор көпке әйгілі импуліс операторының ширатылған немесе кеңейтілген түрі десек-те болады.

Түйін сөздер. Штутм-Лиувилл операторы, операторлың квадрат түбірі, функционәл-дифференциал оператор, аргументі ауытқыған теңдеулер, Катоның гипотезасы, Макинтоштың мысалы, Гурсаның операторы, кері есеп, спектр, меншікті мәндер, меншікті функциялар, унитар опратор, ұқсастық операторы.

УДК 517.43

А.Ш. Шалданбаев[1], А.А. Шалданбаева[2], Б.А. Шалданбай[3]

[1]Международный университет “SILKWAY”, Шымкент;
[2]Региональный социально-инновационный университет, Шымкент;
[3]Южно-казахстанский государственный университет им.М.Ауезова, Шымкент

О КВАДРАТНОМ КОРНЕ ИЗ ОПЕРАТОРА ШТУРМА - ЛИУВИЛЛЯ

Аннотация. В данной работе найден корень квадратный из оператора Штурма - Лиувилля и показан, что этот корень является функционально- дифференциальным оператором первого порядка. Найден вид соответствующей краевой задачи этого функционально - дифференциального уравнения. В качестве наводящей идеи использована одна теорема Путнама. Краевые условия оператора Штурма - Лиувилля имеют весьма специальный вид, и они продиктованы методом исследования. Найденный унитарный оператор обобщает известного оператора импульса.

Ключевые слова: оператор Штурма - Лиувилля, квадратный корень из оператора, функционально-дифференциальный оператор, уравнения с отклоняющимся аргументом, гипотеза Като, пример Макинтоша, оператор Гурса, обратная задача, спектр, собственные значения, собственные функции, унитарный оператор, оператор подобия.

Information about authors:
Shaldanbayev A.Sh. – doctor of physico-mathematical Sciences, Professor, head of the center for mathematical modeling «Silkway» International University, Shymkent; http://orcid.org/0000-0002-7577-8402;
Shaldanbayeva A.A. - Regional Social-Innovative University, Shymkent; https://orcid.org/0000-0003-2667-3097;
Shaldanbay B.A. - M. Auezov South Kazakhstan State University, Shymkent; https://orcid.org/0000-0003-2323-0119.

REFERENCE

[1] U. Rudin, Functional Analysis, M.: Mir, **1975**.

[2] T. Kato, Fractional powers of dissipative operators, II, J. Math. Soc. Japan, 14 (**1962**), pp.242–248.

[3] A. McIntosh, On the compatibility of A1/2 and A∗1/2, Proc. Amer. Math. Soc., 32:2 (**1972**), pp.430–434.

[4] A.M. Selitskiy, Initial data space of the second boundary value problem for a parabolic differential-difference equation, Scientific Bulletin of BelSU, Series: Mathematics. Physics. **2011**. № 23(118). Issue 25, pp. 102-112.

[5] M.S. Agranovich and A.M. Selitskiy, Fractional degrees of operators corresponding to coercive problems in Lipschitz domains, Funct. Analysis and its Appl., **2013**, volume 47, issue 2, pp.2–17.

[6] V. Balakrishnan (**1960**), Fractional powers of closed operators and the semi-groups generated by them. Pacific J. Math., 10:419–437.

[7] Andreas Axelsson, Stephen Keith, and Alan McIntosh (**2006**), The Kato square root problem for mixed boundary value problems. J. London Math. Soc. (2), 74(1):113–130.

[8] Andrea Bonito and Joseph E. Pasciak (**2015**), Numerical approximation of fractional powers of elliptic operators. Math. Comp., 84(295):2083–2110.

[9] Luis Caffarelli and Luis Silvestre (**2007**), An extension problem related to the fractional Laplacian.Comm. Partial Differential Equations, 32(7-9):1245–1260.

[10] Alan McIntosh (**1989**), The square root problem for elliptic operators: a survey. In Functional analytic methods for partial differential equations, Tokyo, volume 1450 of Lecture Notes in Math., pages 122–140. Springer, Berlin, 1990.

[11] M. S. Agranovich (**2012**), Remarks on strongly elliptic second-order systems in Lipschitz domains, Russian J. Math. Phys., 20:4, 405–416.

[12] M.S. Agranovich (**2013**), Sobolev spaces, their generalization and elliptic problems in domains with smooth and Lipschitz bound, M., Izd. MSNMO.

[13] Mihoko Matsuki and Teruo Ushijima (**1993**), A note on the fractional powers of operators approximating a positive definite selfadjoint operator. J. Fac. Sci. Univ. Tokyo Sect. IA Math.,40(2):517–528.

[14] Y. Berg and Y. Lefstrem (**1980**), Interpolation Spaces, Mir, M.

[15] T. Kato (**1972**), Perturbation Theory of Linear Operators, Mir, M.

[16] M.A. Krasnoselsky, P.P. Zabreiko, E.I. Pumulnik and P.E. Sobolevsky (**1966**), Integral operators in spaces of summable functions, Nauka, M.

[17] J.-L. Lyons and E. Madjenes (**1971**), Nonhomogeneous Boundary Value Problems and their Applications, Mir, M.

[18] A. M. Selitsky, Space of initial data of the 3rd boundary value problem for parabolic differential-difference equation in one-dimensional case, Math.Notes, 92: 4 (**2012**), 636–640.

[19] A.M. Selitsky, Modeling of some optical systems on the basis of a parabolic differential-difference equation, Math. Modeling, 24:12 (**2012**), 38–42.

[20] A. L. Skubachevsky and R.V. Shamin, Second-order parabolic differential-difference equations, Dokl. RAN, 379:5 (**2001**), 595–598.

[21] H. Triebel, Theory of Functional Spaces, Mir, M., 1986.

[22] I. Ya. Shneiberg, Spectral properties of linear operators in interpolational families of Banach spaces, Math. investig. 9:2 (**1974**), 214–229.

[23] Sh. Agmon, On the eigenfunctions and on the eigenvalues of general elliptic boundary value problems, Comm. Pure Appl. Math., 15:2 (**1962**), 119–147.

[24] W. Arendt, Semigroups and evolution equations: functional calculus, regularity and kernel estimates, in: Handbook of Differential Equations, Evolutionary Differential Equations, vol. 1, Elsevier/North-Holland, Amsterdam, **2004**, 1–85.

[25] P. Auscher, N. Badr, R. Haller-Dintelmann, J. Rehberg, The square root problem for second order, divergence form operators with mixed boundary conditions on Lp, http://arxiv.org/abs/1210.0780v1.

[26] P. Auscher, S. Hofmann, M. Lacey, J. Lewis, A. McIntosh, P. Tchamitchian, The solution of Kato's conjectures, C. R. Acad. Sci. Paris, S´er. 1, 332:7 (**2001**), 601–606.

[27] P. Auscher, A. McIntosh, A. Nahmod, Holomorphic functional calculi of operators, quadratic estimates and interpolation, Indiana Univ. Math. J., 46:2 (**1997**), 375–403.

[28] P. Auscher, S. Hofmann, A. McIntosch, P. Tchamitchian, The Kato square root problem for higher order elliptic operators and systems on Rn, J. Evol. Equ., 1:4 (**2001**), 361–385.

[29] P. Auscher, P. Tchamitchian, Square root problem for divergence operators and related topics, Ast´erisque, 249 (**1998**), 1–171.

[30] P. Auscher, P. Tchamitchian, Square roots of elliptic second order divergence operators on strongly Lipschitz domains: L2 theory, J. Anal. Math., 90 (**2003**), 1–12.

[31] P. Auscher, P. Tchamitchian, Square roots of elliptic second order divergence operators on strongly Lipschitz domains: Lp theory, Math. Ann., 320:3 (**2001**), 577–623.

[32] A. Axelsson, S. Keith, A. McIntosh, The Kato square root problem for mixed boundary value problems, J. London Math. Soc., 74:1 (**2006**), 113–130.

[33] S. Blunck, P. Kunstmann, Calderron–Zygmund theory for non-integral operators and the H∞ functional calculus, Rev. Mat. Iberoamericana, 19:3 (**2003**), 919–942.

[34] A. F. M. ter Elst, D. W. Robinson, On Kato's square root problem, Hokkaido Math. J., 26:2 (**1997**), 365–376.

[35] J. Griepentrog, K. Gr¨oger, H.-Ch.Kaiser, J. Rehberg, Interpolation for function spaces related to mixed boundary value problems, Math. Nachr., 241 (**2002**), 110–120.

[36] D. Grisvard, Caractrerisation de quelques espaces d'interpolation, Arc. Rational Mech. Anal., 25 (**1967**), 40–63.

[37] M. Haase, (**2006**), The Functional Calculus for Sectorial Operators, Birkh¨auser, Basel.

[38] S. Hoffmann, A short course on the Kato problem, Contemp. Math., 289 (**2001**), 61–67.

[39] T. Hyt¨onen, A. McIntosh and P. Portal, Kato's square root problem in Banach spaces, J.Funct. Anal., 254:3 (**2008**), 675–726.

[40] S. Janson, P. Nilsson, J. Peetre, Notes on Wolff's note on interpolation spaces, Proc. London Math. Soc. (3), 48:2 (**1984**), 283–299.

[41] H. Komatsu, Fractional powers of operators, Pacif. J. Math., 19 (**1966**), 285–346.

[42] J. L. Lions (**1961**), r Equations diffrerentielles operationelles et probl`emes aux limites, Springer-Verlag, Berlin etc.

[43] J. L. Lions, Espaces d'interpolation et domaines de puissances fractionaires d'operrateurs, J. Math. Soc. Japan, 14 (**1962**), 233–241.

[44] A. McIntosh, Square roots of elliptic operators, J. Funct. Anal., 61:3 (**1985**), 307–327.

[45] A. McIntosh, Operators which have an H∞functional calculus, in: Miniconference on Operator Theory and Partial Differential Equations, Proc. Centre Math. Anal.Austral. Nat. Univ., vol. 14, Austral. Nat. Univ., Canberra, (**1986**), 210–231.

[46] A. McIntosh (**1990**), Square Root Problem for Elliptic Operators: a Survey, Lecture Notes in Math., vol. 1450, Springer-Verlag, Berlin.

[47] W. McLean (**2000**), Strongly Elliptic Systems and Boundary Integral Equations, Cambridge Univ. Press, Cambridge, UK.

[48] J. Ne˘cas (**2012**), Les mrethodes directes en threorie des erquations elliptiques, Masson, Paris, 1967; Direct Methods in the Theory of Elliptic Equations, Springer-Verlag, Berlin–Heidelberg.

[49] L. Nirenberg, Remarks on strongly elliptic partial differential equations, Comm. Pure Appl. Math., 8 (**1965**), 649–675.

[50] R.T. Seeley, Norms and domains of the complex powers Az B, Amer. J. Math., 93:2(**1971**), 299–309.

[51] R.T. Seeley, Interpolation in Lp with boundary conditions, Studia Math., 44 (**1972**),47–60.

[52] A.L. Skubachevskii and R. V. Shamin, Mixed boundary value problem for parabolic differential-difference equation, Funct. Differ. Eq., 8:3–4 (**2001**), 407–424.

[53] T.W. Wolff, A note on interpolation spaces, in: Lecture Notes in Math., vol. 918, Springer-Verlag, Berlin–New York, (**1982**), 199–204.

[54] A. Yagi, Coincidence entre des espaces d'interpolation et des domaines de puissances fractionaires d'oprreateurs, C. R. Acad. Sci. Paris, S´er. 1, 299:6 (**1984**), 173–176.

[55] L. Hörmander (**1965**), Linear Partial Differential Operators, Mir, M.

[56] M.I. Vishik, On strongly elliptic systems of differential equations, Math. Sb., 29(71), 3(**1951**), 615–676.

[57] R.V. Shamin, On spaces of initial data for differential equations in a Hilbert space, Math. Sb., 194:9 (**2003**), 141-156.

[58] H. Namsrai, Square Kleino-Gordon operator and physical interpretation, International Journal of Theoretical Physics, (**1998**). T. 37. №5. pp.1531-1540.

[59] R. Putsio (**1994**), On square root of Laplace – Beltrami operator as Hamiltonian, Classical and Quantum Gravity. Vol. 11. No.3. Pp. 609-620.

[60] T.L. Gill and V.V. Zakhari, Analytical representation of square operator, Physical Journal A: Mathematics and general. (**2005**). Vol. 38. №11. Pp. 2479-2496.

[61] P.N. Vabishchevich, Numerical solution of non-stationary spatial-fractional problems with square root of an elliptic operator, Mathematical Modeling and Analysis. (**2016**). Vol. 21. No.2. Pp. 220-238.

[62] A. Bzdak and L. Hadash, Square root of a dirac operator on superspace and Maxwell equations, Physical Letters. Section B: Nuclear Physics, Elementary Particle and High Energy Physics. (**2004**). vol. 582. №1-2. Pp. 113-116.

[63] H.T. Ito, Resonances of square root of the Pauli operator, Publications of Research Institute of Mathematical Sciences. (**2017**). Vol. 53. No.4. Pp. 517-549.

[64] H. Namsray and H.V. Von Geramb, Quantization and nonlocality of square body: Review of International Journal of Theoretical Physics. (**2001**). vol. 40. № 11. pp. 1929-2010.

[65] V.P. Maslov (**1988**), Asymptotic Methods and Perturbation Theory, M.: Mir.

[66] V.A. Marchenko (**1977**), Sturm-Liouville Operators and Their Applications, Kiev, Naukova Dumka.

[67] T.Sh. Kalmenov, S.T. Akhmetova and A.Sh. Shaldanbaev, To spectral theory of equation with deviating arguments, Mathematical Journal, Almaty, (**2004**), vol.4., No.3, pp.41-48.

[68] M.I. Akylbayev, A. Beysebayeva and A.Sh. Shaldanbayev, News of the National Academy of Sciences of the Republic of Kazakhstan, Physico-mathematical Series,Volume 1, Number 317 (**2018**), 34 – 50.

[69] T.Sh. Kal'menov and A.Sh. Shaldanbaev, On a criterion of solvability of the inverse problem of heat conduction, Journal of Inverse and Ill-Posed Problems 18, 352-369 (**2010**).

[70] I. Orazov, A. Shaldanbayev and M. Shomanbayeva, About the Nature of the Spectrum of the Periodic Problem for the Heat Equation with a Deviating Argument,Abstract and Applied Analysis №:128363 DOI: 10.1155/2013/128363 Published: (**2013**),WOS:000325557100001.

N E W S
OF THE NATIONAL ACADEMY OF SCIENCES OF THE REPUBLIC OF KAZAKHSTAN
PHYSICO-MATHEMATICAL SERIES
ISSN 1991-346X **https://doi.org/10.32014/2019.2518-1726.30**
Volume 3, Number 325 (2019), 114 – 119

UDC 539.171

N. Burtebayev[1], Zh.K. Kerimkulov[1,2], D.M. Janseitov[1,3], A.S. Demyanova[4], L.I. Galanina[5], D.K. Alimov[1,2], Y.S. Mukhamejanov[1,6], N. Amangeldi[2], M. Nassurlla[1,6], A. Aimaganbetov[2], Y. Nurtazin[1,6], K. Talpakova[1,2], R. Khodjaev[1,6], A. Sabidolda[1], S.M. Bekbaev[7], D.Ya. Kurban[7], B.S. Mammetov[7]

[1]Institute of Nuclear Physics, Almaty, Kazakhstan;
[2]L.N.Gumilyov ENU, Astana, Kazakhstan;
[3]Joint Iinstitute for Nuclear Rersearch, Dubna, Russia;
[4]National Research Center "Kurchatov Institute", Moscow, Russia;
[5]SINP MSU, Moscow, Russia; [6]al-Farabi KazNU, Almaty, Kazakhstan;
[7]A.Yassawi IKTU, Turkestan, Kazakhstan

STUDY OF ELASTIC AND INELASTIC SCATTERING OF DEUTREONS BY ^{13}C NUCLEI AT ENERGY E_d=18 MeV

Abstract. The differential cross sections of elastic and inelastic ($3/2^-$ excited state of ^{13}C, E_x = 3.684 MeV) scattering of deuterons by ^{13}C nuclei at energy E_d = 18 MeV in the angular range θ_{lab} = 10°-75° have been measured at the U-150M cyclotron (Almaty, Kazakhstan). The total error of the experimental data obtained does not exceed 10%. The standard dE-E method of registration and identification of interaction products was used in the experiment. Thin carbon films with a thickness of about 150 μg/cm2 of about 80% enrichment by ^{13}C were used as targets. A theoretical analysis was made within the framework of the optical model of the nucleus and the coupled channels method. The values of the quadrupole deformation were determined, which are in good agreement with the literature data. It is shown that in order to improve the theoretical description of experimental data, additional mechanisms (reactions, other inelastic processes) that can influence the formation of scattering cross sections must be taken into account in the calculations.

Key words: differential cross sections, optical potentials, deformation parameters.

Introduction. The success of the diffraction mechanism with strong absorption in explaining the elastic and inelastic scattering of alpha particles has stimulated interest in new research on the scattering of other particles, including deuterons, by light nuclei. Since the structure of the alpha particle is strongly coupled, while the deuteron is weakly coupled, it remains an open question whether diffraction with strong absorption in deuteron scattering plays an equally important role, especially in case of light nuclei.

In recent years, the scattering of deuterons by carbon isotopes nuclei has been investigated at energies from 4 to 17 MeV. Analysis of ^{12}C(d,d)^{12}C the reaction in the energy range 9-14 MeV [1,2] with a simple interaction potential, established the applicability of the optical model for light nuclei. To date, there have been few studies on the scattering of deuterons by ^{13}C nuclei. There are only a few works where elastic scattering was studied at energies of 13.7±17 MeV [3-7]. Data on inelastic scattering are completely absent.

The study of elastic and inelastic processes of interaction of deuterons with nuclei is one of the main sources of information on the properties of the ground and low lying excited states of atomic nuclei [8]. These processes, occurring during collisions of nuclei with energies of several tens of MeV, provide valuable information about the structure of specific nuclear states.

Experimental methods and measurement results.

Measurements of the cross sections for deuteron scattering processes on 13C nuclei were carried out on extracted beams of the U-150M isochronous cyclotron of the Institute of Nuclear Physics (Almaty, Kazakhstan) with an energy of Ed = 18 MeV. The interval of measured angles is 10-75 degrees in the laboratory coordinate system.

The deuteron beam was conducted through a collimation system (two collimators 2 mm in diameter, placed 440 mm from each other) and formed a 2 mm spot on the target. Careful adjustment of the collimator system, as well as the mobile device with a detector for measuring the angular distributions, made it possible to reduce the error in determining the angle to ±0.20°. The experiment used a standard experimental ΔE-E method for detecting and identifying particles.

Thin films of ^{13}C (isotopic enrichment of about 80%) made using electron-beam sputtering were used as targets. During the experiments, several self-sustaining films with a thickness of about 150 μg/cm^2 were used. An example of the spectrum of scattered deuterons on the target is shown in Figure 1.

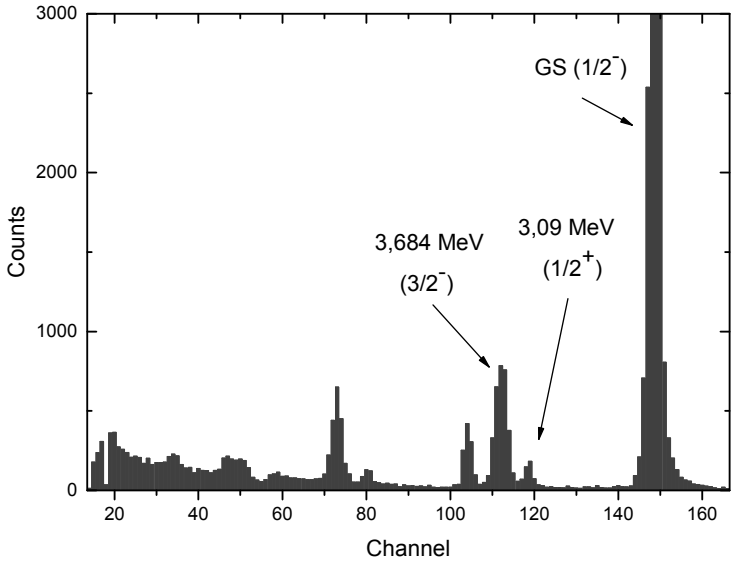

Figure 1 - Spectrum of deuterons scattered by ^{13}C nuclei at an angle of 40 degrees

The total error of the obtained experimental data did not exceed 10 percent. The angular distributions of the measured differential cross sections are presented in Figures 2 and 3 (the symbols are triangles).

Theoretical analysis.

The theoretical elastic scattering cross sections were analyzed using the standard optical model (OM). The calculations were extended using global optical potentials for deuterons obtained in the work of Haixia An [9]. The parameters of the potentials are given in Table 1. Figure 2 presents a comparison of the experimental data with the cross sections calculated within the OM. It can be seen that the calculated cross sections (the solid line in Figure 2) reproduce the experiment quite well.

Table 1 - Optical potential parameters used in the calculations within the framework of optical model and the coupled channels method

V	r_V	a_V	W_S	r_S	a_S	W_D	r_D	a_D	V_{SO}	r_{SO}	a_{SO}	r_C
89,04	1,15	0,75	2,22	1,35	0,62	10,28	1,4	0,68	3,557	0,97	1011	1,303

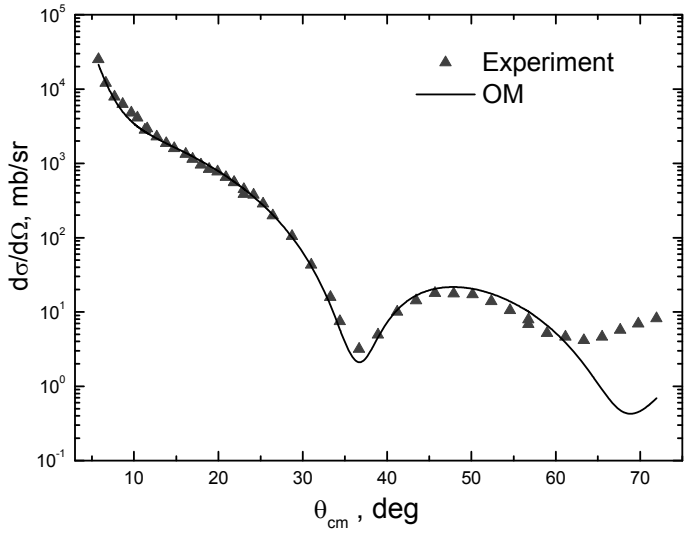

Figure 2. - Comparison of experimental data on elastic scattering with theoretical cross sections calculated within OM using the potentials from Table 1

Inelastic scattering cross sections were calculated within the framework of the coupled channels method (CC) using the FRESCO computer code [10,11]. The coupling between the ground ($1/2^-$) and excited (E_x = 3.684 MeV, $3/2^-$) states of the ^{13}C nucleus in deuteron scattering was taken into account within the framework of the rotational model with the form factor

$$V^{\lambda}(R) = -\frac{\delta_{\alpha}}{\sqrt{4\pi}}\frac{dU(R)}{dR}$$

for quadrupole transitions ($\lambda = 2$), where δ_{λ} is the length of the multipole deformation.

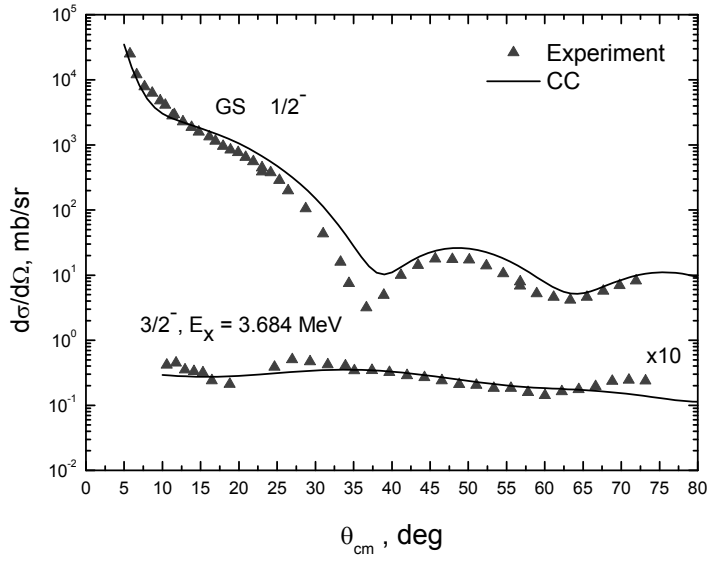

Figure 3 - Comparison of experimental data with theoretical cross sections calculated within the framework of the CC method (elastic scattering is above, inelastic scattering is below)

In the calculations, the potentials from Table 1 were used. The length of the quadrupole deformation was determined from the fit of the calculated cross sections to the experimental data and was $\delta_2 = 0.54$. The found value agrees well with the literature data [12-16]. Figure 3 presents a comparison of the calculated cross sections (solid line) with experimental data. It is seen that the coupling of channels worsened the description of elastic scattering in the region of angles up to 60 degrees. Probably, to eliminate this problem, it is necessary to include additional processes in the coupling: reactions and inelastic channels with excitation of other levels of the ^{13}C nucleus [17-21].

Conclusion. With an error of no more than 10%, the angular distributions of the differential cross sections of elastic and inelastic (excited states of ^{13}C: $3/2^-$, $E_x = 3.684$ MeV) scattering of deuterons on ^{13}C nuclei at an energy $E_d = 18$ MeV in the forward angles region have been measured. The values of the quadrupole defromation are determined, which are in good agreement with the literature data. It is shown that in order to improve the theoretical description of experimental data, additional mechanisms (reactions, other inelastic processes) that can influence the formation of cross sections must be taken into account in the calculations.

ӘОЖ 539.171

Н. Буртебаев[1], Ж.К. Керимкулов[1,2], Д.К. Джансейтов[1,3], А.С. Демьянова[4], Л.И.Галанина[5], Д.К. Алимов[1,2], Е.С. Мухамеджанов[1,6], Н. Амангелді[2], М. Насурлла[1,6], А. Аймаганбетов[2], Е. Нуртазин[1,6], К. Талпакова[1,2], Р. Ходжаев[1,6], А. Сабидолда[1], С.М.Бекбаев[7], Д.Я.Курбан[7], Б.С.Мамметов[7]

[1]Ядролық физика институты, Алматы, Қазақстан;
[2]Л.Н. Гумилев атындағы ЕҰУ, Астана, Қазақстан ;
[3]Біріккен ядролық физики институты, Дубна, Ресей;
[4]«Курчатов институты» Ұлттық зерттеу орталығы, Мәскеу, Ресей;
[5]ММУ ЯФҒЗИ, Мәскеу, Ресей; [6]әл-Фараби атындағы ҚазҰУ, Алматы, Қазақстан;
[7]А.Яссауи атындағы ХҚТУ, Түркістан, Қазақстан

E_d = 18 MeV ЭНЕРГИЯДА ^{13}C ЯДРОЛАРЫНАН ДЕЙТРОНДАРДЫҢ СЕРПІМДІ ЖӘНЕ СЕРПІМСІЗ ШАШЫРАУЫН ЗЕРТТЕУ

Аннотация. $\theta_{lab} = 10^0 - 75^0$ бұрыштар диапазонында E_d = 18 MeV энергиялы дейтрондардың ^{13}C ядроларынан серпімді және серпімсіз (^{13}C ядросының қоздырылған күйі: $3/2^-$, $E_X = 3.684$ MeV) шашырау дифференциалдық қимасы У-150М (Алматы, Қазақстан) циклотронында өлшенді. Алынған эксперименттік мәліметтердің толық қателігі 10% аспайды. Экспериментте әсерлесу өнімдерін тіркеу және сәйкестендірі үшін стандартты dE-E әдісі қолданылды. Нысана ретінде қалындығы шамамен 150 мкг/см^2 болатын 80% байыталған ^{13}C жұқа көміртегі қабықшасы пайдаланылды. Теориялық талдаулар ядроның оптикалық моделі және байланысқан арналар әдісі төңірегінде жүргізілді. Анықталған квадрупольді деформация ұзындығының мәні әдебиеттік мәліметтермен жақсы үйлеседі. Эксперименттік мәліметтерді теориялық тұрғыдан дәлелдеуді жақсарту үшін есептеулерде шашырау қималарының пайда болуына әсер ететін қосымша механизмдерді (реакциялар, басқа серпімсіз процесстер) ескеру қажет.

Түйін сөздер: дифференциалдық қима, оптикалық потенциалдар, деформация параметрлері.

УДК 539.171

Н. Буртебаев[1], Ж.К. Керимкулов[1,2], Д.К. Джансейтов[1,3], А.С. Демьянова[4], Л.И.Галанина[5], Д.К. Алимов[1,2], Е.С. Мухамеджанов[1,6], Н. Амангелді[2], М. Насурлла[1,6], А. Аймаганбетов[2], Е. Нуртазин[1,6], К. Талпакова[1,2], Р. Ходжаев[1,6], А. Сабидолда[1], С.М.Бекбаев[7], Д.Я.Курбан[7], Б.С.Мамметов[7]

[1]Институт ядерной физики, Алматы, Казахстан;
[2]ЕНУ им. Л.Н. Гумилева, Астана, Казахстан;
[3]Объединенный институт ядерной физики, Дубна, Россия;
[4]Национальный исследовательский центр «Курчатовский институт», Москва, Россия;
[5]НИИЯФ МГУ, Москва, Россия;[6]КазНУ им. аль-Фараби, Алматы, Казахстан;
[7]МКТУ им. А.Яссави, Туркестан, Казахстан

ИССЛЕДОВАНИЕ УПРУГОГО И НЕУПРУГОГО РАССЕЯНИЯ ДЕЙТРОНОВ НА ЯДРАХ ^{13}C ПРИ ЭНЕРГИИ E_d = 18 MeV

Аннотация. На циклотроне У-150М (Алматы, Казахстан) измерены дифференциальные сечения упругого и неупругого (уровень возбуждения ядра ^{13}C: $3/2^-$, E_X = 3.684 MeV) рассеяния дейтронов на ядрах ^{13}C при энергии E_d = 18 MeV в диапазоне углов $\theta_{lab} = 10^0 - 75^0$. В эксперименте использовалась стандартная dE-E методика регистрации и идентификации продуктов взаимодействия. В качестве мишеней использовались тонкие углеродные пленки толщиной порядка 150 мкг/см^2 и обогащением по ^{13}C около 80%. Полная погрешность полученных экспериментальных данных не превышает 10%. Выполнен теоретический анализ в рамках оптической модели ядра и метода связанных каналов. Определены значения длин квадрупольной деформации, которые неплохо согласуются с литературными данными. Показано, что для улучшения теоретического описания экспериментальных данных в расчетах необходимо учитывать дополнительные механизмы (реакции, другие неупругие процессы), которые могут влиять на формирование сечений рассеяния.

Ключевые слова: дифференциальные сечения, оптические потенциалы, параметры деформации.

Authors information:

Burtebayev Nassurlla - Professor, Doctor of Physical and Mathematical Sciences, Head of the Laboratory of the Institute of Nuclear Physics, Almaty, Kazakhstan. nburtebayev@yandex.ru, https://orcid.org/0000-0002-4715-9604
Kerimkulov Zh. K. - zhambul-k@yandex.ru, https://orcid.org/0000-0002-9226-2846
Janseitov D. - janseit.daniar@gmail.com, https://orcid.org/0000-0002-8355-3131
Demyanova A.S. - a.s.demyanova@bk.ru, https://orcid.org/0000-0001-5840-7055
Galanina L. - galan lidiyaI @mail.ru, https://orcid.org/0000-0003-1047-0439
Alimov D. K. - diliyo@mail.ru, https://orcid.org/0000-0003-2494-9563
Mukhamejanov Y. S. - craftinho@mail.ru, https://orcid.org/0000-0002-9064-6061
Amangeldi N. - nur19792@mail.ru, https://orcid.org/0000-0002-9416-5425
Nassurlla Marzhan - morzhic@mail.ru, https://orcid.org/0000-0003-0157-0083
Aimagambetov A. - az.aimagambetov@mail.ru, https://orcid.org/0000-0003-3055-5886
Nurtazin Y. - nurtazin@inp.kz, https://orcid.org/0000-0002-3033-2538
Talpakova K. - tkk_777@mail.ru, https://orcid.org/0000-0002-2659-5554
Khojayev R. - ramazan_inp@mail.ru, https://orcid.org/0000-0002-4308-3921
Sabidolda A. - asabidolda@mail.ru, https://orcid.org/0000-0001-6522-9736.
Bekbaev S. - bekbayev.mktu@mail.ru, https://orcid.org/0000-0001-8457-7189.
Kurban D. - dilya.95d@mail.ru, https://orcid.org/0000-0001-6077-4452.
Mammetov B.S. - bekzat.mammetov@mail.ru, https://orcid.org/0000-0003-2628-9853

REFERENCES

[1] Takai M., Kambara T., Tada K., Nakamura M. and Kobayashi S. Two-Step Process in the ^{12}C(d, p)^{13}C reaction. Journal of the Physics Society of Japan, 1977. V. 43. P.17-24.

[2] Nguyen Dai-Ca. Elastic and Inelastic Scattering of Deuterons from ^{9}Be, ^{12}C, ^{14}N and ^{16}O at 14 MeV. Journal of the Physics Society of Japan, 1966. V. 21. P. 2462.

[3] Guratzsch H., Slotta J., Stiller G. A study of deuteron scattering on ^{12}C and ^{13}C. Nuclear Physics A, 1970. V. 140. P. 129-140.

[4] Peterson R.J., Bhang H.C., Hamill J.J. and Masterson T.G. The ^{14}C(α, α')^{14}C and ^{13}C(d, p)^{14}C reactions. Nuclear Physics A, 1984. V. 425. P. 469-492.

[5] Thompson I.J. and Nunes F.M. Nuclear Reactions for AstroPhysicalics: Principles, Calculation and Applications of Low-Energy Reactions. // Cambridge Univ. Press. 2009, P. 115.

[6] Liu Z.H. et. al. Asymptotic normalization coefficients and neutron halo of the excited states in ^{12}B and ^{13}C // Physical Review C. 2001. Vol. 64. P.034312.

[7] Nolte M., Machner H. and Bojowald J. Global optical potential for α particles with energies above 80 MeV // Physical Review C. 1987. Vol. 36. P. 1312.

[8] Nassurlla Maulen, Burtebayev N., Kerimkulov Zh.K., Suzuki T., Sakuta S.B., Nassurlla Marzhan, Khojayev R. Investigation of deuteron scattering by ^{7}Li nuclei at energy of 14.5 MeV // News of the National Academy of Sciences of the Republic of Kazakhstan-Series physico-mathematical, 2018. Vol.6, №322. P.15-22. DOI: https://doi.org/10.32014/2018.2518-1726.12

[9] Haixia An and Chonghai Cai. Global deuteron optical model potential for the energy range up to 183 MeV // Phys. Rev. C. 2006. Vol.73. P. 054605.1-9.

[10] Thompson I.J. Fresco 2.0 // Department of physics, University of Surrey, Guildford GU2 7XH. England, 2006. 129 p.

[11] Abele H. et. al. Measurement and folding-potential analysis of the elastic α-scattering on light nuclei // Atomic nuclei. 1987. Vol. 326. P.373-381.

[12] Mezhevych S.Yu. The ^{13}C+ ^{11}B elastic and inelastic scattering and isotopic effects in the ^{12,13}C+ ^{11}B scattering // Nuclear Physics A. 2003. Vol. 724. P.29–46.

[13] Burtebaev N. Kerimkulov Zh.K., Demyanova A.S., Janseitov D.M., Danilov A.N., Zholdybaev T.K., Alimov D.K. Issledovanie processov uprugogo rasseyaniya ionov ^{3}He na yadrah ^{13}C pri energiyah 50 i 60 MeV v ramkah opticheskogo i folding modelei // Izvestiya NAN RK seriya fiz. mat. 2016. T.306, №2. C. 55.

[14] Burtebayev N., Burtebayeva D.T., Baktybayev M.K., Duisebayev B.A., Ogloblin A.A., Demyanova A.S., Sakuta C.B., Hamada Sh., Janseitov D.M., Nassurlla M. and Artemov S.V. Experimental and theoretical investigation of scattering of alphaparticles from ^{13}C nuclei // Proceedings of the Fifth AASPP Workshop on Asian Nuclear Reaction Database. Mumbai, 2014. P.149-151.

[15] Burtebaev N. Duysebaev B.A., Kerimkulov Zh.K., Muhamedzhanov E.S., Alimov D.K., Janseitov D.M., Saduev N.O., Glushhenko N.V., Sakuta S.B., Peterson R.Zh., Galanina L.I. Analiz uprugih i neuprugih rasseyaniy α-chastic i ionov ^{3}He na yadrah ^{9}Be, ^{13}C i deytronov na yadrah ^{11}B pri nizkih energiyah // Izvestiya NAN RK seriya fiz. mat. 2016. T.305, №1. C.66.

[16] Burtebayev N., Kerimkulov Zh., Demyanova A.S., Sakuta S.B., Morzabayev A.K., Janseitov D.M., Nassurlla M., Alimov D.K., Mukhamejanov Y.S. and Shakirov A.K. Experimental and theoretical investigation of scattering of alpha particles from ^{13}C nuclei // Book of abstracts LXV International conference «NUCLEUS 2015». - Saint-Petersburg, 2015. P.96.

[17] Janseitov D., Burtebayev N., Burtebayeva J., Baktybayev M., Nassurlla M., Demyanova A., Sakuta S. and Mukhamejanov Y. Investigation of α-particle scattering from ^{13}C at energy 29 MeV // Abstract Book Nuclear Physics in Astrophysics 7. York, 2015. - P.60.

[18] Demyanova A.S. et.al. Spectroscopy of exotic states of ^{13}C // EPJ Web of Conferences. 2014. Vol. 66. P.02027. 105 Goncharov S. A. and Izadpanah A. Dispersive semimicroscopic analysis of nuclear-nuclear collisions on the basis of a corrected folding-model potential // Physics of Atomic Nuclei. 2007. Vol. 70. P.21.

[19] Burtebayev N., Sakhiyev S.K., Janseitov D.M. Kerimkulov Zh., Alimov D. and Danilov A.N. Investigation of the elastic and inelastic scattering of α-particles from ^{13}C in the energy range 26.6–65MeV // International Journal of Modern Physics E. 2016. Vol. 25, No.10. P.1650078.

[20] Burtebaev N. Demyanova A.S., Janseitov D.M., Kerimkulov Zh.K., Nasurlla M., Alimov D.K., Shakirov A.K. Vzaimodeystviya al'fa-chastic s yadrami ^{13}C pri energiyah 6.65-16.25 MeV/nuklon // Izvestiya NAN RK seriya fiz. mat. 2016. T.307, №3. C.36.

[21] N. Burtebayev, D. M. Janseitov, Zh. Kerimkulov, Y. S. Mukhamejanov, M. Nassurlla, Demyanova, A. N. Danilov, A.A. Ogloblin, A.S. Aimaganbetov. Investigation of exotic states of ^{13}C at low energy // International Journal of Modern Physics E Vol. 27, No. 3 (2018) 1850025 (7 pages), DOI: 10.1142/S0218301318500258

N E W S
OF THE NATIONAL ACADEMY OF SCIENCES OF THE REPUBLIC OF KAZAKHSTAN
PHYSICO-MATHEMATICAL SERIES
ISSN 1991-346X **https://doi.org/10.32014/2019.2518-1726.31**
Volume 3, Number 325 (2019), 120 – 129

ISSN 2224-5278
UDC539.216: 538.9

D. Kalygulov[2], I. Klinovitskaya[2], T.Turmagambetov[1], A. Pavlov[1], S. Plotnikov[2], B. Mukashev[1], A. Serikkanov[1], Zh. Agabekov[3], D. Kantarbaeva[1]

[1]Satbayev University,Institute of physics and technology, Almaty, Kazakhstan;
[2]D. Serikbayev East Kazakhstan state technical university, Ust-Kamenogorsk, Kazakhstan;
[3]KazPV Ltd, Astana, Kazakhstan
iklinovitskaya@inbox.ru, din.orazbaevna@gmail.com

HIGH-TECH PRODUCTION OF PHOTO-ENERGY IN KAZAKHSTAN BASED ON THE SARYKOL QUARTZ DEPOSIT

Abstract. The technology of silicon purification to solar grade silicon for metallurgical silicon obtained from the Sarykol quartz deposit by carbothermic reduction is presented. This technology is based on metallurgical methods of purification, namely gas-slag refining and directional crystallization. Silicon ingots are grown from the solar grade silicon using "monolike" technology. Photovoltaic converters are manufactured and investigated. Solar cells from "monolike" silicon have a higher efficiency of 17-18.4%, in comparison with solar cells made from multicrystalline silicon. Converters with high efficiency were tested for the light-induced degradation effect.

Key words: solar grade silicon, silicon purification, monolike technology, solar cell.

Introduction. Kazakhstan is implementing the KazPV Project - "Creating of the production of photovoltaic modules based on Kazakhstan silicon", that includes the production of metallurgical grade silicon (MG-Si) and solar grade silicon (SoG-Si), the production of solar cells and photovoltaic modules. The cluster for the production of photovoltaic modules includes three domestic enterprises: MC KazSilicon LLP, Kazakhstan Solar Silicon LLP and Astana Solar LLP.

MG-Si was obtained at the enterprise KazSilicon by the carbothermal method by reduction of high-purity Sarykol quartz by carbon. The MG-silicon purification technology has been developed. SoG-Si was obtained using the developed technology, from which silicon ingots were grown using the "monolike" technology (ML-Si). Solar cells with an efficiency of 17-18.4 % were manufactured based on ML-Si. The solar cell panels were used in the first Kazakhstan Power Plant AstanaSolar with capacity of 250 kW. This technology is the basis for the creation of the industrial production of materials, solar cells, photovoltaic modules and photovoltaic stations.

Methods

MG-Si production and purification up to SoG-Si. The raw materials used for the experiments were studied before melting for the production of metallurgical silicon. Analysis of the quartz of the Sarykol deposit showed that the phosphorus content is the lowest in the world (compared to Australian quartz, considered one of the best in the world, the phosphorus content is 2-6 times lower), the boron content is similar to the Australian deposit and ranges from 1 ppm to 3-4 ppmw. It was found that a distinctive feature of the Sarykol deposit, compared with other global deposits of quartz, is that the impurities of boron, phosphorus and other chemical elements are outside the crystal lattice of the main component of mineral raw materials. This allows, based on the principles of condensed matter physics and materials science, to develop a highly efficient technology for silicon purification to "solar quality" and ensure its use in industrial environments with less financial and resource costs compared to the technologies used in practice. The silicon coming from the furnace needs additional cleaning. One of the options for the purification of metallurgical silicon may be gas-slag refining, i.e. purging of liquid silicon with a special

composition of gases in combination with the addition of fluxes. The article by A. Istratov and others[1] reports on purging the silicon melt with such gases as Cl_2, $SiCl_4$, CO_2, water vapor, or their combinations. These gases react with dissolved impurities in silicon and form volatile compounds that evaporate from the melt. For example, the chlorides of many metals are volatile compounds. According to the authors, this method is effective in Al, Ca, C, Mg, Fe, B, P, and Ti removing.

Mixtures of SiO_2, CaO, $CaCO_3$, Na_2O, Na_2CO_3, Al_2O_3, MgO, BaO, B_2O_3 and CaF_2, and other oxides and fluorides are used as fluxes. During the purification process, at high temperatures, the fluxes react and create a complex glass phase - slag phase, that can react with impurities in the MG-Si melt and create a combination of oxides. These oxides can be solid, liquid or gaseous and can be caught in the slag phase or released in the gas phase from the MG-Si melt. Elements such as Al, Ca and Mg are oxidized and the degree of purification is determined by the Eq. (1), (2), (3):

$$4Al + 3SiO_2 = 3Si + 2Al_2O_3 \quad (1)$$

$$2Ca + SiO_2 = Si + 2CaO \quad (2)$$

$$2Mg + SiO_2 = Si + 2MgO \quad (3)$$

Theoretically, this allows you to remove Al, Ca and Mg to very low levels, but in practice this is hampered by large heat losses occurring during this operation. In order to avoid crystallization of the melt, oxygen is purged, as a result of which an exothermic oxidation of silicon to a dioxide occurs.

After completion of the oxidative refining in the ladle, the slag, that contains some of the impurities, is removed mechanically or settles to the bottom, and the liquid silicon is poured into a special mold. The separation of slag from silicon is due to the difference in density and viscosity of the slag and silicon itself, so that separation is possible. Consequently, a high CaO content will lead to a low viscosity of the slag, which will sink to the bottom of the ladle, while the CaF_2 viscosity will increase, which will cause it's floating up in the molten silicon. Thus, the condition of the difference of properties in density and viscosity for slag-forming additives is necessary to achieve a good separation [2].

When using silicon in photovoltaic applications, special attention is paid to such impurities as boron and phosphorus, since these elements are the main alloying elements in p-type and n-type silicon. These impurities are contained in concentrations of 1^{st}-2^{nd} orders of magnitude higher than the required level in metallurgical silicon.

The slag purification of metallurgical silicon, carried out at MK KazSilicon LLP, is based on a flux containing SiO_2. Carrying out slag purification experiments consisted of adding several components of the corresponding fluxes to the MG-Si melt to remove impurities from the MG-Si melt by selecting of the composition of the slag mixture.

Boron removal process. The boron removal process occurs due to the oxidation of boron elements in the MG-Si melt according to three chemical reactions (4), (5), (6):

1 - Boron oxidation:

$$[B] + (3/4)\ O_2 \rightarrow (1/2)B_2O_3 \quad (4)$$

2 - Boron oxide absorption, that appeared as a result of the first reaction:

$$(1/2)B_2O_3 + (3/2)O^{2-} \rightarrow BO_3^{3-} \quad (5)$$

3 -Final expected boron removal result:

$$[B] + (3/2)O^{2-} + (3/4)O_2 \rightarrow BO_3^{3-} \quad (6)$$

Phosphorus removal reaction process. As for phosphorus, it is possible to purify the MG-Si melt due to the transfer of phosphorus into the slag according to the following two reactions (7) and (8):

$$[P] + (3/4)O^{2-} \rightarrow P^{3-} + (3/4)O_2 \quad (7)$$

or

$$[P] + (3/2)O^{2-} + (5/4)O_2 \rightarrow PO_4^{3-} \quad (8)$$

The oxygen ions required for the oxidation reaction will be supplied into the slag phase due to the decomposition of simple oxides, the slag components that are used for purification. For example, for the SiO_2-CaO slag, oxygen will be supplied according to the following reactions (9), (10):

1 - CaO Flux Disintegration:

$$CaO \rightarrow Ca^{2+} + O^{2-} \quad (9)$$

2 - SiO_2 flux Disintegration:

$$SiO_2 \rightarrow [Si] + O_2 \quad (10)$$

As for the other slags mentioned above, such as BaO, Na_2O, Na_2CO_3, etc., the same decay reactions will occur during the purification process. For example, for Na2O, the following reaction(11) occurs:

$$Na_2O \rightarrow 2Na+ + O_2- \quad (11)$$

When conducting experiments at MC KazSilicon LLP, the flux mixture was added directly during the process of pouring liquid silicon from the furnace into the metallurgical ladle. The average weight of the pouring was about 1 ton.

After the end of the pouring, the ladle was distilled off into a sump to continue refining, the time of which was about 60 minutes. Due to the fact that during this time there was the possibility of crystallization of the molten silicon, the ladle was driven under a special heater designed for this purpose.

The slag resulting from the refining forms creates slag crust on the surface of the liquid metal, which is removed mechanically after the draining of refined liquid silicon into the mold.

For experiments on the removal of boron and phosphorus impurities, several mixtures of flux components were used, representing 2, 3 or 4 component systems, such as, for example, SiO_2-Na_2CO_3, SiO_2-CaO-Al_2O_3, CaO-CaF_2-$BaCO_3$, etc.

Based on the fact that the tests were carried out directly on an industrial scale and given the economic factor, the mass content of the mixture of flux components to the mass of liquid silicon was taken approximately equal to 10%. During the pouring of metallurgical silicon into the ladle from the furnace and refining, the oxygen-air mixture was supplied. The range of consumption of oxygen and air was 1.43 - 2.18 m^3/s and 5.18 - 9.83 m^3/s, respectively.

To determine the effectiveness of slag purification, several tests were carried out, where the time for refining was the same as for cleaning with only one gas-air mixture. Table 1 shows the average value for the removal of Al and Ca in percent, for several issues both with and without fluxes.

Table 1 - Effect of fluxes on the removal of Al and Ca impurities

Name of impurities	Aluminum removal,%	Calcium removal,%
Without fluxes	77,73	91,82
With flux (SiO_2-Na_2CO_3)	94,75	94,63

In the project implementation, an optimized slag purification technology using various fluxes, as well as purification by the crystallization method, was developed [3]. After conducting pilot tests, the SoG-Si obtained by the carbothermic method from the quartz of the Sarykol field after all stages of purification, as well as solar cells created from the material obtained, was investigated.

Table 2 presents the results of analyzes of quartz used to obtain silicon and silicon itself.

Table 2 - Concentrations of impurities after various stages of purification

Material type	Impurities concentration, ppm wt		
	Boron	Phosphorus	Metals
Quartzite	1,3	0,32	125
MG-Si	15,4	68	400
Purified MG-Si (UMG-Si)	<5	8	2500
SoG-Si	0,2	0,57	<3
The analyzes were carried out in certified laboratories Schmid Pilot Production (SPP, Germany) and the National Renewable Energy Laboratory, NREL, USA.			

Growing and investigation of ML-Si ingots. In order to increase the efficiency of solar cells and reduce production costs, a process of silicon ingots production, using the so-called monolike technology has been developed. The aim of this work was to study the effect of a higher concentration of impurities in SoG-Si on the formation of crystalline defects (mainly dislocations) in single-crystal structures. Single-

crystal structure visualization, mapping of the lifetime of minority carriers and photoluminescence were used for studying the properties of a monolike ingot obtained on an industrial scale from Kazakhstan's SoG-Si.

ML-Si ingots of p-type conductivity were manufactured using ECM technology in a PV 600 furnace [4] and weighed about 450 kg. The process of growing ML-Si ingots consists of four stages and takes 78 hours. Silicon is heated to a melting point of 1423°C. Crystallization occurs from the bottom to the top part of the ingot using thermal dissipation, which is carried out under conditions of a homogenized furnace temperature to limit thermal deformations.

Silicon ingots were cut into bricks after the crystallization process. Then ingots were cut into wafers of size 156x156 mm and 180 microns thick. The lifetime of minority charge carriers (electrons) was measured immediately after cutting without additional processing. The measurements were carried out using Microwave Photoconductive Decay (μ-PCD) technology by Semilab WT2000 equipment. This technique does not allow to measure the real lifetime, however, mapping by the obtained values allows to qualitatively evaluate the uniformity of the distribution of the lifetime of the ingot and to identify areas with defects that limit the lifetime. Resistivity was also measured on bricks, using Semilab WT2000 equipment. The uncalibrated photoluminescence (PL) image was obtained on a BT LIS-R2 equipment with laser illumination (915 nm), equivalent to 1 solar constant; the illumination time was 1 s. In addition, the ingots were investigated using infrared Fourier transform spectrometry (IFTS).

The concentration of dopants in the initial SoG-Si needs to be adjusted to achieve the required boron and phosphorus values. As shown in [5]and[6], doping of silicon with gallium allows compensation of phosphorus, despite phosphorus high concentration. Schmidt et al. [7] showed that doping of silicon with gallium does not reduce the carrier lifetime and does not increase the concentration of structural defects in crystalline silicon.

Comparison of the calculated and measured resistivity along ingot height, represented in Fig. 1, shows that doping with gallium can lead to a resistance of the order of 1.5 Ω cm, while the stability of the resistance is maintained until the crystallization fraction reaches 95% without changing the conductivity type of silicon. The carrier mobility (μ) was calculated using the obtained concentrations of boron, phosphorus and gallium, as well as the Arora model [8]. The resistivity (ρ) was calculated from the obtained values of mobility and concentrations of dopants, using Eq. (12):

$$\rho = 1/\mu qp \quad (12)$$

where μ is the mobility of charge carriers, q is the electron charge, p is the effective concentration of charge carriers equal to the difference between the concentrations of acceptor and donor impurities (NB + NGa-NP).

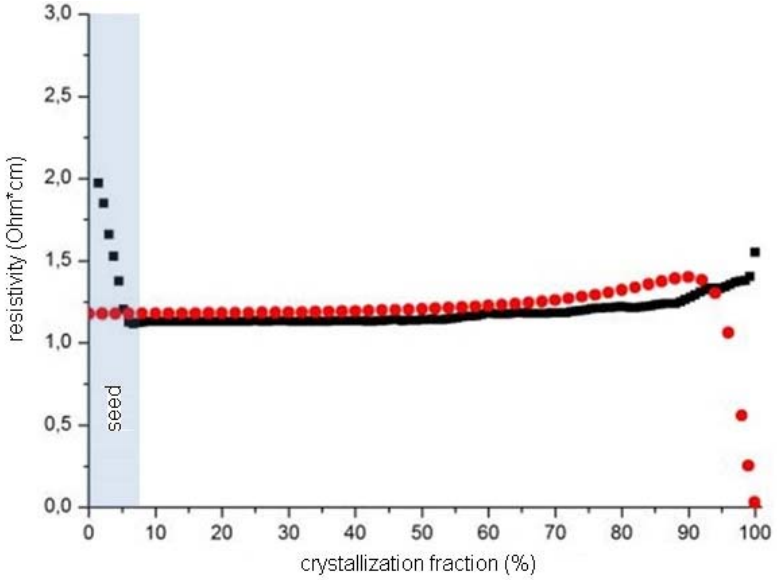

Figure1 - Comparison of the resistivity change dependency along the ingot height, calculated (points) and measured (squares)

Grown ingots contain impurities that lead to the formation of defects that impair the electrical and physical properties of silicon. Namely, oxygen and carbon are the main impurities in standard mc-Si and ML-Si, and are often found in the form of sediment due to the processes occurring during the growth of crystals. Various types of SiO_2 and SiC precipitates and oxygen-containing defects can be observed depending on the temperature conditions and the initial concentration of oxygen and carbon. They can be deposited on the boundaries of the grains and dislocations and, thus, change their electrical characteristics. Therefore, they can affect the recombination in the volume of silicon and the properties of the p – n junction if they penetrate into the space charge region. In addition, it is also known that oxygen forms complexes with boron (B-O), which can significantly reduce the lifetime.

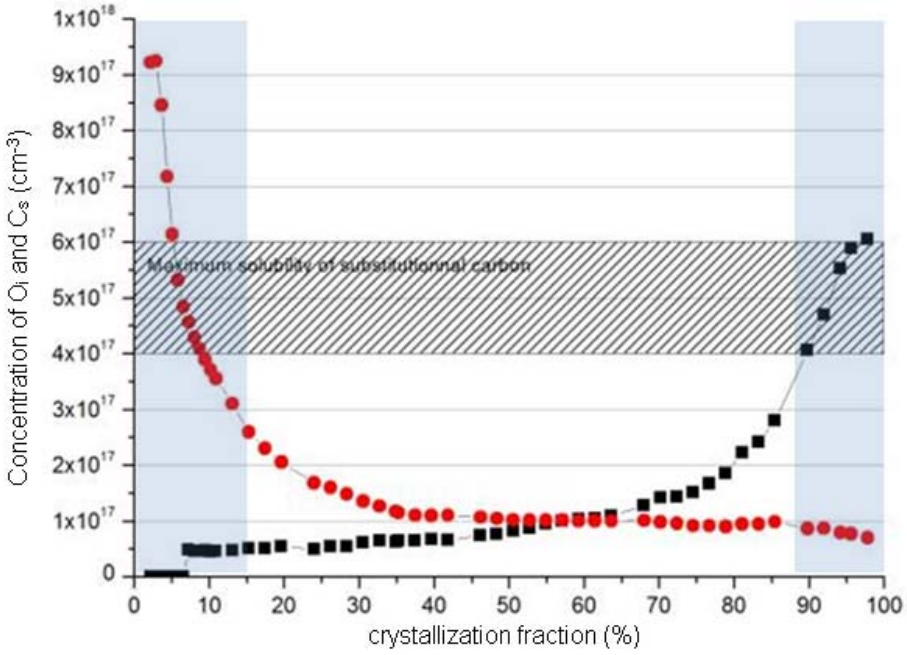

Figuer 2 - The concentration of O_i (points) and C_s (squares) obtained by IFTS measurements along the ingot height. The shaded rectangles highlight the cut off areas on the top and bottom of the ingot, the shaded area shows the maximum solubility of Cs in silicon

Fig. 2 shows the changes in the concentration of interstitial oxygen [O_i] and carbon substitution atoms [C_s] with an increase of the crystallization fraction obtained by IFTS measurements along ingot monolike height. There is a high concentration of oxygen at the bottom of the ingot due to contact with a quartz crucible. The high concentration of carbon in the top of the ingot is due to its low segregation coefficient. From the analysis of grown monolike ingots, it can be seen that the useful part of the ingot contains a rather low concentration of O_i and C_s ($<3 \cdot 10^{17}$ cm^{-3}). At such concentrations, the formation of SiC inclusions is unlikely, and the probability of formation of B – O complexes is significantly reduced.

Damage to the seed with raw materials multiplies and spreads dislocations towards the top of the ingot. A sufficiently high source of stress (3 MPa at the melting point [9]) can occur at high temperatures, and plastic deformation of the seed, which leads to the creation of dislocations. The source of stress can be silicon raw materials loaded on the seed or silicides (SiC, Si_3N_4, SiO_2) formed on the surface of the seed. With the concentration of stresses caused by microscopic points of contact, the dislocation creation threshold is easily exceeded. These mechanisms mainly depend on the flatness and surface state at the seed/crucible and seed/seed boundaries.

Fig. 3 presents the results of photoluminescent analysis performed on the wafers along the height of the marginal and central bricks. The results show that the multiplication of dislocations is higher with a higher curvature of the crystallization front. Thus, temperature conditions and equipment influence on the multiplication of dislocations. The results of the analysis show a clear advantage of monolike ingots compared to standard multicrystalline ingots.

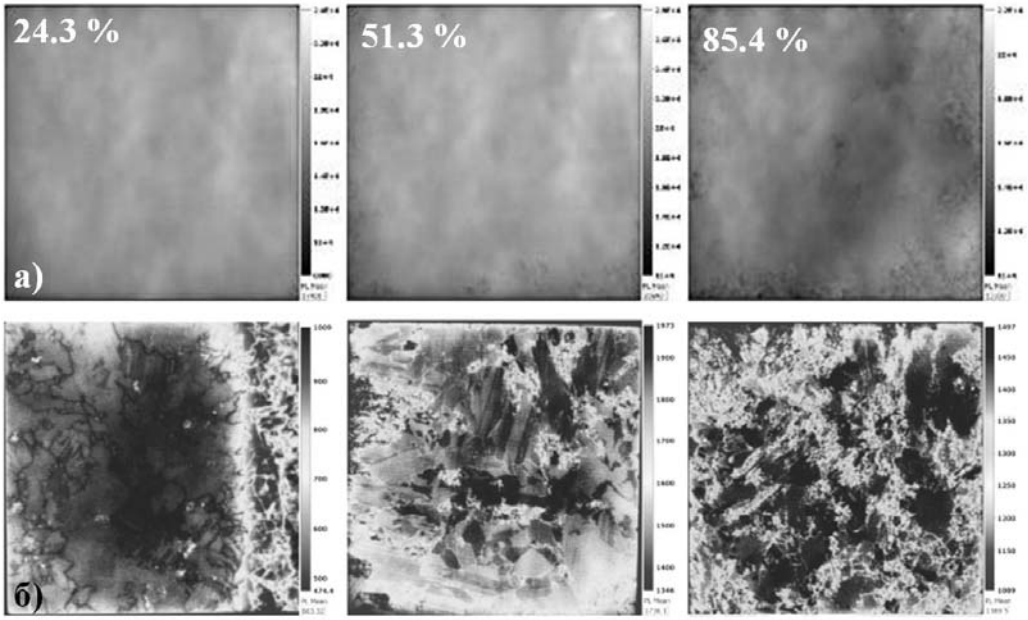

Figure 3 - The uncalibrated image of the photo luminescent analysis of the wafers along the height of the central ML-Si brick (upper row of cells) in comparison with a standard multicrystalline ingot (lower row of cells). The images indicate percent crystallization fraction

Results

Manufacturing and investigation of solar cells. For the study of the possibility of using monolike silicon for the production of high-efficiency solar cells, wafers were chosen along the height of the central ingot. Solar cells were manufactured using the standard Al-BSF architecture [2], according to which the solar cell has a uniform n-type phosphoric emitter on the top part, and is electrically-passivated with SiNx:H layer function also as an anti-reflective coating. The back side of the solar cell is passivated by the p + area, called BSF (back surface field), as a result of screen printing and burning of the back contact from aluminum paste. The charge carriers are assembled on a solid aluminum rear contact and on an H-shaped silver front contact made in the form of a grid.

IV parameters were measured on ready-made solar cells under standard testing conditions (STC). The measured parameters of the solar cells, such as the open-circuit voltage (V_{oc}), short-circuit current (J_{sc}), fill factor (FF) and efficiency (η), were obtained from the measured IV characteristics. In addition, the current-voltage characteristics were measured on solar cells after the degradation test under illumination. The solar cells with the highest efficiency were used to study the effect of degradation of solar cells under lighting (LID). LID measurements were carried out on a device fixing a change in Voc, at a constant temperature (65°C) and illumination (43 mV≈1.1 Sun), every second. Full results are presented in [10].

The influence of gettering effect on the lifetime of charge carriers.

Fig. 4 shows the measurement results of τ_{eff} for silicon wafers before and after gettering. Samples after phosphorus diffusion showed a significant increase in τ_{eff}, regardless of the type of material used. It is known that metallic impurities are one of the main factors reducing τ_{eff} in silicon. Metal impurities can create precipitates in crystallographic defects or can be dissolved in the bulk of silicon, which in turn forms deep energy levels in the forbidden zone, such as interstitial iron atoms (Fe_i), which increases the recombination activity and lowers τ_{eff}. Impurities with a fairly high diffusion coefficient in the process of diffusion of phosphorus diffuse into the n-type layer and form electrically inactive clusters - the gettering process due to the difference in dissolution coefficients at high temperatures. However, it can be seen that the measured τ_{eff} is higher for ML-Si, due to the higher initial (before gettering) τ_{eff} (τ_0) value (Fig. 4). The higher τ_0 for ML-Si is explained by the better crystal structure of this sample and the smaller amount of metallic impurities in the bulk of the wafer.

The measured values of τ_{eff} and τ_0 decrease with an increase in the crystallization fraction, which is explained by an increase in the density of crystallographic defects and an increase in the concentration of impurities due to the effect of segregation during growth. This is confirmed by lower values of $\tau_{eff}$and τ_0 for wafers from the marginal brick of the ingot, due to the higher concentration of defects. It should be noted that the increase in τ_{eff} after the gettering process is lower for the last crystallized fraction (Figure 4). The absence of an increase in τ_{eff} after the gettering process shows that in this case τ_{eff} is more limited by crystallographic defects than by the concentration of impurities.

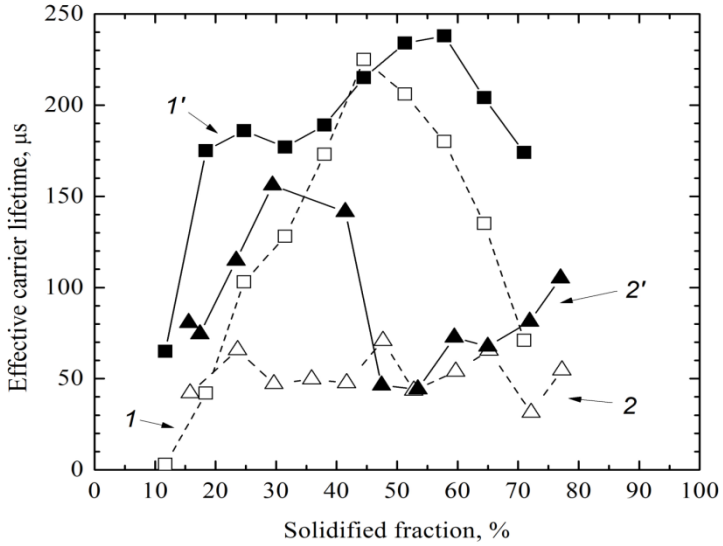

Figure 4 - Comparison of the effective lifetime (with an excessive concentration of charge carriers, $\Delta n = 1 \cdot 10^{15}$ cm^{-3}) on the ML-Si wafers of the central brick and mc-Si, depending on the height of the ingot: 1 - ML-Si wafers before gettering, 1'- ML-Si wafers after gettering, 2 - mc-Si wafers before gettering, 2' - mc-Si wafers after gettering

Based on the data obtained, we can conclude that the use of moonlike technology for growing silicon ingots is more promising; silicon grown using this technology has better electrical characteristics. Therefore, solar cells made of ML-Si should have a higher efficiency.

Fig. 5 shows the distribution of J_{sc} and V_{oc} of solar cells from central ingots of ML-Si and mc-Si, depending on the crystallization fraction. The values of J_{sc} and V_{oc} directly depend on the τ_{eff} and the diffusion length of the electrons and correlate well with the measured values of τ_{eff}. It can also be seen that the values of J_{sc} and V_{oc} are higher for solar cells made of ML-Si, that was expected due to a higher τ_{eff}.

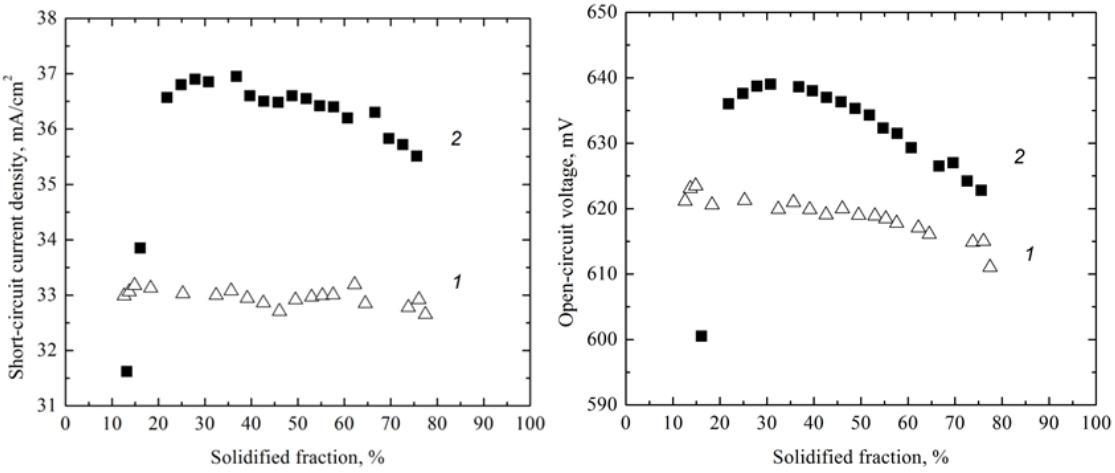

Figure 5 - Comparison of changes in Voc (left) and Jsc (right) along the height of ingots for solar cells made of ML-Si and mc-Si: 1 - mc-Si, 2 - ML-Si

Fig. 6 shows the distribution of the efficiency of Al-BSF solar cells based on silicon wafers along the height of the bricks. As expected, after measuring τ_{eff}, solar cells made from ML-Si have higher efficiency values due to better performance. The maximum value of the efficiency for solar cells made of ML-Si was 18.4%. In[11], a significant decrease in the efficiency along the height of the ML-Si ingot was reported, which was explained by an increase in the density of dislocations. In contrast to our case, very precise control of the crystallization process is not capable of limiting the crystallographic defects formation in the bulk of the crystal. As a result, solar cells produced from a material of this level are less limited in efficiency due to recombination losses, and this explains the presence of a wide area with a very slight decrease in efficiency. These results show that controlled multiplication of dislocations has a significant impact on the production process of solar cells by not only increasing the efficiency limits, but also narrowing the distribution area.

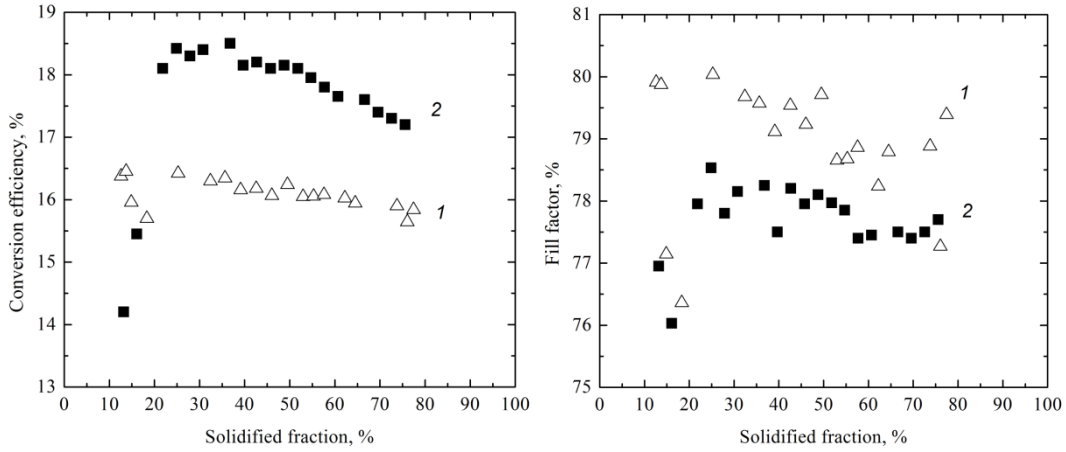

Figure 6 - Comparison of changes in efficiency (left) and fill factor (right) along the height of ingots for solar cells made of ML-Si and mc-Si: 1 - mc-Si, 2 - ML-Si

On the other hand, solar cells made of ML-Si have a fill factor lower than mc-Si solar cells (Fig. 6). These results can be explained by the incomplete refinement of the process and technological regimes for creating solar cells. Since the fill factor depends on the quality of the process of metallization and diffusion of phosphorus (the creation of the n-layer). However, even with smaller values of the fill factor, solar cells made of ML-Si have a higher efficiency. What shows a further opportunity for increasing the efficiency of solar cells by adjustment of technological processes and modes.

At the end of the investigation, solar cells with high efficiency were tested for light degradation to obtain more complete results. These tests are important because of the formation of boron-oxygen complexes (B-O) as a result of exposure to light. These complexes, in turn, are electrically active recombination centers and can significantly reduce the efficiency of solar cells[12].

It was found that the average value of the relative degradation of efficiency is about 1%. The obtained results show an insignificant effect of LID on the efficiency of solar cells produced from ML-Si, that well correlates with theoretical data on the formation of B-O complexes with oxygen concentrations above $3 \cdot 10^{17}$ cm^{-3}. According to measurements the concentration of interstitial oxygen [O_i] in the ML-Si does not exceed $3 \cdot 10^{17}$ cm^{-3} for the regions of the ingot used in the creation of solar cells. Unlike silicon grown by Czochralski technology, in which [Oi] reaches about $8 \cdot 10^{17}$ cm^{-3}, silicon grown by monolike technology is less susceptible to the formation of B-O complexes and consequently the degradation of the efficiency of solar cells when exposed to sunlight.

On the other hand, on the researched solar cells, the LID effect increases with an increase in the crystallization fraction and therefore with decreasing [Oi] and it can be concluded that in this case the LID effect is more associated with other processes and mechanisms than the formation of B-O complexes. A recent paper [13-15]reported that metal impurities such as copper form electrically active precipitates in the bulk of silicon when exposed to light and can cause degradation of the electrical characteristics of solar cells. In addition, [16]reported on the influence of the architecture of solar cells on the effect of

degradation during illumination; it was shown that solar cells with a passivated surface are more sensitive to degradation.

Discussion

Potential production of photovoltaic cells from Kazakhstan p-type silicon purified by metallurgical using the advantages of monolike technology investigated.

It is shown that the content of oxygen and carbon impurities is very low, which prevents the formation of SiO_2 and SiC precipitates. In addition, it has been shown that monolike-grown ingots are practically free of microcrystalline regions, and that a limitation of the dislocation density can be achieved in industrial technology. The optimization of the technology was based on precise control of the curvature of the crystallization front in the process of directional solidification, since the curvature of the front is a key factor in the quality of crystallization.

It is shown that silicon ingots grown using the monolike technology have a higher carrier lifetime compared to standard mc-Si. In addition, it is shown that in the process of creating solar cells, the lifetime of charge carriers increases due to the effect of gettering, without additional purification processes. The advantages of the developed technology were observed at the level of solar cells, by increasing the efficiency and reducing the distribution of efficiency along the ingot height. It is shown that solar cells made of ML-Si have a rather low degradation of efficiency when exposed to light.

The maximum efficiency for solar cells made of ML-Si was 18.4%. In addition, according to the results of recent work, an increase in the efficiency of solar cells up to 20% and higher is expected due to the adjustment of the production process of solar cells to ML-Si wafers.

In conclusion, ML-Si grown from silicon of solar grade in the near future may be a breakthrough in PV industry, due to the high potential for the production of solar cells with high efficiency and significant reduction in production costs.

Д.А. Калыгулов[2], И.А. Клиновицкая[2], Т.С. Турмагамбетов[1], А.А. Павлов[1], С.В. Плотников[2], Б.Н. Мукашев[1], А.С.Серикканов[1], Ж. Агабеков[3], Д.О. Кантарбаева[1]

[1]СәтбаевУниверситеті,Физика-техникалық институты, 050032, Алматы, Қазақстан,
[2]Д.Серикбаеват. ШҚМТУ, 070004, Өскемен, Қазақстан
[3]KazPV Ltd, Астана, Қазақстан

САРЫКӨЛ КВАРЦ КЕН ОРНЫ НЕГІЗІНДЕ ҚАЗАҚСТАНДА ФОТОЭНЕРГЕТИКА ҚҰРУДЫҢ ЖОҒАРЫ ТЕХНОЛОГИЯЛЫ ӨНДІРІСІ

Аннотация. Сарыкөл кен орнынан карботермиялық қалпына келтіру арқылы алынған кварцтан металлургиялық кремнийді күн сапалы кремнийге дейін тазалау технологиясы ұсынылады. Берілген технология тазалаудың металлургиялық әдістеріне – газды қожбен тазарту және бағытталған кристалдануға негізделген. Алынған күндік кремнийден “monolike” технологиясымен құймалар дайындалды. Мульти-кристалданған кремнийден алынған түрлендіргіштермен салыстырғанда өте тиімді – 17-18,4% болатын фотоэлектрлік түрлендіргіштер дайындалып, зерттелді. Өте тиімді түрлендіргіштер жарықтық деградацияның тестінен өткізілді.

Түйін сөздер: күн сапалы кремний, кремнийді тазарту, “monolike” технологиясы, күндік элемент.

Д.А. Калыгулов[2], И.А. Клиновицкая[2], Т.С. Турмагамбетов[1], А.А. Павлов[1], С.В. Плотников[2], Б.Н. Мукашев[1], А.С. Серикканов[1], Ж. Агабеков[3], Д.О. Кантарбаева[1]

[1]Сатпаев Университет, Физико-технический институт, 050032, Алматы, Казахстан;
[2]ВКГТУ им. Д.Серикбаева, 070004, г. Усть-Каменогорск, Казахстан;
[3]KazPV Ltd, Астана, Казахстан

ВЫСОКОТЕХНОЛОГИЧНОЕ ПРОИЗВОДСТВО ПО СОЗДАНИЮ ФОТОЭНЕРГЕТИКИ В КАЗАХСТАНЕ НА ОСНОВЕ КВАРЦЕВОГО МЕСТОРОЖДЕНИЯ САРЫКОЛЬ

Аннотация. Представлена технология очистки металлургического кремния до кремния солнечного качества, полученного из кварца Сарыкольского месторождения карботермическим восстановлением.

Данная технология основана на металлургических методах очистки – газошлаковым рафинированием и направленной кристаллизацией. Из полученного солнечного кремния выращены слитки по технологии “monolike”. Изготовлены и исследованы фотоэлектрические преобразователи, которые имеют более высокую эффективность – 17-18,4%, по сравнению с преобразователями из мультикристаллического кремния. Преобразователи с высокой эффективностью были подвергнуты тестам на световую деградацию.

Ключевые слова: кремний солнечного качества, очистка кремния, технология “monolike”, солнечный элемент.

Information about authors:

D.Kalygulov, D. Serikbayev East Kazakhstan state technical university, Ust-Kamenogorsk, Kazakhstan,107das@mail.ru,https://orcid.org/0000-0003-0723-8567;

I. Klinovitskaya, D. Serikbayev East Kazakhstan state technical university, Ust-Kamenogorsk, Kazakhstan, iklinovitskaya@inbox.ru,https://orcid.org/0000-0001-9608-8470;

T.Turmagambetov, Institute of physics and technology, Satbayev University, Almaty, Kazakhstan, ttleuzhan@yandex.kz ,https://orcid.org/0000-0001-8929-5519;

B. Mukashev, Academician of the National Academy of Sciences of the Republic of Kazakhstan, Institute of physics and technology, Satbayev University, Almaty, Kazakhstan,mukashev2005@mail.ru, https://orcid.org/0000-0003-2206-1093;

A.Pavlov, Institute of physics and technology, Satbayev University, Almaty, Kazakhstan, art_roll@mail.ru, https://orcid.org/0000-0003-0102-1519;

S. Plotnikov, D. Serikbayev East Kazakhstan state technical university, Ust-Kamenogorsk, Kazakhstan, splotnikov@ektu,kzplotsv@ektu.kz,http://orcid.org/0000-0002-3204-0571;

A.Serikkanov, Institute of physics and technology, Satbayev University, Almaty, Kazakhstan, a.serikkanov@gmail.com,https://orcid.org/0000-0001-6817-9586

Zh.Agabekov,KazVP Ltd, Astana, Kazakhstan,janivip@mail.ru, https://orcid.org/0000-0002-3980-0625

D. Kantarbaeva, Institute of physics and technology, Satbayev University, Almaty, Kazakhstan, din.orazbaevna@gmail.com,https://orcid.org/0000-0003-3891-8733

REFERENCES

[1] A.A. Istratov, T. Buonassisi, M.D. Pickett, M. Heuer, E.R. Weber. Materials Science and Engineering B, **134**, PP.282–286, (2006).doi:10.1016/j.mseb.2006.06.023

[2] Handbook of Photovoltaic Science and Engineering, Second Edition, edited by Antonio Luque and Steven Hegedus. John Wiley & Sons Ltd, Second edition (2010).

[3] B.N. Mukashev, A.A. Betekbaev, D.A. Kalygulov,A.A.Pavlov, D.M. Skakov,Physics and Engineering of Semiconductors,Volume 10, 1421, (2015) (in Russ.).

[4] Betekbaev A.A., Mukashev B. N., OunadjelaK. Pavlov A.A., Pellegrin I. and Shcolnik V.S., 24th Workshop on Crystalline Silicon Solar Cells & Modules: Materials and Processes. Breckenridge, Colorado, USA, pp. 101-107, (2014).

[5] Kirscht, F., Heuer, M., Käs, M., Rakotoniaina, J.-P., Jester, T., Metallurgically Refined Silicon for Photovoltaics. Proceedings CSSC-6, Aix-les-Bains, France, (2012).

[6] A.A. Betekbaev, B.N. Mukashev, L. Pelissier , P. Lay , G. Fortin, L. Bounaas, D.M. Skakov, A.A.Pavlov. Journal of Higher Educational Institutions. Materials of Electronic Technology. 103-109, (2015).DOI: 10.17073/1609-3577-2015-2-103-109.ISSN: 1609-3577, (In Russ.).

[7] Schmidt J., Bothe K. Phys. Rev. B, vol. **69**, pp. 24107-24115, (2004).

[8] N.D. Arora, J.R. Hauser, D.J. Roulston. 29th IEEE PVSC. 292 (1982).

[9] Gallien B. PhD Thesis, Université de Grenoble, (2014).

[10] A.A. Betekbaev, B.N. Mukashev, L. Pelissier , P. Lay , G. Fortin, L. Bounaas, D.M. Skakov, D.A. Kalygulov, T.S. Turmagambetov, V.V. Lee, ФТП,**8,** 1106, (2016) (in Russ.)

[11] Trempa M. и др. Journal of Crystal Growth, Vol **351**, pp. 131-140, 2012.

[12] K. Bothe, and J. Schmidt. J. Appl. Phys. **99**, 013701, (2006).

[13] T. Turmagambetov, S. Dubois, J.-P. Garandet, B. Martel, N. Enjalbert, J. Veirman, and E. Pihan. Phys. Status Solidi C. 11, 1697, (2014).

[14] T. Turmagambetov, S. Dubois, J. P. Garandet, H. Lignier and N. Enjalbert. Solar Energy Materials & Solar Cells, 157, p. 558–564, (2016).

[15] E. A. Dmitriyeva, D. M. Mukhamedshina, K. A. Mit’, I. A. Lebedev, I. I. Girina, A. I. Fedosimova, E. A. Grushevskaja. Doping of fluorine of tin dioxide films synthesized by sol-gel method. News of National Academy of Sciences of the Republic of Kazakhstan. Series of geology and technology sciences.Volume 1, Number 433 (2019), PP.73–79, http://dx.doi.org/10.32014/2019.2518-170X.9 ISSN 2224-5278.

[16] M. Cascant, N. Enjalbert, R. Monna, S. Dubois. 29th EU PVSEC, Munich, Germany, 2570, (2014).

N E W S
OF THE NATIONAL ACADEMY OF SCIENCES OF THE REPUBLIC OF KAZAKHSTAN
PHYSICO-MATHEMATICAL SERIES
ISSN 1991-346X **https://doi.org/10.32014/2019.2518-1726.32**
Volume 3, Number 325 (2019), 130 – 139

UDC 521.1 524.4

B. Shukirgaliyev[1,2,3], A. Otebay[2,3], A. Just[4],
P. Berczik[5,4,6], Ch. Omarov[2], A. Naurzbaeva[2,3], M. Kalambay[2,3]

[1]Energetic Cosmos Laboratory, Nazarbayev University, Nur-sultan, Kazakhstan;
[2]Fesenkov Astrophysical Institute, Almaty, Kazakhstan;
[3]Faculty of Physics and Technology, Al-Farabi Kazakh National University, Almaty, Kazakhstan;
[4]Zentrum für Astronomie der Universität Heidelberg, Astronomisches Rechen-Institut, Heidelberg, Germanyl
[5]National Astronomical Observatories of China and Key Laboratory for Computational Astrophysics, Chinese Academy of Sciences, Beijing, Chinal
[6]Main Astronomical Observatory, National Academy of Sciences of Ukraine, Kyiv, Ukraine
bekdaulet.shukirgaliyev@nu.edu.kz, otebay@aphi.kz, omarov@aphi.kz,
aisha.nuryzbaeva@kaznu.kz, kalambay@aphi.kz

VIOLENT RELAXATION IN ISOLATED STAR CLUSTERS

Abstract. We study the effect of initial mass function and stellar evolution on the survivability of isolated star clusters after instantaneous gas expulsion. Our model clusters form with a centrally peaked star-formation efficiency profile according to the local-density-driven cluster formation model. We perform direct $N-$body simulations of $N_* = 10^4$ star clusters with global star-formation efficiencies ranging from 0.13 to 0.50.

We have found that the stellar evolutionary mass-loss does not affect the number of bound stars of star clusters with high global SFE ($SFE_{gl} > 0.2$), and the decrease in final bound mass fraction is only due to stellar evolution. But star clusters with lower global SFE are affected more by stellar evolutionary mass-loss and survive with less number of stars than if it would consist of single-mass non-evolving stars. High-SFE clusters also do not expand much after violent relaxation, while clusters with $SFE_{gl} = 0.15$ and 0.20 expand significantly. The global SFE as low as $SFE_{gl} = 0.30$ is sufficient for a cluster to almost keep its mass and size at the time of gas expulsion in our models.

Keywords. galaxies: star clusters: general – methods: numerical – stars: kinematics and dynamics – open clusters and associations: general.

1 Introduction

Stars do not form in isolation. Instead they form in large groups and clusters within dense clumps in giant molecular clouds. Different stellar-feedback mechanisms as stellar winds, radiation pressure and photo-ionizing radiation coming from massive stars ($> 8M_{SUN}$) can drive the star-forming gas with the speed about $10 km/s$ (i.e. roughly $10 pc/Myr$) [1, 2, 3, 4, 5]. Star-formation efficiency (SFE), the fraction of star-forming gas mass converted into stars, reported by observations of nearby star- forming regions to be usually less than 30% [6, 7, 8]. That means, more than 70% of total mass is driven from the embedded clusters by the gas expulsion, which leads to the instability in the star cluster. Lada and Lada [9] reported that about 90% of star clusters in the solar neighborhood are disrupted after gas expulsion. There are many works dedicated to the topic of survivability of young star clusters after gas expulsion in the literature [eg. 10, 11, 12, 13, 14, 15, 16, 17, among many others].

Shukirgaliyev et al. [16] proposed a new approach to study the survivability of star clusters after instantaneous gas expulsion. They consider star clusters formed according to the local-density-driven cluster formation model of Parmentier and Pfalzner [18]. That is in their model clusters the volume density profile of stars are steeper than that of the residual and total gas, as a consequence of star-

formation taking place with a constant efficiency per free-fall time in a centrally concentrated, spherically symmetric clump gas [18]. They reported that, such star clusters with a centrally peaked SFE profile are more resilient to the instantaneous gas expulsion than the model clusters considered earlier [e.g. 13, and references therein]. The model star clusters of Shukirgaliyev et al. [16] survive the instantaneous gas expulsion with a critical global SFE of $SFE_{gl} = 0.13$ instead of $SFE_{gl} = 0.33$ as estimated previously.

In this study we consider the survivability of isolated cluster models only in contrast to Shukirgaliyev et al. [16], who mainly focused on the survivability of star cluster in the tidal field of our Galaxy, orbiting in the solar neighborhood. The isolated cluster models in Shukirgaliyev et al. [16] have been considered mainly to test their new initial conditions and simulations. Their isolated model clusters are consist of equal-mass, non-evolving stars, while their model clusters of the solar neighbourhood consist of evolving stars with masses sampled according to the initial mass function (IMF) of Kroupa [19]. Therefore, the decrease of the cluster bound fractions at the end of violent relaxation caused by coupled effect of two mass-loss mechanisms: stellar evolution and tidal stripping [16, 20, 21, 22]. The intermediate case of isolated model clusters consist of evolving stars is now being considered in the framework of this study in addition to Shukirgaliyev et al. [16].

We compare the survivability of isolated model clusters of Shukirgaliyev et al. [16], which consist of equal-mass stars with our new simulations with full stellar mass spectrum where additionally stellar evolution taken into account. The gas expulsion is assumed to be instantaneous in both cases.

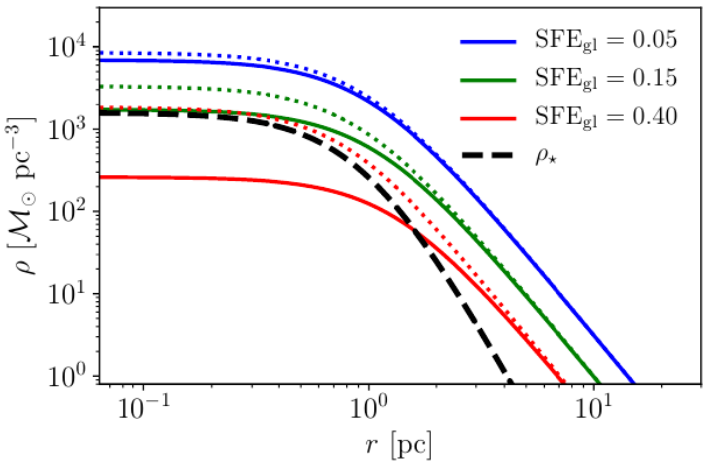

Figure 1 - Density profiles of the star cluster (black dashed line), of the residual (solid lines), and initial (dotted lines) gas for different SFE_{gl} in scaled physical units. A total stellar mass $M_* = 6000 M_{SUN}$ and a 3D half-mass radius $r_h = 1.26 pc$ are assumed. Note that the stellar density profile is a Plummer profile.

2 Model description

Our model clusters have a Plummer density profile and are in virial equilibrium together with the gravitational potential of the residual star-forming gas, immediately before gas expulsion. The density profile of residual gas is recovered for a given global SFE using the Eq. A.7 of Shukirgaliyev et al. [16], assuming that our model clusters have been formed with a constant star-formation efficiency of $\in_{ff} = 0.05$ from centrally concentrated, spherically symmetric gas clump. As a consequence of that, the volume density profiles of the residual and the total gas have a shallower slope that that of stars [18, 16]. Figure 1 shows the volume density profile of stars (black dashed line), of the residual (colored solid lines) and of the initial total gas (colored dash-dotted lines) of $M_* = 6000 M_{SUN}$ cluster with a global SFE of 0.05,0.15 and 0.40 for illustration.

Isolated model clusters of Shukirgaliyev et al. [16] have number of star $N_* = 10000$ in their simulations. In this study, we run a new set of simulations of isolated clusters in order to qualify the effect

of stellar mass function and stellar evolutionary mass loss on the cluster survivability. For that we chose $M_* = 6000 M_{SUN}$ model clusters, which have $N_* = 10455$ stars when we sample stellar masses with IMF of Kroupa [19]. Upper and lower limits of $m_{up} = 100 M_{SUN}$ and $m_{low} = 0.08 M_{SUN}$ have been adopted for the IMF. We use the same normalization of our *N*-body units to physical as in Shukirgaliyev et al. [16] standard case. That is our $M_* = 6000 M_{SUN}$ model clusters have a half-mass radius of $r_h = 1.26 pc$ at the time of gas expulsion.

We generate the initial phase-space distribution of star in our model clusters using the program mkhalo from falcON package [23] with specially developed Gas Potential plug-in [16, 21]. The high-presicion direct *N* -body code phiGRAPE-GPU [24] has been used for our *N* -body simulations, which ended at time about $t = 1 Gyr$.

3 Bound fraction of isolated models

The bound fraction is the fraction of cluster mass immediately after gas expulsion, remaining bound to the cluster at a given time. The bound fraction could be also considered as a number fraction of bound stars. In case of clusters consist of non- evolving (i.e. constant mass) equal-mass stars, the bound fractions in terms of mass and number of stars are the same. But when we consider clusters consist of evolving stars, stellar masses decrease with time and two bound fractions become different. Therefore in this study in contrast to Shukirgaliyev et al. [16] we consider both, bound mass fraction and bound number fraction of our isolated model clusters.

We use the same method as we used in Shukirgaliyev et al. [16] to define the bound fraction of model clusters. That is, instead of defining the bound fraction based on the total (i.e., kinetic + potential) energy of stars as the fraction of stars with a negative

total energy (solid lines in Fig. 2), we eliminate unbound stars by iterative calculations of the total energies of stars after removing of currently unbound ones. This method, described in the appendix of Shukirgaliyev et al. [16] gives us the opportunity to to define the final bound fraction early on in the evolution of clusters. Otherwise, the bound fraction of model clusters, which are super-virial after gas expulsion, can be overestimated by the early method based on the total energies of stars [see the appendix of 16, for more details]. Figure 2, brought here from Shukirgaliyev et al. [16] for the sake of clarity, shows the comparison of the two methods of defining of the bound fraction of isolated model clusters. Dashed lines show the bound fraction calculated by a new technique, while the solid lines correspond to the bound fractions calculated by the old technique. Figure 2 shows that the instantaneous bound fraction converges toward the final bound fraction determined with our technique by the end of the simulations. This shows that with our calculation method we can estimate the final bound fraction even before the inner part of the cluster starts to collapse back and return to virial equilibrium. We caution, however, that with this method we underestimate the final bound fraction of a cluster with a low global SFE during their early evolution after instantaneous gas expulsion. This is caused by removing all un- bound stars, including the centrally concentrated ones, which contribute the most to the gravitational field of the cluster [see Fig. B.2. in 16]. This is the reason for the unusual behavior of the final bound fractions of isolated clusters with a global SFE of 0.13 and 0.15, which is 0 at $t \le 1$ *Myr* , and why they rise at an early time in the evolution instead of decreasing.

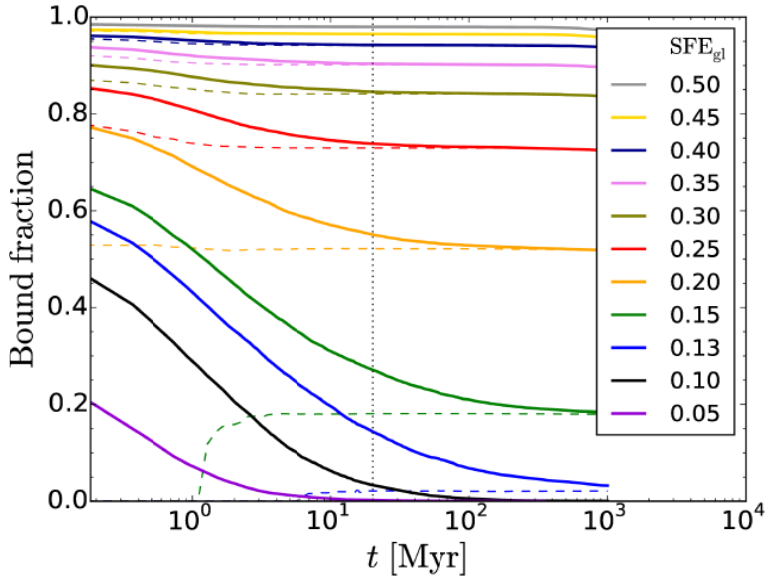

Figure 2 - Time evolution of the bound fraction F_b of isolated models ($N = 10^4$) as defined by two methods: defined by the fraction of stars with a negative total energy (solid lines), and defined by recalculating the total energy of stars in an iterative process (see text for details; dashed lines). The vertical dotted line corresponds to $t = 20\ Myr$ when we scale the isolated models with the same scale factor as for a non-isolated model with $M_* = 6000 M_{SUN}$, which also has $N \approx 10^4$.

(This figure brought here from Shukirgaliyev et al. [16] for the sake of clarity.)

4 Results

We use the technique described above to find the bound fractions of our newly simulated star clusters. Since we are looking at the multi-mass stars and turn on the stellar evolution, we consider two bound fractions, one in terms of number fraction, and the other in terms of mass fraction. In Fig. 3 we compare bound fraction evolution of two isolated models. The left panels show the bound fraction evolution of previous model clusters consist of equal-mass stars. The right panels show the bound number fraction evolution on top panel and bound mass fraction evolution in bottom panel of our newly simulated clusters, consist of IMF sampled evolving stars. The $SFE_{gl} = 13$ model cluster does not survive the instantaneous gas expulsion when is consist of multi-mass evolving stars (see blue lines in the right panels).

Figure 3 shows that after $t = 20\ Myr$ the bound number fraction of all model clusters become almost a constant, so the decreasing of the bound mass fraction of star clusters with IMF is only due to stellar evolution. Therefore we assume that the violent relaxation is over before $t = 20\ Myr$ and then we measure the final bound fraction, that is the bound fraction at the end of violent relaxation at $t = 20\ Myr$.

Figure 4 presents the comparison of the final bound fractions of our model clusters as a function of global SFE, in terms of number fraction in the left and of mass fraction in the right panel. Single mass model clusters and evolving clusters with IMF are represented by green and red colours, respectively. There is almost no difference between the two types of models when we look at the final bound number fraction for a high global SFE ($SFE_{gl} > 0.2$). The decrease in final bound mass fractions of star clusters with IMF mostly caused only by the stellar evolutionary mass-loss and also by Poisson noise in the phase space distribution of stars. The model cluster with the highest SFEs ($SFE_{gl} = 0.5$) save almost all of its stars after instantaneous gas expulsion (see bound number fraction). Therefore its bound mass fraction at the end of violent relaxation is almost the same as if it did not lose any star during its evolution with mass-loss caused by only the stellar evolution (the horizontal dashed line on the right panel of Fig. 4). It also do not too much differ in its bound mass at the end violent relaxation from other two high SFE clusters (

$SFE_{gl} = 0.3$ and $SFE_{gl} = 0.4$). These three model clusters do not expand much after the violent relaxation too (see Fig. 5). The half-mass radius of model clusters at the end of violent relaxation normalized to their half-mass radii immediately after gas expulsion[1] as a function of the global SFE are provided in Fig. 5. As we see from our models, the highest observed SFE, as high as $SFE_{gl} = 0.3$, is sufficient to keep the embedded clusters almost unchanged in terms of mass and size after gas expulsion. [See e.g. 25, to learn about the expansion of star clusters after gas expulsion].

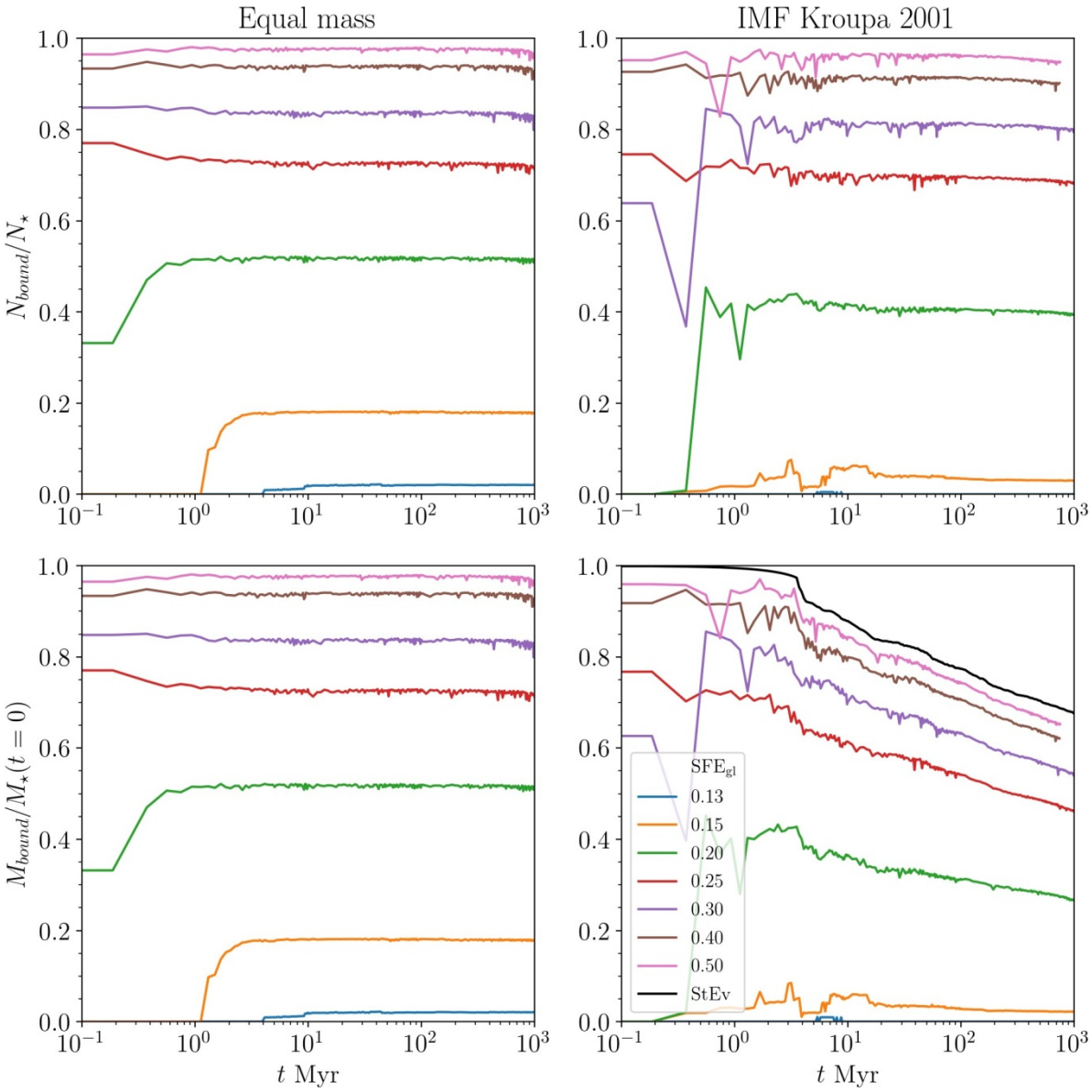

Figure 3 - Bound fraction evolution of isolated clusters. The top panels show the evolution of bound number fraction, while the bottom panels show the evolution of bound mass fraction of equal-mass star clusters in the left panels and IMF sampled evolving star clusters in the right panels. X-axis is given in logarithmic scale. The color-coding corresponds to global SFE shown in the key in the lower right panel. The black line in the lower right panel corresponds to the mass-loss due to pure stellar evolution

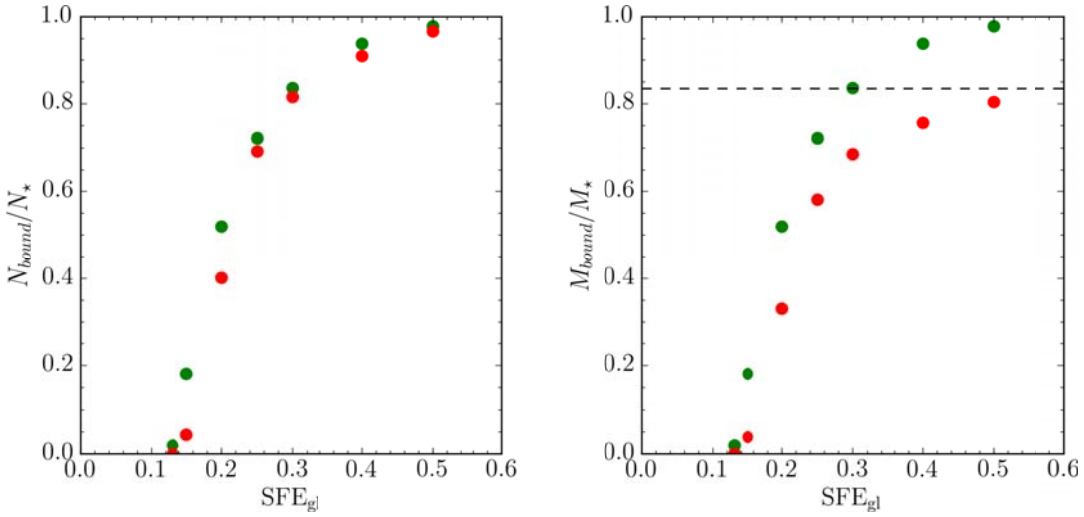

Figure 4 - The final bound fractions of isolated model clusters measured at $t = 20$ *Myr* as a function of global SFE. The left panel shows final bound fractions in terms of number fraction of stars, while the right panel corresponds to the final bound mass fractions. The equal-mass star clusters are marked with green colour, while model clusters with stellar evolution are shown by red

When we look at star clusters with global SFE lower than $SFE_{gl} < 0.25$, their final

bound number fractions are decreased together with their final bound mass fractions when the IMF and the stellar evolution are introduced in the simulations. This is an effect of the fast evolution of most massive stars, when almost 15% of the total stellar mass is lost within early 20 *Myrs* . Due to the stellar evolutionary mass-loss, the central gravitational well of multi-mass clusters becomes much weaker, than that of single-mass clusters, and therefore loses more stars (hence mass). The escape of some very massive stars also have negative influence in the survivability of multi-mass low SFE clusters. The Poisson noise in the initial phase-space distribution of stars also can cause a scatter in the final bound fractions of low-SFE clusters [see 20, for more details].

[1]Since clusters have the same stellar density profile at the time of instantaneous gas expulsion, their half-mass radii immediately after gas expulsion are identical too.

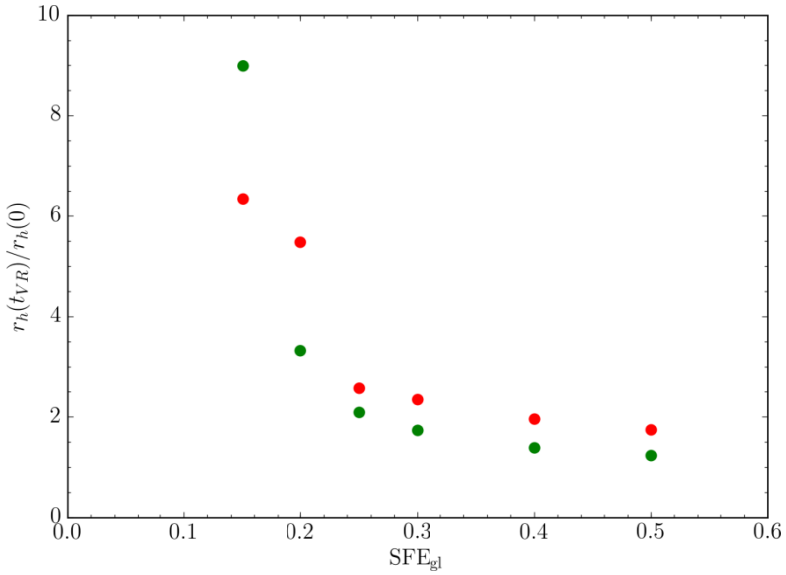

Figure 5 - The half-mass radii of isolated model clusters at the end of violent relaxation as a function of global SFE, normalized to the cluster half-mass radii immediately after gas expulsion ($r_h(0) = 1.26\,pc$). The green and the red filled circles correspond to the single-mass and multi-mass clusters, respectively.

5 Conclusions

We considered the survivability of isolated model clusters, consist of multi-mass evolving stars after instantaneous gas expulsion. Our model clusters formed with a centrally-peaked SFE profile, as a consequence of star formation process happening with a constant efficiency per free-fall time according to the model of Parmentier and Pfalzner [18]. All our model clusters have a Plummer density profile immedi- ately before gas expulsion and are in virial equilibrium with gravitational potential of the residual gas. We consider $M_* = 6000 M_{SUN}$ clusters with different global SFE range from $SFE_{gl} = 0.13$ to $SFE_{gl} = 0.5$. The IMF of Kroupa [19] with the mass limits of $m_{low} = 0.08 M_{SUN}$ and $m_{up} = 100 M_{Sun}$ has been adopted. All stars lose their mass according to the stellar evolution code SSE [26]. We use high-precision direct *N* -body code phiGRAPE-GPU for our simulations.

We calculated the bound fraction of model clusters based on their energies using the technique described in Sec. 3. Then we compare our results with the results in Shukirgaliyev et al. [16] obtained for isolated clusters, consist of non-evolving single- mass stars.

We have found that $SFE_{gl} = 0.3$ is sufficient to save almost all stars ($> 80\%$) and keep the cluster compact after violent relaxation. The model cluster with $SFE_{gl} = 0.13$ does not survive the instantaneous gas expulsion when the IMF and the stellar evolution are introduced in the simulations. The $SFE_{gl} = 0.15$ model cluster survives the instantaneous gas expulsion, although with a small final bound fraction.

The stochastic effect is high in low SFE clusters due to low number of high-mass stars [20]. Therefore in the next study we plan to consider more random realizations and study the stochastic effects due to the mass-function in more detail. We do not consider any effect from dark matter due to relative small scales [27].

Acknowledgments. This work was supported by Sonderforschungsbereich SFB 881 “The Milky Way System” (subproject B2) of the German Research Foundation (DFG). The authors gratefully acknowledge Dr. Genevieve Parmentier (Heidelberg University, Germany) – the former PhD supervisor of B.S. – for her useful comments and suggestions about the content of the paper. The authors gratefully acknowledge Prof. Walter Dehnen (University of Leicester, UK) for his support and discussions in connection with implementing the code mkhalo for our purposes. A.O. and B.S. gratefully acknowledge Prof. Rainer Spurzem for his support with accessing the high-performance computing clusters at JURECA and LAOHU. A.O. and B.S. acknowledge the support within PCF program BR05236322 funded by the Ministry of Education and Science of the Republic of Kazakhstan. P.B. and B.S. acknowledge the support of the Volkswagen Foundation under the Trilateral Partnerships grant 90411 and the support by the National Astronomical Observatories of Chinese Academy of Science (NAOC/CAS) through the Silk Road Project, through the Thousand Talents (“Qianren”) program and (P.B. only) the President’s International Fellowship for Visiting Scientists and the National Science Foundation of China under grant No. 11673032. P.B. acknowledges the special support by the NASU under the Main Astronomical Observatory GRID/GPU computing cluster project. This work benefited from support by the International Space Science Institute, Bern, Switzerland, through its International Team program ref. no. 393 “The Evolution of Rich Stellar Populations & BH Binaries” (2017–18). We acknowledge the use of supercomputers of the Jülich Supercomputing Centre (JSC) JURECA (hhd28), of the Baden-Württemberg HPC infrastructure (bwforCluster, national and state funded through grant INST 35/1134-1 FUGG, and funded by SFB 881), of the KEPLER GPU cluster funded by Volkswagen foundation project I/81 396, and of NAOC/CAS (LAOHU at Centre of Information and Computing).

УДК 521.1 524.4

Б. Шукиргалиев[1,2,3], А.Өтебай[2,3], А.Юст[4], П. Берцик[5,4,6], Ч. Омаров[2], А. Наурзбаева[2,3], М.Қаламбай[2,3]

[1]*Энергетикалық Ғарыш Зертханасы, Назарбаев Университеті, Нұр-сұлтан, Қазақстан* 2*Фесенков ат. Астрофизикалық Институт, Алматы, Қазақстан;*
[3]*Физика-техникалық факультет, Әл-Фараби ат. Қазақ Ұлттық Университеті, Алматы,Қазақстан;*
[4]*Астрономиялық есептеу институты, Хайдельберг Университетінің Астрономия орталығы, Хайдельберг, Германия;*
[5]*Қытайдың Ұлттық Астрономиялық Обсерваториялары мен Есептеуіш Астрофизика Өзекті Зертханасы, Қытай ғылым академиясы, Бейжің, Қытай;*
[6]*Басты Астрономиялық Обсерватория, Украина Ұлттық Ғылым Академиясы, Киев, Украина*

ОҚШАУЛАНҒАН ЖҰЛДЫЗДЫҚ ШОҒЫРЛАРДЫҢ ҚАРҚЫНДЫ РЕЛАКСАЦИЯСЫ

Аннотация. Осы жұмыста бастапқы масса функциясы мен жұлдыздар дамуының жұлдыздық шоғырланудың лездік газ ығыстырылуынан кейінгі сақталуына әсері қарастырылады. Жұлдыз түзілуінің тиімділігі (ЖЖТ) жергілікті тығыздықпен анықталатын модельге сәйкес, зерттеліп отырған жұлдыздық кластерлер орталық шыңға ие ЖЖТ-мен құрылады. Жұлдыз түзілуінің тиімділігі 0.13-пен 0.50 аралығында жататын жұлдыздық шоғырланулардың тікелей *N*-body модельдеуі $N_* = 10^4$ жағдай үшін орындалған.

Массаның жұлдыздар эволюциясы себебінен жоғалуы жаһандық жұлдыз түзілуінің тиімділігі жоғары ($SFE_{gl} > 0.2$) жұлдыздық шоғырланулардағы байланысқан жұлдыздар санына әсер етпейтіні, ақырғы байланысқан фракцияның массасы тек жұлдыздар дамуы арқасында (байланысқан жұлдыздар санының азаюы себебінен емес) кемитіні табылған. Алайда, $SFE_{gl} = 0.15$ төмендеу шоғырланулар жұлдыздар эволюциясынан болатын масса жоғалуының әсеріне ұшырап, массалары бірдей, эволюцияға қатыспайтын жұлдыздардан тұратын кластерлерге қарағанда байланысқан жұлдыздар саны аздау болып сақталып қалады. Оған қоса, SFE_{gl} жоғары шоғырланулар қарқынды релаксациядан кейін қатты кеңеймейтіні, ал $SFE_{gl} = 0.15$ пен 0.20 тең кластерлер – айтарлықтай ұлғайатыны алынған. Біздің модельде $SFE_{gl} = 0.30$ сияқты төмен жаһандық жұлдыз түзілуінің тиімділігі кластер газ ығыстырылу кезінде өзінің массасы мен өлшемін сақтау дерлік үшін жеткілікті болып шықты.

Түйін сөздер. галактикалар: жұлдызды шоғырлар: жалпы - әдістер: сандық- жұлдыздар: кинематика және динамика - шашыраңқы шоғырлар мен бірлестіктер: жалпы

УДК 521.1 524.4

Б. Шукиргалиев[1,2,3], А.Отебай[2,3], А.Юст[4], П. Берцик[5,4,6], Ч. Омаров[2], А. Наурзбаева[2,3], М.Каламбай[2,3]

[1]*Энергетическая космическая лаборатория, Назарбаев Университет, Нур-сұлтан, Казахстан*
[2]*Астрофизический Институт им. В.Г. Фесенкова, Алматы, Казахстан*
[3]*Физико-технический факультет, Казахский Национальный Университет им. Аль-Фараби, Алматы, Казахстан*
[4]*Астрономический вычислительный институт, Центр Астрономии Гейдельбергского Университета, Гейдельберг, Германия*
[5]*Национальная астрономическая обсерватория Китая и Ключевая лаборатория Вычислительной Астрофизики, Академия наук Китая, Пекин, Китай*
[6]*Главная Астрономическая Обсерватория, Национальная академия наук Украины, Киев, Украина*

БУРНАЯ РЕЛАКСАЦИЯ В ИЗОЛИРОВАННЫХ ЗВЕЗДНЫХ СКОПЛЕНИЯХ

Аннотация. В работе исследуется влияние начальной функции масс и звездной эволюции на выживаемость изолированного звездного скопления после мгновенного выдувания газа. Исследуемые модельные кластеры образуются с профилем эффективности звездообразования (SFE), имеющим

центральный пик, в соответствии с моделью формирования кластеров, в которой эта эффективность определяется локальной плотностью. Было выполнено пря- мое N -body моделирование звездных скоплений с $N_* = 10^4$ и глобальной эффективностью звездообразования, лежащей в диапазоне от 0.13 до 0.50.

Было обнаружено, что потеря массы за счет эволюции звезд не влияет на конечное число связанных звезд в звездных скоплениях с высокой глобальной эффективностью звездообразования ($SFE_{gl} > 0.2$), и конечная масса связанной фракции уменьшается только из-за звездной эволюции (не из-за уменьшения числа связанных звезд). Однако звездные скопле- ния с более низкой глобальной $SFE_{gl} = 0.15$ больше подвержены влиянию потери массы за счет звездной эволюции и выживают с меньшим числом звезд, чем скопления, состоящие из неволюционирующих звезд одной массы. Также скопления с высокой SFE_{gl} не расширяются сильно после бурной релаксации, тогда как кластеры с SFE_{gl} = 0.15 и 0.20 значительно расширяются. В нашей модели такой низкой глобальной эффективности звездообразования, как $SFE_{gl} = 0.30$, оказывается достаточно для того, чтобы кластер почти сохранил свою массу и размер во время вытеснения газа.

Ключевые слова. галактики: звездные скопления: общие - методы: численные - звезды: кинематика и динамика - рассеянные скопления и ассоциация: общие

Information about authors:

Shukirgaliyev Bekdaulet - Dr.rer.nat, postdoc, Energetic Cosmos Laboratory, Nazarbayev University and Fesenkov Astrophysical Institute, email: bekdaulet.shukirgaliye;v@nu.edu.kz;

Otebay Aigerim - M.Sc., junior researcher at Fesenkov Astrophysical Institute, PhD student at Faculty of Physics and Technology, Al-Farabi Kazakh National University, email: otebay@aphi.kz.

Andreas Just - Dr.rer.nat, prof. Zentrum für Astronomie der Universität Heidelberg, Astronomisches Rechen-Institut;

Peter Berczik - Dr.rer.nat, deputy Director of Main Astronomical Observatory, National Academy of Sciences of Ukraine.

Omarov Chingis - Dr.rer.nat., President of JSC National center for space research and technology;

Naurzbaeva Aisha - candidate of physical and mathematical sciences, Senior Lecturer, Faculty of Physics and Technology, Al-Farabi Kazakh National University, email: aisha.nuryzbaeva@kaznu.kz;

Kalambay Mukhagali - M.Sc., junior researcher at Fesenkov Astrophysical Institute, PhD student at Faculty of Physics and Technology, Al-Farabi Kazakh National University, email: kalambay@aphi.kz.

REFERENCES

[1] M. R. Krumholz and C. D. Matzner. The Dynamics of Radiation-pressure-dominated H II Regions. // *The Astrophysical Journal*, 703:1352–1362, October 2009. doi: 10.1088/ 0004-637X/703/2/1352.

[2] P. F. Hopkins, D. Narayanan, N. Murray, and E. Quataert. Dense molecular gas: a sensitive probe of stellar feedback models. // *Monthly Notices of the Royal Astronomical Society*, 433: 69–77, July 2013. doi: 10.1093/mnras/stt688.

[3] S. Dib, J. Gutkin, W. Brandner, and S. Basu. Feedback-regulated star formation - II. Dual constraints on the SFE and the age spread of stars in massive clusters. // *Monthly Notices of the Royal Astronomical Society*, 436:3727–3740, December 2013. doi: 10.1093/mnras/stt1857.

[4] D. Rahner, E. W. Pellegrini, S. C. O. Glover, and R. S. Klessen. Winds and radiation in unison: a new semi-analytic feedback model for cloud dissolution. // *Monthly Notices of the Royal Astronomical Society*, 470:4453–4472, October 2017. doi: 10.1093/mnras/stx1532.

[5] K. Grasha, D. Calzetti, A. Adamo, R. C. Kennicutt, B. G. Elmegreen, M. Messa, D. A. Dale, K. Fedorenko, S. Mahadevan, E. K. Grebel, M. Fumagalli, H. Kim, C. L. Dobbs, D. A. Gouliermis, G. Ashworth, J. S. Gallagher, L. J. Smith, M. Tosi, B. C. Whitmore, E. Schinnerer, D. Colombo, A. Hughes, A. K. Leroy, and S. E. Meidt. The spatial relation between young star clusters and molecular clouds in M51 with LEGUS. // *Monthly Notices of the Royal Astronomical Society*, 483(4):4707–4723, Mar 2019. doi: 10.1093/mnras/sty3424.

[6] A. E. Higuchi, Y. Kurono, M. Saito, and R. Kawabe. A Mapping Survey of Dense Clumps Associated with Embedded Clusters: Evolutionary Stages of Cluster-forming Clumps. // *The Astrophysical Journal*, 705:468–482, November 2009. doi: 10.1088/0004-637X/705/1/468.

[7] N. J. Evans, II, M. M. Dunham, J. K. Jørgensen, M. L. Enoch, B. Merín, E. F. van Dishoeck, J. M. Alcalá, P. C. Myers, K. R. Stapelfeldt, T. L. Huard, L. E. Allen, P. M. Harvey, T. van Kempen, G. A. Blake, D. W. Koerner, L. G. Mundy, D. L. Padgett, and A. I. Sargent. The Spitzer c2d Legacy Results: Star-Formation Rates and Efficiencies; Evolution and Lifetimes. // *The Astrophysical Journal Supplement*, 181:321-350, April 2009. doi: 10.1088/0067-0049/181/2/321.

[8] N. Murray. Star Formation Efficiencies and Lifetimes of Giant Molecular Clouds in the Milky Way. // *The Astrophysical Journal*, 729:133, March 2011. doi: 10.1088/0004-637X/729/2/ 133.

[9] Charles J. Lada and Elizabeth A. Lada. Embedded Clusters in Molecular Clouds. // *Annual Review of Astronomy and Astrophysics*, 41:57–115, January 2003. doi: 10.1146/annurev. astro.41.011802.094844.

[10] A. V. Tutukov. Early Stages of Dynamical Evolution of Star Cluster Models. // *Astronomy & Astrophysics*, 70:57, November 1978.

[11] F. C. Adams. Theoretical Models of Young Open Star Clusters: Effects of a Gaseous Component and Gas Removal. // *The Astrophysical Journal*, 542:964–973, October 2000. doi: 10.1086/317052.

[12] C. M. Boily and P. Kroupa. The impact of mass loss on star cluster formation - I. Analytical results. // *Monthly Notices of the Royal Astronomical Society*, 338:665–672, January 2003. doi: 10.1046/j.1365-8711.2003.06076.x.

[13] H. Baumgardt and P. Kroupa. A comprehensive set of simulations studying the influence of gas expulsion on star cluster evolution. // *Monthly Notices of the Royal Astronomical Society*, 380:1589–1598, October 2007. doi: 10.1111/j.1365-2966.2007.12209.x.

[14] R. Smith, M. Fellhauer, S. Goodwin, and P. Assmann. Surviving infant mortality in the hierarchical merging scenario. // *Monthly Notices of the Royal Astronomical Society*, 414: 3036–3043, July 2011. doi: 10.1111/j.1365-2966.2011.18604.x.

[15] P. Girichidis, C. Federrath, R. Allison, R. Banerjee, and R. S. Klessen. Importance of the initial conditions for star formation - III. Statistical properties of embedded protostellar clusters // *Monthly Notices of the Royal Astronomical Society*, 420:3264–3280, March 2012. doi:10.1111/j.1365-2966.2011.20250.x.

[16] B. Shukirgaliyev, G. Parmentier, P. Berczik, and A. Just. Impact of a star formation efficiency profile on the evolution of open clusters. // *Astronomy & Astrophysics*, 605:A119, September 2017. doi: 10.1051/0004-6361/201730607.

[17] J. P. Farias, M. Fellhauer, R. Smith, R. Domínguez, and J. Dabringhausen. Gas expulsion in highly substructured embedded star clusters. // *Monthly Notices of the Royal Astronomical Society*, 476:5341–5357, June 2018. doi: 10.1093/mnras/sty597.

[18] G. Parmentier and S. Pfalzner. Local-density-driven clustered star formation. // *Astronomy & Astrophysics*, 549:A132, January 2013. doi: 10.1051/0004-6361/201219648.

[19] P. Kroupa. On the variation of the initial mass function. // *Monthly Notices of the Royal Astronomical Society*, 322:231–246, April 2001. doi: 10.1046/j.1365-8711.2001.04022.x.

[20] B. Shukirgaliyev, G. Parmentier, A. Just, and P. Berczik. The Long-term Evolution of Star Clusters Formed with a Centrally Peaked Star Formation Efficiency Profile. // *The Astrophysical Journal*, 863:171, August 2018. doi: 10.3847/1538-4357/aad3bf.

[21] B. Shukirgaliyev. *The life of star clusters, from birth to dissolution: a new approach*. PhD thesis, Heidelberg University, 2018.

[22] B. Shukirgaliyev, G. Parmentier, P. Berczik, and A. Just. The star cluster survivability after gas expulsion is independent of the impact of the Galactic tidal field. // *Monthly Notices of the Royal Astronomical Society*, 486(1):1045–1052, Jun 2019. doi: 10.1093/mnras/stz876.

[23] P. J. McMillan and W. Dehnen. Initial conditions for disc galaxies. // *Monthly Notices of the Royal Astronomical Society*, 378:541–550, June 2007. doi: 10.1111/j.1365-2966.2007. 11753.x.

[24] P. Berczik, R. Spurzem, L. Wang, S. Zhong, and S. Huang. Up to 700k GPU cores, Kepler, and the Exascale future for simulations of star clusters around black holes. In *Third International Conference "High Performance Computing", HPC-UA 2013*, pages 52–59, October 2013.

[25] M. P. Geyer and A. Burkert. The effect of gas loss on the formation of bound stellar clusters // *Monthly Notices of the Royal Astronomical Society*, 323(4):988–994, May 2001. doi: 10. 1046/j.1365-8711.2001.04257.x.

[26] J. R. Hurley, O. R. Pols, and C. A. Tout. Comprehensive analytic formulae for stellar evolution as a function of mass and metallicity. // *Monthly Notices of the Royal Astronomical Society*, 315:543–569, July 2000. doi: 10.1046/j.1365-8711.2000.03426.x.

[27] A. Amangeldyieva, D.Kairatkyzy, T.Konysbayev. ON THE NONSTATIONARY PARAMETER OF STATE FOR DARK MATTER. //NEWS OF THE NATIONAL ACADEMY OF SCIENCES OF THE REPUBLIC OF KAZAKHSTAN. PHYSICO MATHEMATICAL SERIES, ISSN 1991-346X. Volume 6, Number 322 (2018), 44 – 48. https://doi.org/10.32014/2018.2518-1726.16

N E W S
OF THE NATIONAL ACADEMY OF SCIENCES OF THE REPUBLIC OF KAZAKHSTAN
PHYSICO-MATHEMATICAL SERIES
ISSN 1991-346X **https://doi.org/10.32014/2019.2518-1726.33**
Volume 3, Number 325 (2019), 140 – 152

Wojcik Waldemar[1], S.A.Kulmamirov[2], Zh.M.Alimzhanova[2], L.M. Alimzhanova[2], A.M. Akhmetova[2], V.I. Karyukin[2]

[1]The Lublin University of Technology;
[2]Kazakh National University al-Farabi

STUDY OF THE STABILITY OF THE REGULATOR BALANCING ROBOT NI MINDSTORMS

Abstract. The article presents the results of studying the steady state of a balancing robot when the control is carried out in a closed state. The synthesis of the controller's coefficients was carried out by estimating the root of the characteristic equation and the linear quadratic regulator. Under the action of the PID controller, algorithms for controlling the robot servos were compiled. The results of the experimental studies allowed us to construct transient characteristics in a closed robot control system while balancing the state of the robot in a steady state and in motion.

Evaluation of the stability of the robot. The control system of the balancing robot is asymptotically stable if its steady-state value at the time of its movement or at the moment of stopping will tend to zero regardless of the initial conditions, in the absence of input influences: $\lim_{t\to\infty} x(t) = 0$.It is assumed that the movement of the robot is described by a standard equation of the form: $\dot{x}(t) = Ax(t) + Bu(t)$ [1].In order for the robot to be asymptotically stable, it is necessary and sufficient that the real part of all the eigenvalues of the matrix be negative [2-6].

Feedbacks object state control. Let us consider that the robot under the study of a control object is a closed system, the block diagram of which is shown in Figure 1. The feedback control action is determined by the product of the proportionality coefficient K and the difference between the desired values and the measured values.

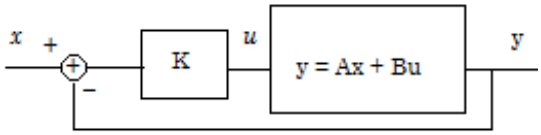

Figure 1 Feedback control

The control action and the status of SIS threads shown in Figure 1 describe the following equations:

$$u(t) = -K(y(t) - x(t),$$
$$\dot{x}(t) = (A - BK)y(t) + BKx(t). \quad (1)$$

It is necessary to maintain the system under the study of a steady statem by dividing by thecount value of the matrix *K*. Changing these valuesentails a change of b-governmental numbers of the matrix *(A – B *K)*. For sustainable regulation of a closed robot system, it is necessary for it to be controlled. The system will be controllable if the rank of the matrix *M* coincides with the rank of the matrix *A*. Here $M_c = [B, AB, \dots, A^{n-1}B]$ you can use the ctrb command to determine manageabilityinthe ControlSystemToolbox environment. There are 2 main methods for calculating feedback coefficients:

1) Calculation of the desired roots. The method describesthecalculation of the coefficients *K* with the creation of the desired eigenvalues of the matrix *A – B * K*.Inthe ControlSystemToolbox for the calculation, you can use the place function.

Example 1. K coefficients are describedin the first communication system with closed CONCRETE and GOVERNMENTAL parameter values A = [0,1; -2; -3] and B = [0;1]. Pole values are [-5, -6].

$$\begin{bmatrix} \gg A = [0{,}1, -2, -3]; B = [0, 1]; \\ \gg poles = [-5, -6]; \\ \gg K = place\ (A, B, poles) \\ K = 28{,}0\ \ 8{,}0 \end{bmatrix}$$

2) Linear square regulator M is received by calculating the coefficients of the matrix *K* on the basis of minimizing the value of the functional *J* calculated in the following form: $J = \int_0^\infty (x\,(t)^T Qx(t) + u(t)^T Ru(t))dt$. Parameters are adjusted by selecting the weight matrices of the state *Q* and the input action *R*, which are selected on the basis of the physical nature of the processes. The ControlSystemToolbox application can use the lqr functions to calculate a controller.

Example P 2. A = [0,1; -2, -3], B = [0; 1], Q = [100, 0; 0, 1]; R = 1.

$$\begin{bmatrix} \gg \lambda = [0{,}1, -2, -3]; B = [0, 1]; \\ \gg Q = [100, 0; 0, 1]; R = 1; \\ \gg K = lqr\ (A, B, Q, R) \\ K = 8{,}198\ \ 2{,}137 \end{bmatrix}$$

The control of the servos of the robot is carried out to generate the desired movement of the robot. For this purpose, the PID controller is most often used [16], i.e. a device in the feedback circuit used by an open-loop control system to generate a robot control signal. The PID controller generates a control signal which is the sum of 3 terms, the first of which is proportional to the input signal, the second is the integral of the input signal and the third is the derivative of the input signal.

The purpose of the PID controller is to maintain a given value x0 of a certain value x by changing another value of u. The value of x0 is called the "setpoint", and the difference e = (x - y) is called the "non-residual" or mismatch. The output signal of the regulator u is determined by three terms:

$$u(t) = P + I + D = K_p e(t) + K_i \int_0^t e(\tau)d\tau + K_d \frac{de}{dt}, \quad (2)$$

where K_p, K_i, K_d, are proportional, integral and differential components of the regulatorrespectively.

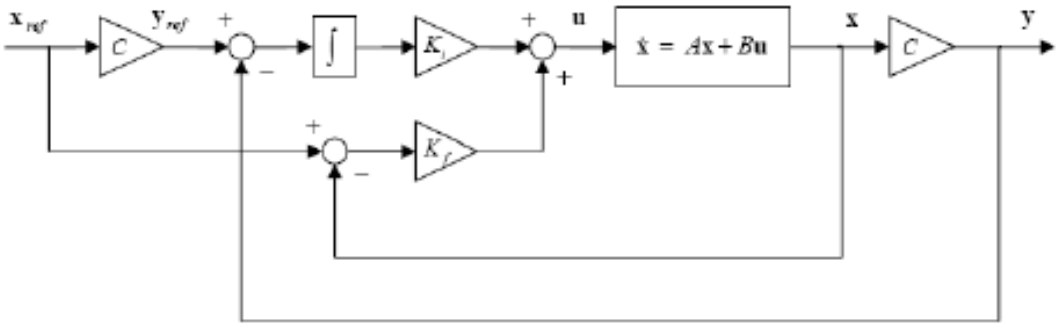

Figure 2 - PID controller

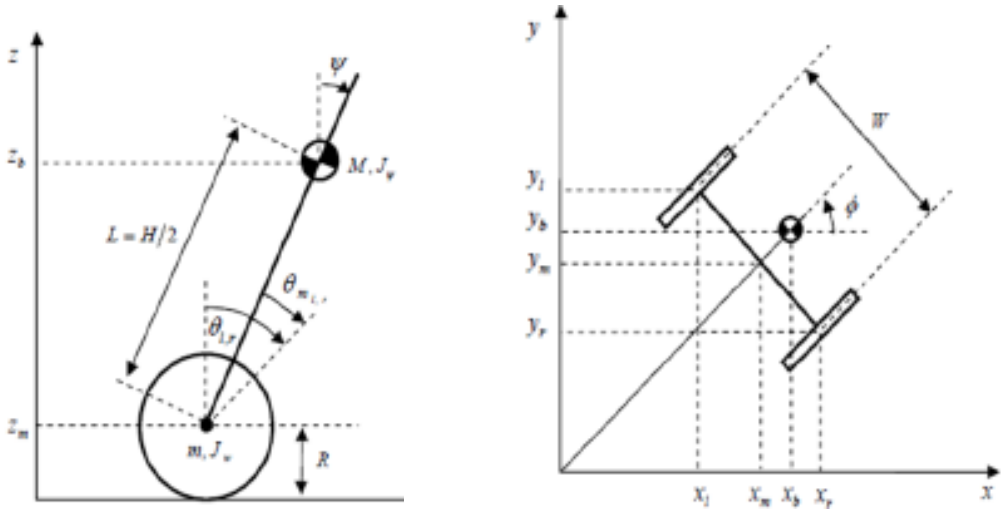

Figure 3 Model Parameter Designation

Figure 3 shows the model parameters indicated for robots: mobile robots of the “Motobot” type [2] and a balancing robot of the “Segway” type [3]. For use in specific studies below are the values of their parameters:

g = 9.81 (m / s2) acceleration of gravity;
m = 0.03 (kg) wheel weight;
R = 0.035 (m) wheel radius;
Jw = mR2 / 2 (kgm2) the moment of inertia of the wheel;
M = 0.6 (kg) body weight;
W = 0.14 (m) body width;
D = 0.04 (m) body thickness;
H = 0.144 (m) body height;
L = H / 2 (m) distance to the center of mass from the axis of the wheels;
JΨ = 2 (M * L) / 3 (kgm2) the moment of inertia of the body is tilted;
Jφ = M (W2 + D2) / 12 (kgm2) rotational moment of inertia;
Jm = 10-5 (kgm2) the moment of inertia of the engine;
Kb = 0.468 (V * s / rad) is the counter-emf constant;
Kt = 0.317 (N * m / A) is the motor torque constant.

Now we know everything to compile the source code of the program for organizing the movement of the robots. Let's call this program “Segway”. First of all, we compose the main control circuit of the robot. The diagram shown in Figure 4 reflects the main window of the program. The key blocks of the program are described above when they conducted an experimental study on assembling a Motobot robot. The rest of the schemes are contained in the nxtway_appblock.

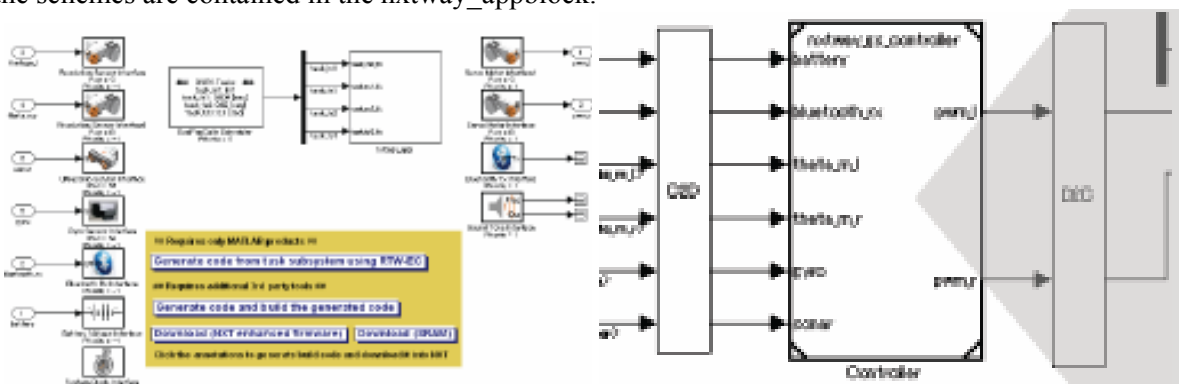

Figure 4 - The program «Segway» (left)
for the organization of the movement of the robot with the controller (right)

Figure 5 shows a general diagram of the model with all adjustable registrable inputs/outputs. Shown here are the signals that transmit data on the record, which is conducted via Bluetooth protocol.

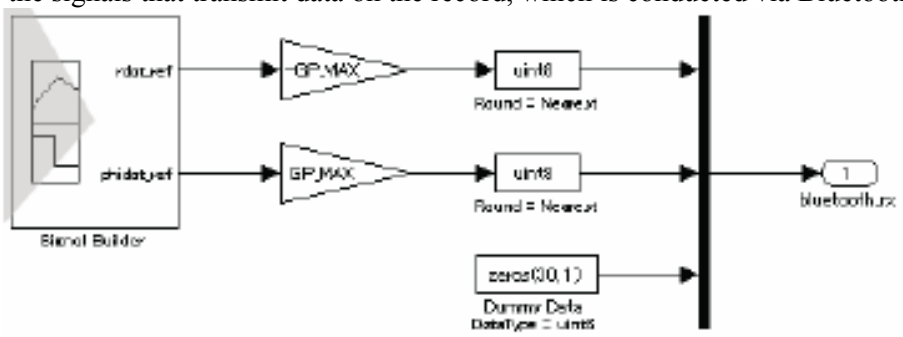

Figure 5 - Control generator diagram

The results of the study made it possible to examine some of the constituent blocks of the robot model in details. ReferenceGenerator is a unit that transmits and limits control actions on the controller. The "Controller" shown in Figure 4 is the block designating the NXT controller. On the left side there are blocks that serve to receive data from sensors, encoders and Bluetooth.On the right side there are blocks that serve to transmit signals to the engines and Bluetooth (Figure 6). The controller unit operates in the discrete time system, and the model unit operates in continuous time mode; therefore, it is necessary to convert the transmitted values.

Figure 7 shows the "NXTway-GS" subsystem, consisting of sensors, drivers, and a linearized model of the robot. It converts the type of input data signals into real values. The subsystem calculates the dynamics of the robot, and displays the recorded data of the results after performing the data sampling procedure. This subsystem defines the parameters of the environment of the robot.

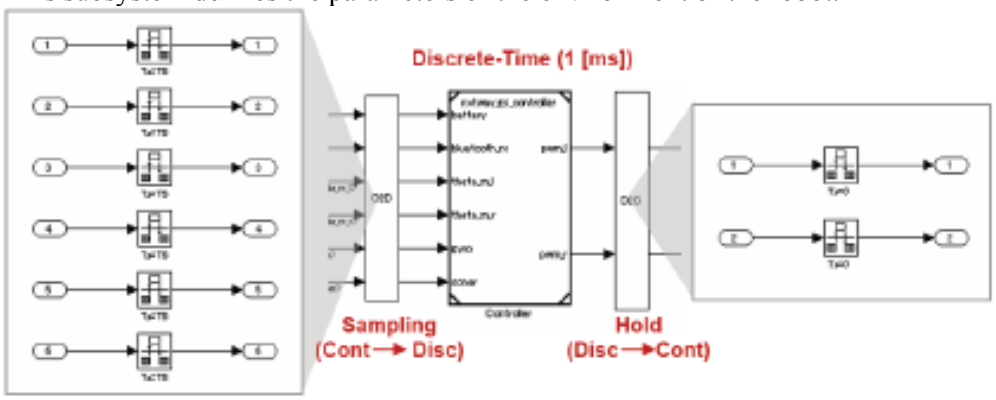

Figure 6 - Circuits of ADC and DAC blocks in models for signal conversion

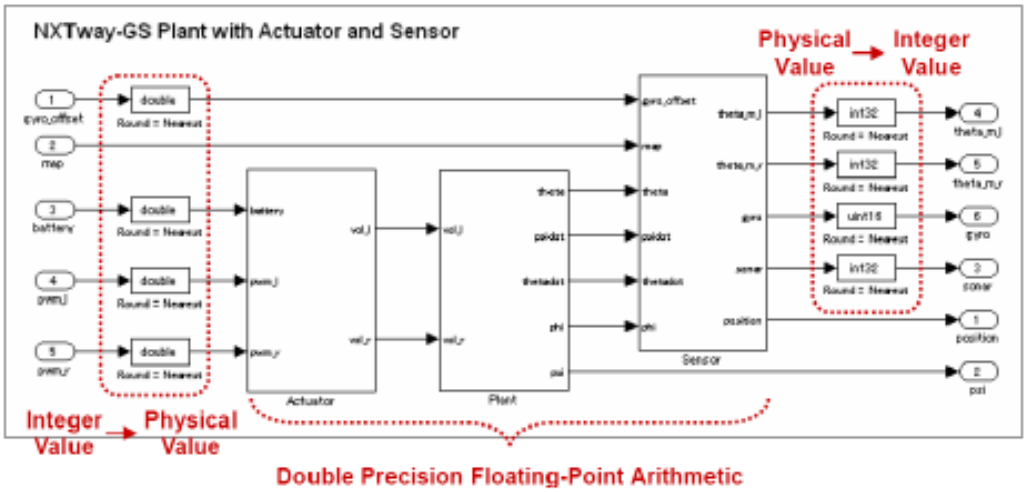

Figure 7 - Scheme servo control depending on the testimony sensors development

The block shown in Figure 7 “Actuator” is a subsystem that converts the power set by the controller to the voltage supplied to the motors. Designated block «Plant» is the model described by equations of double inverted pendulumtaking into account the calibration of the gyroscope.

The “Sensor” block converts the values obtained on the state of the model into the output signals of the sensors. Additionally, the distance to obstacles obtained from the ultrasonic distance sensor is calculated. This information may be used for detecting obstructions and avoid collisions with them.

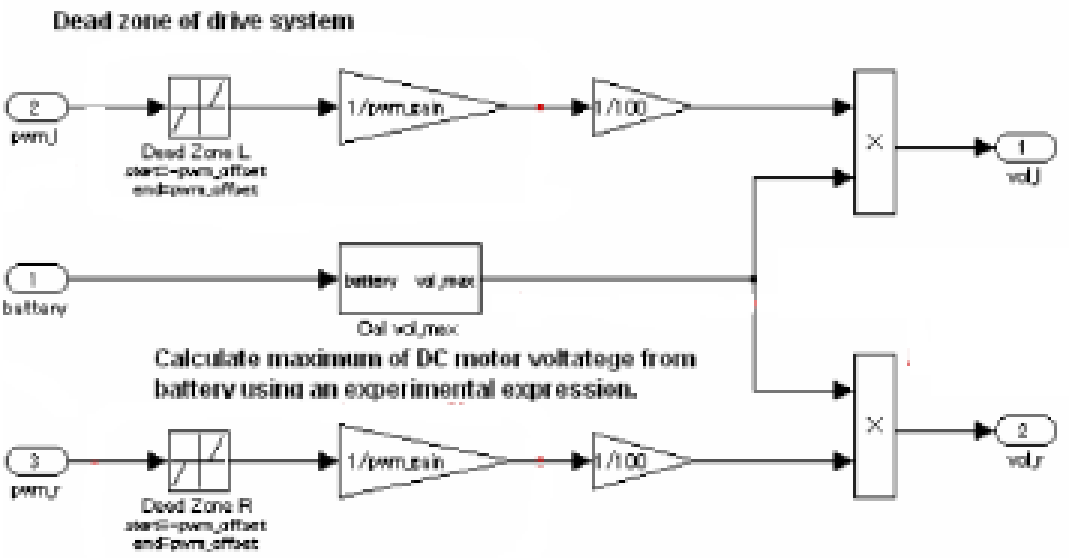

Figure 8 - Drive subsystem

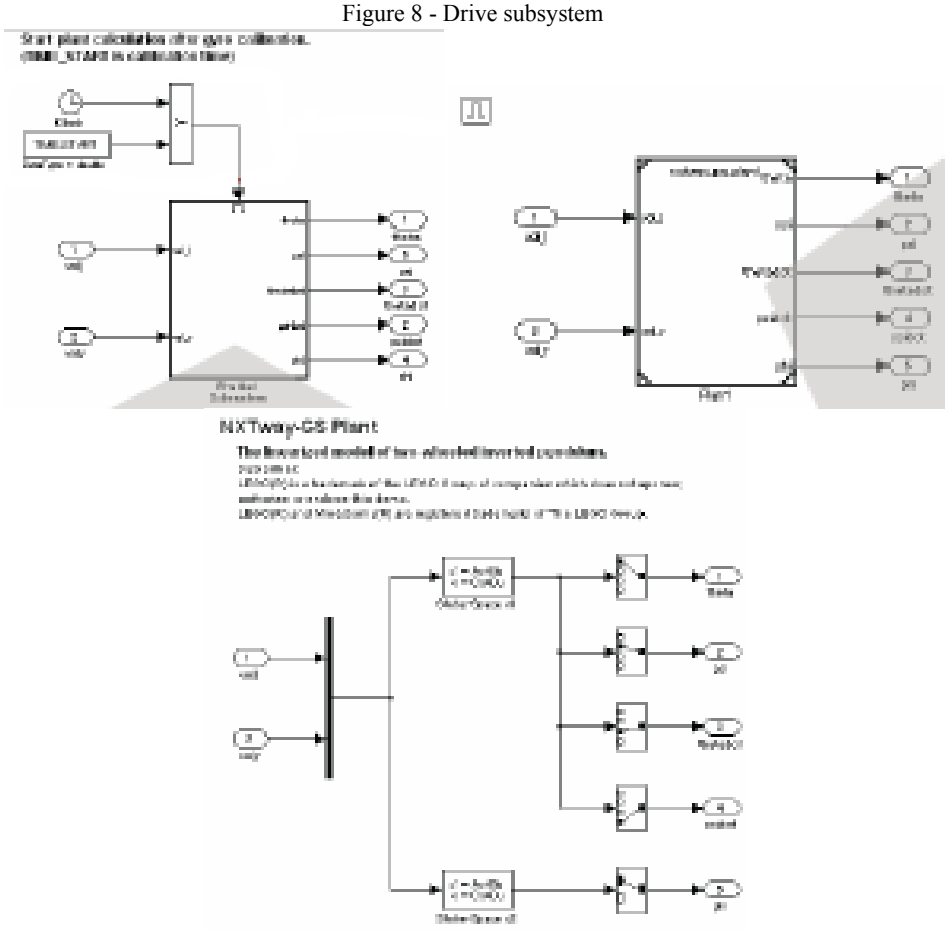

Figure 9 - Model Subsystem

The “Data”, “Store”, and “Memory” blocks are used as general blocks for distributing data between subtasks. Block “task_ts2” is responsible for detecting obstacles of Corollary robot and evading them.The “task_ts3” block is responsible for counting the time and checking the battery level of the robot.

Block “task_ts1” serves for calibration and balancing the gyroscope and for controlling the sound level and writing data. Balancing and control start after calibrating the Osprey Gear. The calibration time is saved as “time_start”.

Further, in the constructed schemes, the subsystems of balancing and control are presented. In the circuit shown in Figure 17 is a block “DiscreteDerivativeBlock”, which calculates the time constant of reverse differentiation block and “DiscreteIntegratorBlock”, which calculates the time integral by Euler method.

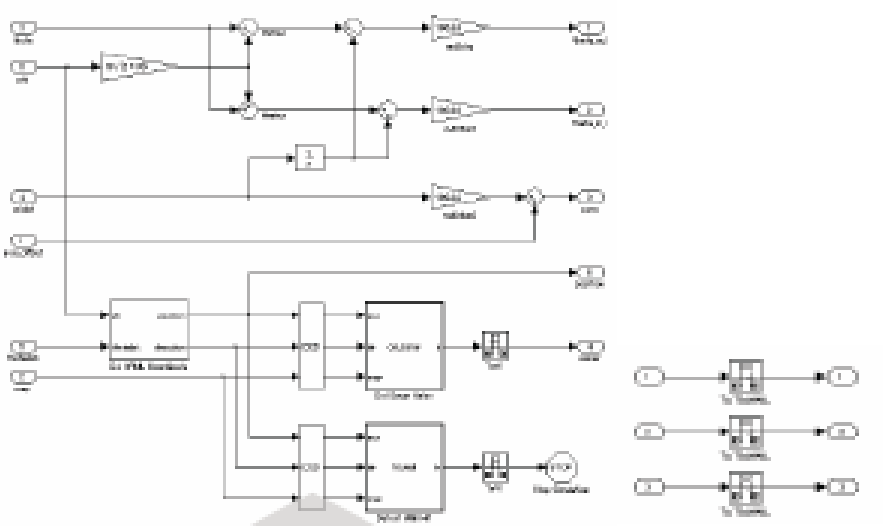

Figure10 - Sensor Subsystem

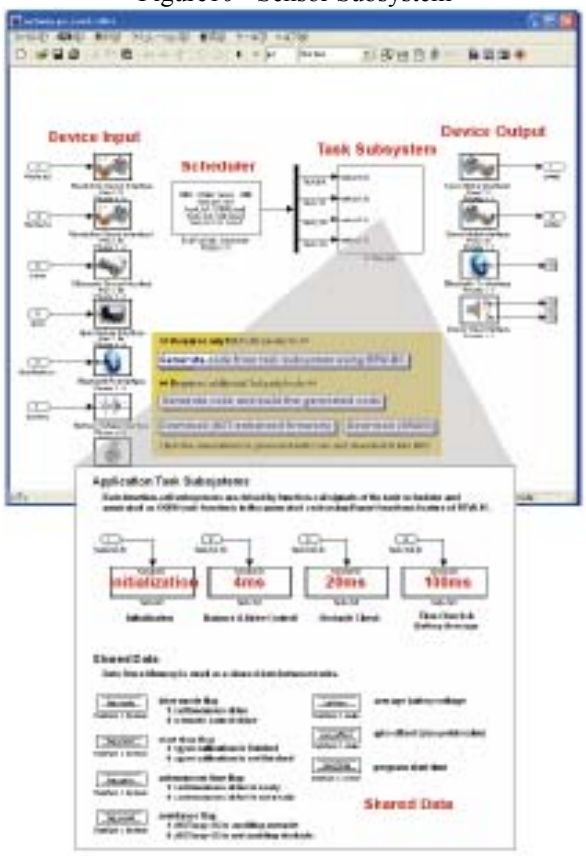

Figure 11 - Operation scheme nxtway_gs controller applications.mdl

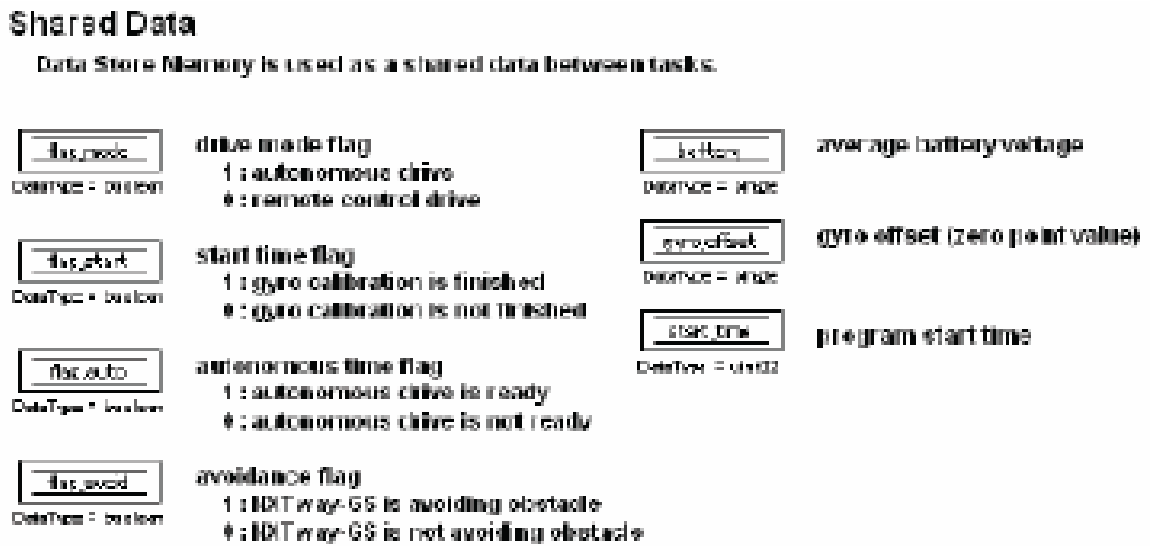

Figure 12 - Distributed data blocks

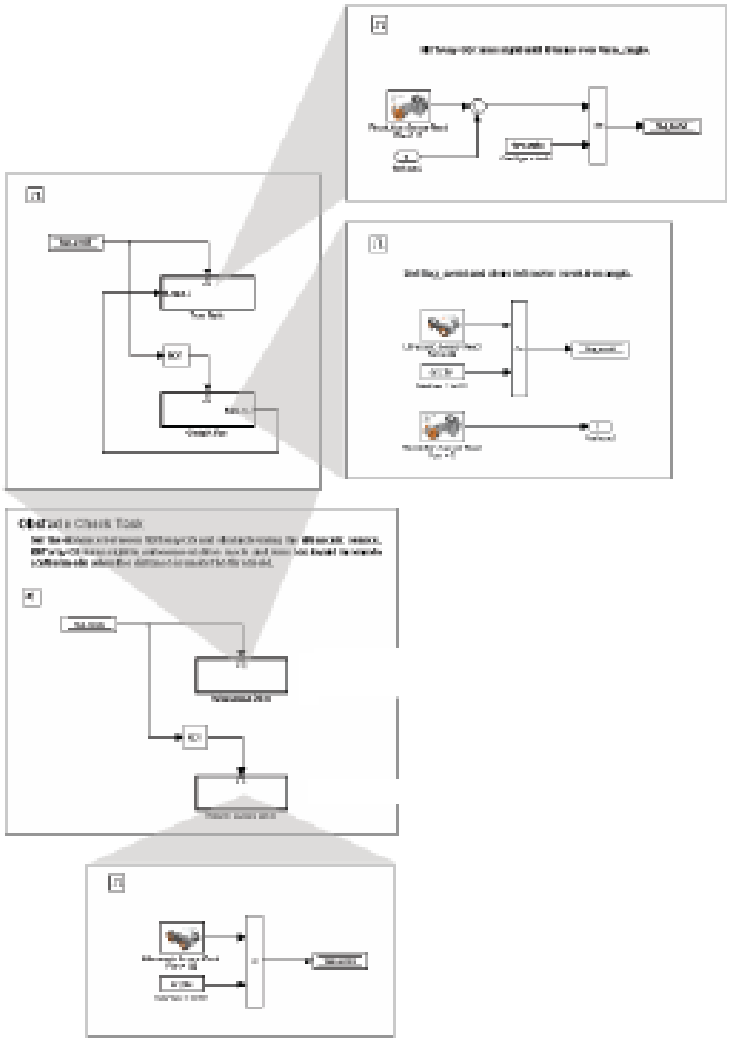

Figure13 - The task_ts2 subsystem responds
for detecting and avoiding robbery

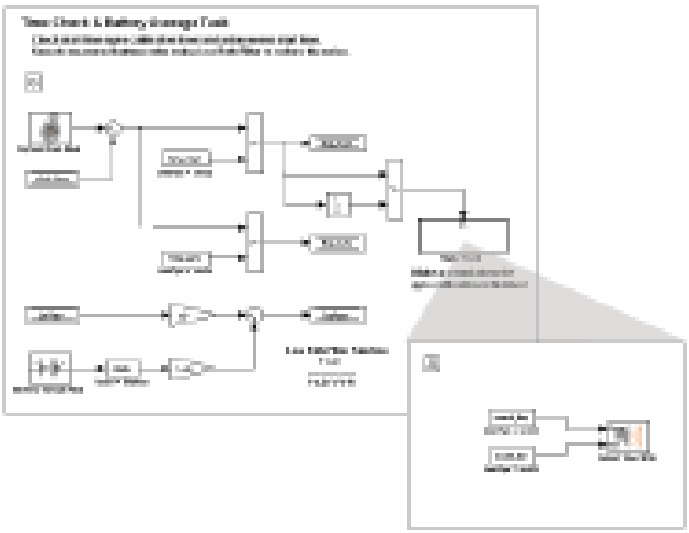

Figure 14 - The task _ts3 subsystem is responsible for counting time. and check the battery level of the robot

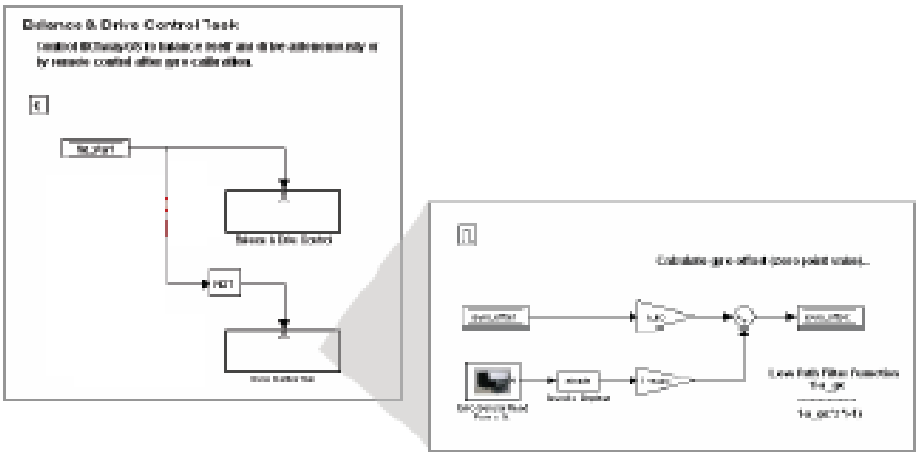

Figure15 - The task_ts1 subsystem is used to calibrate the gyroscope and balancing, as well as for managing and recording data

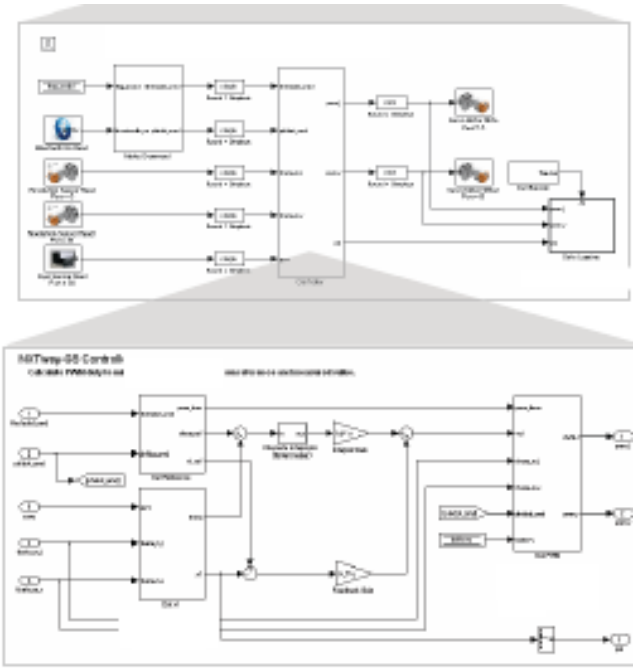

Figure16 - Controller model for control in balance mode

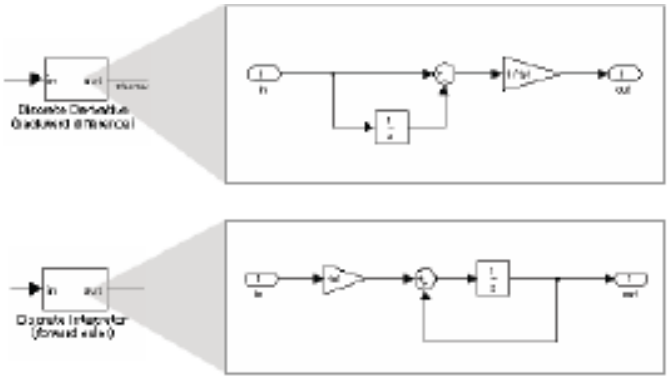

Figure17 - Blocks of the controllers «Discrete Derivative» and «Discrete Integrator Block»

Figure 17 also contains the blocks responsible for the calculation of the signal level, and with the use of a low pass filter for reducing surges caused by abrupt changes in speed of the generated signal. Figure 18 shows the method for calculating the generated controls.

Subsystem shown in Figure 19 calculates the state of the system using the sensor output signals. Long gyro data is used to remove "girodrifta" (gidrodreyfa), and a low pass filter is used for removing away move speed signal. The subsystem shown in Figure 20 is responsible for calculating the supply of the required power to the servo drives.

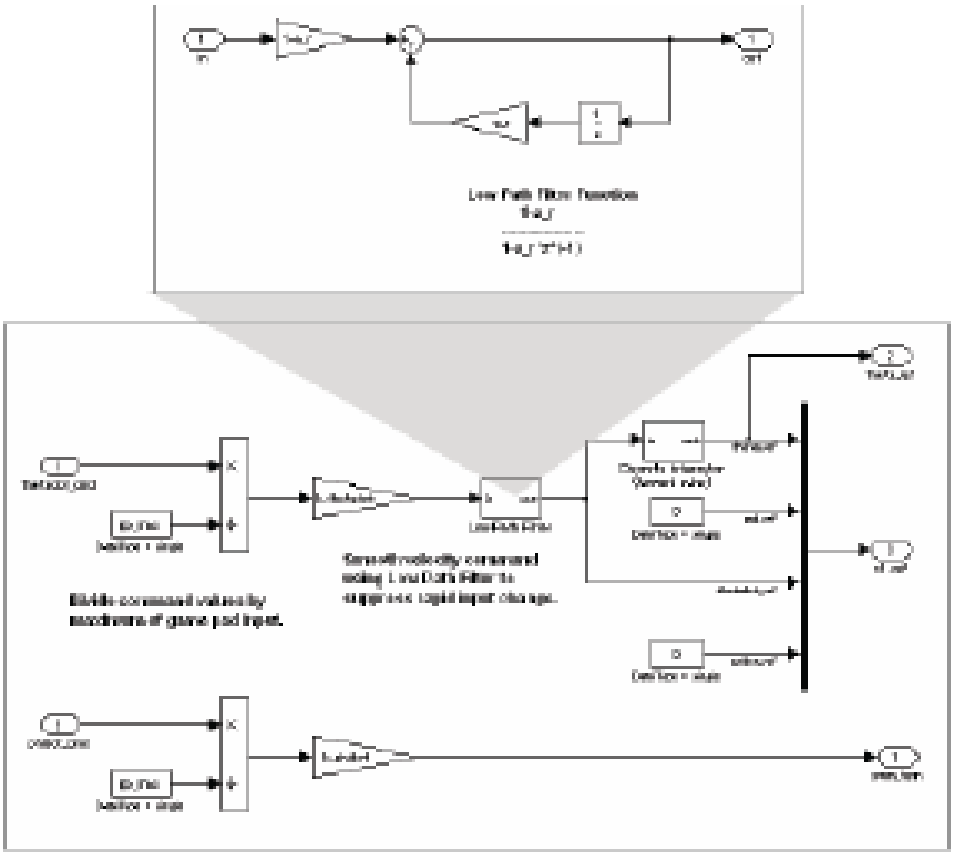

Figure 18 - Procedure for Calculating p and controls generated

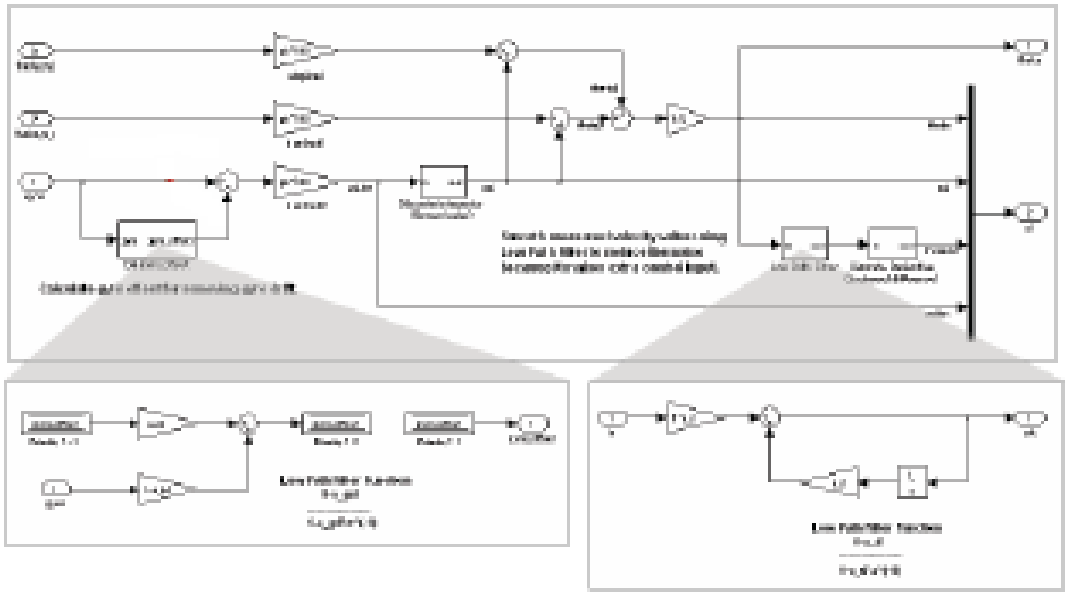

Figure 19 - Monitoring and monitoring the state of the model as a closed system

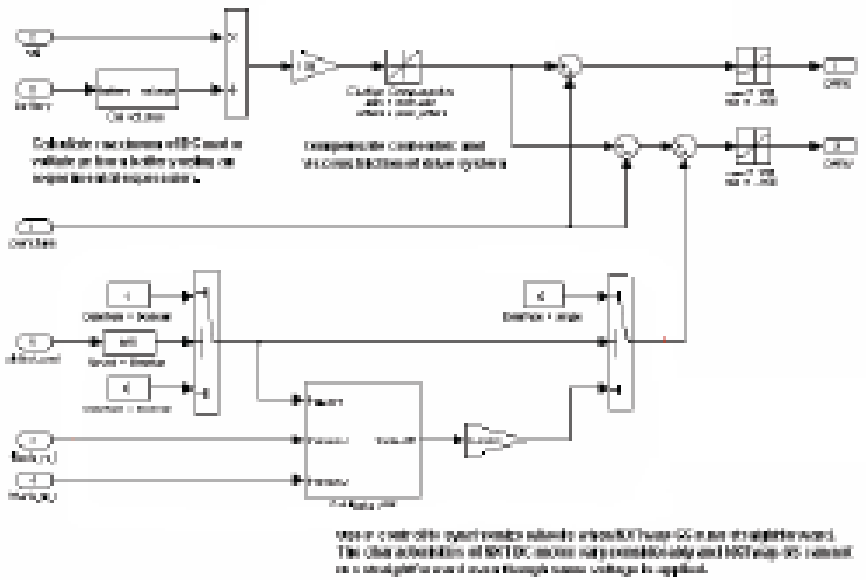

Figure 20 - Procedure for calculating p and the power supplied to the robot servo

The simulation results. The use of the utility "NXT GamePad" can register and record the value of an angle of inclination of the robot of the gyroscope and the robot regarding to the beginning of the movement using the values of the encoder of one of the servomotors. Figures 21 and 22 show the results of experimental research in the form of a graph of the data obtained by balancing the robotin a steady state and in a motion, respectively.

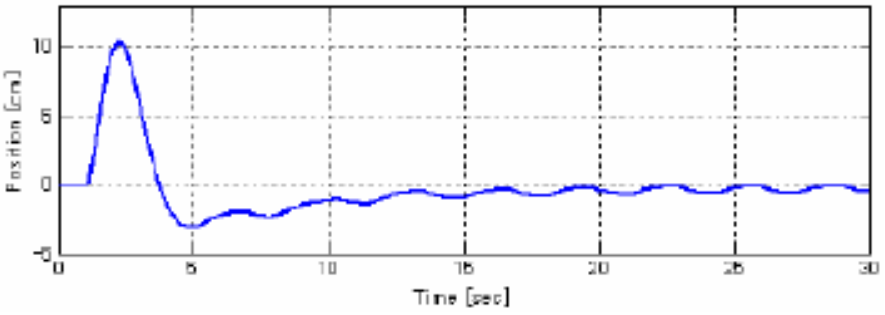

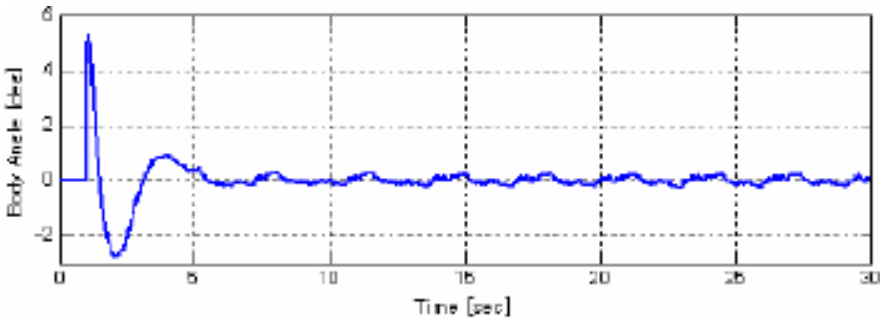

Figure 21 - Model results in a steady state

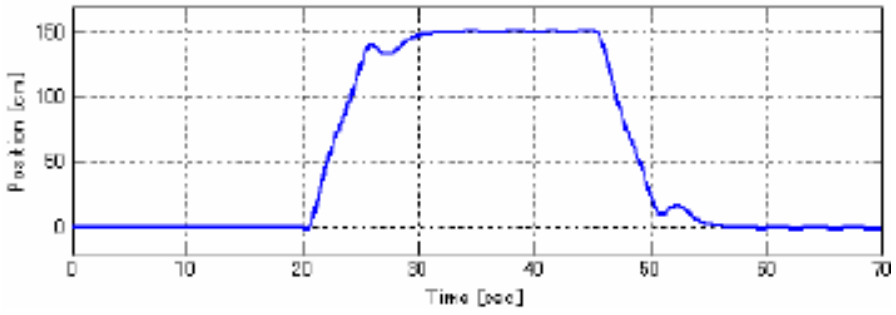

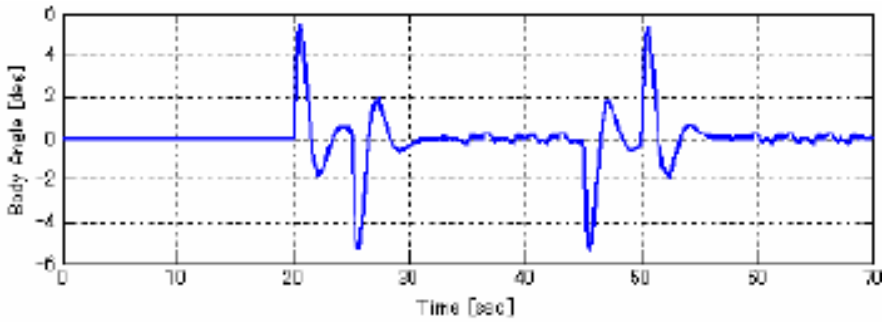

Figure 22 - Simulation resultsinmotion

Findings. The article addresses the problems of stability of a balancing robot in motion in accordance with the laws of TAU. The stability of a closed system on the basis of feedback has been investigated. The coefficients were synthesized using the following methods: calculation by the desired roots and the linear quadratic regulator method. According to the defined parameters of the PID controller, functional diagrams are compiled for controlling the robot servos. The results of experimental studies of balancing a robot in static and dynamic conditions were obtained using the NINXT GamePad utility, taking into account the value of the tilt angle of the robot from the gyroscope relative to the start of movement, using the encoder value of one of the servomotors. Registered statistics for specific values of the parameters of the controller of the robot show the degree of compliance with its stability when the robot moves in the closed state.

[1]Waldemar Wojcik, С.А. Кульмамиров[2], Ж.М.Алимжанова[2], Л.М.Алимжанова[2] , А.М.Ахметова[2], В.И.Карюкин[2]

[1]Люблинский технологический университет;
[2]Казахский национальный университет им. аль-Фараби

ИССЛЕДОВАНИЕ УСТОЙЧИВОСТИ РЕГУЛЯТОРА БАЛАНСИРУЮЩЕГО РОБОТА NI MINDSTORMS

Аннотация. В статье представлены результаты исследования устойчивого состояния балансирующего робота, когда управление осуществляется в замкнутом состоянии. Синтез коэффициентов регулятора осуществлялся оценкой корня характеристического уравнения и линейного квадратичного регулятора. При действии ПИД-регулятора составлены алгоритмы управления сервоприводами робота. Результаты проведенных экспериментальных исследований позволили построить переходные характеристики в замкнутой системе управления роботом при балансировании состояния робота на месте и в движении.

[1]Waldemar Wojcik, С.А. Кульмамиров[2], Ж.М.Алимжанова[2], Л.М.Алимжанова[2] , А.М.Ахметова[2], В.И.Карюкин[2]

[1] люблюблин технологиялық университеті;
[2]әл-Фараби атындағы қазақ ұлттық университеті

РОБОТ NI MINDSTORMS РЕГУЛЯТОРДЫҢ ТҰРАҚТЫЛЫҒЫН ЗЕРТТЕУ ТЕҢДЕСТІРУ

Аннотация. Мақалада теңдестіру роботының тұрақты күйін зерттеудің нәтижелері келтірілген, ол бақылау жабық жағдайда орындалады. Реттеуші коэффициенттерді синтездеу тәндік теңдеудің түбірін және сызықтық квадраттық реттегішті бағалау арқылы жүзеге асырылды. PID контроллерінің әрекеті бойынша робот серверлерін басқару алгоритмдері жасалады. Эксперименттік зерттеулердің нәтижелері біз роботтың жай-күйі мен қозғалу жағдайын теңестіру кезінде жабық циклдық роботты басқару жүйесінде өтпелі сипаттамаларды құруға мүмкіндік берді.

Information about authors:

Waldemar Wojcik - PhD of informatics and electronics, The Lublin University of Technology,professor;

Kulmamirov S.A. - Associate Professor of the Department "Information Systems", Ph.D., Academician MAIN. Kazakh National University al- Farabi;

Alimzhanova Zh.M. - Associate Professor of the Department "Information Systems", Ph.D., Kazakh National University al-Farabi;

Alimzhanova L.M. - Associate Professor of the Department "Information Systems", Ph.D., Kazakh National University. al-Farabi;

Akhmetova A.M. - Department "Artificial Intelligence and BigData " PhD Kazakh National University. al- Farabi;

Karyukin V.I. - teacher of the department "Information Systems", Kazakh National University. al- Farabi

REFERENCES

[1] Bobtsov A.A., Kapitanuk Yu. A., Kapitonov A. A., Kolyubin S. A., Pyrkin A. A., Chepinsky S. A., Shavetov S. V. LEGO MINDSTORMS NXT technology in studing Dents of the basics of adaptive management // Scientific and Technical Bulletin of St. Petersburg State University ITMO. 2011. No. 1. P.103-108.

[2]Information Control Problems in Manufacturing, V. 1-14.

[3]Bobtsov AA, Pyrkin AA, Borgul AS, Zimenko KA Control Approaches for Com-plicated Self-Unstable Plants with Two-Wheel Mobile Robot Motobot // Preprints of the 9th IFAC Symposium on Advances in Control Education (ACE2012), Nizhny Novgorod, Russia, 2012, pp. 107-111.

[4]Bobtsov AA, Kolyubin SA, Pyrkin AA, Borgul AS, Zimenko KA, Rabysh EY Mechatronic and Robotic Setups for Modern Control Theory Workshops // Precinints of the 9th IFAC, Nizhny Novgorod, Rus-sia, 2012, pp. 348-353.

[5] Bobtsov A. A., Pyrkin A. A., Borgul A. S., Zimenko K. A. Algorithms for managing the autonomous two-wheeled mobile robot “Motobot” // Scientific and Technical Newsletter of St. Petersburg State University ITMO, 2011, # 75, ss . 63–68.

[6] Borgul A. S., Gromov V. S., Zimenko K. A., Maklashevich S. Yu. System and Bolbota Stabilization Algorithms // Scientific and Technical Bulletin of St. Petersburg State University ITMO, 2011, # 75, ss. 58–63.

[7] Korolkova M. A., Krasnova S. A. Using NXTOSEK and EMBEDDED CODER ROBOT NXT for programming the LEGO MINDSTORMS NXT robot // Reports of the Fifth International Conference “Parallel Computing and Control Problems” PACO 2010, Moscow. P.1489-1496.

[8] Luchin R.M. Programming embedded systems: from model to robot // SPb.: Nauka, 2011. 184 p.

[9] LEGO firmware. http://mindstorms.lego.com

[10] leJOS. http://lejos.sourceforge.net

[11] nxtOSEK. http://lejos-osek.sourceforge.net

[12] OSEK. http://portal.osek-vdx.org

[13] ECRobotInstaller. www.mathworks.com/matlabcentral/fileexchange/25207

[14] Explorer. www.nxtprograms.com/NXT2/explorer/index.html

[15] NXT GamePad http://lejos-osek.sourceforge.net/nxtgamepad.htm.

[16] US Navy Academy to Acquire 50 RobotisBioloid Humanoid Robot Kits from KumoTek http://www.azonano.com/news.aspx?NewsID=4498

[17] Programming Bioloid robot in C. http://support.robotis.com/en /software/embeded_c/cm510_cm700.htm.

[18] ROBOTIS BIOLOID http://www.robotis.com/xe/BIOLOID_main_en.

[19] Benedettelli D., Casini M., Garulli A., Giannitrapani A., Vicino A.A. LEGO Mindstorms experimental setup for multi-agent systems // Control Applications, (CCA) & Intelligent Control, (ISIC), 2009 IEEE, pp. 1230-1235.

[20] Brigandi S., Yunfeng Wang, Field J. A LEGO Mindstorms NXT based multirobot system // Advanced Intelligent Mechatronics (AIM), 2010 IEEE / ASME International Conference, pp. 135-139.

[21] Akhtaruzzaman, M., Shafie A. A. Geometrical analysis of humanoid system by BIOLOID humanoid system standing on single leg // Mechatronics (ICOM), 2011 4th International Conference, pp. 1-5.

[22] RoboCup. http://www.robocup.org.

[23] Kalimoldayev, M.N., Pak, I.T., Baipakbayeva, S.T., Mun, G.A., Shaltykova, D.B., Suleimenov, I.E. Methodological basis for the development strategy of artificial intelligence systems in the republic of Kazakhstan in the message of the president of the Republic of Kazakhstan // News of the National Academy of Sciences of the Republic of Kazakhstan, Series of Geology and Technical Sciences 6(432), - c. 47-54. - 2018. https://doi.org/10.32014/2018.2518-170X.34

[24] RoboPlus. Software for robot BIOLOID. http://www.wertech.ru/Blog/23-roboplus-bioloid.aspx.

[25]Samigulina, G.A., Nyusupov, A.T., Shayakhmetova, A.S.Analytical review of software for multi-agent systems and their applications // News of the National Academyof Sciences of the Republic of Kazakhstan,Series of Geology and Technical Sciences. - 3(429), c. 173-181. – 2018

[26] Askarova A.S., Bolegenova S.A., Safarik P., Bolegenova S.A., Maximov V.Yu., Beketayeva M.T., Nugymanova A.O. **(2018)** Modern computing experiments on pulverized coal combustion processes in boiler furnaces. N e w s of the National academy of sciences of the Republic of Kazakhstan. Physico-mathematical series Volume 6, Number 322 (2018), Pp. 5 – 14. ISSN 1991-346X https://doi.org/10.32014/2018.2518-1726.11

N E W S
OF THE NATIONAL ACADEMY OF SCIENCES OF THE REPUBLIC OF KAZAKHSTAN
PHYSICO-MATHEMATICAL SERIES
ISSN 1991-346X **https://doi.org/10.32014/2019.2518-1726.34**
Volume 3, Number 325 (2019), 153 – 157

UDK54.7-327

E.K. Denissyuk, R.R. Valiullin

Fesenkov Astrophysical Institute, Almaty, Kazakhstan
eddenis@mail.ru, rashit_valiullin@mail.ru

ROTATING CURVE OF THE GALAXY NGC 1068

Abstract. The matter in the body of spiral galaxies (stars, nebulae, clusters), judging by their images, is distributed very non-uniformly. Moreover, all objects have their own velocities in space. However, in general, they are affected by the gravitational field of the total mass, referred to the center of the galaxy. One of the main aim is to evaluate this mass. In order to weaken the effect of random velocities, the average spectrum from fairly large sections of the galaxy along the entrance slit of the spectrograph is recorded.

In the Fesenkov Astrophysical Institute (FAPHI) the spectral observations of the bright Seyfert galaxy NGC 1068 were carried out in the red region of the spectrum. The telescope AZT-8 with a diameter of 0.7 m and a slit spectrograph designed and manufactured in FAPHI was used. The spectra were recorded on a SBIG CCD ST-8 (1530x1020, 9μ). The spectrograms obtained with the long slit were used to measure the profiles of the Hα and [NII], 6583Å, emission lines, namely, the radial velocities were determined at different distances from the center in the 9 "x10" areas. Further processing assumes that the galaxy is a thin circular disk whose matter rotates around the center so that at each distance from the center the rotation velocity is constant and it depends only on the distance to the center, and the disk itself is observed as an ellipse due to the inclination to the line of sight.

In order to obtain a real dependence of the rotational velocities on the distance from the center under these assumptions, it is necessary to translate the distances along the slit and the radial velocities measured at these points into the galaxy plane by taking into account its inclination to the line of sight. As a result, the dependence of the rotation velocities of matter on the distance to the center was obtained. The mass of the disk with a radius of 6 parsec was estimated.

Keywords: seyfert galaxies, emission lines rotating curve; individual: Sy NGC 1068.

Introduction

NGC 1068 is one of the closest and brightest Seyfert galaxies (Sy). It has a complex structure. The velocity field of the matter motion in this galaxy was studied in detail with the large telescopes [1, 2]. A map of isolines of the equal radial velocities was obtained, which shows a very complex picture [1]. Mass estimation is usually performed using the laws of mechanics and experimental data on the velocities of the mass movement along the rotation curve. Obtaining of a rotation curve for galaxies, visible from the edge is the simplest procedure. In such case, the distances from the center are measured directly from the spectrogram, however, the measured positions of the line can differ markedly from the true rotation velocities. At each distance from the center in this case, the total radiation of objects falling on the line of sight in this direction is recorded. Contribution is made by all regions, including distant objects, which also appeared on the line of sight. This leads to large errors in the estimates of the true velocities.

More accurate rotation curves can be obtained for galaxies with such an inclination to the line of sight, at which the integration during spectroscopy occurs in a fairly narrow volume of the galaxy. At the same time, galaxies, having the form of an ellipse, should not have an eccentricity close to zero, so that the projections of the measured velocities are not commensurate with measurement errors. It should be noted that the transition to the true velocities and distances implies that the galaxy is flat, thin enough and has circular symmetry. The galaxy NGC 1068 - one of the most studied in a wide range of wavelengths seyfert galaxies, satisfies to such criterion. Its global characteristics, in particular the mass, are known not very well. To obtain general characteristics, observational data should be averaged. Averaging can be carried out directly during observations.

This paper uses the results of spectral studies of NGC 1068 obtained with a small telescope. The procedure for processing and accounting for the orientation of the galaxy is describes in details below.

Observations and processing

Observations were carried out in the 11.2 m Cassegrain focus of the telescope AZT-8 (diameter of 0.7 m) with the diffraction spectrograph made in FAPHI [3]. CCD camera SBIG ST-8 (1530x1020, 9μ) was used as a receiver. For the wavelength calibration, the spectrum of the lamp with HeI, NeI and ArI emission lines was used. The observations were carried out on 2007, October 28. Three 30 minutes exposures were made. To use the different parts of the matrix, the center of the galaxy was shifted along the slit by 15" at different exposures. The broad 10" slit of spectrograph was oriented parallel to the celestial equator. Along the dispersion, the scale was 0.183Å/pixel, and across the dispersion - 0."65/pixel.

Processing was carried out separately for each of the three spectrograms. The wavelengths of the two emission lines Hα and [NII] 6583 Å were determined. The measurements were carried out in the 6" bands close to each other from the center in both directions until at least one of these lines remained measurable. The results are presented in Table 1. It was especially difficult to carry out measurements in the central band. Figure 1 shows a fragment of the spectrum in this central band, where narrower emissions are superimposed on the broad asymmetric lines Hα and [NII] 6583 Å. There is also an example of a fragment of the spectrum at a distance of +18 ", where there are no difficulties with measurements. For this reason, a number of authors, for example [1], do not give any data on the velocities in the central region of the galaxy NGC 1068.

If to assume that the galaxy has axial symmetry, then, having the radial velocity along the section passing through the center, the angle of inclination of the galaxy plane «i» or the eccentricity of the observed galaxy «e» and the angle between the observed major axis and the «φ» section, it is possible to get a true rotation curve in the plane of the galaxy itself. To do this, one can use any section that passes through the center, except for that one along the minor axis.

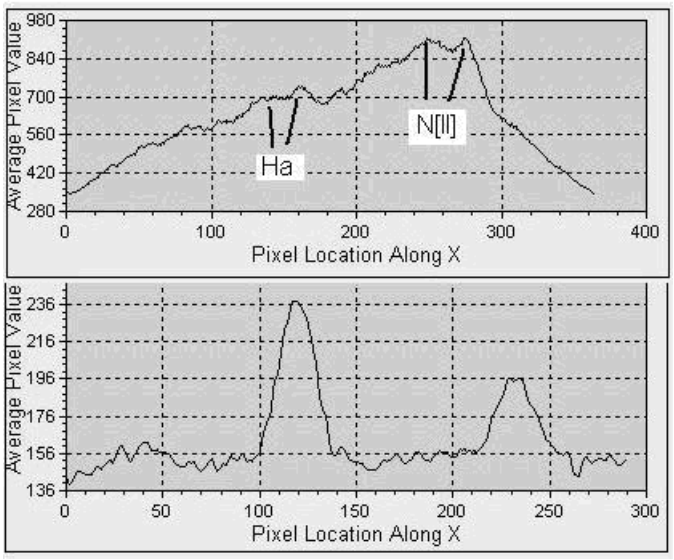

Figure 1 - Fragments of the spectrograms near emission lines of Hα and [NII], 6583Å in the 9 image lines. Axis X shows the numbers of pixels. The upper panel – the spectrum of the central band, where besides the broad lines, the narrower emission, shifted to the «red» side, are visible. The bottom panel – fragment of the spectrogram on the 18" distance from the centre, where the wavelengths of these lines are unambiguously measurable

Further, the result must be corrected for the effect of the projection of the section distances from the center and radial velocities for the inclination of the galaxy to the line of sight. The transition to the true distances «r» under the assumption that the galaxy is a circular disk tilted to the line of sight at an angle «i» can be made using the following formula, where «e» is the eccentricity of the visible image and «φ» is the angle between the major axis of the galaxy image and the slit direction

$$r = r_{obs} \cdot \frac{\sqrt{(1-e^2 \cdot \cos^2 \varphi)}}{(1-e)} \quad (1)$$

In this case, the true rotation velocities in the galactic plane V at the corresponding distances «r» are related to the observed Vr values by the formula:

$$V=Vr/\cos \varphi/\sin i \quad (2)$$

We used the following parameters: i = 32.50 [4], e = 0.5373, φ = 450. Thus, r"= r" obs · 1.8483 and V = Vr / 0.2687 for all distances from the center.

The results of the observations given in Table 1 allow us to obtain the dependence of the rotational velocitis of the annular zones in the galaxy plane on their distances from the center, expressed in parsecs. For this the redshift of the galaxy and the Hubble constant are required. The values Vr = +1137 km / s [4] and H = 72 km/s/Mpc were assumed.

Table 1 – The wavelengths of the emission lines Hα and [NII], measured on the different distances from the centre

R"	Hα (A)	N[II] (A)	Hα (B)	N[II] (B)	Hα (C)	N[II] (C)
-42			6585.6	6605.3		
-36	6585.6	6605.7	6585.2	6605.3	6585	6606.6
-30	6583.8	6605.3	6583.2	6606.6	6585.2	6605.9
-24	6584.3	6605.2	6584.3	6605	6584.7	6605.5
-18	6584.5	6605.7	6584.7	6605.9	6584.5	6605.3
-12	6585.2	6606.4	6584.9	6605.7	6584.9	6606.3
-6	6585.4	6606.1	6585.8	6607.2	6584.5	6605.9
0	6589.4	6609.4	6585.4	6605	6584.9	6586.7
6	6590.7	6610.1	6591.1	6607.2	6590.7	6610.7
12	6590.3	6610.8	6590.2	6610.7	6590.3	6611.1
18	6590.2	6610.8	6589.6	6610.7	6589.8	6610.5
24	6590	6610.5	6589.8	6611	6589.8	6610.7
30	6588.7	6610.5			6590	6610.1
36	6588.7	6609.7			6590.5	
42	6587.6	6608.8				

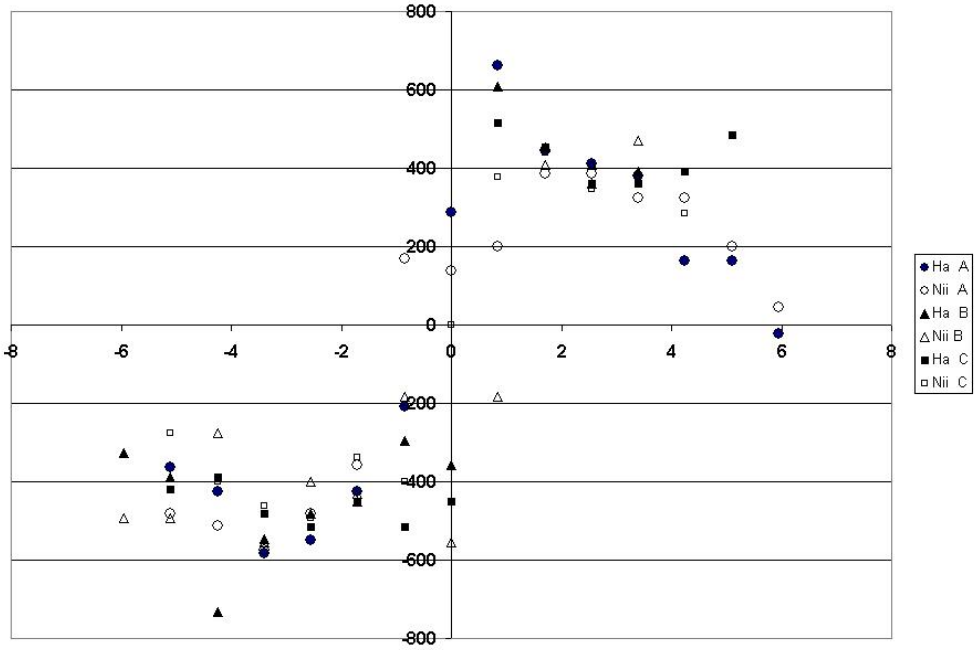

Fig. 2 - The Y axis shows the true rotational velocities of the regions of the galaxy NGC 1068 at distances through the 6″ to both sides of the center. The distances in kpc are on the X axis. For each distance, the values are obtained for each of the spectrograms (A, B and C) along Hα and [NII]]6583Å lines (see the icons on the right)

Obtained results

Figure 2 shows the rotation curve of the galaxy NGC 1068. It is based on the results of measuring the position of the line (in radial velocities) at different distances from the center. The emission lines Hα и [NII], 6583 were used. Measurements were taken every 6" in three spectrograms. It can be seen that there are differences in the rotation of the eastern and western (relative to the center) parts of the galaxy. In the region of ± 1.5 kpc, the rotation is close to solidstate. If to assume that at a distance of 6 kpc, the average rotational speed is about 300 km/s (see Fig. 2), then the mass inside this radius can be estimated by the formula $M = V^2 \cdot r / G$, and will be equal to ~ $1.25 \cdot 10^{11}$ M☼. Earlier for r = 5.7 kpc, the mass estimate of $6.4 \cdot 10^{10}$ M☼ was obtained [4].

The work was carried out within the framework of Project No. BR05236322, financed by the Ministry of Education and Science of the Republic of Kazakhstan.

УДК 524.7-327

Э.К. Денисюк, Р.Р. Валиуллин

«В.Г.Фесенков атындағы Астрофизика институты» ЕЖШС, Алматы, Қазақстан

NGC 1068 ҒАЛАМЫНЫҢ АЙНАЛУ ҚИСЫҒЫ

Аннотация. Ірімді ғаламдарда материя (жұлдыздар, тұмандықтар, шоғырланулар), олардың суреттеріне қарағанда біртексіз таралатындығын көреміз. Сонымен бірге, кеңістікте барлық объектілердің өзіндік жылдамдықтары бар. Ғаламның центріне бағытталған, жиынтық массаның гаравитациялық өрісі әсер етеді. Солардың ең негізгі бір есебі массаларын анықтау болып табылады. Спектрографтың саңылауына кіретін бойымен, кездейсоқ жылдамдықтардың әсерін әлсіретуге ғаламның анағұрлым үлкен бөлігінің орташа спектрі тіркеледі.

ФАФИ спектрдің қызыл аймағында аса жарық сейферт ғаламының спектрлік бақылаулары жүргізілді. ФАФИ құрастырылған және жасалған саңылаулы спектрограф және диаметрі 0.7 м АЗТ-8 телескобы қолданылды. Спектрді ЗБА SBIG ST-8 (1530x1020, 9μ) камерасы арқылы тіркелді. Алынған ұзын спектрограммаларда Hα және [NII], 6583Å эмиссиялық сызықтарының кескіндері, соның ішінде центрден әртүрлі қашықтықтан ауданының өлшемі 6"x10" болатын сәулелік жылдамдықтар анықталды. Өңдеулерден кейін ғалам жуан, дөңгелек диск, материя центрдің айналасында айналады, центрден әрбір қашықтықтағы жылдамдық тұрақты және тек қана центрден қашықтыққа ғана тәуелді деп болжанады және де, көру сәулеленуіне көлбеулігіне байланысты диск эллипс болып бақыланады.

Осы болжамдардан, айналу жылдамдығының центрден қашықтыққа нақты тәуелділігін алуға көру сәулеленуінің көлбеулігін есепке алып ғалам жазықтығында сәулелену жылдамдығы өлшенген осы нүктелерді және саңылау бойындағы қашықтыққа аудару қажет. Нәтижесінде, материя айналу жылдамдығының центрден қашықтыққа тәуелділігі алынды және радиусы 6 парсек дисктің массасы анықталды.

Түйін сөздер: сейферт ғаламдары, эмиссиялық сызықтар; айналу қисығы; жеке объектілер: Sy NGC 1068.

УДК 524.7-327

Э.К. Денисюк, Р.Р. Валиуллин

Астрофизический Институт им Фесенкова, Алматы, Казахстан

КРИВАЯ ВРАЩЕНИЯ ГАЛАКТИКИ NGC 1068

Аннотация. Материя в теле спиральных галактик (звезды, туманности, скопления), судя по их изображениям, распределяется весьма неоднородно. При этом все объекты имеют свои скорости в пространстве. Однако в целом на них действует гравитационное поле суммарной массы, отнесенной к центру галактики. Одна из основных задач состоит в том, чтобы оценить эту массу. Для того, чтобы ослабить влияние случайных скоростей, регистрируется средний спектр от достаточно больших участков галактики вдоль входной щели спектрографа.

В АФИФ проведены спектральные наблюдения яркой сейфертовской галактики NGC 1068 в красной области спектра. Использовался телескоп АЗТ-8 диаметром 0.7 м и щелевой спектрограф, спроектированный и изготовленный в АФИФ. Регистрация спектров велась на ПЗС камеру SBIG ST-8(1530x1020, 9μ). На спектрограммах, полученных с длиной щелью, измерялись профили эмиссионных линий Hα и [NII], 6583Å,

а именно определялись лучевые скорости на разных расстояниях от центра в площадках размером 6"x10". При дальнейшей обработке предполагается, что галактика является толстым круглым диском, материя которого вращается вокруг центра так, что на каждом расстоянии от центра скорость вращения постоянна и зависит только от расстояния до центра, а сам диск наблюдается как эллипс из-за наклона к лучу зрения.

Для того, чтобы в этих предположениях получить реальную зависимость скоростей вращения от расстояния от центра, необходимо перевести расстояния вдоль щели и измеренные в этих точках лучевые скорости в плоскость галактики путем учета ее наклона к лучу зрения. В результате получена зависимость скорости вращения материи от расстояния до центра и оценена масса в диске с радиусом 6 парсек.

Ключевые слова: сейфертовские галактики, эмиссионные линии; кривая вращения; индивидуальные объекты: Sy NGC 1068.

Information about authors:
Denissyuk E.K. - Doctor of Physical and Mathematical Sciences, Fesenkov Astrophysical Institute. eddenis@mail.ru
Valiullin R.R., Doctor of Physical and Mathematical Sciences. Deputy Director for Science
Fesenkov Astrophysical Institute. rashit_valiullin@mail.ru

REFERENCES

[1] Kaneko N., Satoh T. , Toyama K., et al. Observations of the velocity curves of NGC 1068 // A.J. 1992. V 103. P. 422 .

[2] Weinberger A. J., Neugebauer G., Matthews K. Diffraction-limited Imaging and Photometry of NGC 1068//A.J. 1999. V 117. P. 2748.

[3] Denissyuk E. K. Spectrograph for faint objects: the device and the main results of observations// AA TRANS. 2003. V 22. P. 175.

[4] Galletta G. & Recillas-Cruz E. The Large Scale Trend of Rotation Curves in the Spiral Galsxies NGC 1068 and NGC 3310// A&A. 1982. V 112. P.361.

N E W S
OF THE NATIONAL ACADEMY OF SCIENCES OF THE REPUBLIC OF KAZAKHSTAN
PHYSICO-MATHEMATICAL SERIES
ISSN 1991-346X **https://doi.org/10.32014/2019.2518-1726.35**
Volume 3, Number 325 (2019), 158 – 165

UDC 523.45

V.G. Teifel, P.G. Lysenko, A.M. Karimov,
G.A. Kirienko, V.A. Filippov, G.A. Kharitonova, A.P. Hozhenets

Fessenkov Astrophysical Institute, Almaty, Kazakhstan
tejf@mail.ru, lyssenko_petr@mail.ru, karalik0@yandex.ru, gak39@mail.ru,
filipp.va@mail.ru, gah38@mail.ru, hogenez@gmail.com

JUPITER: ZONAL SPECTROPHOTOMETRY OF WEAK AMMONIA ABSORPTION BANDS IN 2018

Abstract. Based on measurements of zonal spectrograms obtained by scanning the Jupiter disk in March – June 2018, the profiles of the 645 and 787 nm weak absorption bands of NH3, and the character of the zonal absorption variations at different latitudes are derived. A standard has been prepared for processing and analyzing data in relation to further studies of possible seasonal and sporadic variations based on Jupiter's spectral observations for the full period of its rotation around the Sun. The zonal and latitudinal variations of ammonia absorption are shown. As in previous years, the NH3 absorption depression is particularly prominent at the latitude of about + 150 in the NEB region. As in previous years, some differences in the latitudinal absorption of the 645 and 787 nm NH3 bands remain.

Keywords: Jupiter, Atmosphere, Clouds, Ammonia, Methane, Molecular Absorption Bands, Spectrophotometry.

Introduction

Ammonia in the atmosphere of Jupiter, despite a low relative abundance, plays a decisive role as the main cloud-forming factor in the upper troposphere. In the program of atmospheric research of Jupiter, which we carry out, special attention is now being paid to studying the behavior of the absorption bands of ammonia in the visible and near infrared region of the spectrum. These are two fairly weak bands in the region of the wavelengths of 645 nm and 787 nm. The bands are weak in intensity and very little have been studied so far, since no special observations of these bands have actually been made. The exception is a lot of data, possibly unique, from Jupiter's spectrophotometric observations, which we have carried out since 2004. We obtained the uniform observational data with a single technique during the full 12-year period of Jupiter's revolution around the Sun, which makes it possible to trace certain seasonal changes in the atmosphere and in the cloud layer of the planet. Some results, but far from all ones, have been published recently [1- 4].

The program of research of ammonia absorption on Jupiter as well as the characteristics of the planet's atmosphere depending on it, should cover a long period. Therefore, in order to preserve the homogeneity of the observation and processing, a standard procedure has been developed for the general problem of studying molecular absorption and atmospheric structure from spectral observations. This technique is described here using the example of processing one of the Jupiter scans received in 2018.

There are no descriptions of the observations of these two absorption bands of ammonia on Jupiter in the literature for the last decades. But it does not mean the absence of considerable attention to the problem of studying ammonia absorption on this planet. A whole series of works was carried out, one way or another, related to the content of ammonia and its variations in the atmosphere of Jupiter. The fact is that the absorption of radiation by NH_3 molecules can significantly affect the passage of infrared or microwave radiation in the Jupiter troposphere in those areas of the electromagnetic spectrum where there are fairly intense NH_3 absorption bands. An example of this is the observation of long waves of

microwave radio emission in the region of 8–12 GHz [5-6]. In addition, both molecular absorption by gaseous ammonia and the cloud layer in the upper troposphere, consisting mainly of crystals of frozen NH_3, affect the transmission and output of infrared radiation in the 4÷8-micron range [7-13].

Studies of the behavior of the weak absorption bands of ammonia (NH_3 535, 645 and 787 nm) give some possibilities for optical sounding of the Jovian troposphere. Their formation occurs both inside the ammonia cloud layer and in deeper layers of the atmosphere. But there is some peculiarity in the conditions of their formation. Unfortunately, so far there have been a little laboratory studies of these bands [14-15]. Recently, in 2018, two publications were published [16-17]. But still, no completely reliable values of absorption coefficients have been obtained for these bands. This is due, in particular, to their complex rotational-vibrational structure.

Observations

The observations of Jupiter described here, were made on the night of 9 to 10 of May 2018, using an SGS diffraction spectrograph with a ST7-XE CCD camera installed in a 7.5-meter Kassegren focus of the 0.6-meter telescope RZ-600. The CCD matrix consists of 765x550 elements-pixels of 9x9 microns in size. The spectrograph dispersion is 4.3 Angstroms per pixel. An entrance slit width of 25 micrometers provides a resolution of about 8 Angstrom along wavelengths, and a formal resolution on the image of the planet is about 0.65 angular seconds. The actual resolution in the image, of course, is worse due to the influence of atmospheric turbulence. In the image of the spectrum, the scale is 4.08 pixels for 1 arc second.

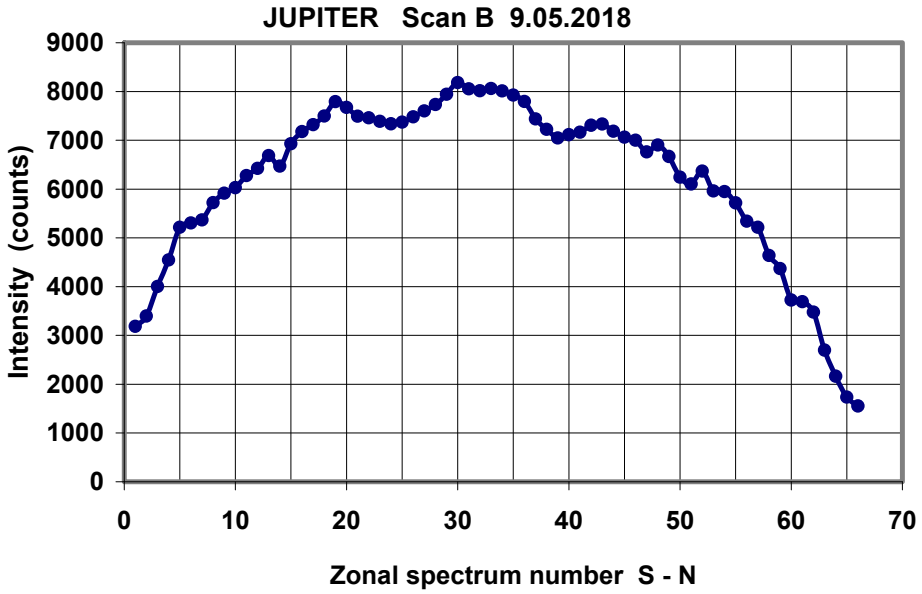

Figure 1 - Photometric profile of Jupiter's disc scan. Each point corresponds to a separate zonal spectrogram

The entrance slit of the spectrograph was oriented parallel to the planet's equator, and when scanning the Jupiter disk, 66 zonal spectra were obtained from the South to the North Pole. Figure 1 shows the brightness profile along the central meridian of Jupiter, constructed from the intensity readings in each of the spectra.

The duration of exposure of each spectrum was 20 seconds, and the entire scanning process lasted 24 minutes. During this time, Jupiter rotates by 15 degrees, so the observations belong to the visible hemisphere of Jupiter with the longitude of the central meridian of 220 ± 7 degrees in the 2 rotation system. Figure 2 shows a longitudinal sweep map in Jupiter's second rotation system [18], where the longitude interval of the central meridian during the scan period and the entire longitude interval covered by the zonal spectra, are marked.

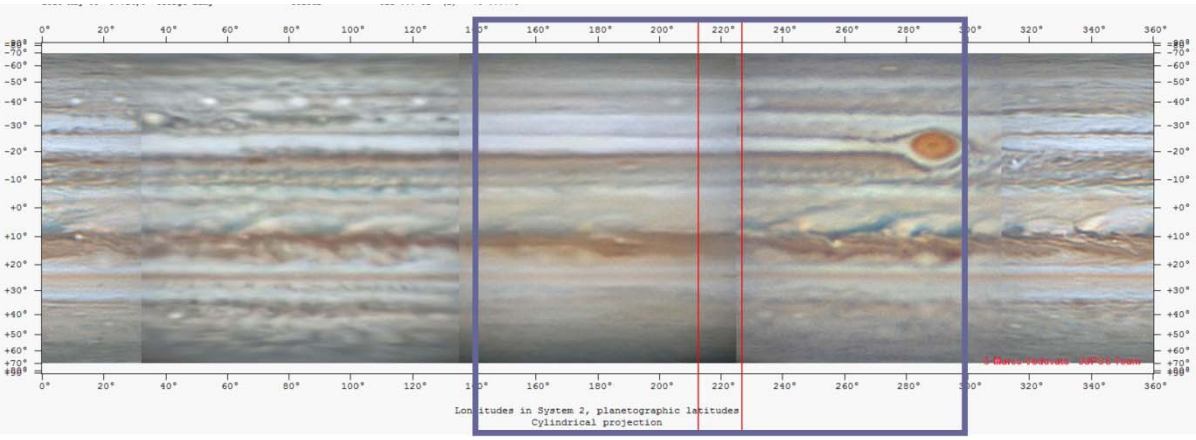

Figure 2 - The scanned region of Jupiter on the map for May 2018 (ALPO Japan)

Spectrogram processing

We perform the initial digitization of spectrograms using the standard program for CCD Camera. An area of 765x220 pixels is selected. The resulting digital array is transferred to an Excel spreadsheet, where a wavelength calibration is performed so that H-alpha line of the Fraunhofer spectrum always falls on the same line number. Then the array is transferred to the processing Excel-program. All further operations are carried out in this program automatically up to the output of the corresponding resulting graphs. The processing includes following stages: background accounting, calculation of the relation to the reference spectrum, interpolation of the continuous spectrum in the region of the molecular absorption bands of methane and ammonia for further calculation of the profiles of these bands in units of residual intensity. Then, for each band, the absorption band equivalent widths are calculated for each point of the zonal profile of the Jupiter disk. All this is done within the same file pertaining to the same spectrogram. In this way, the plots of the absorption band equivalent widths course along one or another zone are obtained. We show some examples of such graphs in Figure 3.

Separation of the NH_3 645 and 787 nm absorption bands is a complicated enough procedure, since both of these bands overlap with the absorption bands of methane. The 645 nm band falls on the weak wing of the methane absorption band, so that its separation is carried out simply by interpolating the methane band profile, which is almost linear in that spectral region, which the ammonia band profile belongs to. For similar spectral regions, the spectrum of the Saturn ring is used as a reference, because it does not contain any absorption bands. For the 787 nm band, which falls in the middle of the more intense methane band, we used the spectrum of the center of the Saturn disk as a reference. This spectrum also contains methane absorption bands, but ammonia absorption is practically absent there, so the ammonia band profile stands out in the relation of the Jupiter spectrum to the Saturn's one, as described in [2]. At the time, it was paid attention to the presence of the ammonia band in the relation of the Jupiter spectrum to the Saturn's one [19], but no special measurements of this band were made. The results obtained for each spectrum are then transferred to another summary table for the derivation and comparative analysis of absorption variations at different Jupiter latitudes.

The absorption bands profiles

From each zonal spectrogram, profiles of ammonia absorption bands in units of residual intensity were obtained. From them we calculated equivalent widths of the bands. To study the latitudinal absorption of ammonia on each zonal spectrum, we selected and averaged equivalent widths over ten pixels corresponding to the position near the central meridian of Jupiter. These results are presented as a set of 66 profiles for each of the two NH_3 bands. We show the absorption band profiles for zones with numbers 25, 30, 35, 40 in Figures 3 and 4 as the samples.

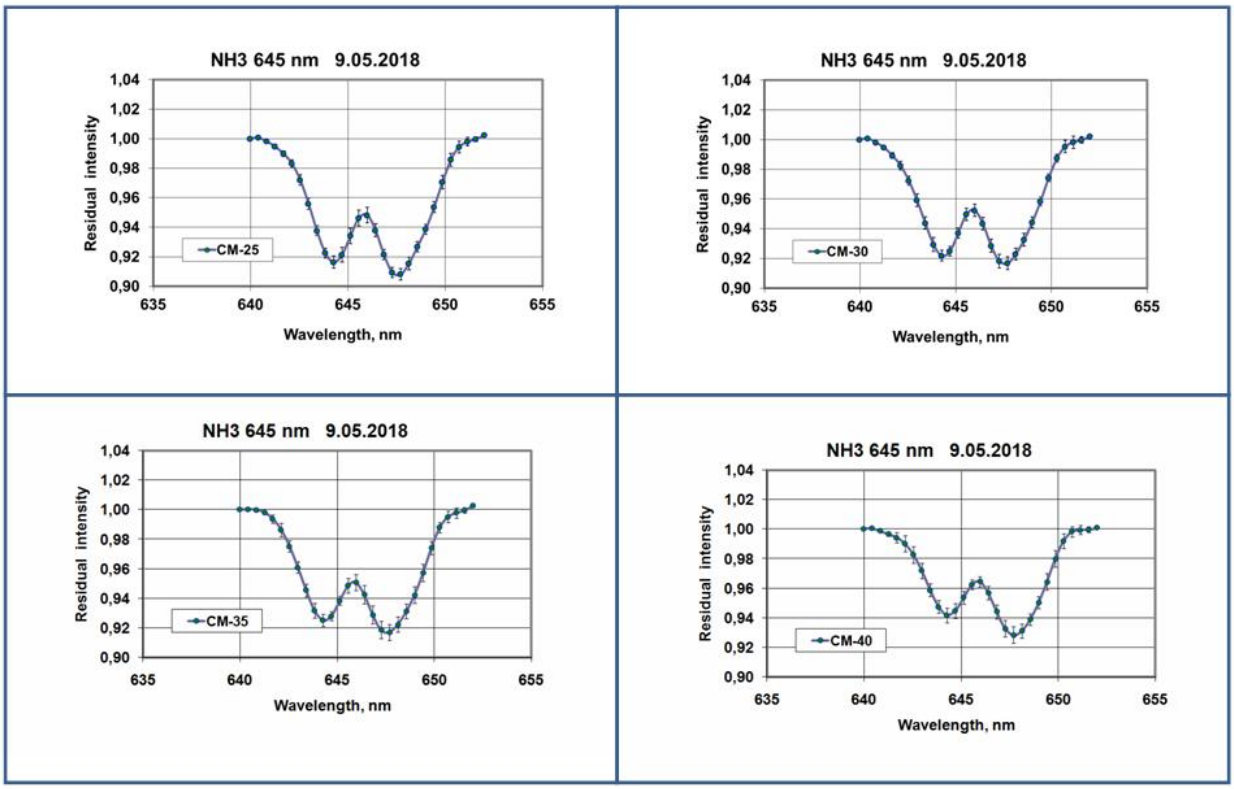

Figure 3 - Fragment of a set of profiles of the 645 nm absorption band

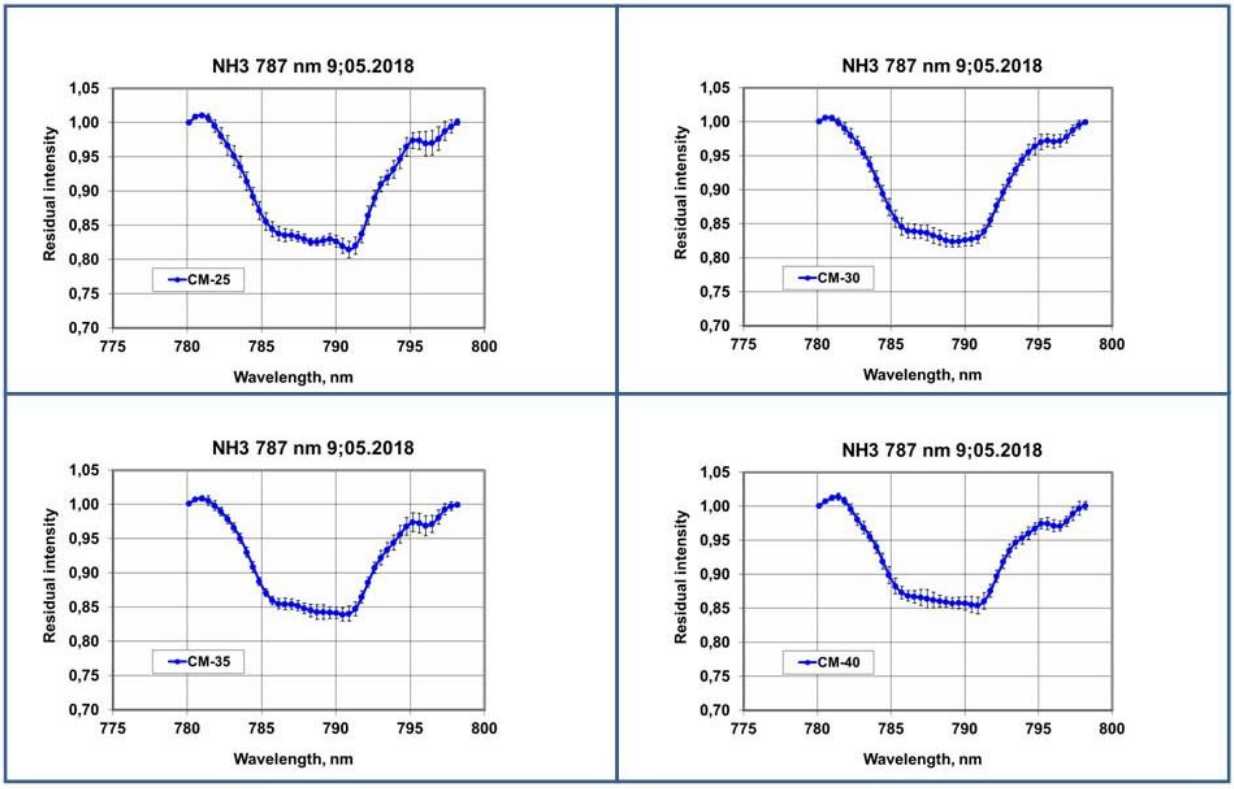

Figure 4 - Fragment of a set of profiles of the 787 nm absorption band

To compare the profiles of the studied lines, we selected seven of them, corresponding to the seven following belts and zones of Jupiter: southern temperate belt (STB), southern tropical zone (STrZ), southern equatorial belt (SEB), equatorial zone (EZ), northern equatorial belt (NEB), northern tropical zone (NTrZ), and Northern temperate zone (NTB). The comparison results we present in Fig. 5 and 6. These figures show a pairwise comparison of the absorption bands corresponding to the symmetric zones or belts. One can see that the both absorption bands corresponding to the Northern Equatorial Belt (NEB), have the lowest intensities.

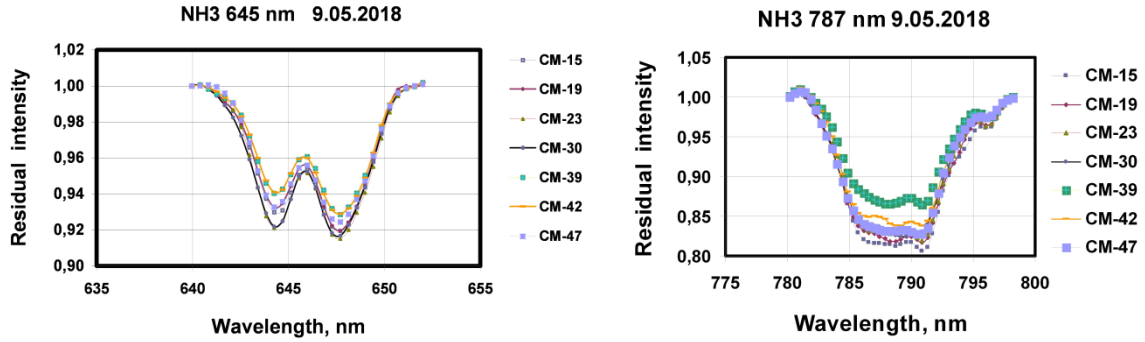

Figure 5 - Comparison of the profiles of the NH_3 absorption bands for 7 Jupiter belts and zones (STB, STrZ, SEB, EZ, NEB, NTrZ, NTB) at the central meridian

Zonal variations of the ammonia absorption

The main objective of this study is primarily considering the behavior of ammonia absorption during the transition from the central meridian to the edges of the Jupiter disk within each of the zones (or belts). In our previous publications [1-2], we have already noted that the intensity of the weak NH_3 absorption bands decreases to the limb rather steeply, so that the zonal absorption variations differ from the latitudinal variations observed along the central meridian, where the decline occurs mainly at high latitudes.

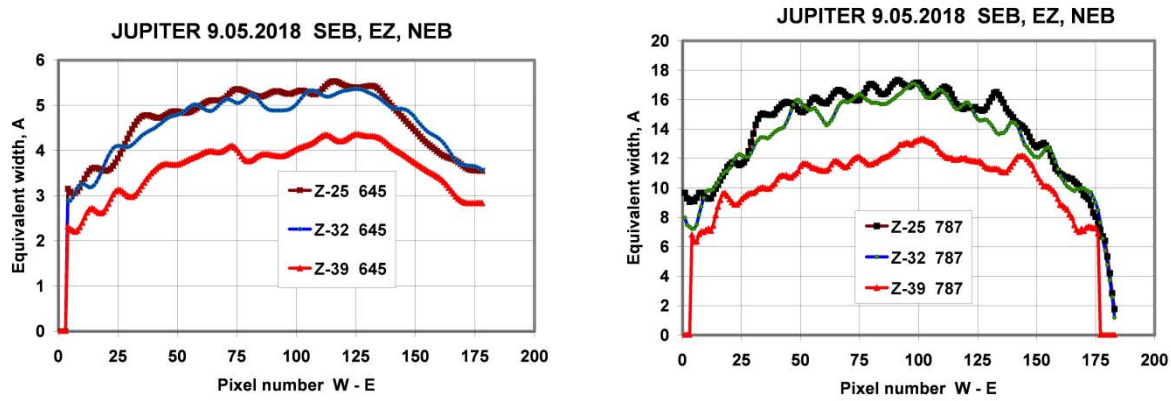

Figure 6 - Comparison of profiles of the ammonia absorption zonal variations in the three Jupiter belts (SEB, EZ and NEB)

A decrease in the absorption to the edges of the disk is observed for all zones of Jupiter and is inherent to the studied weak molecular absorption bands of 645 and 787 nm of ammonia and 702 and 619 nm of methane. The formation of weak absorption bands occurs mainly in the Jupiter troposphere inside the upper cloud layer. If the cloud cover optical thickness is large enough, the multiple light scattering on cloud particles plays an important role, because this increases the optical absorption path in the gaseous medium. Theoretical calculations show that, with the approach to the edges of the planet's disk, the number of scattering events decreases and, accordingly, the effective optical absorption path decreases.

In fact, those things are not so simple. While we cannot exclude the fact that the ammonia cloud layer has a finite optical thickness, and absorption in weak bands also occurs in a sub-cloud layer of pure gas. In

addition, large-scale images from the JUNO space probe, which is next to Jupiter, indicate a very complex horizontal vortex and turbulent cloud structure of Jupiter [16]. Therefore, many of the effects observed in the cloud zones of Jupiter may manifest themselves differently depending on the scale and spatial resolution.

Latitude variations of ammonia absorption

The study of latitudinal differences in intensities of the ammonia absorption bands one can carry out in two ways: by zonal spectra and by the spectra of the central meridian, when the spectrograph slit is oriented in the south-north direction. In digital arrays derived from zonal spectrograms, we selected and averaged the values of equivalent widths of the ammonia bands near the central meridian (10 points on each side). Within these longitude intervals, the absorption is almost the same, so averaging just gives a smaller random scatter of estimates. Figure 7 presents absorption graphs for each ammonia band, indicating standard deviations. One can see that they are small, whereas the resulting latitudinal differences in some zones clearly superior to them. This figure also shows the meridional course of brightness in the continuous spectrum. We recall that each point on the curves corresponds to a separate zonal spectrogram.

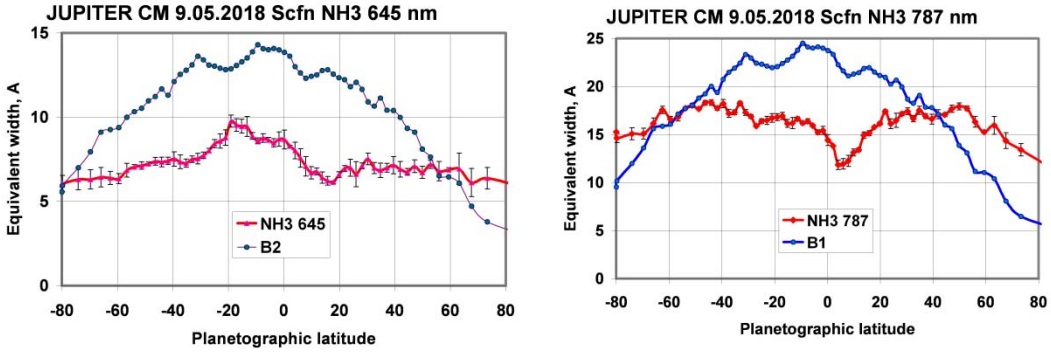

Figure 7 - Variations of equivalent widths of the ammonia absorption bands in latitudes at the central meridian of Jupiter from measurements of zonal spectrograms

Interestingly, the latitudinal courses of intensities of the two ammonia absorption bands always show very noticeable differences, as one can see, for example, from figure 8. In that figure there are the both bands' variations normalized to the equatorial zone and shown in the scale of planetographic latitudes. Here one can see the mismatch of absorption minima located north of the equator. In the NH_3 787 nm absorption band, the minimum occurs at a latitude of about 15 degrees, and in the NH_3 645 nm band it is shifted to the north, i. e. to a latitude of about 20 degrees. From radio observations of Jupiter in the microwave spectrum [6], the researchers also note that the minimum of ammonia absorption, which corresponds to the maximum output of thermal radio emission, falls not in the middle of the Northern Equatorial Belt (NEB), but on the border between Equatorial zone and NEB.

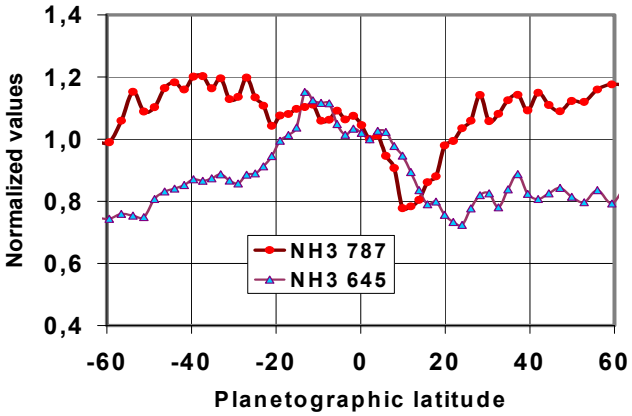

Figure 8 - Comparison of latitudinal variations of equivalent widths of the 645 and 787 nm absorption bands normalized to EZ

Another difference in the absorption latitudinal course is that the 645 nm band has a greater decrease in absorption when moving to temperate latitudes.

Conclusion

Because of a limited scope of this article we cannot present all the results and details of the conducted research. Really, even only the 2018 observational material comprises more than 4,500 spectrograms of individual zones.

There is still a number of problems and tasks, including the search of the most correct methods for the best separation of ammonia absorption from methane one, as well as the problems of interpretation of the obtained data using different models of absorption band formation.

The study of the behavior of the ammonia weak absorption bands is of interest, in particular, because their formation in the cloud layer is most susceptible to the influence of multiple scattering, especially if the optical thickness of the clouds is considered as semi-infinite. But an occasion of the relatively small optical thickness of the cloud layer is also possible. Then the observed features of the absorption bands should be largely determined by their variations in latitude and longitude. The local values of the density and thickness of the ammonia cloud layer must be interrelated with the temperature regime and the concentration of gaseous ammonia. So comprehensive studies in this direction are necessary in the future.

This research was carried out in accordance with the grants of MES RK 0073 / F4 and AP05131266.

УДК 523.45

В.Г. Тейфель, П.Г. Лысенко, А.М. Каримов,
Г.А. Кириенко, В.А. Филиппов, Г.А. Харитонова, А.П. Хоженец

Астрофизический институт им. В.Г. Фесенкова, Алматы, Казахстан

ЮПИТЕР: ӘЛСІЗ ЖОЛАҚТЫ АММИАК ЖҰТЫЛУЫНЫҢ АЙМАҚТЫҚ СПЕКТРОФОТОМЕТРИЯСЫ

Аннотация. 2018 жылдың наурыз-шілде айларында Юпитер дискасын сканерлеуден кейінгі алынған аймақтық спектрограммалар негізінде әлсіз жұтылу жолақтары NH3 645 және 787 нм кескіндері өлшенді және әртүрлі ендіктегі жұтылудың аймақтық өзгерістерінің сипаттамалары анықталды. Юпитердің толық Күнді айналу периодының спектрлік бақылау мәліметтері бойынша кездейсоқ және мезгілдік мүмкін болатын болашақтағы зерттеулерге қолданылатын мәліметтерді өңдеуге және талдауға арналған әдіснама дайындалды. Ендік және аймақ бойынша аммиактың жұтылуының айнымалылығы көрсетілген. NEB ауданында шамамен +15 градус ендікте NH3 жұтылуының тоқырауы былтырғы жылдағыдай ерекше байқалады. Өткен жылдағыдай, NH3 645 және 787 нм жолақтарының ендік бойындағы жұтылу жолдарының кейбір айырмашылықтары сақталады.

Түйін сөздер: Юптер, атмосфера, бұлт, аммиак, метан, молекулалық жұтылу жолағы, спектрофотометрия.

УДК 523.45

В.Г. Тейфель, П.Г. Лысенко, А.М. Каримов,
Г.А. Кириенко, В.А. Филиппов, Г.А. Харитонова, А.П. Хоженец

Астрофизический институт им. В.Г. Фесенкова, Алматы, Казахстан

ЮПИТЕР: ЗОНАЛЬНАЯ СПЕКТРОФОТОМЕТРИЯ СЛАБЫХ ПОЛОС ПОГЛОЩЕНИЯ АММИАКА

Аннотация. На основе измерений зональных спектрограмм, полученных при сканировании диска Юпитера в марте-июне 2018 года, измерены профили слабых полос поглощения NH3 645 и 787 нм, и выведены характер зональных вариаций поглощения на разных широтах. Подготовлен стандарт методики обработки и анализа данных применительно к дальнейшим исследованиям возможных сезонных и спорадических вариаций по материалам спектральных наблюдений Юпитера за полный период его обращения вокруг Солнца. Показаны вариации аммиачного поглощения по зонам и по широте. Как и в прошлые годы особенно выделяется депрессия поглощения NH3 на широте около +15 градусов в районе

NEB. Как и в предыдущие годы сохраняются некоторые различия в широтном ходе поглощения у полос NH3 645 и 787 нм.

Ключевые слова: Юпитер, атмосфера, облака, аммиак, метан, молекулярные полосы поглощения, спектрофотометрия.

Information about authors:

Expecting a miracle Victor Germanovich - SLLP Astrophysical Institute. V. G. Fesenkova, doctor of physical-Mat. Professor, head of the laboratory of Physics of the moon and planets, tejf@mail.ru, https//orcid.org/ 0000-0003-0093-1975;

Kirienko G. A. - senior researcher, gak39@mail.ru, https//orcid.org/ 0000-0002-1753-4813;

Karimov A. M. - B. S., karalik0@yandex.ru, https//orcid.org/ 0000-0003-0797-6252;

Lysenko P. G. - B. S., lyssenko_petr@mail.ru, https//orcid.org/ 0000-0002-4292-782X;

Filippov V. A., senior researcher, filipp.va@mail.ru, https//orcid.org/0000-0001-9013-849X;

Kharitonova G. A., senior researcher, gah38@mail.ru, https//orcid.org/0000-0003-0366-4761;

Hogenes A. P., B. S., hogenez@gmail.com, https//orcid.org/0000-0002-0830-0345

REFERENCES

[1] Tejfel` V.G., Karimov A.M., Vdovichenko V.D. (2005) Strange latitudinal variations of the ammonia absorption on Jupiter, Bulletin of the American Astronomical Society, 37(3): 682 (in Eng).

[2] Tejfel` V.G., Vdovichenko V.D., Lysenko P.G., Karimov A.M., Kirienko G.A., Bondarenko N.N., Filippov V.A., Kharitonova G.A., Khozhenets A.P. (2018) Ammonia in Jupiter` s atmosphere: spatial and temporal variations of the NH3 absorption bands at 645 and 787 nm, Solar System Research, 52: 480-494 (in Eng).

[3] Tejfel V.G., Vdovichenko V.D., Kirienko G.A., Karimov A.M., Lysenko P.G., Filippov V.A., Kharitonova G.A., Khozhenets A.P. (2019) The weak ammonia absorption bands study from zonal spectrophotometry of Jupiter, EPSC Abstracts V.13, EPSC – DPS2019 – 134, 2P. Geneva, Switzerland, (in Eng).

[4] Tejfel` V.G., Vdovichenko V.D., Lysenko P.G., Karimov A.M., Kirienko G.A., Filippov V.A., Kharitonova G.A., Hozhenets A.P. (2018) The Great Red Spot on Jupiter: some features of the ammonia absorption, Proceedings of NAS RK [Izvestia NAN RK], 3: 23 – 31 (in Eng).

[5] Pater I., Sault R.J., Butler B., de Boer D., Wong MH. (2016) Peering through Jupiter's clouds with radio spectral imaging, Research Reports Gas Giant Planets. Science, 352: 1198-1201 (in Eng).

[6] Pater I., Sault R.J., Wong M.H., Fletcher L.N., Boer D., Butler B. (2019) Jupiter`s ammonia distribution derived from VLA maps at 3 – 37 GHz, arXiv: 1902.07294V1 [astro – ph. EP] 19 Feb 2019 (in Eng).

[7] Fletcher L.N., Orton G.S., Mousis O., Yanamandra-Fisher P., Parrish P.D., Irwin P.G.J., Edkins E., Baines K.H., Line M.R., Vanzi L., Fujiyoshi T., Fuse T. (2010) Jupiter's Great Red Spot: High-resolution thermal imaging from 1995 to 2008, Icarus, 208: 306-328 (in Eng).

[8] Fletcher L.N., Orton G.S., Sinclair J.A., Donnelly P., Melin H., Rogers J.H., Greathouse T.K., Kasaba Y., Fujiyoshi T., Sato T.M., Fernandes J., Irwin P.G.J., Giles R.S., Simon A.A., Wong1 M.H., Vedovato M. (2017) Jupiter's North Equatorial Belt expansion and thermal wave activity ahead of Juno's arrival, Geophys. Res. Letters, 44 (Issue 14): 7140-7148, DOI:10.1002/2017GL073383 (in Eng).

[9] Antunano A., Fletcher L.N., Orton G.S., Rogers J.H., Harrington J., Donnelly P.J., Rowe-Gurney N., Blake J.S.D. (2018) Infrared characterization of Jupiter s equatorial disturbance cycle, Geophysical Research Letters, 45: 10,987-10,995 (in Eng).

[10] Giles R.S., Fletcher L.N., Irwin P.G.J., Orton G.S., Sinclair J.A. (2017) Ammonia in Jupiters troposphere from highresolution 5 μm spectroscopy, Geophys. Res. Letters, 44 (Issue 21): 10838-10844 (in Eng).

[11] Fletcher L.N., Greathouse T.K., Orton G.S., Sinclair J.A., Giles R.S., Irwin P.J., Encrenaz T. (2016) Mid-Infrared mapping of Jupiter's temperatures, aerosol opacity and chemical distributions with IRTF/TEXES, arXiv: 1606.05498. V.1 [astro-ph. EP] 17.06 (in Eng).

[12] Simon A. A., Tabataba-Vakili F., Cosentino R., Beebe R. F., Wong M. H., Orton G. S. (2018) Historical and Contemporary Trends in the Size, Drift, and Color of Jupiter's Great Red Spot, Astronomical Journal, V. 155 P.1-15 (in Eng).

[13] Loeffler M.J., Hudson R. L. (2018) Coloring Jupiter's Clouds: Radiolysis of Ammonium Hydrosulfide (NH4SH), Icarus, 302: 418-425 (in Eng).

[14] Giver LP., Boese, RW., Miller, JH. (1969) Laboratory studies of the visible NH3 bands with applications to Jupiter, J. Atm. Sci., 26: 941-942 (in Eng).

[15] Giver LP. Miller JH., Boese RW. (1975) A laboratory atlas of the 5 1 NH3 absorption band at 6475 A with applications to Jupiter and Saturn, Icarus, 25: 34-48 (in Eng).

[16] Irwin P.G.J. (2009) Giant planets of our Solar system. Atmospheres, composition, and structure. (second edition), Springer – Praxis, 403 (in Eng).

[17] Irwin P.G.J., Bowles N., Braude A.S., Garland R., Calcutt S. (2017) Analysis of gaseous ammonia (NH3) absorption in the visible spectrum of Jupiter, Icarus, 302: 426-436 (in Eng).

[18] ALPO Japan –http://alpo-j.asahikawa-med.ac.jp/indexE.htm (in Eng).

[19] Karkoschka E.(1994) Spectrophotometry of the jovian planets and Titan at 300- to 1000-nm wavelength: the methane spectrum, Icarus,111: 174-192 (in Eng).

N E W S
OF THE NATIONAL ACADEMY OF SCIENCES OF THE REPUBLIC OF KAZAKHSTAN
PHYSICO-MATHEMATICAL SERIES
ISSN 1991-346X **https://doi.org/10.32014/2019.2518-1726.36**
Volume 3, Number 325 (2019), 166 – 175

УДК 539.17

B.K. Kozhakhmet[1], G.G. Kulikov[2], G.S. Nurbakova[1], S.B. Rustembayeva[1]

[1]Kazakh National University named after al-Farabi, Almaty, Kazakhstan;
[2]National Research Nuclear University "MEPHI", Moscow, Russia
bauyr.ko@gmail.com, GeGKulikov@rosatom.ru, g.nurbakova@gmail.com, rustembayeva@gmail.com

USE OF MOLYBDENUM AS A STRUCTURAL MATERIAL OF FUEL ELEMENTS IN LEAD OR LEAD-BISMUTH EUTECTIC COOLED FAST REACTOR TO IMPROVE ITS SAFETY

Abstract. In our previous works has been described that the mean prompt neutron lifetime in fast reactors can be significantly elongated [1,2]. But if the last parameter is not comparable with the time required for the heat generated in the fuel elements to transport from a fuel to a coolant, feedback on the effect of changes in coolant parameters on reactivity during this time will not have time to manifest. Here was studied that the thermal constants of fuel elements can be shortened by using molybdenum as a structural material of fuel elements. Other aspects related to the use of molybdenum in nuclear reactors have also been studied.

When performing the study the neutron-physical properties of isotopes of natural molybdenum (nuclear data library JENDL-4.0) and thermal properties of metallic molybdenum were used.

The following results were obtained:

1. A method for reducing the thermal constant of fuel elements for light water and fast reactors by using dispersion fuel in cylindrical fuel rods containing, for example, granules of metallic U-Mo-alloy into Mo-matrix was proposed.
2. The necessity of molybdenum enrichment by weakly absorbing isotopes was shown.
3. Total use of isotopic molybdenum will be more than 50%.
4. Mo has a good corrosion resistance to Pb and Pb-Bi eutectic

A decrease in thermal constants of fuel elements, in combination with an increase in the mean prompt neutron lifetimes in the absence of the heat transfer crisis in fast reactors, can be promising way for a better reactor operation safety even under the conditions of the prompt neutron excursions.

Keywords: improvement of fast reactor safety, physic-mechanical characteristics of molybdenum, thermal constant of fuel elements, corrosion resistance in lead and LBE.

Introduction

It is well known fact that the safety of nuclear reactor in the case of introduction of reactivity comparable with delayed neutrons fraction depends largely on the properties of fuel and materials constituting fuel element [3]. Sharp reactivity increase initiates neutron flash, which is suppressed by means of feedback due to fuel heating and increase of neutron absorption by fertile nuclide (^{238}U or ^{232}Th) thanks to the Doppler effect. If there is enough time for heat transfer from fuel to coolant then there would be feedback caused by heating of the coolant. This second feedback depends largely on thermal-physical characteristics of the fuel element and materials constituting it.

As is known, a refractory material based on molybdenum is characterized by good thermal-physical properties [4]. Therefore, such a material appears to be attractive when using dispersion fuel elements with good heat-conducting molybdenum matrix. However, there are some difficulties to use such a material in the reactor core. Firstly, molybdenum of a natural isotopic composition is quite a strong absorber of neutrons. Secondly, it is necessary to take into account its compatibility with fuel material on the one hand and with coolant on the other hand. Resolving these issues is the subject of the present paper.

Physico – mechanical characteristics of molybdenum and some peculiarities of its nuclear – physical properties

Natural isotopic composition of molybdenum and some peculiarities of its nuclear-physical properties

Natural isotopic composition of molybdenum is represented by seven stable isotopes with mass numbers 92, 94–98, and 100, of which ^{98}Mo is the most common (23.75%).

Molybdenum has a favorable complex of physico - mechanical characteristics, due to which it is one of the best structural metals (Table 1).

Table 1 - Physico-mechanical characteristics of molybdenum

Characteristic	unit of measurement	Value
Crystal cell, α_0	nm	0,314737
Atomic radius r_a	nm	0,139
Atomic volume Ω	м^3/mole	9,42E-06
Atomic mass A	a.t.u.	95,941
Ionization potential U	eV	7,29
Density at 20^{0}C ρ	кg/m^3	10,2E+03
Melting temperature T_{melt}	^{0}C	2587(2625)
Boiling temperature $T_{boiling}$	^{0}C	5227
Spesific heat of fusion L_m	J/кg	0,382
Spesific heat of evaporation L at $T_{boiling}$	J/кg	6,191
Thermal conductivity at 20^{0}C λ	W/(m*K)	162
Heat capacity at 20^{0}C C_c	J/(кg*K)	240-250
Thermal expansion at 20^{0}C α_t	K^{-1}	5,1-5,2E-06
Vapor pressure при $T_{пл}$	Pa	2,94(3,47)E-02
Electrical resistivity at 20^{0}C ρ_e	Om*m	5,0-5,7E-08
Magnetic susceptibility при 20^{0}C χ_{ms}	m^3/кg	0,82-0,93E-09
Electron work function A	eV	4,33
Emissivity on a smooth surface ρ		0,4
Modulus of normal elasticity at 20^{0}C	kgs/mm^2	32000
Shear modulus at 20^{0}C	кgs/mm^2	12200

Important advantages of Mo are its high values of melting point, normal elasticity modulus and thermal conductivity with a relatively low density and low coefficient of linear expansion [5,6,7,8,9,10,11]. Since the density of Mo (10200 kg / m3) is almost two times less than the density of W (19300 kg / m3), the Mo-based alloys have a much higher specific strength (at temperatures below 1370 ° C). Molybdenum has a rather low neutron capture cross section; the capture values of some molybdenum isotopes, in the thermal spectrum is smaller than the zirconium (zirconium alloys are used as a basic structural material in the core of thermal reactors) capture cross-section ($\sigma_{(n,\ y)thermal}$(Zr) = 0.18 barn), and in the fast spectrum is smaller than iron capture cross-section ($\sigma_{(n,\ y)1\ MeV}$(Fe) = 0.06 barn) (Table 2) [12,13]. Mo has good heat resistance and high radiation resistance [14,15,16], it is characterized by high corrosion resistance in most alkaline solutions, in liquid metals, as well as in sulfuric, hydrochloric and hydrofluoric acids at different temperatures and concentrations.

Table 2: Isotopic composition and radiative neutron capture cross-sections of molybdenum at thermal point (En = 0.025 eV) and in the fast spectrum

Nuclide, atomic number of molybdenum isotope	Natural composition [%]	nuclei concentration ρ, 1-E24 cm^{-3}	$\sigma_{(n,y)}$, barn (E_n=0,0253 eV)	$\sigma_{(n,y)}$, barn (E_n=1 MeV)
Monat		0,06403	2,55	0,035
92	14,8		0,019	0,033
94	9,3		0,015	0,036
95	15,9		14	0,054
96	16,7		0,5	0,028
97	9,6		2,1	0,055
98	24,1		0,13	0,028
100	9,6		0,199	0,017

At the same time molybdenum of a natural isotopic composition is characterized by a significantly larger neutron capture cross-section in the thermal energy range

It means that technology of isotopic enrichment should be applied in order to use molybdenum as a construction material in thermal reactors. It can be seen from the table that isotopes ^{92}Mo and ^{94}Mo account for almost a quarter of the natural material and are located on the "light" end of isotopes natural mixture. Their mixture provides about the same neutron capture cross-section as natural zirconium does. Isotope ^{95}Mo provides a dominant contribution to the total capture cross-section, the atomic weight of which is intermediate in molybdenum isotopic composition. Use of ^{98}Mo and ^{100}Mo is not excluded, of course. Dependence of capture cross-section of these light and heavy isotopes of molybdenum on neutron energy is shown in figures 1 and 2 (here reactor energy range is considered). One can see that capture cross-section is generally inversely proportional to neutron velocity, and, generally speaking, the resonance integral is more than an order of magnitude smaller than that of ^{238}U [12].

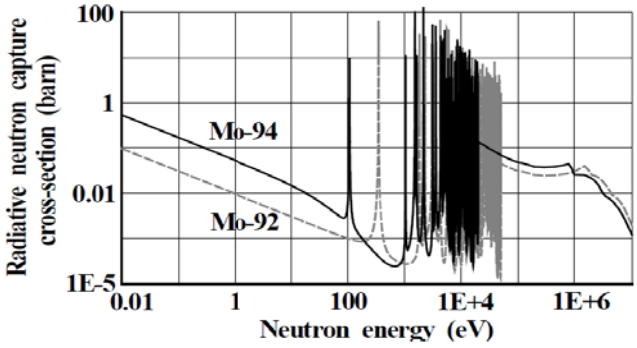

Figure 1: Radiative neutron capture cross-section of molybdenum isotopes ^{92}Mo and ^{94}Mo on neutron energy (nuclear data library JENDL-4.0)

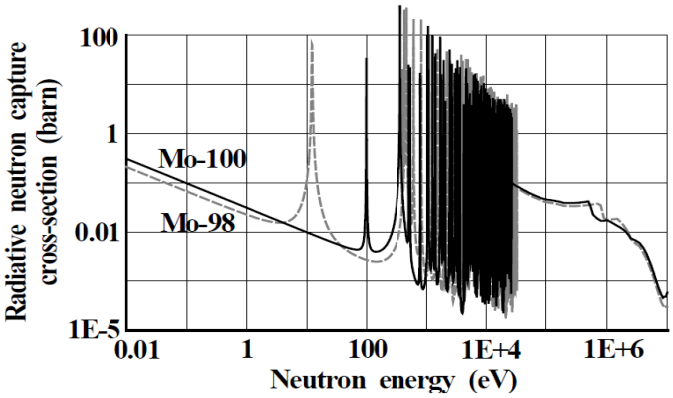

Figure 2. Radiative neutron capture cross-section of molybdenum isotopes ^{98}Mo and ^{100}Mo on neutron energy (nuclear data library JENDL-4.0)

Isotopic enrichment of molybdenum for medical purposes and for reducing its radiative neutron capture.

As is known, the isotopic enrichment is a high-level technology requiring the use of multi-step separation cascades, and therefore is very expensive. However, for the case of production of enriched molybdenum there is one important factor that can significantly facilitate the solution of this issue.

There is already a commercial enrichment of molybdenum [17] with the production of the desired isotopes ^{98}Mo and ^{100}Mo for medical diagnosis of early formation of cancerous tumors. Currently, the diagnosis is the most advanced in the world in the field of medicine and, therefore, the need for these heavy isotopes of molybdenum is high and continues to rise.

Keeping this fact in mind, it can be assumed that the process of obtaining molybdenum enriched by the light isotopes $^{92+94}$Mo can be successfully combined with the process of producing heavy isotopes ^{98}Mo and ^{100}Mo. Heavy isotopes are the product at one end of enrichment cascade, while light isotopes are

the product at the other end. Of course, the structure of the cascade requires to be changed to get rid of the strong neutron absorber - isotope ^{95}Mo, atomic weight of which is intermediate in a series of atomic weights. Since this isotope is in the middle of the spectrum of the atomic weights of molybdenum natural isotopes (see table 1), a cascade of isotope separation with additional selection in the middle of the cascade should be used. This problem is considered in [17].

Thermo – physical parameters of metallic molybdenum, important for use as a structural material of the fuel element

Table 3. Shows some thermo-physical parameters of molybdenum and zirconium that are important for heat transfer in the fuel element [4, 12, 18].

Table 3 - Nuclear-physical and thermo-physical properties of fuel and structural materials.
[a]Granules – U-9%Mo; matrix – Mo; the proportion of granules $V_f = 0.5$

Material	Density [g/cm^3] (20ºC)	$T_{melting}$ [ºC]	Heat capacity [10^7J/(m^3·K]	Thermal conductivity [W/(m·K)] (1000ºK)	Time constant of cylindrical fuel element (rod) τ_{th} [s] (d = 9.1 mm)
Zr	6.5	1855	0.23	21.5	0.36
Mo	10.22	2623	0.30	112	0.20
U-9%Mo	17.6	1300	0.35	40	0.36
Dispersion fuel[a]	-	-	0.32	71.5	0.26

Apart from the fact that molybdenum has a melting point substantially greater, it also has a more than 5 times greater coefficient of thermal conductivity. Model fuel element of metallic molybdenum is characterized by a time constant of transferring heat to the environment [3] which is almost two times smaller than that for zirconium. These attractive properties of molybdenum can be used to create a new concept of a fuel element for thermal and fast reactors. This structural material is compatible with the well-known metallic uranium-molybdenum fuel good thermal properties of which are shown in table 3.

Rod fuel element with a small time constant τ_{th} for fast reactor and thermal reactor

As is known, fuel material of fuel elements of the world's first nuclear power plant built in the USSR (Obninsk) in 1954, was an alloy U-9%Mo. Molybdenum was chosen not only because it is able to stabilize γ-phase of uranium, but also because its alloy with uranium is characterized by a high thermal conductivity and high nuclear density of uranium (see table 3).

It can be seen that among materials presented in table 3, for creating a fuel element it is preferable to use dispersion fuel containing granules of a metal alloy U-9%Mo, dispersed into the molybdenum matrix. To improve the thermal contact of fuel with cladding, the latter also should be produced, for example, from Mo-based alloy [19].

Experimental studies [20] performed with a model nuclear fuel have confirmed the possibility of creating such a dispersion fuel (U-Mo - fuel granules, Mo - matrix) both in terms of compatibility over a wide temperature range of fuel granules, matrix and cladding, and at high fuel burn-up.

Since the thermal conductivity of fuel granules (U-9%Mo) is 2.8 times smaller than that of a molybdenum matrix, the average thermal conductivity of dispersion fuel material depends to a significant extent on the proportion of fuel granules, and on their forms. Assuming that fuel granules have a spherical shape, when their share Vf = 0.5 in dispersion fuel material, the average coefficient of thermal conductivity of the fuel rod is 71.5 W/(m·K) [18], and the time constant of the fuel element with a diameter d = 9.1 mm will be $\tau_{th} = 0.26$ sec (see table 3).

Prospects for the use of dispersion fuel elements with molybdenum as a structural material in fast reactors and corrosion resistance of molybdenum to lead and lead-bismuth eutectic

As for the apparent attractiveness of the possibility of using molybdenum and its alloys as a structural material in fast reactors (fuel - uranium-molybdenum alloy, the matrix material - molybdenum in dispersion fuel elements, cladding material - possibly also refractory material), the need for use of molybdenum enriched by light isotopes still requires to be considered.

It is known that molybdenum and its alloys are compatible with both aqueous coolant (in thermal reactors), and liquid metals Na, Pb and Pb-Bi [5,21,22,23,24,25,26,27] in fast reactors. Here some results of different studies, that shows high corrosion resistance to Pb and Pb-Bi coolants.

In work [27] The relative resistance of 21 metals and alloys to mass transfer in liquid lead has been

measured. Tests were performed in small, quartz thermal-convection loops. The test temperature was about 800°C, with a thermal gradient of 300 ^{0}C existing across the loops. All the metals and alloys studied, only niobium and molybdenum exhibited a high resistance to mass transfer (Figure 3). Neither of these metals suffered noticeable mass transfer or corrosion under the test conditions. A transverse section of the hot-leg specimen from a molybdenum loop is shown in Fig. 4.

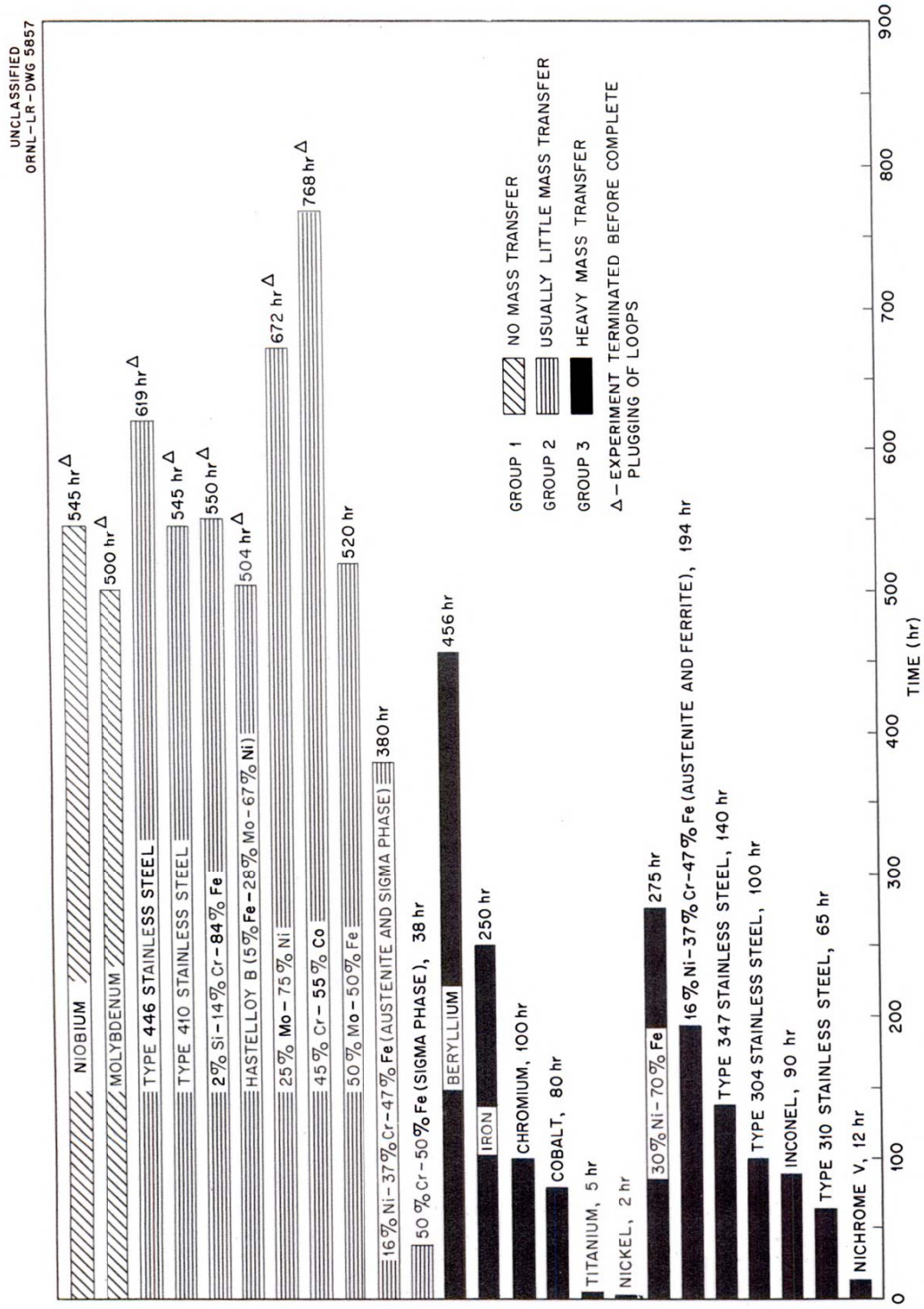

Figure 3: Mass transfer in liquid lead

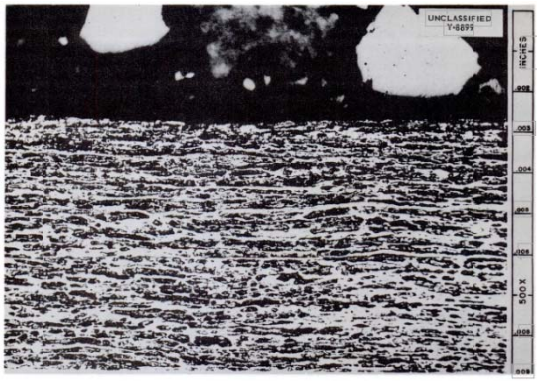

Figure 4 - Transverse Section of Hot-Leg Specimen from
a Molybdenum Loop in Which Liquid Lead Was Circulated. 500X

The specimens of molybdenum were immersed in the stirred lead-bismuth for 1000 h, that was heated up to 700 ^{0}C [28]. Oxygen concentration was 5*10^{-6} wt.%.

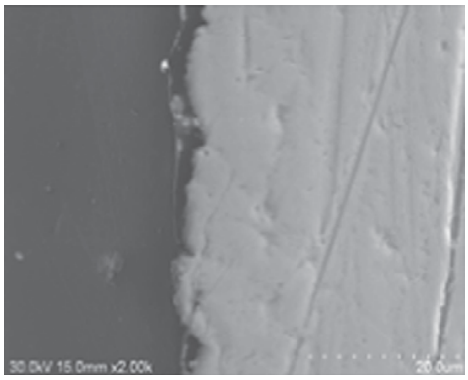

Figure 5 - SEM micrograph of Mo after immersion in 700 ^{0}C LBE for 1000 h

Fig. 5 shows the SEM micrograph of the cross section of the molybdenum. There is no significant weight change of the molybdenum specimen. These results show that after the immersion in high temperature LBE for 1000 h. At lower temperature, high corrosion resistance of molybdenum in liquid LBE has been also reported in another works. Fazio et al. (2003) reported that in flowing LBE at 400 ^{0}C molybdenum exhibited smooth surface with no evidence of LBE on the surface and growth of oxide layer. Hata and Takahashi (2005) reported that in the stirred LBE pool at 450 ^{0}C molybdenum had good corrosion resistance.

The result of the molybdenum after immersion in Pb–Bi is shown in Fig. 6 [29]. Oxygen concentration was 10^{-6} wt.%. (550 ^{0}C) - 2* 10^{-}5(800 ^{0}C)).

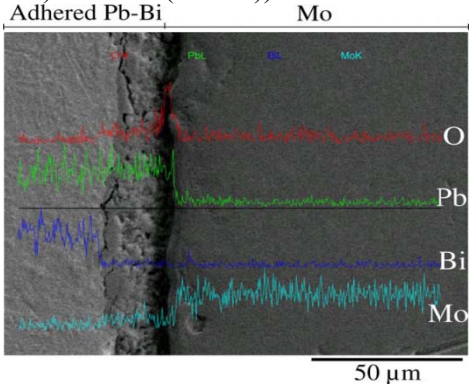

Figure: 6 SEM-EDX micrograph analysis of molybdenum after immersion in Pb–Bi at 550 ^{0}C for 12 h
and then the temperature was increased up to 800 ^{0}C and kept there for 12 h

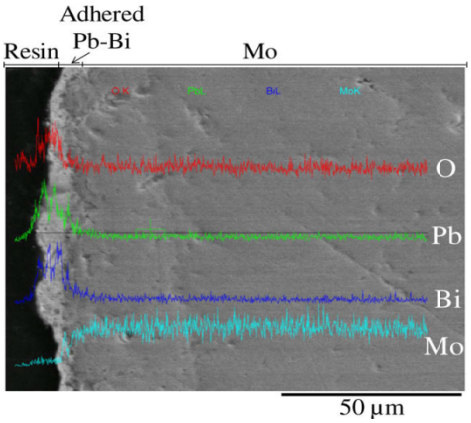

Figure 7 - SEM-EDX micrograph analysis of molybdenum after immersion in Pb–Bi at 550 ^{0}C for around 500 h and then the temperature was increased up to 800 ^{0}C and kept there for 15 h.

Fig. 7 shows the SEM-EDX micrograph analysis of the cross section of the molybdenum after immersion in Pb–Bi [29]. Oxygen concentration was 10^{-6} wt.% (550 ^{0}C - 800 ^{0}C).

The compatibility test was performed at 673 K and the corrosion and tensile results reported concern the first 1500-h run of the loop operation [30]. All the materials tested suffered from liquid metal attack exhibiting a weight loss. The consequent evaluation of the corrosion rate showed that, under the given test conditions, the refractory metals are more resistant than the steels. The measured weight loss of molybdenum sample was $9.1*10^{-7}$mg/mm^2 ($4.7*10^{-5}$ µm/h). From a metallographic point of view, as is shown in the SEM micrograph of Fig. 8 metal exhibited an almost smooth interface with the lead–bismuth alloy. No evidence of liquid metal attack on the surface of material, or of the growth of an oxide layer, could be detected.

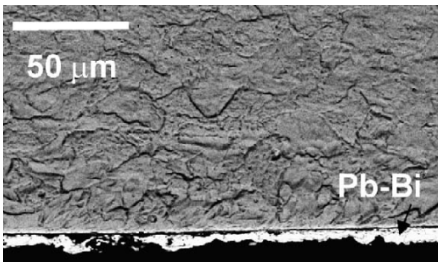

Figure 8: SEM – micrograph of the Mo cross section

The weight loss measured could be associated with both the uniform dissolution and the low solubility of Mo in Pb–Bi liquid at 673 K.

In another work [31] the specimens of molybdenum were immersed in the lead for 500 h, that was heated up to 700 ^{0}C. Oxygen concentration was $4.5*10^{-7}$ wt.%.

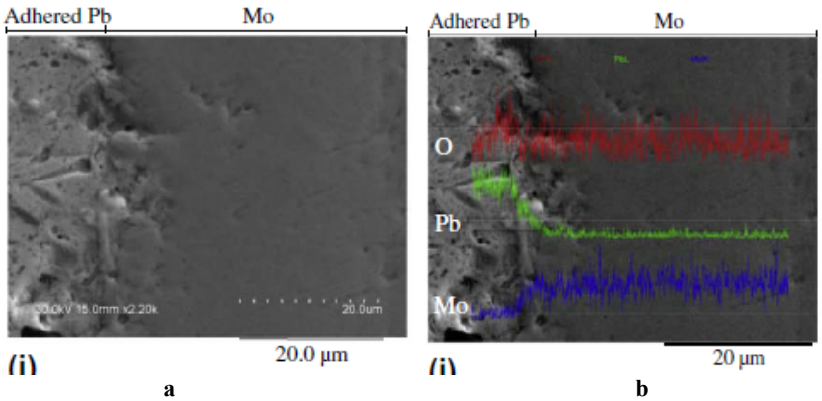

Figure 9 - SEM(a)-EDX(b) micrograph of cross section of tested molybdenum specimen after immersion in lead at 700 ^{0}C for 500 h

The figures 4, 5, 6, 7, 8, 9 shows that no penetration of Pb–Bi or Pb into the molybdenum matrix and no dissolution of molybdenum atoms from specimen into Pb–Bi/Pb. Moreover, no crack on the surface of the specimens after immersion in Pb–Bi/Pb under transient temperature up to 800 ^{0}C/700 ^{0}C was observed.

Fig. 8a shows that neither cracks nor a friable molybdenum oxide layer on the surface of the specimen occurred.

This results showed that the molybdenum exhibited high corrosion resistance to Pb–Bi up to 800 ^{0}C and to Pb up to 700 ^{0}C. In all this work molybdenum specimen has a purity of at least 99.95 wt.% .

However, it is important to note that in a core the combination of a high melting point liquid metal coolant (e.g., Pb, Pb-Bi et al.) and the fuel element with a cladding based on a refractory (molybdenum-based) material [19] and with a molybdenum matrix can significantly increase the stability of the core with respect to the possibility of a crisis in the heat transfer at a jump of reactivity. Using uranium-molybdenum fuel fits well into the concept of protected fuel cycle based on a mixture of (^{233}U+^{238}U) [32].

If two heavy isotopes $^{98+100}$Mo would be used for medicine purposes (these isotopes account for about 1/3 of the total of molybdenum), and two light isotopes $^{92+94}$Mo would be used for reactor purposes (these isotopes account for about 1/4 of the total of molybdenum), then the total use of the isotopic molybdenum would be over 50%. The rest of the molybdenum without damage may be used in the national economy.

Summary conclusion

All the results presented above allowed us to make the following conclusions:

1. A method for reducing the time constant of the fuel elements allowing us to increase the safety of light water reactors and fast reactors by using dispersion fuel in cylindrical fuel elements containing, for example, granules of metallic U-Mo-alloy into Mo-matrix with enrichment by weakly absorbing molybdenum isotopes was proposed.
2. The use of the isotopic molybdenum would be more than 50%.
3. Molybdenum has the good resistance to lead and LBE.

Б.К. Қожахмет[1], Г.Г. Куликов [2], Г.С. Нурбакова [1], С.Б. Рустембаева [1]

[1]Әл- Фараби атындағы Қазақ Ұлттық Университеті, Алматы, Қазақстан ;
[2]Ұлттық Ядролық Зерттеу Университеті "МИТИ", Мәскеу, Ресей

ҚАУІПСІЗДІКТІ ЖОҒАРЫЛАТУ ҮШІН, ҚОРҒАСЫН НЕМЕСЕ ҚОРҒАСЫН-ЕВТЕТИВТІ САЛҚЫНДАТЫЛҒАН ЖЫЛДАМ РЕАКТОРДА, ОТЫН ЭЛЕМЕНТТЕРІНІҢ ҚҰРЫЛЫМДЫҚ МАТЕРИАЛЫ РЕТІНДЕ МОЛИБДЕНДІ ПАЙДАЛАНУ

Аннотация. Зерттеудің негізгі мақсаты – ядролық реакторлардың қауіпсіздігін арттыру үшін, отын элементтерінің құрылымдық материалы ретінде, молибденді пайдалануды түсіндіру болып табылады. Қолданылған молибденнің ерекшелігі, оның изотоптық құрамы, қатерлі ісіктің медициналық диагностикасында пайдаланылатын, бөлу каскадының жұмысы кезінде қалдық ретінде алынған молибденнің құрамына сәйкес келеді.

Зерттеу барысында табиғи молибденнің нейтронды-физикалық қасиеттері (JENDL-4.0 ядролық деректер кітапханасы) және металл молибденінің жылулық қасиеттері пайдаланылды.

Келесі нәтижелер алынды:

1. Шар тәрізді микротвэлдарды пайдалану жолымен жүретін жеңіл сулы реакторлар үшін, сонымен қатар, молибденнің әлсіз жұтылатын изотоптарымен байытылған Mo-матрицасында металл U–Mo-түйіршіктерінің құймасынан тұратын, дисперсті отын пайдалану жолымен жүретін жылдам реакторлар үшін де, твэлдардың тұрақты уақытын азайту әдісі ұсынылған.
2. Молибденді әлсіз жұтылатын изотоптармен байытудың қажеттілігі көрсетілген.
3. Молибденнің изотоптық құрамының жалпы қолданылуы 50%-дан жоғары.
4. Mo-нің Pb және Pb-Bi евтетивінде коррозияға жақсы төзімділігі бар екендігін дәлелдейтін жұмыстарға шолу жасалынды.

Молибденнің әлсіз жұтылатын изотоптарымен байытылған Mo-матрицасында металл U–Mo-түйіршіктерінің құймасынан тұратын, цилиндр тәрізді отынды білікшелердегі дисперстік отынды пайдалану жолымен жүретін, жылу бөлетін элементтер твэлдарының тұрақты уақытын азайту, жеңіл сулы және жылдам ядролық реакторлардың қауіпсіздігін арттырудың лайықты тәсілі болуы мүмкін.

Түйін сөздер: жылдам реакторлардың қауіпсіздігін арттыру, молибденнің физика-механикалық сипаттамалары, жылу бөлетін элементтердің жылулық тұрақтысы, қорғасын мен LBE-дегі коррозияға төзімділігі.

Б.К. Кожахмет [1], Г.Г. Куликов [2], Г.С. Нурбакова [1], С.Б. Рустембаева [1]

[1]Казахский Национальный Университет имени Аль-Фараби, Алматы, Казахстан ;
[2]Национальный Исследовательский Ядерный Университет “МИФИ”, Москва, Россия

ИСПОЛЬЗОВАНИЕ МОЛИБДЕНА В КАЧЕСТВЕ СТРУКТУРНОГО МАТЕРИАЛА ТОПЛИВНЫХ ЭЛЕМЕНТОВ В СВИНЦЕВОМ ИЛИ СВИНЦЕВНОМ-ЭВТЕТИЧЕСКОМ ОХЛАЖДЕННОМ БЫСТРОМ РЕАКТОРЕ ДЛЯ ПОВЫШЕНИЯ ЕГО БЕЗОПАСНОСТИ

Аннотация. Основной целью исследования является обоснование использования молибдена в качестве конструкционного материала топливных элементов для повышения безопасности ядерных реакторов. Особенностью используемого молибдена является то, что его изотопный состав соответствует молибдену, который получается в качестве хвоста при работе разделительного каскада для изготовления материала для медицинской диагностики рака.

При проведении исследования использовались нейтронно-физические свойства изотопов природного молибдена (библиотека ядерных данных JENDL-4.0) и теплофизические свойства металлического молибдена.

Были получены следующие результаты:

1. Предложен способ уменьшения постоянной времени твэлов как для легководных реакторов путем использования шаровых микротвэлов, так и для быстрых реакторов путем использования дисперсного топлива, содержащего, например, гранулы металлического U–Mo - сплава в Mo - матрице с обогащением слабопоглощающими изотопами молибдена.
2. Показана необходимость обогащения молибдена слабо поглощающими изотопами.
3. Общее использование изотопного состава молибдена составит более 50%.
4. Выполнен обзор по работам, где доказывается, что Mo имеет хорошую коррозионную стойкость в Pb и евтетике Pb-Bi.

Уменьшение постоянной времени твэлов тепловыделяющих элементов, путем использования дисперсионного топлива в цилиндрических топливных стержнях, содержащих, например, гранулы металлического U-Mo-сплава в Mo-матрице с обогащением слабо поглощающими изотопами молибдена, может оказаться заслуживающим внимание способом повышения безопасности легководных и быстрых ядерных реакторов.

Ключевые слова: повышение безопасности быстрых реакторов, физико-механические характеристики молибдена, тепловая постоянная тепловыделяющих элементов, коррозионная стойкость в свинце и LBE.

Information about authors:

Kozhakhmet B.K. - al-Farabi Kazakh National University, Almaty, Kazakhstan, 2nd course PhD student, bauyr.ko@gmail.com, ORCID: https://orcid.org/0000-0001-6370-7511

Kulikov G.G. - National Research Nuclear University, Moscow, Russia, professor, GeGKulikov@rosatom.ru, ORCID: https://orcid.org/0000-0001-7580-2823

Nurbakova G.S. - al-Farabi Kazakh National University, Almaty, Kazakhstan, c.ph.-m.sc., docent, g.nurbakova@gmail.com, ORCID: https://orcid.org/0000-0001-5999-8635

Rustembayeva S.B. - al-Farabi Kazakh National University, Almaty, Kazakhstan, 1st course PhD student, rustembayeva@gmail.com, ORCID: https://orcid.org/0000-0001-9520-2518

REFERENCES

[1] Kulikov G.G., Apse V.A., Kulikov E.G., Kozhakhmet B.K., Shkodin A.O. and Shmelev A.N. (2017). Radiogenic lead from poly-metallic thorium ores as a valuable material for advanced nuclear facilities. Kerntechnik: Vol. 82, No. 1, pp. 87-91.

[2] Kozhakhmet B.K., Kulikov G.G., Nurbakova G.S. (2018) Improvement of neutron-physical characteristics of BN-600 fast reactor by using ^{208}Pb based neutron reflector. News of the National Academy of Scieces of the Republic of Kazakhstan. Physico-mathematical series. V.4, № 320, pp.22-35.

[3] Hummel H.H. and Okrent D. (1970) Reactivity Coefficients in Large Fast Power Reactors, American Nuclear Society, La Grange Park, Illinois, USA

[4] Kalin B.A., Platonov P.A., Tuzov Yu.V., Chernov I.I. and Shtrombakh Ya.I. (2012) Fizicheskoe materialovedenie: Uchebnik dlya vuzov, Vol. 6, Konstruktcionnye materialy yadernoy tekhniki, NRNU MEPhI, Moscow, Russia

[5] Zelikman A.N. (1970) Molibden, Metallurgiya, Moscow, USSR.
[6] Nikonov N. (2014) Molibden. Svoistva, primenenie, proizvodstvo, produkciya. Metotekhnika. Russia
[7] Perelman F.M., Zvorykin A.Ya. (1968) Molibden i volfram, Nauka, Moscow, USSR.
[8] Morgunova N.N. etc (1975) Splavy molibdena, Metallurgiya, Moscow, USSR.
[9] III Vsesouznye soveshaniya po himii i tekhnologii molibdena i volframa (1977) Tezisy dokladov, Orjonikidze, USSR
[10] Agte K., Vacek I. (1964) Volfram i molibden, Energiya, Leningrad, USSR
[11] Plyushev V.E. (1961) Spravochnik po redkim metallam, Mir, Moscow, USSR
[12] Grigor'ev I.S. and Meylikhov E.Z. (1991) Fizicheskie velichiny: Spravochnik, Energoatomizdat, Moscow, Russia
[13] Wolter A., Reinolds A. (1986) Reaktory - razmnojiteli na bystrykh neitronah:Per. s angl., Enerdoatomizdat, Moscow, USSR
[14] Nelson A.T., Sooby E.S., Kim Y.J., Cheng B., Maloy S.A. (2013) High temperature oxidation of molybdenum in water vapor environments,Journal of nuclear materials
[15] Gelles D.S., Peterson D.T., Bates J.F. (1981) Void swelling in the molybdenum alloy TZM irradiated to hihg fluence, Journal of nuclear materials, North-Holland publishing company
[16] Cockeram B.V., Smith R.W., Hashimoto N., Snead L.L. (2011) The swelling microstucture, and hardening of wrought LCAC, TZM, and ODS molybdenum following neutron irradiation, Journal of nuclear materials
[17] Smirnov A.Yu. and Sulaberidze G.A. (2014) Sravnenie sposobov obogascheniya promezshutochnykh komponentov v kaskadakh iz odinakovogo chisla razdelitel'nykh komponentov, Atomnaya energiya 117 №5 pp 274–279
[18] Baranov V.G., Godin Yu.G., Tenishev A.V., Khlunov A.V. and Novikov V. (2012) Fizicheskoe materialovedenie: Uchebnik dlya vuzov, Vol. 7, Yadernye toplivnye materialy, NRNU MEPhI, Moscow, Russia
[19] Dolgov A.B., Novikov V.V. and Ivanov A.S. (2013) Novoye toplivo dlya VVER, Atomniy ekspert 6-7 pp 30–34
[20] Shornikov D.P. (2008) Distinctive Features of Interaction of the U-Mo Fuel Composition Fission
[21] Sorokin A.P., Kalyakin S.G. and Kozlov F.A. (2014) Visokotemperaturnaya yadernaya energotekhnologiya na osnove bistrikh reaktorov s natrievim teplonositelem dlya proizvodstva vodoroda, Atomnaya energiya 116 №4 pp 194–283
[22] Gromov B.F., Demishonkov A.P. and Toshinskiy G.I. (1993) Patent of RF №2066710 Class C23F 11/00 Date of filing 10.03.1993,Products and the Al Matrix with Barrier Coating Proc. of the 12th International Conference on Research Reactor Fuel Management pp 26–29 [Sposob zaschity konstruktcionnykh materialov ot korrozii pri povyshennykh temperaturakh v zhidkom svintce, vismute i ikh splavakh]
[23] Vasko A.T., Kovach S.K. (1983) Elektrokhimiya tugoplavkih metallov, Tekhnika, Kiev, USSR
[24] Shreir L.L. (1976) Corrosion. Volume 1: Metal / Environment Reactions Hardcover, Newnes-Butterworths, ISBN 0408001097
[25] Gulyaev A.P. (1982) Korrosionnostoikie splavy tugoplavkih metallov, Nauka, Moscow, USSR
[26] Tufanov D.G. (1990) Korrosoinnaya stoikost' nerzhaveushikh stalei, splavov i chistykh metallov, Metallurgiya, Moscow, USSR
[27] Cathcart J.V., Manly W.D., (1956) The Mass Transfer Properties of Various Metals and Alloys in Liquid Lead, CORROSION, 12(2):43-47.
[28] Rivai A.K., Takahashi M. (2008)Compatibility of surface-coated steels, refractory metals and ceramics to high temperature lead - bismuth eutectic, Progress in nuclear energy, 560-566
[29] Rivai A.K., Takahashi M. (2008) Corrosion characteristics of materials in Pb–Bi under transient temperature conditions, Journal of nuclear materials
[30] Fazio C., Ricapito I., Scaddozzo G., Benamati G. (2003) Corrosion behaviour of steels and refractory metals and tensile features of steels exposed to flowing PbBi in the LECOR loop, Journal of nuclear materials, 325-332.
[31] Rivai A.K., Takahashi M. (2009) Corrosion investigations of Al–Fe-coated steels, high Cr steels, refractory metals and ceramics in lead alloys at 700 ^{0}C, Journal of nuclear materials
[32] Shmelev A.N., Kulikov G.G., Kulikov E.G. and Apse V.A. (2014) O potentciale gibridnykh (sintezdelenie) narabotchikov topliva dlya yadernykh reactorov: stabilizirovannye razmnozhayuschie svoystva, glubokoe vygoranie, zaschischennoe toplivo, NRNU MEPhI, Moscow.

N E W S
OF THE NATIONAL ACADEMY OF SCIENCES OF THE REPUBLIC OF KAZAKHSTAN
PHYSICO-MATHEMATICAL SERIES
ISSN 1991-346X **https://doi.org/10.32014/2019.2518-1726.37**
Volume 3, Number 325 (2019), 176 – 187

УДК:535.4+004.9

A.M. Tatenov, U.B. Baytukayev,
N. Sandibayeva, G.T. Tugelbayeva, G.E. Bibosynova

Kazakh National Women's Pedagogical University. Almaty, Kazakhstan
tatenov_adambek@mail.ru; umirbek.baytukaev@mail.ru;
nazira.s@mail.ru; g_tugelbaeva@mail.ru; g_u_l_z_h_a_n@inbox.ru

INTERACTIVE VIRTUALIZATION IN THE PROGRAM DELPHY ENVIRONMENT OF ALGORITHMS AND PHENOMENA OF THE SECTION OF PHYSICS OF "ELECTRICITY", FOR HIGHLY EFFECTIVE TUTORING

Abstract. The training program assumes not only studying of theoretical material, but also performance of laboratory works. They are necessary for development of skills of measurement of physical quantities, performance of physical experiences, ability to draw the correct conclusions from the observations. Modern computer technologies allow to add this traditional scheme of training. The training programs modeling physical processes and the phenomena which not always manage to be shown "in live" in the training conditions can provide to pupil's substantial assistance [1,2,3,7]. Processes the phenomenon of the section of physics "Electricity" are visualized and online virtualized by means of the computer program Delphy environments. The made, laboratory work on a research of processes the phenomenon of the section of physics "Electricity" are very effective at development of this course, and the technology of creation of the virtual and interactive laboratory described in this article is very relevant for creation of the similar virtual and interactive laboratories (VIL) in other objects. This virtual interactive laboratory development is introduced in educational process of the Eurasian technological university and is successfully applied in training.

Keywords: Algorithm, virtual interaktivization, virtual and interactive laboratory (VIL), electricity, multimeter, two-channel oscillograph, capacity, inductance, electrical circuit, computer program Delphy, Pascal.

Introduction. Physics - science experimental. Therefore, the training program assumes not only studying of theoretical material, but also performance of laboratory works. They are necessary for development of skills of measurement of physical quantities, performance of physical experiences, ability to draw the correct conclusions from the observations.

Modern computer technologies allow to add this traditional scheme of training. The training programs modeling physical processes and the phenomena which not always manage to be shown "in live" in classroom conditions can provide to pupil's substantial assistance. The value of such programs, however, should not be exaggerated. It is necessary to remember - nothing can replace a real physical experiment in which a part a natural phenomenon, but not the copy of "virtual reality" simulated by the person talks to the researcher!

The "Virtual and Interactive Laboratory of the Section of Physics "Electricity"" program can be used in the course of training differently.

First, with its help it is possible to show demonstrations during an explanation of new material. Such demonstrations are very evident, improve perception and awaken interest in a subject. Advantage of such demonstrations, in comparison with usual videos, also that the teacher can quickly, changing parameters in the program, to answer questions of pupils: "And what will be if …?" The answer is simple - let's make and we will look!

Secondly, the program can be used as a "laboratory" practical work. It is the best of all to give these classes in a computer class. In this case each pupil will be able to perform the laboratory work

independently. Preliminary preparation is usually necessary for such occupation - when the theory of the phenomenon is already known, then intelligent work with experimental installations can bring benefit in deeper understanding of a subject. A set of laboratory works and demonstrations offered by us far does not exhaust all opportunities of the program, and the teacher can always complement this list with own developments.

In the third, on the basis of the program it is possible to perform research works and projects. Within the opportunities, the program allows to conduct researches enough difficult electric processes and the phenomena which theory is beyond the program of training. Inquisitive pupils could open, for example, for themselves laws of Ohm, Kirchhoff for a branched chain, the law of Joule Lenz, etc. if to think over the scheme of an experiment and to take the corresponding measurements. Below examples of laboratory works and demonstrations which can be used in the program are given. It must be kept in mind that the calculations which are carried out by our program for model of real electrical circuits have qualitative character. The list of laboratory works the physics offered for performance on the computer according to the section "Electricity".

Laboratory work № 1 - Studying of dependence of resistance of real conductors on their geometrical parameters and specific resistance of materials.

Laboratory work № 2- Research of resistance of conductors at parallel and consecutive connection.

Laboratory work № 3- EMF and internal resistance of DC power sources. The law of Ohm for a complete chain.

Laboratory work № 4 - Research of difficult chains of direct electric current. Laboratory work № 5- Power in a chain of a direct current.

Laboratory work № 6- The principles of operation of fuses in electrical circuits.

Laboratory work № 7- Elements of chains of alternating current. Capacitive and inductive resistance, their dependence on the frequency of alternating current and parameters of elements. Laboratory work № 8- The resonance phenomenon in a chain of alternating current.

Realization virtual-interaktivization stages of works in the program environment Delphi-7.

The present requirement of time, visualization and interaktivization, including animation images in movements physical the phenomenon and work with them demands the convenient software for realization. The modern visual programming system of Delphi-7 provides convenient means for creation of the environment of modeling of any physical task. We use the Delphi programming language and its Delphi development environment [5.6]. This environment was created by the Borland company with use of the Object Pascal language. Now development of Delphi it is carried out by the Embarcadero company, and the environment supports several languages: Delphi, C, C, C#. The Delphi environment allows to compile the same codes of the program for Windows, Mac OS, iPhone, Android, etc. For reduction of capacity of use of memory for virtual – interaktivization of Delphi-7 technologies is very effective. Delphi is the system of visual object-oriented programming in the Object Pascal language for the Windows operating system. The programs written for Windows are called applications. The technology of visual programming gives to the user an opportunity to create applications by means of a mouse and to observe on the screen results of work in the course of application programming. By the way, the Delphi environment is written to Delphi. [4].

The program in Delphi consists, at least, of four types of files:

1. *.dpr – the file project (for example, Project1.dpr) connects other files in the uniform program. Project options (settings kompilyator, names of office catalogs …) are stored in the file *.dof;

2. *.pas – descriptions and the operators trained by the programmer for what decision - or parts of a programmable task contain files of modules (for example, Unit1.pas). The compiled module is a file *.dcu;

3. *.res – the binary file of resources (for example, Project1.res) stores the Delphi resources used in the program – pictograms, the image of the cursor of a mouse, etc. It is created automatically during creation of the project.

4. *.dfm – *.res is similar, keeps properties of setting up the interface
(forms) of the program. [4,5,6].

After compilation we receive one executable *.exe the file, for example, Project1.exe which comprises the *.res and *.dfm files.

The program of the project has the following sections:

-**program**< program heading (coincides with a name of the file of the project)>;

*(** The section of announcements *(to the first* ***begin****): *)*

-uses < the list of the used modules >;

[Announcements of tags; constants; types; variables; procedures and functions]

-begin

(Section of operators: *)*

<*operator*1>; <*operator*2>; <…>;

<operatorN>

end. *// End of the project*

The first **Begin** means the end of announcements and the beginning algorithmic part of the program which consists of the operators divided by a symbol ";". The program comes to an end with the word end. (with a point). When the new project opens, its text (code) is created automatically and looks as follows:

```
program Project1;
uses
    Forms,
    Unit1 in 'Unit1.pas' {Form1};
{$R *.RES}
begin
    Application.Initialize; // initialization of the
    application Application.CreateForm(TForm1, Form1); // creation of a form
    Application.Run; // application
    launch
    end.
```

The body of the project consists of three operators: preparation of initial data of the program (initialization), creation of the interface on the basis of the main Form1 form and, at last, application launch.

Appointment and general features of the program.

The product is intended for the aid to pupils (and to teachers) average and also average special educational institutions for studying of sections of a course of physics "Electricity". It naturally supplements the classical scheme of training consisting of digestion of theoretical material and development of practical skills of experimenting in physical laboratory.

The program represents the electronic designer allowing to imitate on the monitor screen processes of assembly of electric circuits, to investigate features of their work, to take measurements of electrical quantities as it becomes in a real physical experiment. By means of the designer it is possible:

• to study dependence of resistance of conductors on the specific resistance of its material, length and cross section;

• to study laws of a direct current - Ohm's law for sub circuit and the law of Ohm for a complete chain;

• to study laws of consecutive and parallel connection of conductors, condensers and coils;

• to study the principles of use of safety locks in electronic schemes;

• to study laws of allocation of thermal energy in electric and lighting fixtures, the principles of coordination of sources of current with loading;

• to study the principles of carrying out measurements of current and tension in electronic schemes by means of modern measuring devices (a multimeter, a two-channel oscillography), to observe a type of alternating current on separate details, shift of phases between current and tension in chains of alternating current;

• to study manifestation of capacitive and inductive resistance in chains of alternating current, their dependence on the frequency of the generator of alternating current and face values of details;

• to study allocation of power in chains of alternating current;

• to investigate the resonance phenomenon in chains with a consecutive and parallel oscillatory contour;

• to determine parameters of an unknown detail;

to investigate the principles of creation of electric filters for chains of alternating current. The designer it is also possible to use within his opportunities and for other tasks in independent creative work of pupils.

One of the main features of a complex is the greatest possible imitation of real physical process. For this purpose, following is provided, for example:

• images of details of the designer and measuring devices are provided not schematically, and in such look as "actually";

• at excess of rated power of the electric current proceeding through resistance the last "burns down" and takes a form of the turned black detail;

• the bulb and the electric heater at the rated power begin to shine and "fuse" if the power disseminated on them exceeds working value;

• at excess of operating voltage on the condenser, the last also "fails";

• at excess of rated working current via the safety lock, it "fuses";

• the majority of operations and their results are followed by sound effects.

It becomes in order that the pupil visually saw consequences of the mistakes, learned to understand the reasons of this or that unsuccessful experiment and developed necessary skills of the preliminary analysis of the scheme.

For use of the program enough initial skills of work in the Windows system.

Maintenance of a working window and basic principles of work with a complex.

At start of the program, the monitor of the computer is displayed:

• the bench with contact platforms on which it is possible to collect and analyze work of electric circuits (in the center of the screen);

• the panel of details containing a set of electric elements (in the right part of the screen);

• "recycle bin" where the fused and unnecessary details are thrown out (it is located in the left bottom corner of the screen);

• the control panel of the program with buttons for a call of auxiliary tools (it is located in the top part of the screen);

• the panel of comments (in the lower part of the screen).

Bench.

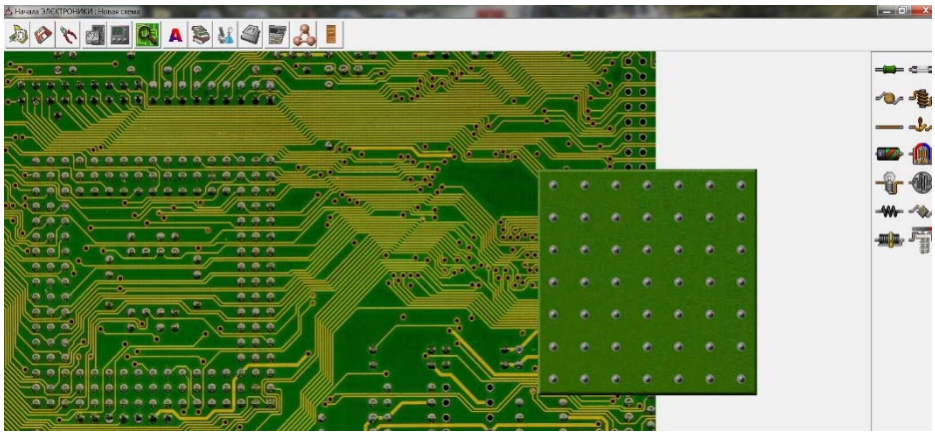

The bench is set of 7 x 7 = 49 contact platforms to which electric details, for assembly of various electric circuits "are soldered". Each detail can be located only between two next contact platforms or vertically or horizontally. In points of their connection with contact platforms, it is possible to connect probes of measuring devices to details. The choice of details from construction set and their "soldering" on a desktop is made by means of the mouse manipulator. It becomes standard for Windows – applications in the way – it is necessary to place the index of "mouse" on the necessary detail (the index takes a tweezers form), then to press the left mice button and, holding it in the pressed state, to move a

detail to the right place of the bench. After release of the left mice button, the detail will be established in the specified place. The unnecessary and "spoiled" details can be removed from a table in "recycle bin" in the same way.

It is possible to delete details from a table and other method. It is necessary "to right-click" on a detail of "mouse" – the window with the inscription "Throw Out a Detail" will appear. After confirmation (click on the button), the detail will be removed in a basket.

The details which are "thrown out" out of bench limits, but not in a basket collect in the lower part of the bench.

On a table sources of an alternating and direct current cannot be at the same time located.

Panel of details of the designer.

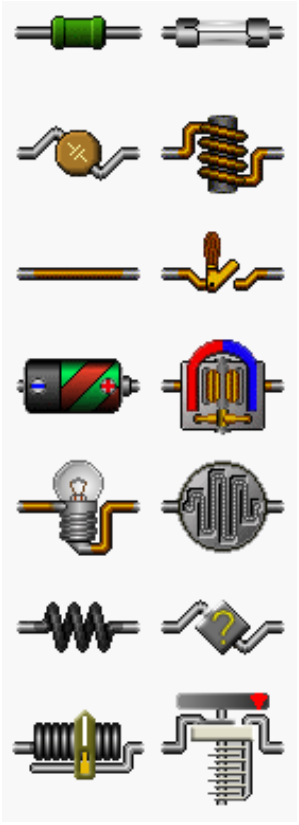

In the designer it is possible to use the following details:

- the resistor (it is characterized by resistance in Ohms and power in Watts, "burns down" at its excess);
- the safety lock (it is characterized by the maximum working current, "burns down" at its excess);
- the condenser (it is characterized by capacity in Farads and operating voltage, fails at its excess);
- the inductance coil (it is characterized by inductance in Henry, has very small active resistance);
- an assembly wire (has very small resistance);
- the switch (it is characterized by two states - "is opened" and "closed");
- a battery (it is characterized by polarity, EMF in Volts and internal resistance in Ohms);
- the generator of sinusoidal tension (it is characterized by amplitude and frequency of alternating voltage);
- a bulb (it is characterized by operating voltage in Volts, working current in milliamperes or power in Watts, "fuses" at their excess);
- the electric heater (it is characterized by the operating voltage and operating power, "fuses" at their excess);
- the real conductor (it is characterized by material, length and cross-sectional area);
- an unknown detail (can be the resistor, the condenser, the coil, the battery or the generator);
- a rheostat (it is characterized by the maximum resistance in Ohms);
- the condenser of variable capacity (it is characterized by the maximum capacity in Farads).

Panel of comments. Data on details and hints about purpose of buttons of the control panel are output to panels of comments. This information appears after installation of the index of "mouse" on the corresponding elements.

Digital multimeter.

General view and details purpose of a multimeter. Rules of work with a miltimeter.

Measurements by means of a multimeter: Measurement of tension. Measurement of force of a direct current. Measurement of resistance**.**

General view and details purpose of a multimeter.

In the drawing are shown arrangement of control elements and nests for connection of a multimeter to the electronic scheme. Switching of operating modes and limits of measurement is made by "click" of the mouse manipulator on tags of the corresponding limits (at installation of the index on limits it takes a hand form).

Rules of work with a multimeter.

1. The multimeter is caused on the screen (desktop) by pressing of the Receive a Multimeter button on the top panel of a window of the program. The following pressing this button calls the second device

(at the same time the button is blocked). For removal of the device it is necessary to click on the button in the right top corner of a window of a multimeter. The device together with the clips disappears from the screen.

2. Connection of a multimeter to points of the studied scheme is made by installation to the right places of the general (dark blue) and measuring (red) the clips connected to the corresponding nests of the device.

The general view of a multimeter is shown below in the drawing:

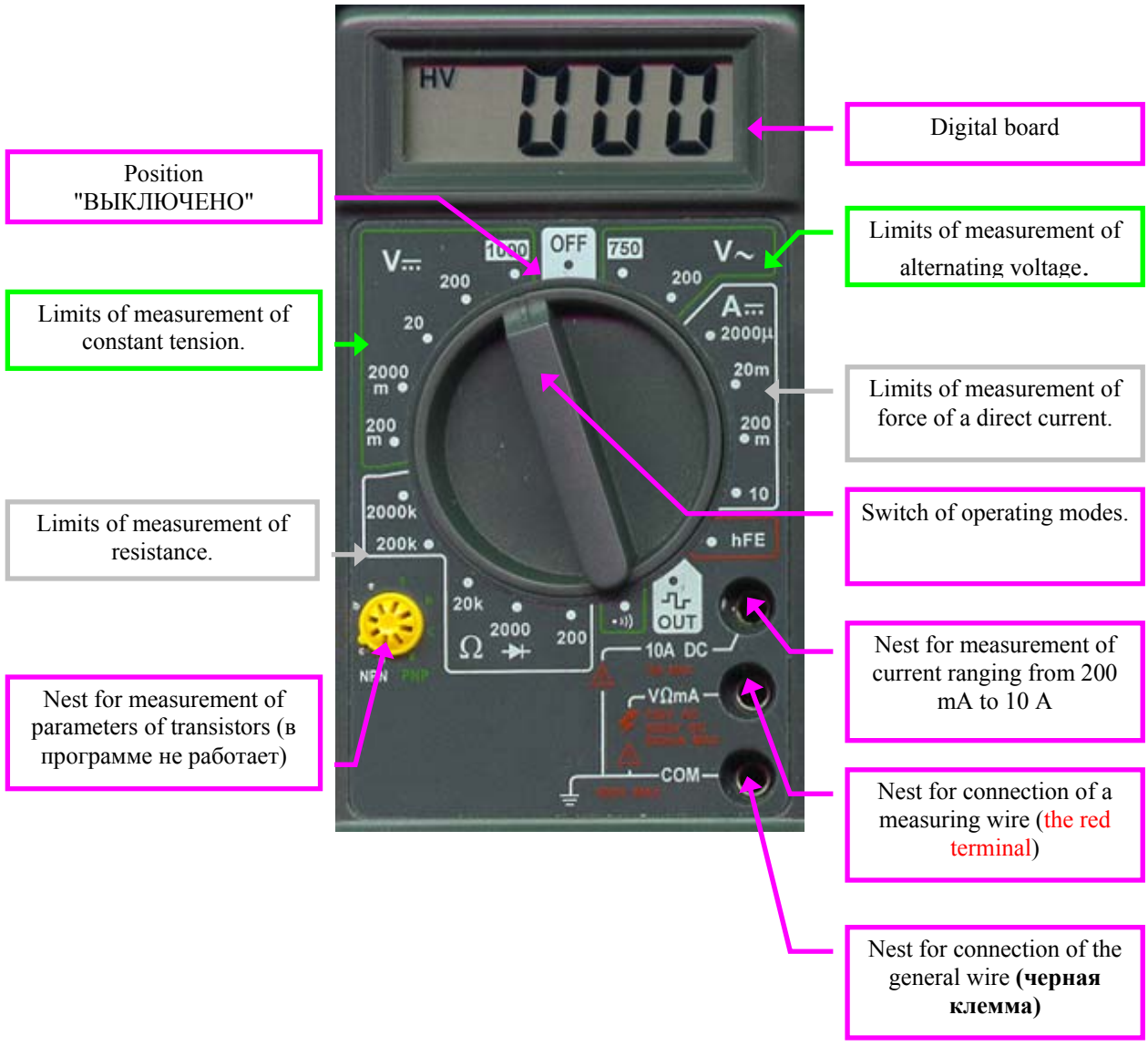

Connecting wires of the device on the screen are not shown not to encumber the bench. It is necessary for connection of the device to the studied scheme:

- to establish the index of "mouse" on the necessary clip of the device (the index will take a hand form);
- to press and hold the left mice button:
- to drag a clip (holding the button) in the necessary point of the scheme and to release the mice button.

If in the course of work it is required to switch clips to other places of the scheme, then the same procedure is used. Transfer of a clip on area of the device brings to its automatic "parking" on the corresponding entrance nest of a multimeter.

3. Switching of operating modes of the device is carried out by installation of the index of "mouse" on the corresponding point of the panel of the device (at the same time the index changes the look) and click of the left mice button. The switch of operating modes of a multimeter turns in noted position.

4. On a digital board of the device the numerical value of the measured size (current, tension, resistance) in units specified on the chosen measurement limit is displayed. If in the left part of a board it is highlighted-1 (overflow) it means that the value of the measured size exceeds the maximum value of the chosen measurement limit. It is necessary to switch the device to other limit.

5. You can use one or two multimeters which have number 1 and 2 for work. Clips of devices also have the corresponding numbers. Devices can be used at the same time and independently. For example, it is possible to measure by the first device tension, and the second - current, in different parts of the studied scheme.

Measurements by means of a multimeter.

The multimeter allows to take measurements:

• tension of direct and alternating current;

• forces of a direct current;

• resistance of sites of a chain of a direct current.

to check existence of contacts with use of the sound alarm system.

Measurement of tension.

For voltage measurement on the site of the studied chain it is necessary to consider the following:

The voltmeter always turns on parallel to the site of a chain on which measure tension (the real voltmeter can fail at the wrong inclusion!).

What type of current - constant or variable, proceeds in a chain? The switch of operating modes needs to be installed in the corresponding position.

The voltmeter shows effective value of alternating voltage.

At measurement of constant tension, the voltmeter shows value taking into account polarity - if potential on a measuring clip less, than on the general, on a board the sign "minus" is highlighted.

Limits of measurement of constant tension: 1000 V, 200 V, 20 V, 2000 mV, 200 mV.

Limits of measurement of alternating voltage: 750 V, 200 V.

Entrance resistance of the device is equal in the mode of the voltmeter to 1 megOm.

Measurement of force of a direct current. For measurement of current on the site of the studied chain it is necessary to consider the following:

The ampermeter always turns on consistently in the site of a chain where current is measured (the real ampermeter can fail at the wrong inclusion!).

Our ampermeter can measure only force of a direct current.

At measurement of current in chains, the ampermeter shows its value taking into account polarity: if current via the device flows from the general terminal to measuring, on a board the sign "minus" is highlighted.

Limits of measurement of force of a direct current: 10 A, 200 mA, 20 mA, 2000 mA.

Entrance resistance of the ampermeter is not enough (near 10^{-6} Om)

Measurement of resistance. For measurement of resistance it is necessary to consider the following: The ohmmeter can measure only the active resistance of elements of the scheme; Limits of measurement of resistance: 2000 kOm, 200 kOm, 20 kOm, 2000 Ohms, 200 Ohms and a special limit for definition of contacts with the sound alarm system; On the measured site of the scheme the device gives voltage of 2 V; It is possible to determine by the Device existence of contact in the scheme, at the same time, if resistance of the measured site is less than 75 Ohms, the sound signal is given. mereny forces of a direct current. For measurement of current on the site of the studied chain it is necessary to consider the following:

The ampermeter always turns on consistently in the site of a chain where current is measured (the real ampermeter can fail at the wrong inclusion!).

Our ampermeter can measure only force of a direct current.

At measurement of current in chains, the ampermeter shows its value taking into account polarity: if current via the device flows from the general terminal to measuring, on a board the sign "minus" is highlighted.

Limits of measurement of force of a direct current: 10 A, 200 mA, 20 mA, 2000 mkA**.**

Entrance resistance of the ampermeter is not enough

Dual trace oscilloscope. General view and details purpose of an oscillograph of the Rule of work with an oscillograph: Description of governing bodies of an oscillograph. Measurements by means of an oscillograph.

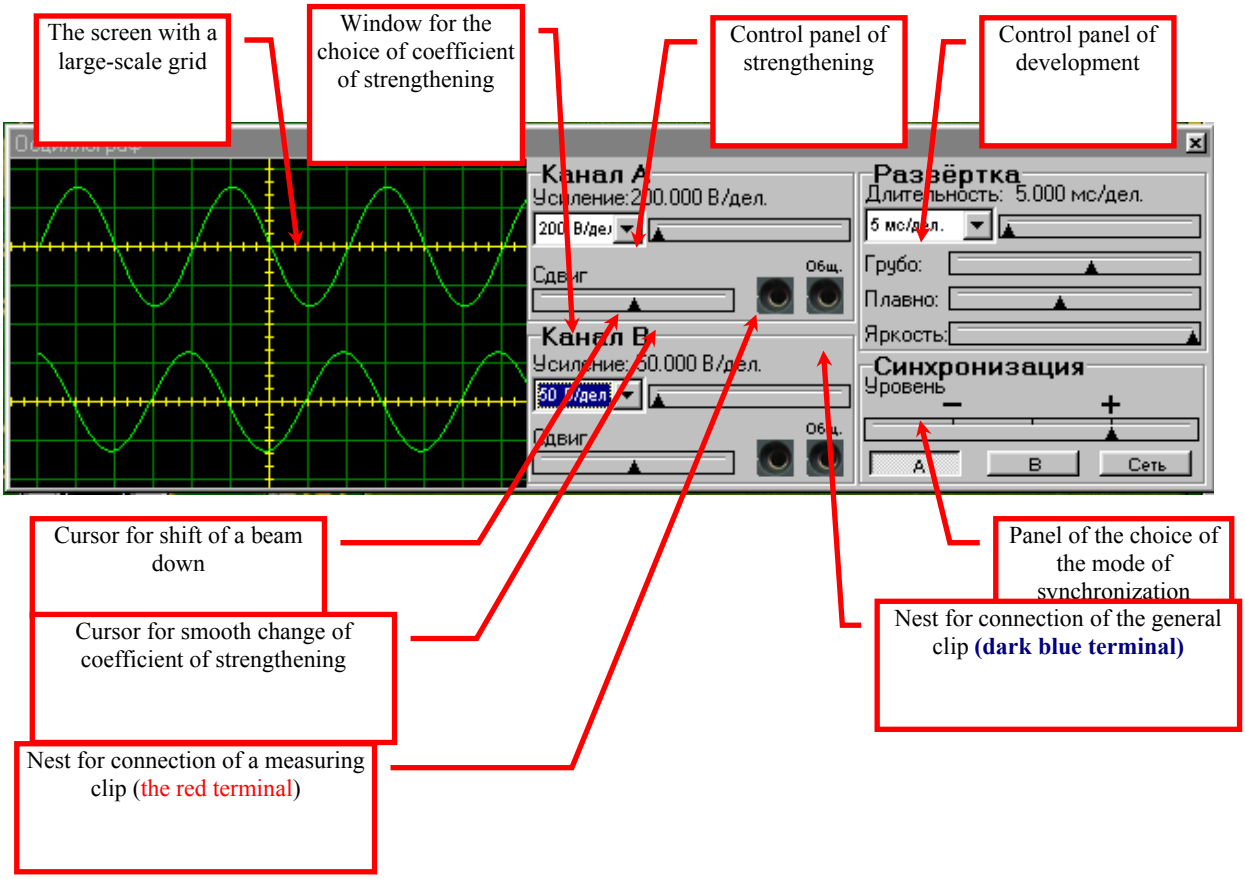

General view and details purpose of an oscillography:

The front panel of an oscillography contains the following parts:

- The screen with a large-scale grid for observation of a form of a signal and quantitative measurements;
- Control panel of strengthening of channels and shift of beams down;
- Control panel of development, shift of beams across, choice of the modes of synchronization and some support functions.

The oscillography is intended for visual observation of a form of alternating voltage. It allows to define quantitative characteristics of a signal also: frequency and amplitude of alternating voltage, impulse duration, shift of phases between two periodic signals (for this purpose the oscillography has to be two-channel).

Entrance resistance of an oscillography is rather high (near 10 megOms).

General view and details purpose of an oscillography:

The front panel of an oscillography contains the following parts:

- The screen with a large-scale grid for observation of a form of a signal and quantitative measurements;

- Control panel of strengthening of channels and shift of beams down;
- Control panel of development, shift of beams across, choice of the modes of synchronization and some support functions.

Rules of work with an oscillography.

1. The oscillography is caused on the screen (desktop) by pressing of the Receive an Oscillography button on the top panel of a window of the program. For removal of an oscillography it is necessary to click on the button ☒ in the right top corner of its window. The oscillography together with the clips disappears from the screen.

2. Connection of an oscillography to points of the studied scheme is made by installation to the right places of the general (dark blue) and measuring (red) the clips connected to the corresponding nests of an oscillography. Connecting wires on the screen are not shown not to encumber the bench. Clips have designations (letter A and B) corresponding to channels of an oscillography. It is necessary for connection of an oscillography to the studied scheme: to establish the index of "mouse" on the necessary clip of the device (the index will take a hand form); to press and hold the left mice button: to drag a clip (holding the button) in the necessary point of the scheme and to release the mice button. If in the course of work it is required to switch clips to other places of the scheme, then the same procedure is used. Transfer of a clip on area of the device brings to its automatic "parking" on the corresponding entrance nest of an oscillography.

3. Installation of operating modes of an oscillography is carried out by means of adjustment of coefficients of strengthening of channels, the choice of duration of development, the mode of synchronization and adjustment of support functions.

4. On the screen of an oscillography the measuring grid by means of which it is possible to take quantitative measurements of parameters of a signal is put.

5. You can use for work one or two channels at the same time. Clips of an oscillography have designations "A" and "B", according to channels "A" and "B"".

Description of governing bodies of an oscillography.

Installation of coefficient of strengthening.

In order that the image of a signal on the screen of an oscillography did not go beyond the screen or had no too small amplitude, it is necessary to choose coefficient of strengthening of the channel correctly.

The coefficient of strengthening of an oscillography is set in Volts/divisions. It means, for example, that the price of division of a scale of the screen of an oscillography will be down equal to 500 mV if value of coefficient of strengthening to choose equal 500 mV / put.

The coefficient of strengthening of an oscillography can be changed in the Strengthening window by the choice of the necessary value from the offered list. This list opens when pressing the button located to the right of a window. Besides, it is possible to change smoothly strengthening coefficient in some limits by means of a cursor of located more to the right of a window with the button. For this purpose, it is necessary to establish the index of "mouse" on this badge, to press the left mice button and, holding it in the pressed state to move a cursor to the necessary position.

The cursor "Shift down" allows to displace an oscillography beam up or down.

Choice of the mode of development.

For the correct display of a periodic signal it is necessary to choose the corresponding duration of development of an oscillography also.

Duration of development is set in units time/division. It means, for example, that the price of division of a scale of the screen of an oscillography will be equal to 20 ms across if value of duration of development to choose equal 20 ms / put. The numerical value of duration of development is set by the ways similar for installation of coefficient of strengthening.

The cursor "The synchronization level" determines the time point of the beginning of development of a signal corresponding to a preset value of its amplitude. This adjustment can be useful to numerical definition of phase shift between two signals. Buttons "A" and "B" choose the channel on which development synchronization is carried out. The button "Network" changes development of both channels of an oscillography from the internal generator of sinusoidal tension. This mode is used for observation of addition of perpendicular fluctuations – Lissazhu's figures.

Cursor "Brightness" can be changed intensity of a luminescence of beams of an oscillography (at the same time brightness of a large-scale grid does not change).

Measurements by means of an oscillography.

The oscillography allows to take measurements: amplitudes of tension of alternating current; frequencies of alternating voltage; shift of a phase between two signals.

here is an assembly of the electric circuit

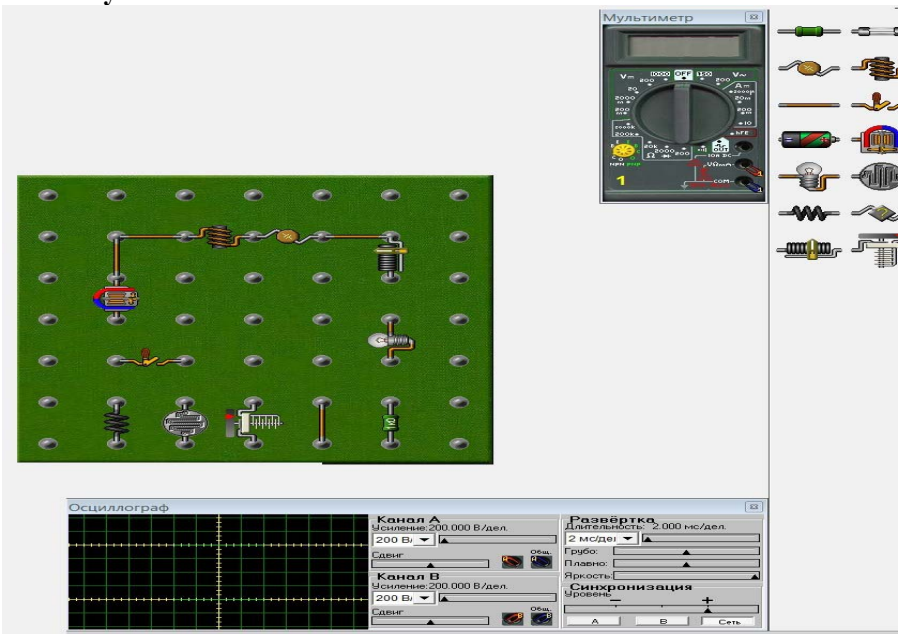

After final assembly of the scheme, there will be a process of measurement of parameters of a chain.

Performance of laboratory works on a physics course – electricity, begins with assembly of an electrical circuit, with calculation of parameters of details and half-cooking to measurements of current, tension, resistance of resistors, frequencies and amplitudes of alternating current, shift of phases electric fluctuation, the power of electroinstallations of a chain.

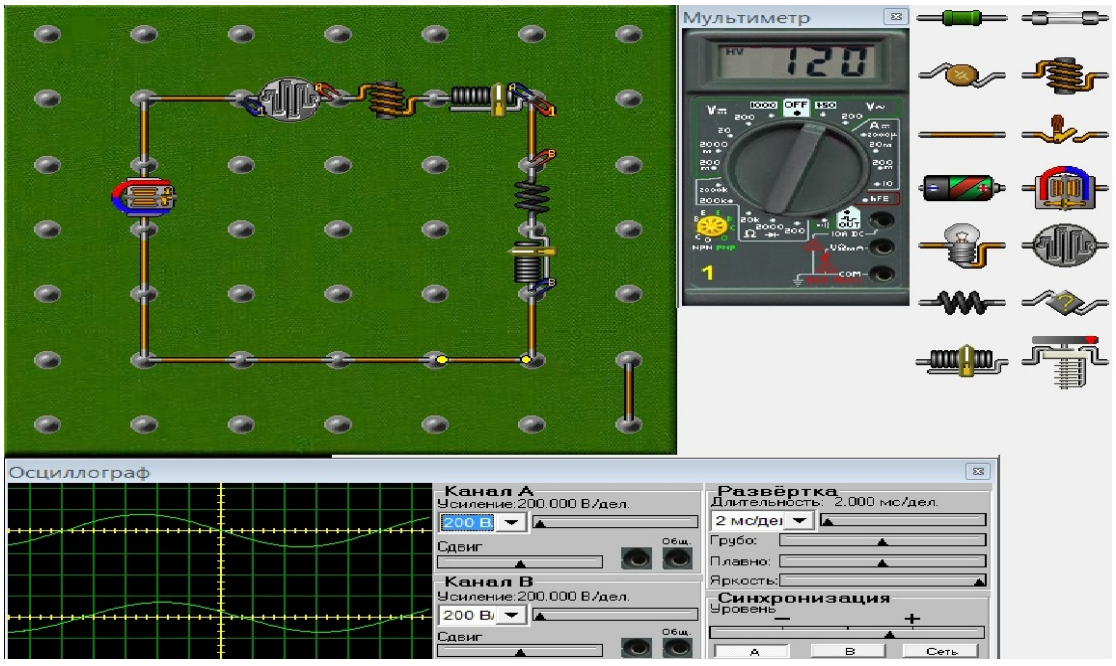

Measurement of devices and characteristic of all details of the scheme work in the real mode

Conclusion.

As a part of information technologies the new industry develops - it is a virtual interaktivization and visualization of the hardly understood subjects of physics, chemistry, biology and other objects [2,3,7]. And creation is virtual – interactive laboratories in the called objects meet the operated measuring devices very seldom. Therefore the technology of creation of the virtually-interactive laboratory (VIL) for the section of physics "Electricity" given in this work will be very relevant to creators similar to VIL – at higher step in other objects of knowledge. Such VIL – on the computer are very effective for development of a certain course of knowledge and develop independent research skills and awaken to creative search of methods of a research. Given VIL according to the section of physicists Electricity, due to visuality and interactive intervention in change process an experiment condition, it is very useful to fast development of a subject of physics by students and to development of skills a research. Brought VIL – according to the section of a course section of physicists Electricity, are introduced in educational process of the Eurasian Technological University and are successfully applied.

УДК:535.4+004.9

А.М. Татенов, У.Б. Байтукаев, Н. Сандибаева, Г.Т.Тугельбаева, Г.Е.Бибосынова.

Казақ Ұлттық Қыздар Педагогикалық Университеті. Алматы қ. Казақстан.

ФИЗИКАНЫҢ «ЭЛЕКТРЛІК» БӨЛІМІНДЕГІ ҚҰБЫЛЫСТАРДЫҢ АЛГОРИТМДЕРІН DELPHY БАҒДАРЛАМА ОРТАСЫНДА ИНТЕРАКТИВТІ ВИРТУАЛДАУ, ЖОҒАРЫ САПАЛЫ ОҚЫТУДЫҢ ҚҰРАЛЫ

Аннотация. Бұл оқыту бағдарламасы тек теориялық материалдарды үйрету ғана емес, сонымен бірге лабораториялық зертханалық жұмыстарды орындауға болады. Зертханалық жұмыстар, физикалық шамаларды өлшеу әдістерін үйренуге, физикалық тәжірибелерді орындауды меңгеруге, өзінің зерттеу нәтижелерінен дұрыс қорытынды шығаруға қажет. Қазіргі компьютерлік технологиялар дәстүрлі оқытуға қажетті қосымшаларды жасауға мүмкіндігі бар. Физикалық процестер мен құбылыстарды модельдеу арқылы жасалған оқыту бағдарламалары, оқыту кезіндегі «тірілей» көрсете алмайтын процестерді , көрсете алады және оқушыға түсіну үшін зор көмек береді.[1,2,3,7]. Физиканың «электрлік» бөліміндегі процестер мен құбылыстар Delphy компьютерлік бағдарлама ортасында көрнекілік-ке ие болды және интерактивті түрде виртуалданды. Жасалынған виртуалды-интерактивті лабораториялық жұмыстар физиканың «электрлік» бөліміндегі процестер мен құбылыс-тарды зерттеу нәтижесінде осы курсты меңгеруге өте пайдалы, ал мақаладағы келтірілген виртуалды-интерактивті лабораторияны құрудың технологиясы, басқа пәндерден осы сия-қты виртуалды-интерактивті лабораториялар (ВИЛ) құруға көмек ретінде өте актуалды. Келтірілген виртуалды-интерактивті лаборатория қондырғылары Евразия технологиялық университетінің оқыту процесіне толығынан енгізілген және оқыту барысында қолданыс-та.

Түйін сөздер: Алгоритм, виртуалды интерактивтендіру, виртуалды-интерактивті лаборатория (ВИЛ), электрлік, мультиметр, екіканалды осциллограф, сиымдылық, индук-тивтілік, электр тізбегі, компьютерлік бағдарлама, делфи, паскаль.

УДК:535.4+004.9

А.М. Татенов, У.Б. Байтукаев, Н. Сандибаева, Г.Т.Тугельбаева, Г.Е.Бибосынова.

Казахский Национальный Женский Педагогический Университет, г.Алматы, Казахстан

ИНТЕРАКТИВНАЯ ВИРТУАЛИЗАЦИЯ В ПРОГРАММНОЙ СРЕДЕ DELPHY АЛГОРИТМОВ ЯВЛЕНИИ РАЗДЕЛА ФИЗИКИ «ЭЛЕКТРИЧЕСТВА», ДЛЯ ВЫСОКОЭФФЕКТИВНОГО ОБУЧЕНИЯ

Аннотация. Обучающая программа предполагает не только изучение теоретического материала, но и выполнение лабораторных работ. Они необходимы для выработки навыков измерения физических величин, выполнения физических опытов, умения делать правильные выводы из своих наблюдений. Современные компьютерные технологии позволяют дополнить эту традиционную схему обучения. Обучающие программы, моделирующие физические процессы и явления, которые не всегда удается показать "в живую"

в обучающих условиях, могут оказать учащимся существенную помощь.[1,2,3]. Процессы явлении раздела физики «Электричество» визуализированы и интерактивно виртуализированы с помощью компьютерных программных сред Delphy**.** Сделанная, лабораторная работа по исследованию процессов явлении раздела физики «Электричество» очень эффективны при освоении данного курса, а технология создания виртуально-интерактивной лаборатории описанной в данной статье, очень актуальна для создания аналогичных виртуально-интерактивных лаборатории(ВИЛ) по другим предметам. Данная виртуально- интерактивная лабораторная разработка внедрена в учебный процесс Евразийского технологического университета и успешно применяется в обучении.

Ключевые слова: Алгоритм, виртуальная интерактивизация, виртуально-интерактивная лаборатория(ВИЛ), электричество, мультиметр, двухканальный осциллограф, емкость, индуктивность, электрическая цепь, компьютерная программа,делфи, паскаль.

REFERENCES

[1] Tatenov A.M., Savelyeva V.V. The manual on physics for technical specialties. Almaty, Medet group, 2017.

[2] Adambek Tatenov, Akerke Amirkhanova, Victoria Savelyeva

[3] Virtual-interactive visualization of atomic structures, electron configurations, energy levels in 3D format for the construction of virtual-interactive laboratories with the mechanisms of chemical reactions in inorganic and organic chemistry.- International Journal of Applied Engineering Research ISSN 0973-4562 Volume 11, Number 5 (2016) pp 3319-3321 © Research India Publications. http://www.ripublication.com 3319

[4] Tatenov A.M. Information technologies in modeling of processes in oil layers and power stations//Works of the International conference "High Technologies - Guarantee of Sustainable Development".-Almaty: КазНТУ, 2011. Page 312-315.

[5] Programming in the environment of Delphi: studies. - a method. A grant for bachelors of engineering and physical specialties / сост. V.K. Tolstykh. – Donetsk: To DONN, 2010. 128 pages: silt.

[6] Rubenking N. Programming in Delphi for "teapots". Kiev:

[7] "Dialectics", 1996. 304 pages.

[8] Hoffman V.E., Homonenko A.D. Delphi 6. SPb.: BHV is St. Petersburg, 2001. – 1152 pages.7.Tatenov A.M., Askarova Sh.M. Virtual and Interactive Information Technology in Modeling Researches of Processes of Applied Problems of

[9] a Science. World Applied Sciences Journal,-30.(Management, Economics,

[10]Technology), 2014.pp.-144-148. ISSN.1818-4952.

[11]ISSN 1991-346X 2. 2019 53 N E W S OF THE NATIONAL ACADEMY OF SCIENCES OF THE REPUBLIC OF KAZAKHSTAN PHYSICO-MATHEMATICAL SERIES ISSN 1991-346X https://doi.org/10.32014/2019.2518-1726.12 Volume 2, Number 324 (2019), 53 – 59 УДК:535.4+004.9 A.M. Tatenov, V.V. Savelyeva, N.A. Sandibayeva, L.S. Baykadamova, D.Baitukayeva. Kazakh National Women's Pedagogical University. Kazakhstan, Almaty tatenov_adambek@mail.ru; vika-sova@mail.ru;nazira.s@mail.ru; laura83-askar@mail.ru; baitukaeva_dana@mail.ru INTERACTIVE VIRTUALIZATION IN THE ENVIRONMENT OF FLASH-CC, JAVA SCRIPT OF ALGORITHMS THE PHENOMENON OF THERMOPHYSICS AND MOLECULAR PHYSICS, AS ACHIEVEMENT OF HIGHLY EFFECTIVE TRAINING Abstract. The training program assumes not only studying of theoretical material, but also performance of

МАЗМҰНЫ

СОДЕРЖАНИЕ

CONTENTS

Publication Ethics and Publication Malpractice in the journals of the National Academy of Sciences of the Republic of Kazakhstan

For information on Ethics in publishing and Ethical guidelines for journal publication see http://www.elsevier.com/publishingethics and http://www.elsevier.com/journal-authors/ethics.

Submission of an article to the National Academy of Sciences of the Republic of Kazakhstan implies that the described work has not been published previously (except in the form of an abstract or as part of a published lecture or academic thesis or as an electronic preprint, see http://www.elsevier.com/postingpolicy), that it is not under consideration for publication elsewhere, that its publication is approved by all authors and tacitly or explicitly by the responsible authorities where the work was carried out, and that, if accepted, it will not be published elsewhere in the same form, in English or in any other language, including electronically without the written consent of the copyright-holder. In particular, translations into English of papers already published in another language are not accepted.

No other forms of scientific misconduct are allowed, such as plagiarism, falsification, fraudulent data, incorrect interpretation of other works, incorrect citations, etc. The National Academy of Sciences of the Republic of Kazakhstan follows the Code of Conduct of the Committee on Publication Ethics (COPE), and follows the COPE Flowcharts for Resolving Cases of Suspected Misconduct (http://publicationethics.org/files/u2/New_Code.pdf). To verify originality, your article may be checked by the Cross Check originality detection service http://www.elsevier.com/editors/plagdetect.

The authors are obliged to participate in peer review process and be ready to provide corrections, clarifications, retractions and apologies when needed. All authors of a paper should have significantly contributed to the research.

The reviewers should provide objective judgments and should point out relevant published works which are not yet cited. Reviewed articles should be treated confidentially. The reviewers will be chosen in such a way that there is no conflict of interests with respect to the research, the authors and/or the research funders.

The editors have complete responsibility and authority to reject or accept a paper, and they will only accept a paper when reasonably certain. They will preserve anonymity of reviewers and promote publication of corrections, clarifications, retractions and apologies when needed. The acceptance of a paper automatically implies the copyright transfer to the National Academy of Sciences of the Republic of Kazakhstan.

The Editorial Board of the National Academy of Sciences of the Republic of Kazakhstan will monitor and safeguard publishing ethics.

Правила оформления статьи для публикации в журнале смотреть на сайтах:

www:nauka-nanrk.kz

http://physics-mathematics.kz/index.php/en/archive

ISSN 2518-1726 (Online), ISSN 1991-346X (Print)

Редакторы *М. С. Ахметова, Т.А. Апендиев, Д.С. Аленов*
Верстка на компьютере *А.М. Кульгинбаевой*

Подписано в печать 10.06.2019.
Формат 60x881/8. Бумага офсетная. Печать – ризограф.
8,3 п.л. Тираж 300. Заказ 3.

Национальная академия наук РК
050010, Алматы, ул. Шевченко, 28, т. 272-13-18, 272-13-19